ISSN 2518-7198 (Print)
ISSN 2663-5089 (Online)

BULLETIN
OF THE KARAGANDA UNIVERSITY

PHYSICS
Series

№ 4(108)/2022

ISSN 2663-5089 (Online)
ISSN-L 2518-7198 (Print)
Индексі 74616
Индекс 74616

ҚАРАҒАНДЫ УНИВЕРСИТЕТІНІҢ ХАБАРШЫСЫ

ВЕСТНИК КАРАГАНДИНСКОГО УНИВЕРСИТЕТА

BULLETIN OF THE KARAGANDA UNIVERSITY

ФИЗИКА сериясы

Серия ФИЗИКА

PHYSICS Series

№ 4(108)/2022

Қазан–қараша–желтоқсан
30 желтоқсан 2022 ж.
Октябрь–ноябрь–декабрь
30 декабря 2022 г.
October–November–December
December, 30th, 2022

1996 жылдан бастап шығады
Издается с 1996 года
Founded in 1996

Жылына 4 рет шығады
Выходит 4 раза в год
Published 4 times a year

Қарағанды, 2022
Караганда, 2022
Karaganda, 2022

Редакцияның мекенжайы: 100024, Қазақстан, Қарағанды қ., Университет к-сі, 28
Тел.: +7 701 531 4758; факс: (7212) 35-63-98.
E-mail: vestnikku@gmail.com; karabekova71@mail.ru
Сайты: physics-vestnik.ksu.kz

Атқарушы редактор

PhD д-ры **Г.Б. Саржанова**

Редакторлары

Ж.Т. Нурмуханова, С.С. Балкеева, И.Н. Муртазина

Компьютерде беттеген

М.С. Бабатаева

Қарағанды университетінің хабаршысы. «Физика» сериясы.
ISSN-L 2518-7198 (Print). ISSN 2663-5089 (Online).

Меншік иесі: «Академик Е.А. Бөкетов атындағы Қарағанды университеті» КЕАҚ.

Қазақстан Республикасы Ақпарат және қоғамдық даму министрлігімен тіркелген. 30.09.2020 ж. № KZ38VPY00027378 қайта есепке қою туралы куәлігі.

Басуға 29.12.2022 ж. қол қойылды. Пішімі 60×84 1/8. Қағазы офсеттік. Көлемі 15,0 б.т. Таралымы 200 дана. Бағасы келісім бойынша. Тапсырыс № 137.

«Акад. Е.А. Бөкетов ат. Қарағанды ун-ті» КЕАҚ баспасының баспаханасында басылып шықты.
100024, Қазақстан, Қарағанды қ., Университет к-сі, 28. Тел. (7212) 35-63-16. E-mail: izd_kargu@mail.ru

Адрес редакции: 100024, Казахстан, г. Караганда, ул. Университетская, 28
Тел.: +7 701 531 4758. Факс: (7212) 35–63–98.
E-mail: vestnikku@gmail.com; karabekova71@mail.ru
Сайт: physics-vestnik.ksu.kz

Вестник Карагандинского университета. Серия «Физика».
ISSN-L 2518-7198 (Print). ISSN 2663-5089 (Online).

Собственник: НАО «Карагандинский университет имени академика Е.А. Букетова».

Зарегистрирован Министерством информации и общественного развития Республики Казахстан. Свидетельство о постановке на переучет № KZ38VPY00027378 от 30.09.2020 г.

Подписано в печать 29.12.2022 г. Формат 60×84 1/8. Бумага офсетная. Объем 15,0 п.л. Тираж 200 экз. Цена договорная. Заказ № 137.

Отпечатано в типографии издательства НАО «Карагандинский университет им. акад. Е.А. Букетова». 100024, Казахстан, г. Караганда, ул. Университетская, 28. Тел. (7212) 35-63-16. E-mail: izd_kargu@mail.ru

Postal address: 28, University Str., 100024, Karaganda, Kazakhstan

Tel.: +7 701 531 4758; Fax: (7212) 35-63-98.

E-mail: vestnikku@gmail.com; karabekova71@mail.ru

Web-site: physics-vestnik.ksu.kz

Bulletin of the Karaganda University. "Physics" Series.

ISSN-L 2518-7198 (Print). ISSN 2663-5089 (Online).

Proprietary: NLC "Karagandy University of the name of academician E.A. Buketov".

Registered by the Ministry of Information and Social Development of the Republic of Kazakhstan. Rediscount certificate No. KZ38VPY00027378 dated 30.09.2020.

Signed in print 29.12.2022. Format 60×84 1/8. Offset paper. Volume 15,0 p.sh. Circulation 200 copies. Price upon request. Order № 137.

Printed in the Publishing house of NLC "Karagandy University of the name of acad. E.A. Buketov".
28, University Str., Karaganda, 100024, Kazakhstan. Tel. (7212) 35-63-16. E-mail: izd_kargu@mail.ru

МАЗМҰНЫ — СОДЕРЖАНИЕ — CONTENT

КОНДЕНСАЦИЯЛАНҒАН КҮЙДІҢ ФИЗИКАСЫ
ФИЗИКА КОНДЕНСИРОВАННОГО СОСТОЯНИЯ
PHYSICS OF THE CONDENSED MATTER

ТЕХНИКАЛЫҚ ФИЗИКА
ТЕХНИЧЕСКАЯ ФИЗИКА
TECHNICAL PHYSICS

ЖЫЛУФИЗИКАСЫ ЖӘНЕ ТЕОРИЯЛЫҚ ЖЫЛУТЕХНИКАСЫ
ТЕПЛОФИЗИКА И ТЕОРЕТИЧЕСКАЯ ТЕПЛОТЕХНИКА
THERMOPHYSICS AND THEORETICAL THERMOENGINEERING

DOI 10.31489/2022PH4/6-13

UDC 535.37

D. Temirbayeva*[1], N. Ibrayev[1], E. Seliverstova[1], M. Kudinova[2], A. Ishchenko[2]

[1]Institute of Molecular Nanophotonics, Buketov University, Karaganda, Kazakhsta
[2]Institute of Organic Chemistry, NAS of Ukraine, Kyiv, Ukraine
*(*E-mail: dilara.temirbayeva@gmail.com)*

Plasmon effect on triplet-singlet energy transfer in the dye-doped Langmuir-Blodgett films

The effect of silver plasmonic nanoparticles on triplet-singlet energy transfer in the donor-acceptor pair of organic dyes was studied. Layered dye films were prepared on the surface of glass and island silver films using the Langmuir-Blodgett method. Amphiphilic analogs of Rose bengal and polymethine dye were used as donor and acceptor of energy. A polymer monolayer was deposited between monolayers of donor and acceptor molecules to exclude the competing triplet-triplet energy transfer. The spectra of delayed fluorescence and phosphorescence of donor-acceptor films and the delayed luminescence lifetime of donor in these films have been measured. It is shown that a threefold increase in the fluorescence intensity and a twofold increase in the donor phosphorescence intensity are observed on silver island films. The successful triplet-singlet energy transfer is evidenced by both the quenching of donor centers and appearance of sensitized delayed fluorescence of the acceptor with the duration close to the donor triplet lifetime. In the presence of silver nanoparticles, in addition to enhancement in the intensity of the donor emission, an increase in the efficiency of triplet-singlet energy transfer was observed. The obtained results can be used in various optical devices.

Keywords: Rose bengal; polymethine dye; silver island film; plasmon; delayed fluorescence; phosphorescence; triplet-singlet energy transfer; Langmuir-Blodgett films.

Introduction

Intermolecular energy transfer is one of the main processes in various applications of photonics [1, 2], optics, optoelectronics [3, 4, 5] and photovoltaics [6, 7]. The electron excitation energy transfer between molecules is one of the possible ways to influence the rate of photochemical reactions. The mechanism, the theoretical description of which was first proposed by Förster in the 1940s, allows distances up to 10 nm to be measured and it is based on the nonradiative dipole-dipole interaction of the giving and receiving molecules [8].

The triplet-singlet energy transfer was predicted by Förster [8] and confirmed by Ermolaev and Sveshnikova [9], who discovered this type of energy transfer using several phosphorescent donors and fluorescent acceptors in solid media. Thus, it was experimentally shown that Förster's theory can be applied to donor-acceptor pairs undergoing triplet-singlet energy transfer [9, 10].

The triplet-singlet energy transfer is widely used to obtain high-efficiency fluorescent organic light-emitting devices [3, 11, 12], to create biochemical and biophysical sensors [12], and can be used as a method to increase the rate of light emission from excited triplet states [13]. In [11], the authors used nonradiative energy transfer to increase the efficiency of a fluorescent red organic light-emitting device in four times. The triplet-singlet energy transfer is used in a new emitter concept for organic light-emitting diodes (OLEDs) called as thermally activated delayed fluorescence (TADF) [12, 14]. In [15], simultaneous and efficient energy transfer from both donating singlet and triplet states of a single photoluminescent molecular species was demonstrated, showing that cooperation between these two exciton transfer channels is possible.

At present, there are few publications devoted to the study of the effect of plasmonic nanoparticles on the triplet-singlet energy transfer. In [16], a decrease in the efficiency of triplet-singlet energy transfer on the surface of a silver island film was observed. And in [17], the influence of the plasmon effect of Ag nanoparticles (NPs) on singlet-singlet (S-S) and triplet-singlet (T-S) energy transfer in the same donor–acceptor pair of organic molecules was studied, and it was shown that the plasmon effect affects both S–S and T–S energy transfer.

In this work, the Langmuir-Blodgett (LB) technology was used to obtain structured films. The LB method is a useful and well-established tool for the fabrication of ultrathin films. The composition and thickness of such films can be precisely controlled at the molecular level. In addition, the orientation of fluorescent probes to the metal surface is fixed and the probes are in a monolayer, which is favorable for studies of metal-enhanced processes [18–20].

In the present work, we studied the effect of plasmonic nanoparticles on the T–S energy transfer in langmuir films in a pair of Rose bengal and polymethine dye. In contrast to [17], where the donor and acceptor molecules are arranged randomly, in the present work, the molecules are arranged structured using the Langmuir–Blodgett technology.

Experimental

Amphiphilic analogs of the dyes of Rose Bengal (RB) and indotricarbocyanine (PD) [21] were used as an energy donor (D) and acceptor (A), respectively. The structural formulas are shown in Fig. 1.

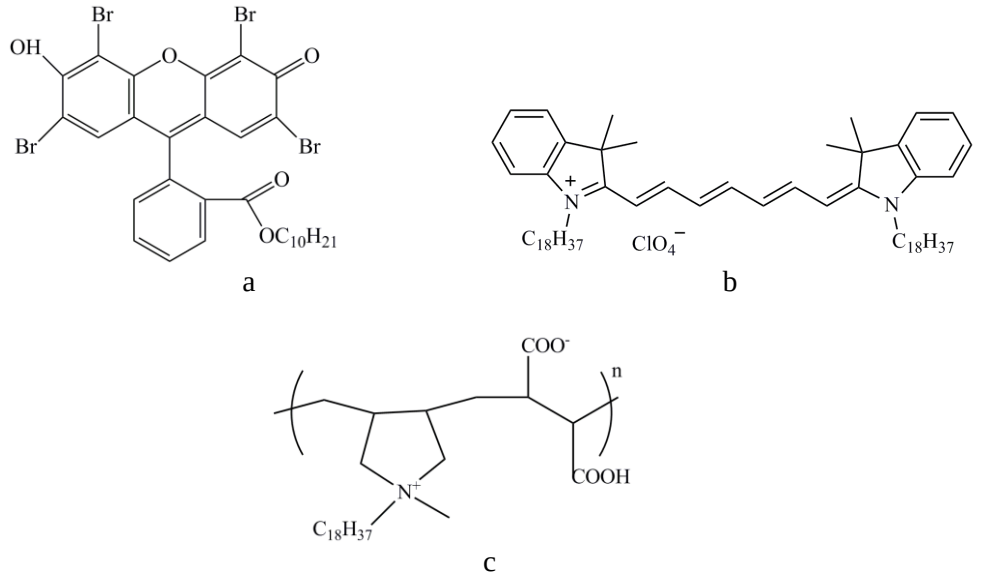

Figure 1. Structural formulas: a) RB; b) PD; c) PDOAM

Silver island films (SiFs) were prepared by magnetron sputtering, as described in [20]. After silver deposition, the films were annealed at a temperature of 240°C in a muffle furnace for 30 minutes. MIRA 3LMU scanning electron microscope (SEM, Tescan) was used for the studying of morphology and structure of the films. As shown by SEM (Fig. 2a), clusters of Ag particles with a radius of 40–50 nm are formed after annealing. The absorption spectrum of the SiF has a maximum at a wavelength of 435 nm (Fig. 2b).

Samples were prepared using the Langmuir-Blodgett (LB) method in a KSV Nima trough. In LB films, the distance between molecules can be changed up to their direct contact. The subphase was deionized water purified with AquaMax water purification system.

To prepare the samples, the dyes were dissolved in chloroform and mixed in the required ratios with the amphiphilic polymer poly (N,N-dialyl-N-octadecylamine-alt-maleic acid) (PDOAM) [21]. A mixed solution of amphiphilic polyampholyte and a dye makes it possible to obtain more stable and condensed films on the water surface. The relative concentration of dyes was 20 and 80 mol% for RB and PD, respectively. Transfer of monolayers to solid substrates was carried out according to the Z-type with the vertically method at a surface pressure of π=35 mN/m for RB, π=30 mN/m for PD. The π–A isotherm of PD is shown in Fig. 3. A pol-

ymer monolayer was deposited between the acceptor and donor monolayers (Fig. 2c). The polymer provides a distance between the donor and the acceptor of more than 2 nm. This makes it possible to eliminate the competing triplet-triplet energy transfer as an additional channel for energy transfer from the donor to the acceptor. Polymer monolayers were transferred to the substrate at a surface pressure of π=35 mN/m in a Z-type. It is known that a certain distance from the surface of plasmonic NPs is required to obtain the maximum effect [20, 22]. Therefore, in this work, several samples were prepared with different distances from the SiF surface (Fig. 2c). In one case, donor molecules were deposited directly onto the SiF surface; in the other case, three monolayers of PDOAM were deposited between SiF and donor molecules. In total, 3 RB monolayers and 1 PD monolayer were deposited in each film.

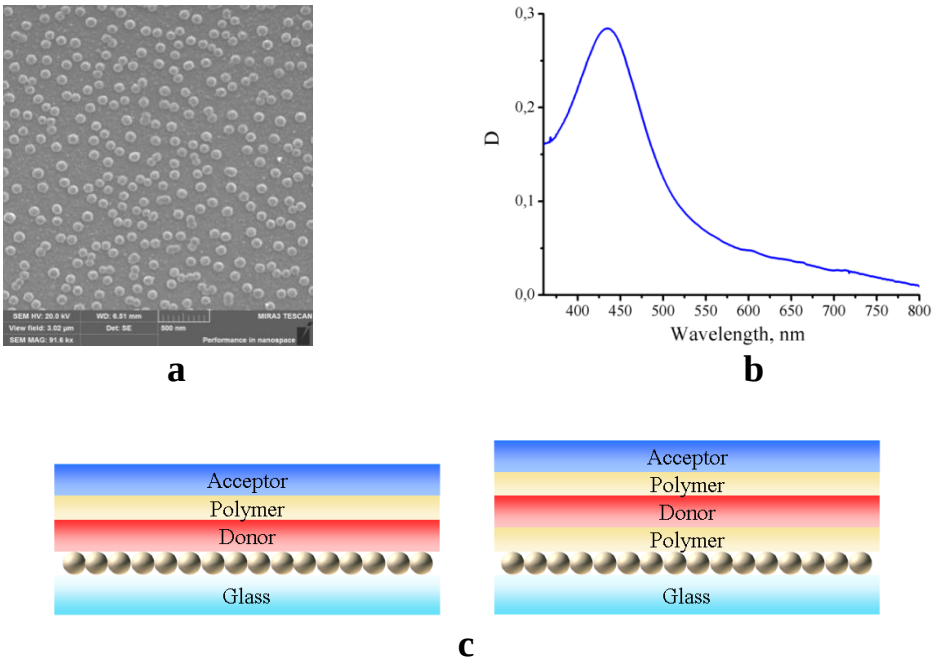

Figure 2. SEM image (a) and absorption spectrum (b) of SiF, and schemes of multilayer samples (c)

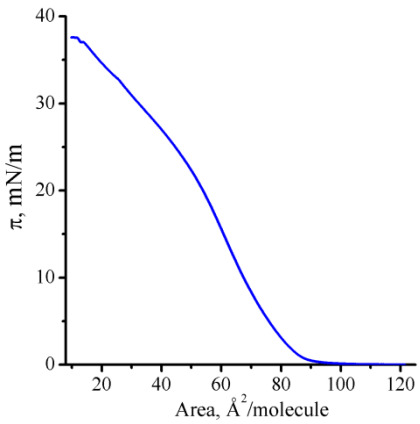

Figure 3. Surface pressure-area (π–A) compression isotherm of PD

The absorption spectra of the samples were measured using a Cary 300 spectrophotometer (Agilent Technologies). The emission spectra and lifetime were performed on a Cary Eclipse spectrometer (Agilent Technologies). Delayed fluorescence (DF) and phosphorescence measurements were carried out using a cryostat OptistatDN (Oxford Instruments). Phosphorescence mode: delay time = 0.1 ms; gate time = 0.5 ms. The DF and phosphorescence lifetimes were determined using the Cary Eclipse software using the following equation:

$$I(t) = I_0 \exp(-kt),$$

where, I_0, $I(t)$ — luminescence intensity at zero and arbitrary times, respectively; $k=1/\tau$ — is the rate constant of the luminescence decay calculated from the graph plotted in the coordinates $\ln(I_0/I)$ versus t.

The energy transfer efficiency (E_{ET}) was estimated according to equation [23-25]:

$$E_{ET} = 1 - \frac{\langle \tau_D \rangle}{\langle \tau_{0D} \rangle}$$

where $\langle \tau_D \rangle$, $\langle \tau_{0D} \rangle$– average fluorescence lifetime of RB in donor-acceptor and donor films, respectively.

The energy transfer rates in the presence of plasmonic NPs (k_{ET}^{pl}) and without them (k_{ET} $k_{ET\ E}$) were estimated according to the following formulas) [17, 23-24]:

$$E = \frac{k_{ET}}{\tau_{0D} + k_{ET}} \text{ and } E_{ET}^{pl} = \frac{k_{ET} + k_{ET}^{pl}}{\tau_{0D} + k_{ET} + + k_{ET}^{pl}},$$

where E_{ET}^{pl} is the energy transfer efficiency in the presence of plasmon NPs.

Results and Discussion

The normalized absorption and luminescence spectra of RB and PD in the LB films are shown in Fig. 4. When excited in the absorption bands of RB, the fluorescence spectrum of RB has a maximum at a wavelength of λ_{max}^{fl} =562 nm. The DF and phosphorescence spectra of RB at room temperature have a maximum approximately at 565 nm and 695 nm, respectively. The absorption spectrum maximum of PD is exhibits at 755 nm, and the fluorescence spectrum — at 785 nm. The absorption and fluorescence spectra have a universal shape characteristic of dyes of the polymethine series [26-27]. The overlap integral of the phosphorescence spectrum of RB and absorption of PD is equal to I =$2.87 \cdot 10^{-12}$ $M^{-1}cm^3$ [17].

The optical density of the dye LB film on glass at the absorption band maximum is about ~0.006 for RB and ~0.01 for PD. It is difficult to estimate the optical density of LB films on the SiF surface due to the effects of light scattering by Ag islands.

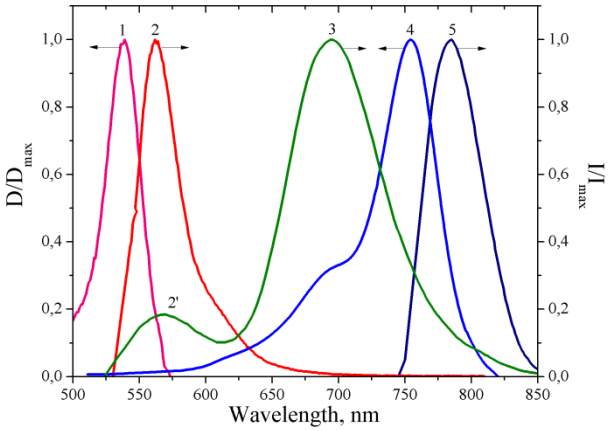

Figure 4. Normalized absorption (1, 4) and fluorescence (2, 5) spectra of RB (1, 2), PD (4, 5) films and delayed fluorescence (2') and phosphorescence (3) spectrum of RB

The fluorescence spectra of the LB films of the donor and the donor-acceptor pair on a glass substrate and on the SiF with a polymer are shown in Figure 5. The fluorescence intensity of the donor increased in 1.8 times directly on the SiF, and in 2.8 times on the SiF coated with three polymer monolayers compared with the control sample on the glass. In the presence of an acceptor, the intensity of the donor decreased, and a sensitized fluorescence of the acceptor appeared in the range of 700–800 nm. When the acceptor is excited with a wavelength of λ_{exc}=530 nm in the absence of donor molecules, no radiation is detected. These data indicate that energy transfer proceeds from excited singlet RB molecules to unexcited acceptor molecules.

The influence of the SiF on the singlet–singlet energy transfer by the inductive–resonant mechanism was considered in previous works [17, 18, 25].

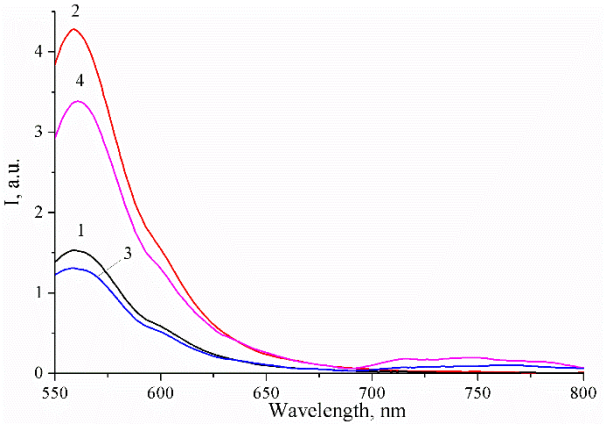

Figure 5. Fluorescence spectra of donor films (1, 2) and donor-acceptor films (3, 4) at λ_{exc}=530 nm on glass (1, 3), SiFs (2, 4) and SiFs coated with polymer monolayers (3)

The results of measurements of DF and phosphorescence of deoxygenated films of a donor and a donor-acceptor pair on glass and SiFs are shown in Figure 6a. When RB films on glass were photoexcited at λ_{exc}=532 nm, the maximum of the DF band of dye is recorded at approximately λ_{max}=565 nm, and the phosphorescence maximum at λ_{max}=695 nm. The lifetimes of phosphorescence and DF of RB are practically the same and equal to 0.3 ms.

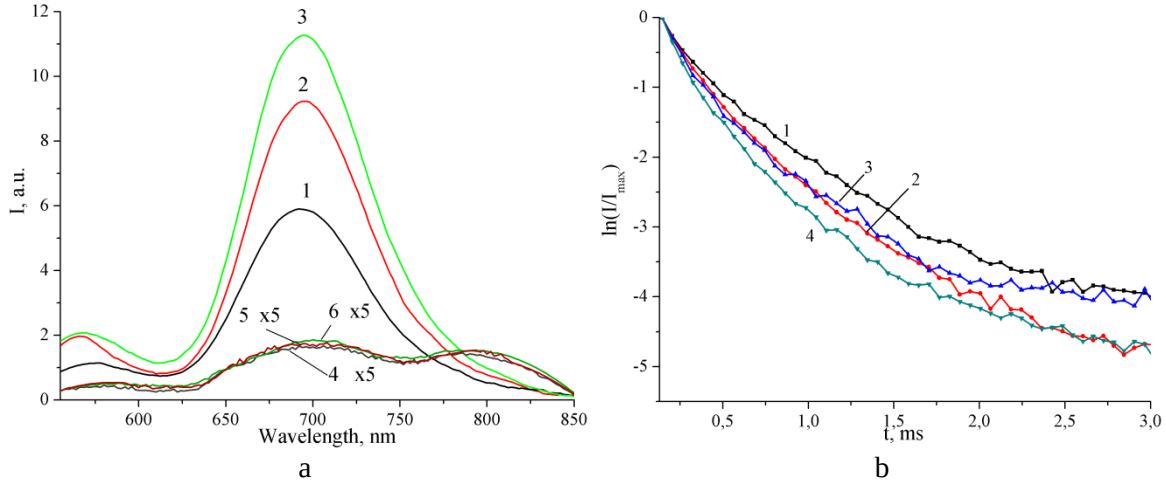

Figure 6. Spectra of DF and phosphorescence (a) and phosphorescence decay kinetics (b) of donor (1, 2, 3) and donor-acceptor films (4, 5, 6) at λ_{exc}=530 nm on glass (1, 4), on SiFs (2, 5) and SiFs coated with polymer monolayers (3, 6)

In the presence of an acceptor, quenching of the intensity of both DF and donor phosphorescence is observed, and the donor lifetime was decreased to 0.22 ms (Figure 6b). When a pure PD film was excited at λ_{exc}=532 nm, no radiation was registered. Because of the great overlapping of the sensitized luminescence of PD with the long-wavelength wing of the donor band, acceptor luminescence lifetimes, were recorded taking into account the donor phosphorescence contribution. The lifetime of acceptor in this case was equal to ~0.1 ms.

The observed quenching of the delayed luminescence RB and the sensitized luminescence of PD indicate the T–S energy transfer from triplet donor molecules to acceptor molecules in the ground electronic state.

In the presence of silver NPs, the intensity of DF and phosphorescence was increased almost 1.6 times directly on the SiFs and 1.9 times on the SiFs coated with three polymer monolayers. In this case, the duration of the luminescence is slightly reduced. In the presence of an acceptor, a similar spectrum is observed on SiFs, as on glass (Table 1).

Table 1

Intensity of DF and phosphorescence of donor (D), sensitized luminescence of acceptor, phosphorescence lifetime of donor τ_D^{Ph} (λ_{reg}=695 nm), T–S energy transfer rate in the presence (k_{ET}^{pl}) and without SiF (k_{ET}) in donor-acceptor (DA) films, λ_{ecx}=530 nm

Samples	I_D^{DF} , r.u.	I_D^{Ph} , r.u.	I_A^{Fl} , r.u.	τ_D^{Ph}, ms	s^{-1} or $k_{ET\ E}^{TS\ pl}$ k_{ET}^{pl} s^{-1}	$\frac{k_{ET}^{pl}}{k_{ET}}$
On glass substrates						
D	1.2	5.9	–	0.295	–	–
DA	0.1	0.34	0.3	0.220	$1.13 \cdot 10^3$	–
On SIF						
D	1.9	9.2	–	0.230	–	–
DA	0.1	0.35	0.3	0.165	$1.32 \cdot 10^3$	1.17
On SIF with polymer						
D	2.1	11.2	–	0.240	–	–
DA	0.1	0.35	0.3	0.178	$1.2 \cdot 10^3$	1.06

In the presence of Ag NPs, an increase in the rate of spin-forbidden energy transfer is observed. For a sample in which donor molecules were located directly on the SiF, the rate of T–S energy transfer increases by almost 1.2 times. Even though at 6–8 nm from the SiF, the maximum intensity of the donor radiation was observed, the rate of T–S energy transfer from the energy donor to the acceptor is lower. This can be explained by the fact that molecules located far from the SiF are less affected by the plasmon field.

Conclusions

The effect of plasmonic silver NPs on the T–S energy transfer in a donor–acceptor pair in planar nanostructures has been studied. Ag island films exhibit a threefold increase in the fluorescence intensity and a twofold increase in the phosphorescence intensity of the energy donor. An increase in the T–S energy transfer efficiency was registered recorded in the plasmon field of Ag NPs. In this case, the maximum growth in the rate of T-S energy transfer was observed for a sample deposited directly on the SiF surface.

Acknowledgements

This research is funded by the Science Committee of the Ministry of Science and Higher Education of the Republic of Kazakhstan (Grant No. AP14870117).

References

1 Jin, X.-H., Price, M.B., Finnegan, J.R., Boott, C.E., Richter, J.M., & et al. (2018). Long-range exciton transport in conjugated polymer nanobers prepared by seeded growth. *Science. 360*, 897−900. doi:10.1126/science.aar8104.

2 Currie, M.J., Mapel, J.K., Heidel, T.D., Goffri, S., & Baldo, M.A. (2008). High-Efficiency Organic Solar Concentrators for Photovoltaics. *Science*. *321*(5886), 226–228. doi:10.1126/science.1158342.

3 Baldo, M.A., Thompson, M.E., & Forrest, S.R. (2000). High-efficiency fluorescent organic light-emitting devices using a phosphorescent sensitizer. *Nature*. *403*(6771), 750–753. doi:10.1038/35001541.

4 Reineke, S., Thomschke, M., Lüssem, B., & Leo, K. (2013). White organic light-emitting diodes: Status and perspective. *Reviews of Modern Physics*. *85*(3), 1245–1293. doi:10.1103/revmodphys.85.1245.

5 Ishchenko, A. (2002). Molecular engineering of dye-doped polymers for optoelectronics. *Polymers for Advanced Technologies*, *13*(10-12), 744–752. doi:10.1002/pat.269.

6 Cao, W., & Xue, J. (2014). Recent progress in organic photovoltaics: device architecture and optical design. *Energy & Environmental Science*. *7*(7), 2123. doi:10.1039/c4ee00260a.

7 Bulavko, G.V., & Ishchenko, A.A. (2014). Organic bulk heterojunction photovoltaic structures: design, morphology and properties. *Russian Chemical Reviews*, *83*(7), 575–599. doi:10.1070/rc2014v083n07abeh00441.

8 Förster, T. (1949). Experimentelle und theoretische Untersuchung des zwischenmolekularen Übergangs von Elektronenanregungsenergie. *Zeitschrift für Naturforschung*. *4*, 321−327.

9 Ermolaev, V.L. & Sveshnikova, E.B. (1963). Inductive resonance energy transfer from aromatic molecules in the triplet state. *Russian Academy of Sciences*. 1295–1298.

10 Bennett, R.G., Schwenker, R.P., & Kellogg, R.E. (1964). Radiationless Intermolecular Energy Transfer. II. Triplet→Singlet Transfer. *The Journal of Chemical Physics*. *41*(10), 3040–3041. doi:10.1063/1.1725671.

11 D'Andrade, B.W., Baldo, M.A., Adachi, C., Brooks, J., Thompson, M.E., & Forrest, S.R. (2001). High-efficiency yellow double-doped organic light-emitting devices based on phosphor-sensitized fluorescence. *Applied Physics Letters*. *79*(7), 1045–1047. doi:10.1063/1.1388159.

12 De Sousa, L.E., dos Santos Born, L., de Oliveira Neto, P.H., & de Silva, P. (2022) Triplet-to-Singlet Exciton Transfer in Hyperfluorescent OLED Materials. *Journal of Materials Chemistry C. 10*(12), 4914–4922. https://doi.org/10.1039/D1TC05596H.

13 Cravcenco, A., Hertzog, M., Ye, C., Iqbal, M.N., Mueller, U., Eriksson, L., & Börjesson, K. (2019). Multiplicity conversion based on intramolecular triplet-to-singlet energy transfer. *Science Advances*. *5*(9), eaaw5978. doi:10.1126/sciadv.aaw5978.

14 Yanai, N., & Kimizuka, N. (2017). New triplet sensitization routes for photon upconversion: thermally activated delayed fluorescence molecules, inorganic nanocrystals, and singlet-to-triplet absorption. *Accounts of Chemical Research*. *50*(10), 2487–2495. doi:10.1021/acs.accounts.7b00235.

15 Kirch, A., Gmelch, M., & Reineke, S. (2019). Simultaneous singlet-singlet and triplet-singlet förster resonance energy transfer from a single donor material. *The Journal of Physical Chemistry Letters*. *10*, 310–315. doi:10.1021/acs.jpclett.8b03668.

16 Kislov, D.A., & Kucherenko, M.G. (2014). Nonradiative triplet-singlet transfer of electronic excitation energy between dye molecules in the vicinity of the silver-film surface. *Optics and Spectroscopy*. *117*, 784–791. doi:10.1134/S0030400X14090112.

17 Ibrayev, N., Seliverstova, E., Temirbayeva, D., & Ishchenko, A. (2022). Plasmon effect on simultaneous singlet-singlet and triplet-singlet energy transfer. *Journal of Luminescence*. *251*, 119203. doi:10.1016/j.jlumin.2022.119203.

18 Ibrayev, N., Seliverstova, E., Zhumabay, N., & Temirbayeva, D. (2019). Plasmon effect in the donor-acceptor pairs of dyes with various efficiency of FRET. *Journal of Luminescence*. *214*, 116594. doi:10.1016/j.jlumin.2019.116594.

19 Cui, Q., He, F., Li, L., & Möhwald, H. (2014). Controllable metal-enhanced fluorescence in organized films and colloidal system. *Advances in Colloid and Interface Science*. *207*, 164–177. doi:10.1016/j.cis.2013.10.011.

20 Temirbayeva, D., Ibrayev, N., & Kucherenko, M. (2022). Distance dependence of plasmon-enhanced fluorescence and delayed luminescence of molecular planar nanostructures. *Journal of Luminescence*. *243*, 118642. doi:10.1016/j.jlumin.2021.118642.

21 Yeroshina, S.A., Ibrayev, N.K., Kudaibergenov, S.E., Rullens, F., Devillers, M., & Laschewsky, A. (2008). Spectroscopic properties of mixed Langmuir–Blodgett films of rhodamine dyes and poly (N,N-diallyl-N-octadecylamine-alt-maleic acid). *Thin Solid Films*. *516*(8), 2109–2114. doi:10.1016/j.tsf.2007.05.056.

22 Ray, K., Badugu, R., & Lakowicz, J.R. (2007). Sulforhodamine adsorbed Langmuir−Blodgett layers on silver island films: effect of probe distance on the metal-enhanced fluorescence. *The Journal of Physical Chemistry C. 111*, 7091–7097. doi:10.1021/jp067635q.

23 Lakowicz, J.R. (2011). *Principles of Fluorescence Spectroscopy.* Springer.

24 Szmacinski, H., Ray, K., & Lakowicz, J.R. (2009). Effect of plasmonic nanostructures and nanofilms on fluorescence resonance energy transfer. *Journal of Biophotonics*. *2*(4), 243–252. doi:10.1002/jbio.200910003.

25 Seliverstova, E.V., Temirbayeva, D.A., Ibrayev, N.K., & Ishchenko, A.A. (2019). Plasmon effect of Ag nanoparticles on Förster resonance energy transfer in a series of cationic polymethine dyes. *Theoretical and Experimental Chemistry. 55*, 115–124. doi:10.1007/s11237-019-09602-9.

26 Temirbaeva D., Seliverstova E., Ibrayev N.Kh., Ishchenko A. (2016). Experimental study and calculations of spectral-luminescence properties of cyanine dye. *Bulletin of the University of Karaganda-Physics, 3*(83), 52–59.

27 Ibrayev N.Kh., Seliverstova E.V., Zhumabay N.D., Omarova G.S., Ishchenko A.A. (2018). Effect of plasmon resonance of metal nanoparticles on spectral-luminescent properties of polymethine dye. *Bulletin of the University of Karaganda-Physics. 3*(91), 37–41.

Д. Темирбаева, Н. Ибраев, Е. Селиверстова, М. Кудинова, А. Ищенко

Боялған Ленгмюр-Блоджетт қабыршақтарындағы триплет-синглеттік энергия тасымалдауына плазмон әсері

Мақалада органикалық бояғыштардың донор-акцептор жұбындағы триплет-синглеттік энергия тасымалдауына плазмондық күміс нанобөлшектерінің әсері зерттелген. Ленгмюр-Блоджетт технологиясын қолдана отырып, шыны төсемелері мен күміс аралдық қабыршақтарына бетіне қабатты боғыш қабыршақтары дайындалды. Энергия доноры және акцепторы ретінде бенгалдың қызғылт және полиметиндік бояғыштарының амфифильді аналогтары пайдаланылды. Бәсекелес триплет-триплеттік энергияның тасымалдауын болдырмау үшін донорлық және акцепторлық молекулалардың моноқабаттары арасында полимер моноқабаты орналастырылды. Донор-акцепторлық қабыршақтардың баяуланған флуоресценция және фосфоресценция спектрлері және осы қабыршақтардағы донордың ұзақ мерзімді люминесценциясының өмір сүру ұзақтығы өлшенді. Күміс қабыршақтарында донордың флуоресценциясының қарқындылығы үш есе және фосфоресценция қарқындылығы екі есе артуы байқалатыны көрсетілген. Триплет-синглет энергия тасымалдануы донор сәулеленуінің өшуімен де, донорлық триплеттердің өмір сүру ұзақтығына жақын сенсибилизацияланған акцептордың баяуланған флуоресценцияның пайда болуымен де дәлелденеді. Күміс нанобөлшектері болған жағдайда энергия донор қарқындылығын арттыруынан басқа, триплет-синглеттік электрондық энергия тасымалдау эффективтілігінің жоғарылауы байқалады. Алынған нәтижелерді әртүрлі оптикалық құрылғыларда қолдануға болады.

Кілт сөздер: бенгалдың қызғылты, полиметиндік бояғыш, күміс аралдық қабыршағы, плазмон, баяуланған флуоресценция, фосфоресценция, триплет-синлеттік энергия тасымалдау, Ленгмюр-Блоджетт қабыршақтары.

Д. Темирбаева, Н. Ибраев, Е. Селиверстова, М. Кудинова, А. Ищенко

Влияние плазмонного эффекта на триплет-синглетный перенос энергии в окрашенных пленках Ленгмюра–Блоджетт

Исследовано влияние плазмонных наночастиц серебра на триплет-синглетный перенос энергии в донорно-акцепторной паре органических красителей. По технологии Ленгмюра-Блоджетт были приготовлены слоистые пленки красителей на поверхности стекла и островковых пленок серебра. В качестве донора и акцептора энергии были использованы амфифильные аналоги бенгальского розового и полиметинового красителя. Между монослоями молекул донора и акцептора был нанесен монослой полимера для исключения конкурирующего триплет-триплетного переноса энергии. Измерены спектры замедленной флуоресценции, фосфоресценции донорно-акцепторных пленок и время жизни длительной люминесценции донора в этих пленках. Показано, что на островковых пленках серебра наблюдается трехкратное увеличение интенсивности флуоресценции и двухкратное увеличение интенсивности фосфоресценции донора. Об успешном триплет-синглетном переносе энергии свидетельствует как тушение донорных центров, так и появление сенсибилизованной замедленной флуоресценции акцептора с длительностью, близкой ко времени жизни триплетов донора. В присутствии наночастиц серебра, помимо усиления интенсивности излучения донора, наблюдается рост эффективности триплет-синглетного переноса электронной энергии. Полученные результаты могут быть использованы в различных оптических устройствах.

Ключевые слова: бенгальский розовый, полиметиновый краситель, островковая пленка серебра, плазмон, замедленная флуоресценция, фосфоресценция, триплет-синглетный перенос энергии, пленки Ленгмюра-Блоджетт.

DOI 10.31489/2022PH4/14-21

UDC 541.145

T.M. Serikov, P.A. Zhanbirbayeva, A.S. Baltabekov, A.B. Kuanyshbekova

Karaganda University of the name of academician E.A. Buketov, Kazakhstan
*(*e-mail: serikov-timur@mail.ru)*

Photocatalytic activity of the TIO_2/Ag/rGO nanocomposite

The paper presents the results of a study of the photocatalytic activity of films formed by titanium dioxide nanorods doped with silver nanoparticles and reduced graphene oxide. The obtained nanocomposite materials were studied by optical spectroscopy, scanning electron microscopy, X-ray diffractometry, and Raman spectroscopy. The photocatalytic activity of the samples was evaluated by generating a photocurrent when the surface was illuminated by a modulated light source of a xenon lamp. In addition, the photocatalytic activity of the samples was evaluated by the degradation of the methylene blue dye, which is a model. It was found that the introduction of silver nanoparticles and reduced graphene oxide into the pores of films made of titanium dioxide nanorods leads to an increase in the spectral sensitivity of the sample in the region of 400-500 nm. The increased sensitivity of the sample to visible light leads to an increase in photocurrent generation and is 2.3 times higher than that of the original sample. Degradation of the methylene blue dye after 100 minutes of irradiation in the presence of a TiO_2/Ag/rGO sample was 19 %. This is 3 times higher than in TiO_2 nanorods films and 2.3 times higher than TiO_2/Ag films. The results of the conducted studies have shown that the improvement of photocatalytic activity is associated with a decrease in film resistance, an expansion of spectral sensitivity and an increase in the surface area of the nanorods.

Keywords: titanium dioxide nanorods, silver nanoparticles, reduced graphene oxide, photocatalysis

Introduction

Recently, semiconductors based on metal oxides with high photosensitivity and excellent physicochemical properties have attracted wide attention due to their widespread use for environmental restoration and solar energy conversion [1-3]. As one of the promising semiconductors, TiO_2 nanostructures have been extensively investigated for photocatalysis and photocatalytic splitting of water, due to availability, low cost and good stability [4]. The most commonly used structures in photocatalysis are titanium dioxide nanoparticles, but they have a significant disadvantage associated with the implementation of 3–dimensional electron transport. In addition, when films are made from nanoparticles, unformed contacts between them affect the possibility of electron transfer from one nanoparticle to another [5]. One-dimensional nanostructures, such as titanium dioxide nanorods, may have a number of advantages over nanoparticles. For example, in nanorods, electron transport is carried out in one direction — along the walls. This can lead to a decrease in the electron travel time from the charge generation centers to the current-removing electrodes [6]. Despite the advantages of TiO_2 (TNR) nanorods over nanoparticles, the wide band gap (~ 3.0–3.2 eV) and the rapid recombination of photogenerated electron-hole pairs in TiO_2 still limit its widespread use in photocatalysis. Increasing the sensitivity of TiO_2 in the visible region of the spectrum and reducing the recombination rate can be achieved by adding nanoparticles of noble metals, such as silver and carbon nanostructures, such as graphene. It has been reported that alloying with noble metals is an effective way to improve the optical and photoelectrochemical properties of the TiO_2 photocatalyst.

LF of noble metals with surface plasmon resonance (SPR) not only contributes to the generation of electron-hole pairs by electromagnetic fields, but also increase light scattering in order to capture most of the light for bonded semiconductors [7-10]. Numerous successful systems have been created using TiO_2 in combination with various noble metals, and represent great potential for electrochemistry and photocatalysis.

Graphene with a two-dimensional planar structure has many advantages, such as high electron mobility, ease of solution synthesis, unique optical, thermal and mechanical properties, with a wide range of applications from photocatalysis, electrochemical detection, transparent electrodes to lithium-ion batteries. Graphene in its pure form is rarely used in photocatalysis, as it is hydrophobic. Therefore, it is more convenient to use graphene oxides, for example, reduced graphene oxide (rGO), since it forms stable dispersions in water. It is noteworthy that nanocomposite photocatalysts based on reduced graphene oxide (rGO) can quickly transfer electrons and prolong the lifetime of charge carriers, which leads to an increase in quantum efficiency. Graphene or its derivatives can also significantly improve the adsorption capacity of the target molecule

due to its large specific surface area. In addition, due to the adjustable band gap and high transparency, the light intensity practically does not change before it reaches the surface of the catalyst.

Thus, the creation of a triple hybrid system combining noble metal, TiO_2 and nanolists (rGO) to improve the photocatalytic characteristics of the photocatalyst and the study of their mechanisms of action is a very urgent task.

The aim of this work is to synthesize and study the photocatalytic activity of a nanocomposite material, which consists of a film of titanium dioxide nanorods doped with silver nanoparticles and reduced graphene oxide deposited on their surface.

Experimental

Films formed by TiO_2 nanorods were obtained on FTO substrates (7 ohms/cm^2, Sigma–Aldrich) by hydrothermal synthesis in a sealed autoclave with a volume of 50 with a solution content containing 15 ml of deionized water (H_2O), 15 ml of hydrochloric acid (HCl) (36.5–38.0 %, Sigma–Aldrich) and 0.25 ml of titanium butylate $C_{16}H_{36}O_4Ti$ (titanium butoxide, 97 %, Sigma–Aldrich) at a temperature of 180^{0}C and a synthesis duration of 18 hours. Then the samples were calcined at a temperature of 500 ^{0}C for 2 hours. Silver nanoparticles were recovered on the surface of TiO_2 nanorods in a solution containing 0.2 g of polyvinylpyrrolidone (PVP, molecular weight 40,000), 40 ml of deionized water and ethylene glycol, with the addition of 2 mmol $NaBH_4$. Then the film from the nanorods was immersed to the bottom of the vessel with the rods up and kept in an oven at a temperature of 70 °C for 1 hour, removed and dried at room temperature. rGO (99 %, Cheaptubes) was deposited on the surface of a film made of titanium dioxide nanorods containing silver nanoparticles from a phosphate solution (0.5 g/l) by electrochemical method using a standard three-electrode system. After 5 minutes of deposition, the films were removed and washed several times with deionized water. The deposition time is optimal, at which the maximum photocatalytic activity of the samples is observed [11, 12].

The phase composition of the samples was studied by X-ray diffraction using an automatic powder diffractometer STOE STADI-P (STOE & Cie GmbH) in the angle range 2 ° 5-80°. X-ray images were analyzed using the PDF-2 powder database, as well as the standard WinXPow software package. The morphology of the surface was studied using a MIRA 3LMU scanning electron microscope (Tescan, Czech Republic). The optical density of all samples was recorded on a CM 2203 spectrofluorimeter (Solar, Belarus). Raman spectra were studied using a Confotec MR520 microscope (Sol Instruments), laser wavelength λ=532 nm. The photocatalytic activity of the samples was evaluated by measuring the magnitude of the photoinduced current with an illuminated area of 1 cm^2 in a standard three-electrode cell using a CS350 potentiostat/galvanostat with a built-in EIS analyzer (Corrtest Instruments, China) in an electrolyte of 0.1 M NaOH. In addition, the photoactivity of the films was evaluated by photodegradation of the methylene blue (MV) dye. A xenon lamp with a power of 300 W/cm^2 (Newport, USA) served as a laboratory light source. The surface area of the samples was estimated by the number of adsorbed dye molecules as follows: an aqueous solution of methylene blue dye with a concentration of 10 — ^{6} mol/l was poured into three containers with a volume of 25 ml. Then, the films were lowered into the solutions for 20 hours. At the same time, the optical density of the dye was determined every 1 hour and the concentration of adsorbed molecules was calculated by the formula

$$C = \frac{N_A C' V}{S}\left(1 - D_1 / D_2\right)$$

where N_A is the Avogadro constant, C′ is the concentration of dye molecules in the solution, V is the volume of the solution, S is the area of the adsorbent, D1 and D2 are the optical densities of the solution before and after sorption. The active surface of the films was calculated from the calculation of the area of one molecule of methylene blue 130 Å2.

Results and Discussion

Figure 1 shows SEM images of TiO_2 nanorods (a), TiO_2 nanorods with the addition of silver nanoparticles (b) and deposited sheets of reduced graphene oxide (c).

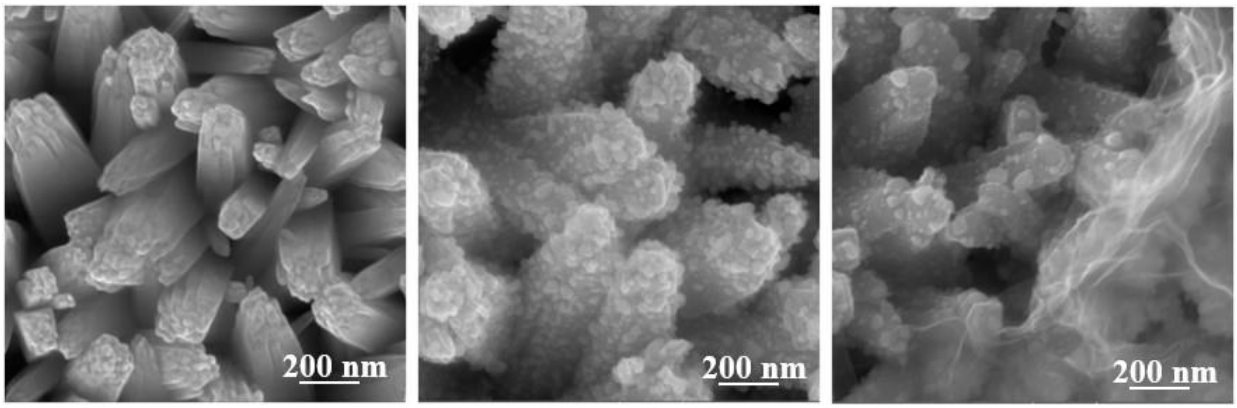

a) b) c)

Figure 1. SEM images TNR (a), TNR/Ag (b), TNR/Ag/rGO (c)

Figure 1a shows that TNRS is formed on the surface of the FTO substrate as a result of hydrothermal synthesis. As a result of image processing, it was found that the diameter of the nanorods varies from 100 to 180 nm. TiO_2 nanorods are mainly located perpendicular to the substrate surface and have a length of about 4.1 microns. As a result of the chemical reduction of silver nitrate, silver nanoparticles are formed on the surface of the nanorods. The diameter of silver nanoparticles varies from 20 to 40 nm. In addition, the sizes of silver nanoparticles were confirmed by the method of dynamic light scattering on Zeta Seizer (Malvern) (Figure 2b). Electrochemical deposition of rGO on the surface of TNT/Ag films leads to the formation of rGO sheets on its surface. Figure 1c shows that graphene oxide sheets partially envelop the surface of the rods.

Figure 2a shows the spectrum of maps of the presence of chemical elements in the TNR/Ag/rGO sample.

a)

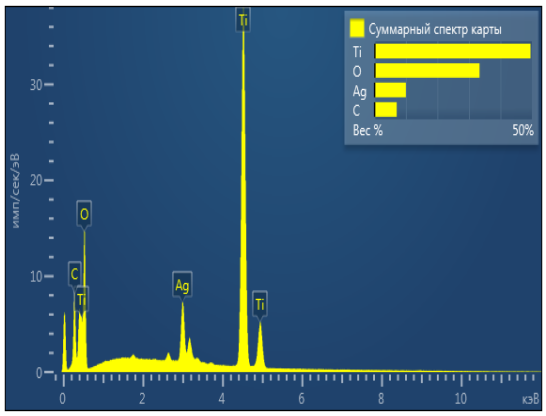

b)

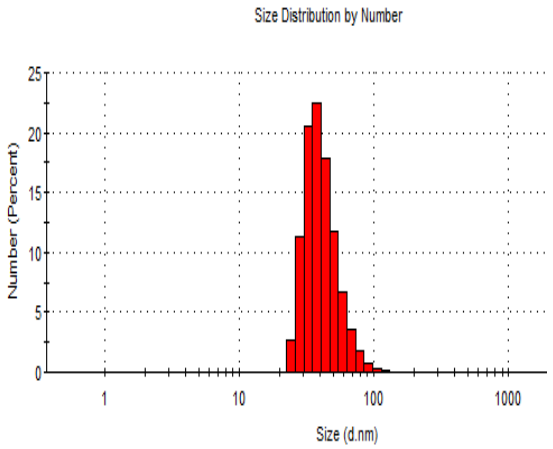

Figure 2. EDX analysis of TNR/Ag/rGO (a) and size distribution of silver nanoparticles determined on Zeta Seizer

According to the results of studies of the elemental composition of the TNR/Ag/rGO sample, it was shown that 4 elements were identified in the samples, such as Ti, O, Ag and C. The elements Ti and O belong to titanium dioxide, which form the basis of the film, therefore its percentage ratio is significantly greater than the rest and amounts to 50 and 32 % respectively. The presence of Ag (10 %) and C (8 %) is a confirmation of the formation of silver and nanoparticles on the surface of the semiconductor film.

Figure 3 shows the mapping of chemical elements on the TNR/Ag/rGO surface.

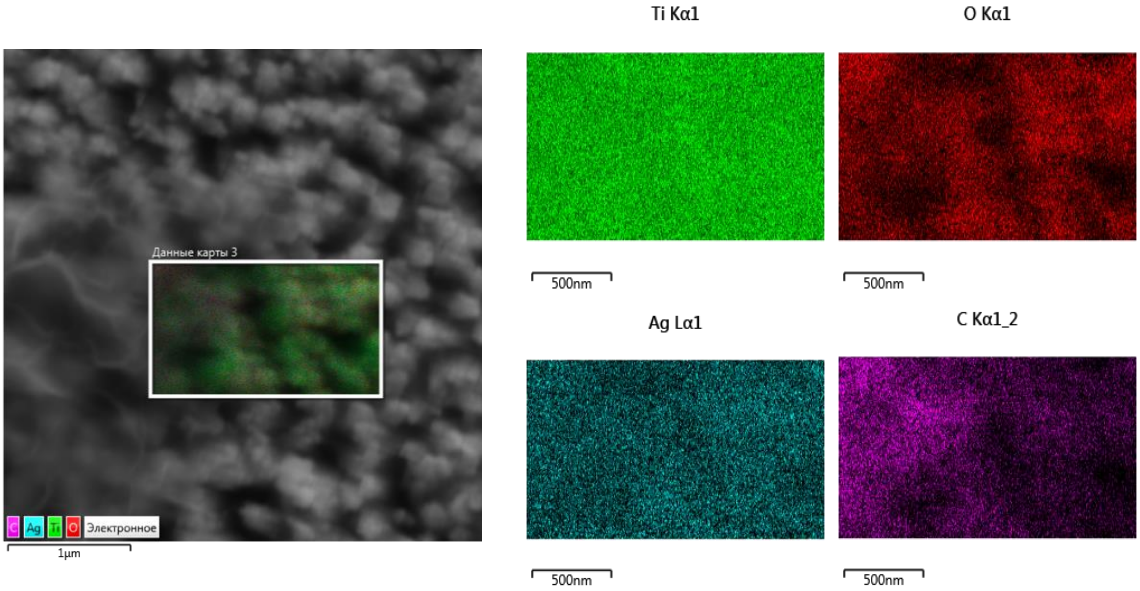

Figure 3. Mapping of chemical elements on the TNR/Ag/rGO surface

It can be seen from the presented data that Ag is evenly distributed over the entire surface and excludes aggregation of nanoparticles.

Figure 4 shows the X-ray diffraction of the studied samples. It was found that the films formed by TNR belong to the tetragonal modification of rutile (JCPDS, No. 21-1276), which is characterized by reflexes in the 27.4°, 36.1°, 41.3°, 54.4°, 62.9° and 69.9°. When silver nanoparticles are deposited, four additional peaks appear on the X-ray at 38.11°, 44.27°, 64.42° and 77.47° corresponding to the lattice planes (111), (200), (220) and (311) (JCPDS No. 07-0783). There was no registration of peaks corresponding to graphene in our experiments, due to the low detection limit.

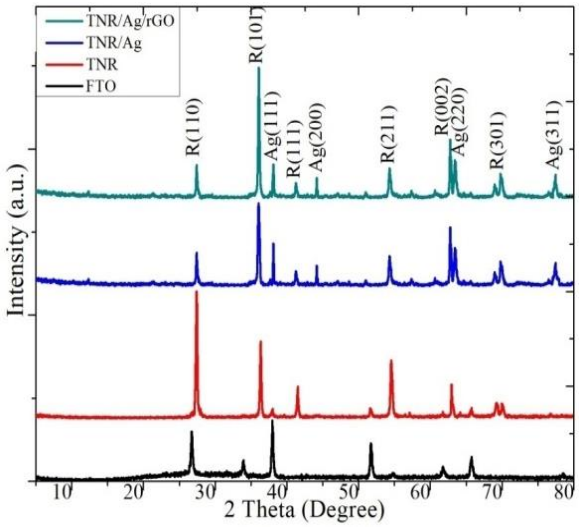

Figure 4. X-ray diffraction patterns of TNR, TNR/Ag, and TNR/Ag/rGO samples

Figure 5 shows the Raman spectra of TR, TNR/Ag and TNR/Ag/rGO. For TNR, intense three combinationally active optical phonon modes 144, 445 and 610 cm-1 are observed, which belong to the B1g, Eg, A1g modes.

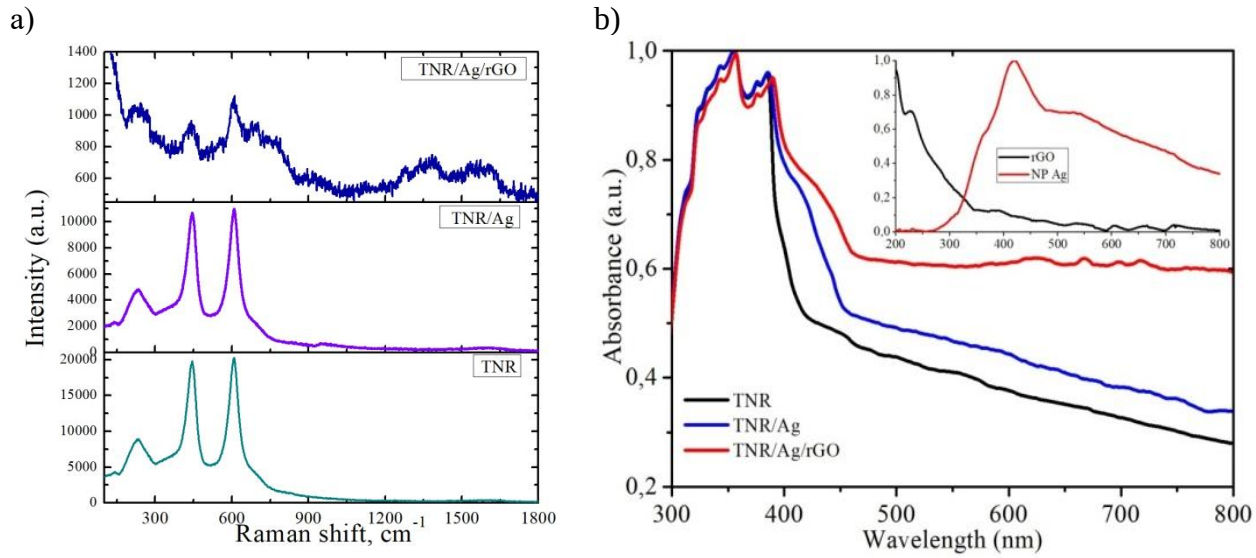

Figure 5. Raman spectra (a) and absorption spectra (b) of TR, TNR/Ag and TNR/Ag/rGO samples

The addition of silver nanoparticles to the structure of titanium dioxide nanorods does not lead to the appearance of new bands, since metals are not combinationally active. However, we observed a 2-fold decrease in the intensity of the bands compared to the original sample, which may be due to the partial blocking of the surface of the nanorods by silver nanoparticles, preventing excitation by laser radiation. With the deposition of rGO, the peaks of raman scattering from the nanorods noticeably decreased, while peaks of raman scattering of light from rGO appear in the region of 1350, 1590 cm^{-1}, which characterize the degree of graphene defectiveness.

Figure 5b shows the normalized absorption spectra of nanostructured films. The absorption of TiO_2 nanorods is in the ultraviolet region, the edge of the spectrum is in the region of 380-400 nm. The introduction of Ag nanoparticles leads to a change in the absorption spectrum and is characterized by the presence of a small shoulder in the region of 420-430 nm. Obviously, this is due to the absorption capacity of Ag nanoparticles in this area. It can be seen from the insertion of Figure 4b that the maximum absorption spectrum of Ag nanoparticles is in the region of 410-430 nm. The TNR/Ag/go nanocomposite material allows to absorb much more light in the visible region of the spectrum compared to pure titanium dioxide and with doped Ag nanoparticles. The edge of the absorption band of the nanocomposite is shifted relative to the TiO2 band, which indicates a decrease in the band gap of the composite material.

Figure 6a shows the dependence of the density of the generated current when the surface is illuminated by a light source and when it is turned off. The samples demonstrate excellent stability over the time period presented. When the surface is illuminated, the current density instantly reaches its maximum. From the data obtained, it can be seen that sensitization of the surface of the nanorods by Ag and rGO nanoparticles leads to an increase in photocurrent, as for TNR. Thus, for TNR/Ag/rGO, the photocurrent density is 2.3 and 1.3 times higher than TN and TNR/Ag, respectively.

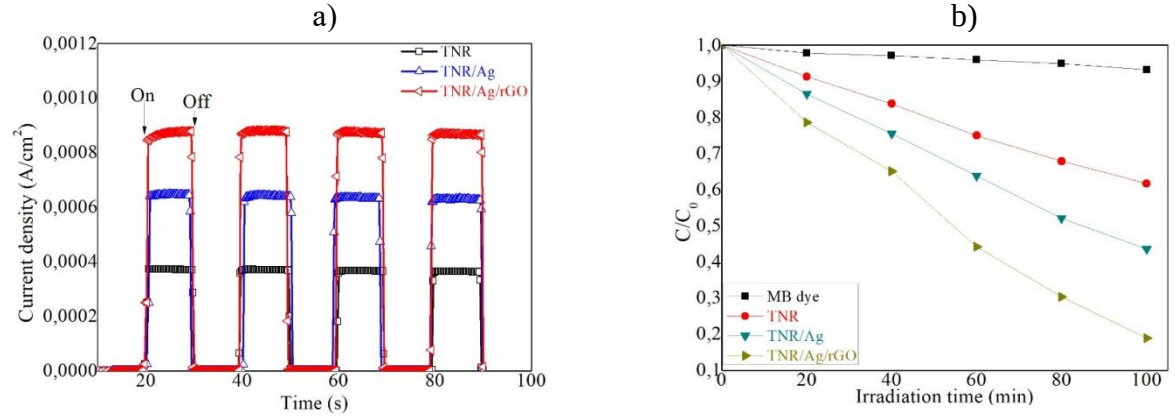

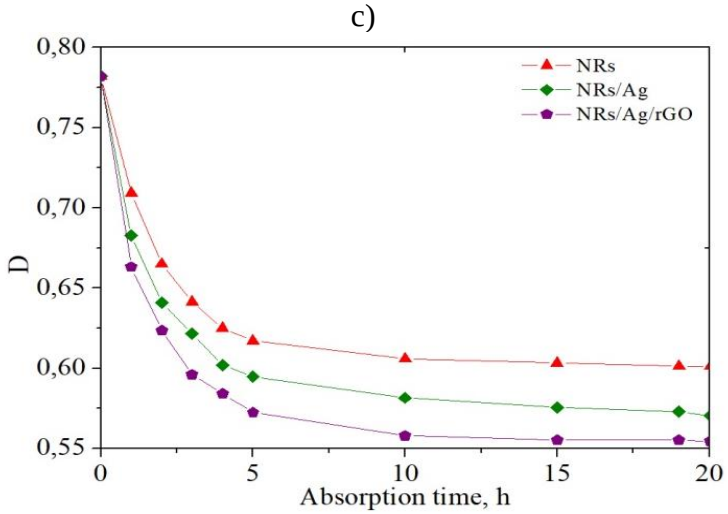

Figure 6. Photocurrent density (a), degradation of the dye MV (b) and the dependence of the optical density of the dye on the sorption time (c) for TNR, TNR/Ag and TNR/Ag/rGO

The photocatalytic activity of the samples was studied by observing the discoloration of the heterocyclic dye MV under the action of UV radiation. The photodegradation curves of MG are shown in Figure 6b, where C0 is the initial concentration, and C is the dye concentration at the time of measurement. MV itself shows almost no self-decomposition during prolonged irradiation. In contrast, MB demonstrates a clearly positive degradation process in the presence of TR, TNR/Ag and TNR/Ag/rGO nanocomposite. The degradation of MV after 100 min of irradiation in the presence of a TNR/Ag/rGO sample was 19 %, which is 3 times higher than in TNR and 2.3 times higher than TNR/Ag. It is obvious that the nanocomposite TNR/Ag/rGO exhibits a significant increase in photocatalytic activity than individually. Next, the active surface area of the samples was estimated. To do this, the samples were kept in a container with a dye with a known concentration for 20 hours. At the same time, the optical density of the dye was measured at certain intervals (Figure 6c). It can be seen from the figure that after 5 hours of sorption, the change in the optical density of the dye is insignificant, which indicates their saturation. Thus, it was found that 36.18*1014 were sorbed in TNR films, and 44.66*1014 and 49.37*1014 molecule/cm^2 respectively were sorbed in TNR/Ag and TNR/Ag/rGO. If we take into account, that the area occupied by 1 MV dye molecule is 130 A2, then the active surface area for TNR will be 4.7*1017 A2, for TNR/Ag 5.8*1017 A2 and for TNR/Ag/rGO 6.4*1017 A2. The results obtained indicate that the addition of Ag and rGO nanoparticles leads to an increase in the active surface area of the nanorods.

Conclusion

Thus, the influence of Ag nanoparticles and rGO impurities on the structural, optical, structural and photocatalytic properties of films formed by TiO_2 nanorods has been studied. The formation of Ag nanoparticles with a cubic structure and gan layers on the TNR surface is confirmed by the presence of reflexes on X-ray and sRaman spectra, respectively. Measurements of the optical characteristics of the synthesized material showed that the absorption spectrum of the TNR/Ag/rGO and TNR/Ag nanocomposite is shifted to the long-wavelength region relative to the absorption spectrum of TNR, possibly as a result of changes in the band gap of the semiconductor and the absorption capacity of Ag. The synthesized TNR/Ag/rGO nanocomposite showed a significant increase in photocatalytic activity with respect to the degradation of MV under the action of UV light and generation of photocurrent. In the presence of TNR/Ag/rGO film, MG degradation was 19 %, which is 3 times higher than in TNR and 2.3 times higher than TNR/Ag. The increase in photocatalytic activity is associated with an expansion of spectral sensitivity and an increase in the active surface area of the samples.

Acknowledgments

The work was carried out within the framework of the grant of the Committee of Science of the Ministry of Education and Science of the Republic of Kazakhstan AP08052675.

References

1 Zhang, L., Hu, J.S., Huang, X.H., Song, J., & Lu, S.Y. (2018). Particle-in-box nanostructured materials created via spatially confined pyrolysis as high performance bifunctional catalysts for electrochemical overall water splitting. *Nano Energy, 48,* 489-499.

2 Ito, S., Murakami, T.N., Comte, P., Liska, P., Grätzel, C., Nazeeruddin, M.K., & Grätzel, M. (2008). Fabrication of thin film dye sensitized solar cells with solar to electric power conversion efficiency over 10 %. *Thin Solid Films, 516,* 4613-4619.

3 Lee, J., Hong, K.S., Shin, K., & Jho, J.Y. (2012). Fabrication of dye-sensitized solar cells using ordered and vertically oriented TiO2 nanotube arrays with open and closed ends. *Journal of Industrial and Engineering Chemistry, 18,* 19-23.

4 Blanco-Vega, M.P., Guzmán-Mar, J.L., Villanueva-Rodríguez, M., Maya-Treviño, L., Garza-Tovar, L.L., Hernández-Ramírez, A., & Hinojosa-Reyes, L. (2017). Photocatalytic elimination of bisphenol A under visible light using Ni-doped TiO2 synthesized by microwave assisted sol-gel method. *Materials Science in Semiconductor Processing, 71,* 275-282.

5 Serikov, T.M., Ibrayev, N.Kh., Ivanova, T.M., & Savilov, S.V. (2021). Influence of the hydrothermal synthesis conditions on the photocatalytic activity of titanium dioxide nanorods. *Russian Journal of Applied Chemistry, 94*(4), 438-445.

6 Serikov, T.M., Ibrayev, N.Kh., Isaikina, O.Ya., & Savilov, S.V. (2021). Nanocrystalline TiO2 films: synthesis and low-temperature luminescent and photovoltaic properties. *Russian Journal of Inorganic Chemistry, 66*(1), 117-123.

7 Patil, S.S., Mali, M.G., Tamboli, M.S., Patil, D.R., Kulkarni, M.V., Yoon, H., Kim, H., Al-Deyab, S.S., Yoon, S.S., Kolekar, S.S., & Kale, B.B. (2016). Green approach for hierarchical nanostructured Ag-ZnO and their photocatalytic performance under sunlight. *Catalysis Today, 260,* 126-134.

8 Hajkova, P., Matousek, J., & Antos, P. (2014). Aging of the photocatalytic TiO2 thin films modified by Ag and Pt. *Applied Catalysis B: Environmental, 160,* 51–56.

9 Liu, Y., Chi, M., Dong, H.L., Jia, H.S., Xu, B.S., & Zhang, Z.X. (2014) Ag/CdS heterostructural composites: fabrication, characterizations and photocatalysis. *Applied Surface Science, 313,* 558–562.

10 Gao, W.Y., Wang, M.Q., Ran, C.X., Yao, X., Yang, H.H., Liu, J., He, D.L., & Bai, J.B. (2014). One-pot synthesis of Ag/r-GO/TiO_2 nanocomposites with high solar absorption and enhanced anti-recombination in photocatalytic applications. *Nanoscale, 6,* 5498-5508.

11 Zhumabekov, A.Z., Ibrayev, N.K., & Seliverstova, E.V. (2020). Photoelectric properties of a nanocomposite derived from reduced graphene oxide and TiO2. *Theoretical and Experimental Chemistry, 55,* 398-406.

12 Serikov, T.M. (2020). The effect of electric transport properties of titanium dioxide nanostructures on their photocatalytic activity. *Bulletin of the University of Karaganda-Physics,* 3, 13-21.

Т.М. Сериков, П.А. Жанбирбаева, А.С. Балтабеков, А.Б. Куанышбекова

TIO_2/Ag/rGO нанокомпозитінің фотокаталитикалық белсенділігі

Мақалада күміс нанобөлшектерімен және тотықсыздандырылған графен оксиді тұндырылған титан диоксиді наноөзекшелерінен түзілген қабыршақтардың фотокаталитикалық белсенділігін зерттеу нәтижелері келтірілген. Алынған нанокомпозиттік материалдар оптикалық спектроскопия, сканерлеуші электронды микроскопия, рентгендік дифрактометрия және Раман спектроскопиясы арқылы зерттелді. Үлгілердің фотокаталитикалық белсенділігі бетіне ксенон шамының модуляцияланған жарық көзімен жарықтандырылған кездегі фототоктың генерациясынан бағаланды. Сонымен қатар үлгілердің фотокаталитикалық белсенділігі мысал ретінде қолданылған метилен көк бояғышының ыдырауы арқылы бағаланған. Титан диоксиді наноөзекшелерінен түзелген қабыршақтардың кеуектеріне күміс нанобөлшектерін және тотықсыздандырылған графен оксидін енгізу 400–500 нм аймағында үлгінің спектрлік сезімталдығының жоғарылауына әкелетіні анықталды. Үлгінің көріну облысында жарыққа сезімталдығының жоғарылауы фототок генерациясының жоғарылауына әкеледі және бастапқы үлгіге қарағанда 2,3 есе жоғары екені көрсетілді. TiO_2/Ag/rGO үлгісінің қатысуымен 100 минут сәулеленуден кейін метилен көк бояғыштың ыдырауы 19 % құрады. Бұл TiO_2 наноторлы қабыршақтарына қарағанда 3 есе және TiO_2/Ag қабыршақтарына қарағанда 2,3 есе жоғары. Жүргізілген зерттеулердің нәтижелері фотокаталитикалық белсенділіктің жақсаруы қабыршақтардың кедергісінің төмендеуімен, спектрлік сезімталдықтың кеңеюімен және қабыршақтардың бетінің ұлғаюымен байланысты екенін көрсетілді.

Кілт сөздер: титан диоксидінің наноөзекшелері, күміс нанобөлшектері, тотықсыздандырылған графен оксиді, фотокатализ.

Т.М. Сериков, П.А. Жанбирбаева, А.С. Балтабеков, А.Б. Куанышбекова

Фотокаталитическая активность нанокомпозита TIO2/Ag/rGO

В статье представлены результаты исследования фотокаталитической активности пленок, образованных наностержнями диоксида титана, допированных наночастицами серебра и восстановленного оксида графена. Полученные нанокомпозитные материалы исследованы методами оптической спектроскопии, сканирующей электронной микроскопии, рентгеновской дифрактометрии, раман-спектроскопии. Фотокаталитическую активность образцов оценивали по генерации фототока при освещении поверхности модулированным источником света ксеноновой лампы. Кроме того, фотокаталитическая активность образцов была оценена по деградации красителя метиленового голубого, который является модельным. Установлено, что внедрение в поры пленок из наностержней диоксида титана наночастиц серебра и восстановленного оксида графена приводит к повышению спектральной чувствительности образца в области 400–500 нм. Повышенная чувствительность образца к видимому свету приводит к росту генерации фототока и в 2,3 раза выше, чем у исходного образца. Деградация красителя метиленового голубого после 100 мин облучения в присутствии образца TiO_2/Ag/rGO составила 19 %. Это в 3 раза выше, чем в пленках из наностержней TiO_2 и 2,3 раза выше, чем пленках TiO_2/Ag. Результаты проведенных исследований показали, что улучшение фотокаталитической активности связано с понижением сопротивления пленки, расширением спектральной чувствительности и ростом величины площади поверхности наностержней.

Ключевые слова: наностержни диоксида титана, наночастицы серебра, восстановленный оксид графена, фотокатализ.

DOI 10.31489/2022PH4/22-31

UDC 621.45.038.7

A.B. Kengesbekov[2], B.K. Rakhadilov[2], L.G. Zhurerova[1], G.K. Uazyrkhanova[3], Ye.Ye. Kambarov[3]

[1]S. Amanzholov East Kazakhstan University, Ust-Kamenogorsk, Kazakhstan;
[2]PlasmaScience LLP, Ust-Kamenogorsk, Kazakhstan;
[3]D. Serikbayev East Kazakhstan Technical University, Kazakhstan, Ust-Kamenogorsk, Kazakhstan.
(E-mail: aidar.94.01@mail.ru)

Formation of TiN coatings by air plasma spraying

Titanium nitride (TiN) coatings were obtained on the surface of 12Kh18N10T steel by air plasma spraying (APS) of TiN powders using an arc plasmatron made by the authors. The plasmatron has a node of circular input and gas-dynamic focusing of the powder and the output apertures of the nozzle-anode are made in the form of rectangular narrowing-expanding channels (No.34334 RK: IPC H05H 1/42). A study of operation modes of a plasmatron for spraying of powder coatings was carried out. The structural-phase state, microhardness and wear resistance of TiN coatings were systematically investigated. The optimum APS operating mode for deposition of TiN powder was determined: current 250 A, voltage 68 V, argon gas flow 34 L/min, spraying distance 150 mm. To reduce the oxidation of TiN powder in the APS process, a method of creating a nitrogen environment at the outlet of the anode nozzle, nitrogen flow rate 2.3 bar was used. The results of structural analysis showed that TiN is the main phase of the coating. The mechanism of formation of TiN structures was characterized by analyzing SEM results of TiN coating surface morphology and TiN droplets sprayed on the surface of the sample. The results showed that the TiN(1) coating has better wear resistance than the TiN(2) and TiN(3) coatings. The cross-sectional and longitudinal microhardness of the TiN coating was investigated. The highest cross-sectional hardness of TiN coating is 1250 HV0.1, which is in accordance with mode 1.

Keywords: plasmatron, air plasma spraying, TiN, wear resistance, SEM analysis, anode nozzle.

Introduction

In recent years in all industrially developed countries technologies of creation of wear-resistant materials based on nitrides and methods of coating from them are intensively developed. Titanium nitride (TiN) has excellent wear resistance, erosion resistance, heat resistance and low friction coefficient [1-3], so it is widely used in some areas as the solid, wear-resistant coatings. The choice of methods for applying TiN coatings is determined by the geometric parameters of the coated parts and products, their design and technological features, conditions of future operation, as well as the required thickness of the functional protective coating [4,5]. The only factor uniting all the available methods is thermal influence in the process of applying a protective coating, necessary for formation of a stable adhesive bond of coating with a substrate.

The following coating deposition methods are currently most widely used in industry [6-9]: detonation spraying; high velocity oxide-fuel spraying (HVOF); air plasma spraying. Each of the above methods has its own advantages and disadvantages determining its effective area of application, but the first two methods can be implemented only in the presence of special chambers and gas communications. Moreover, their application is also limited by energy problems arising during heating of large-sized parts, since the required density and adhesion are achieved by the subsequent heat treatment of the formed layer. Therefore, one of the most economical and easy-to-implement methods of applying TiN coatings is the air plasma spraying method, which allows to form and melt the coating in one operation.

The essence of air plasma spraying is that powder particles pass through a zone of ionized gas (plasma) formed by an electric gas discharge, are melted and deposited on the substrate surface heated in the contact zone in the course of coating formation [10, 11]. The main element of technological equipment is a plasma torch that combines the functions of a plasma source and atomizer of disperse material. Plasma-forming gas (argon, nitrogen, air) passes through the electric arc zone, is ionized and exits through the nozzle of the plasma gun in the form of a plasma jet (flow). A significant disadvantage of this technology so far is the low thermal and overall efficiency of the process, amounting to only 3-8 %, which is an urgent problem of air-plasma spraying. In most technological processes of plasma treatment of materials, electric arc linear plasmatrons are most commonly used, which, compared to plasmatrons of other circuits, have a simple design, a

relatively long life of electrodes, the possibility of controlling the discharge power not only by changing the arc current, but also by changing the voltage at the arc.

Thus, the purpose of this study is to obtain wear-resistant nitride coatings by air plasma spraying.

Technology

Depending on the set tasks, an experimental air plasma spraying installation designed for surface treatment with plasma and application of powder coatings at atmospheric pressure was developed for protective coatings application.

The installation includes power supply, control panel, switching module with start-up unit, dispenser and autonomous plasma torch cooling unit. The installation is equipped with a plasma torch, which can be used in both manual and mechanized versions.

Fig. 1 shows schematically the installation for powder coatings, showing: plasmatron 1 which consists of anode 2, cathode 3, interelectrode ceramic insert 4, tubes 5 for feeding plasma gas — argon 6, tubes 7 for feeding inert gas — nitrogen 8 and sprayed powder 9, fittings for inlet 10 and outlet 11 of cooling fluid 12, powder batcher 13, power supply 14, off-line unit of water cooling 15.

The installation works as follows. Before starting work, the cooling system is switched on. Distilled water is used to cool the plasmatron, which enters the cavity of the anode assembly housing through a fitting and then the heated water is discharged through a fitting. The coolant is in circulating mode and the temperature of the coolant is automatically regulated by an autonomous water cooling module. Then the plasma-forming gas-argon is fed through the radial feed tube of the cathode assembly, to the discharge area of the plasmatron. When voltage is applied to the electrodes, an electric arc occurs between the nozzle-anode and the cathode and the plasma-forming gas – argon is ionized and exits the nozzle-anode at high speed, forming a plasma stream. Then the metering device is connected and through the inert gas channel the powder to be sprayed is fed into the plasma stream.

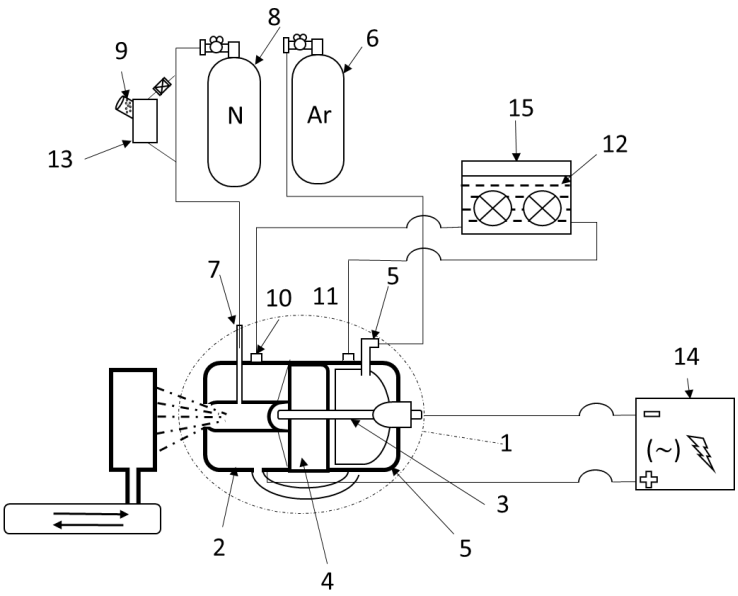

Figure 1. Schematic diagram of a powder coating installation

Plasmatron (Figure 2) is a thermal plasma generator of DC coaxial design with tungsten cathode with diameter of 5 mm, embedded in the copper rod in the center, and all-welded nozzle anode of copper, which has a radiator profile, which will allow to disassemble and assemble the plasmatron during repair work without deteriorating its quality. The key element of the plasmatron design is a node of annular input and gas-dynamic focusing of the powder, as well as the outlet holes of the nozzle-anode are made in the form of rectangular tapering-expanding channels. This design scheme provides input of the sprayed powder into the axial high-temperature and high-speed part of the plasma flow, which significantly increases the efficiency of heating and acceleration of particles and sputtering productivity [12]. The lifetime of the plasma torch is more than 200 hours, the cathode is replaced after 50 hours of operation. The plasma torch is capable of sta-

tionary operation with various media, primarily with oxidizing media. AC electric arc plasmatron operates in argon (nitrogen, air, gels) with a maximum power of up to 34 kW at a low pressure of about 0.01 MPa.

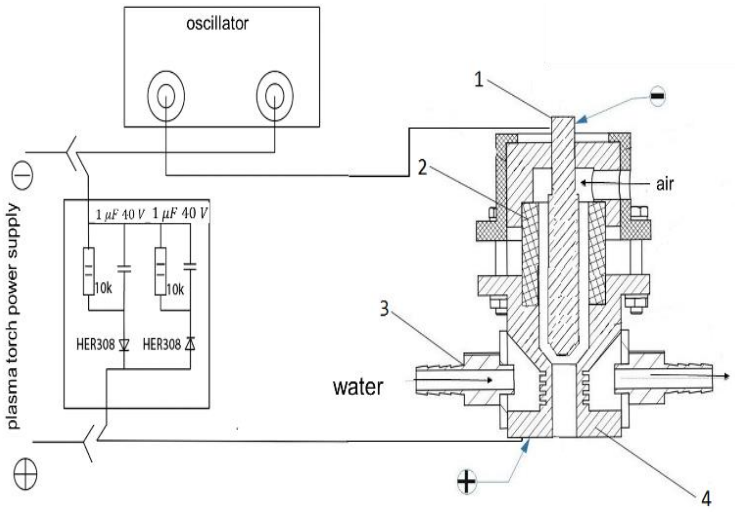

1 — cathode, 2 — insulator, 3 — cooling connector, 4 — anode
Figure 2. Scheme of connection of the plasma torch to the power supply

Materials and Methods

Stainless steel 12Kh18N10T (0.12 % C, 18 %Cr, 10 %Ni, Ti) was used as a substrate material. To improve the adhesion between the coating and the substrate, the flat surface of a 50×50×4 mm steel sample was cleaned in acetone and sandblasted before spraying. TiN powder with a dispersion of 15-40 μm was used for coating spraying (Figure 3).

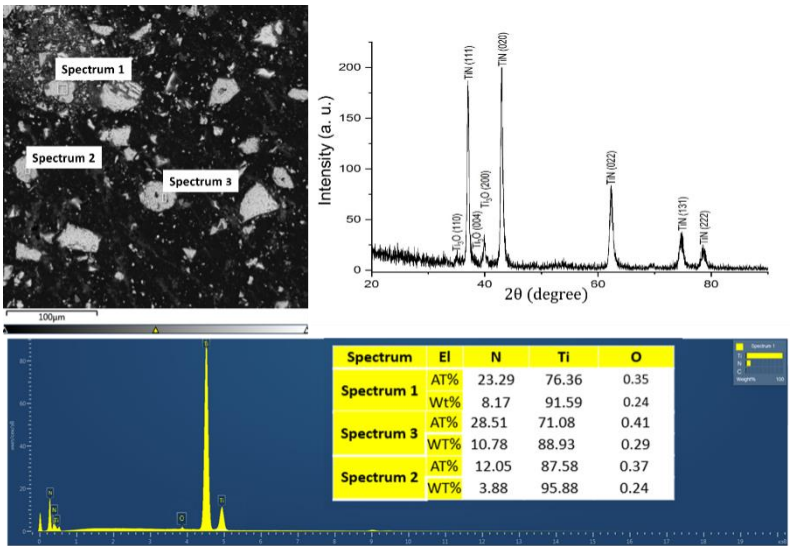

Figure 3. Structure-phase states of sprayed titanium nitride powder

An air-plasma system was used for the experiment, the design of which is shown in Figure 1. First, the substrate was preheated to 250 °C using a plasma jet, which was controlled by a HT-819 pyrometer. Then, TiN coatings were applied to the substrate using a plasma torch. The surface morphology was studied by scanning electron microscopy on a JSM-6390 scanning electron microscope with an energy dispersive spectrometer (EDS).

The microhardness of the samples was measured by a diamond indenter on the device Metolab 502 (Russia) in accordance with GOST 9450-76 [13], at a load of 100 g and exposure time of 10 s. The samples were tested for abrasive wear on the experimental stand (Figure 4) against soft stationary abrasive particles

by the scheme "rotating roller — flat surface" in accordance with GOST 23.208-79, which corresponds to the American standard ASTM C 6568 [14].

Measurements of corrosion resistance were carried out on potentiostat-galvanostat "P-150", using a three-electrode connection scheme to the electrochemical cell using a chlorosilver reference electrode and an auxiliary platinum electrode. For corrosion resistance tests, a 3 % NaCl solution in distilled water was used as an aggressive medium. Measurements were carried out at ambient temperature 20±2 °C.

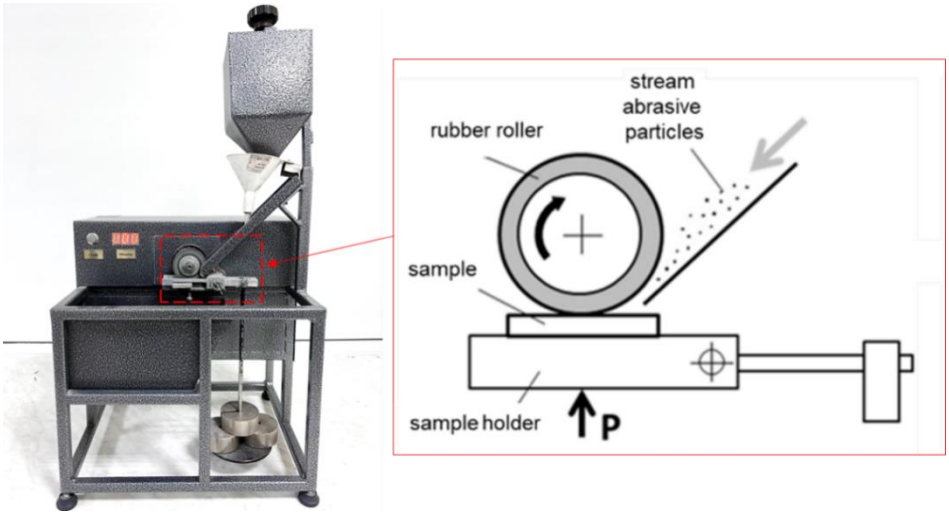

Figure 4. The experimental test stand for testing of samples abrasive wear according to the “rotating roller–flat surface” scheme

The formation of a dense homogeneous coating layer is influenced not only by the spraying parameters, but also by the quality of the powder. In addition, the main quality parameters of air plasma spraying, which include hardness, layer thickness and wear resistance, depend on several factors: spraying distance, current strength, voltage, gas pressure. Among these factors, electric current and working gas (Ar) pressure play an important role. In this regard, for the spraying modes the corresponding technological parameters listed in Table 1 were selected.

Table 1

Modes of air plasma spraying

Sample	Spraying distance, mm	Gas flow rate Ar, ltr/min	Gas flow rate N, bar	Current, A	Processing time, s	Coating thickness, μm	Voltage, V
TiN(1)	150	35	2.4	250	60	~70	68
TiN(2)	150	35	2.7	350	60		
TiN(3)	150	35	3	450	60		

Results and Discussion

The microstructure of the cross-sectional microslip is shown in Figure 5. The cross-sectional microslip shows porosity in the applied layer, probably having a diffusion character. The microstructure of 20 μm thick TiN(1) coating is characterized by high density, low porosity, smooth boundary with the substrate. The volume fraction of the pores formed at large distances from each other is 0.13 % of the surface area of the coating. There are also very small pores formed, apparently, as a result of degassing of the molten material of the particles during their crystallization.

Fig. 5 b, c shows the microstructure of TiN(2) and TiN(3) coatings, which is characterized by the presence of porosity throughout the thickness, the pores have an irregular shape and sizes from a few microns to 10 μm. The porosity of the TiN coating is 2.96 % and 8.04 % at 75 and 200 μm thickness, respectively. The coating section at the border with the substrate is characterized by a more uniform structure. The structure with few pores should be attributed to the gas that exists between the tiny liquid droplets and does not have time to be released during coating formation, which seems to contribute to the formation of small character-

istic micro-cracks in the thick coating structures seen in Figure 5 b, c. Therefore, to this day, the problem of reducing pores and cracks, as well as improving the structure of coatings remains an urgent task that requires thorough research.

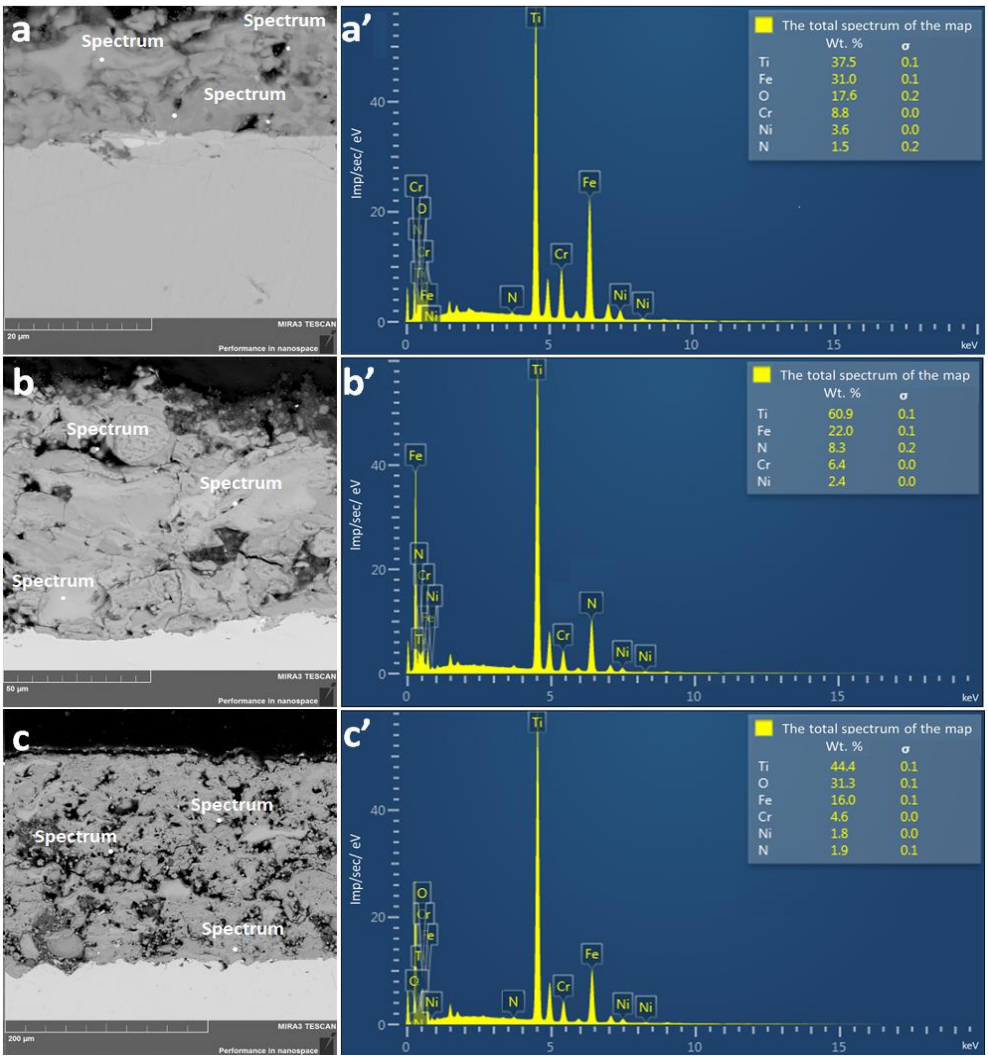

Mode 1 (20 μm), (b) mode 2 (75 μm), (c) mode 3 (200 μm)
Figure 5. SEM images of cross-sectional morphology of TiN coating

From the mapping data in Figure 6 we can also conclude that the distribution of the main components (Ti, N, Cr, Ni, O and Fe) is uniform throughout the thickness of the coatings and in the substrate. In accordance with the data on the distribution of elements in the surface layer obtained both in the mapping mode and in the point mode (Figure 6), the layer consists of pronounced spectra of Ti and N, demonstrating the contrasting composition of TiN coatings. According to this, it can be assumed that the predominant phase in this area is TiN.

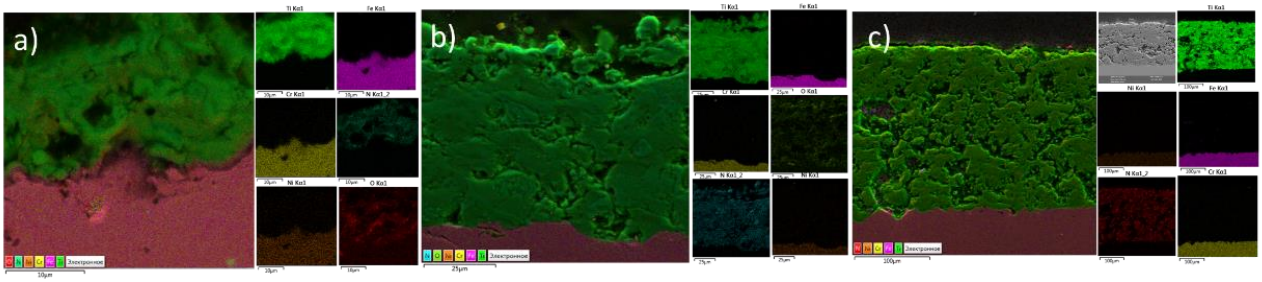

a)TiN(1); *b) TiN(2);* *c)TiN(3)*

Figure 6. Cross-section morphology and corresponding EDS maps of coating samples

The study of the structure was supplemented by microhardness measurements along the entire cross section of the coating. Figure 7 shows the results of microhardness measurements of TiN coatings of different modes. All coatings in general are characterized by high microhardness. Similar results were obtained in [15, 16]. The dependence of microhardness on an arrangement of measuring points on height of a layer is not found. The comparatively high hardness is observed on the surface of the coating processed by mode 1, has value 1250 $HV_{0.1}$. This may be due to the low content of pores and cracks in the structure of the sample TiN(1).

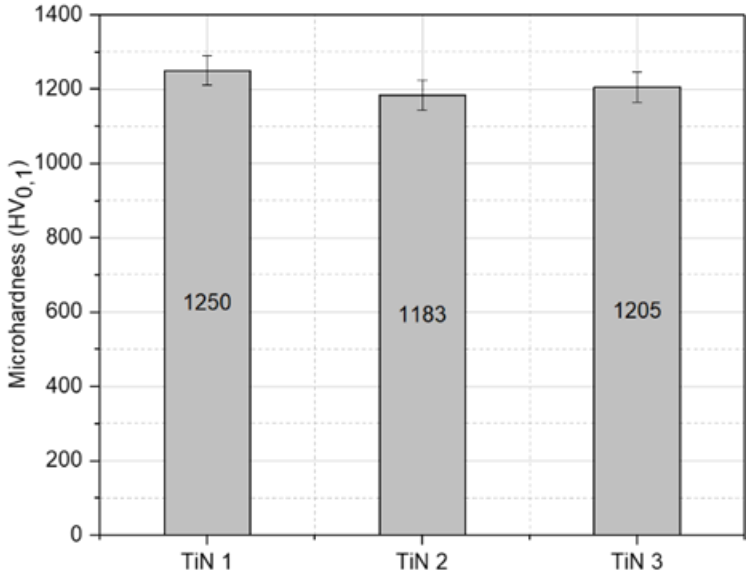

Figure 7. Results of the microhardness of TiN coatings obtained by the APS method

An abrasion test was performed to evaluate the wear resistance of the coatings. The abrasion results in terms of mass loss and relative wear resistance for the coatings are shown in Figure 8. It can be seen that there was little difference in the resistance against abrasive wear of the samples. The best material among all the coatings studied was TiN(1), which showed a higher abrasion resistance compared to the coatings obtained by the TiN(2) and TiN(3) modes, by about 83-87 %.

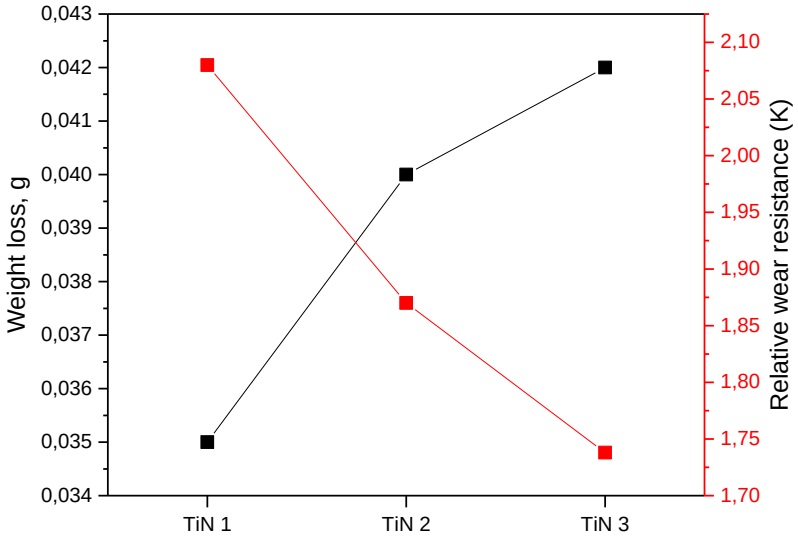

Figure 8. Results of mass loss and relative wear resistance of coatings

According to the thermodynamics of corrosion, a higher intrinsic corrosion potential can lead to greater resistance to the electrochemical reaction, indicating a stronger ability to resist the addition and loss of electrons, as well as better corrosion resistance of the material. Generally, based on corro-

sion kinetics, the lower the intrinsic corrosion current density, the higher the corrosion resistance [17, 18]. Figure 9 shows that the corrosion resistance of TiN(1) coatings is better than that of TiN(2) and TiN(3) coatings. In the coatings obtained by TiN(2) and TiN(3) modes the corrosion rate Rcorr =0.905 cm/year and Rcorr =0.486 cm/year respectively is higher than that of TiN(1) coating with value Rcorr=0.078 cm/year (Table 2). It was determined that the corrosion resistance reaches the highest value when spraying under the regime TiN(1).

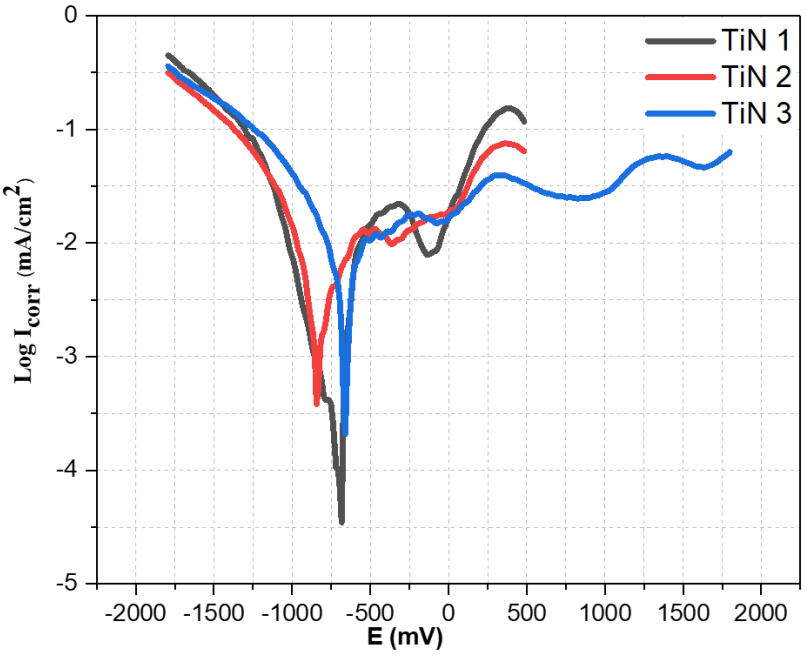

Figure 9. Polarization curves of coatings obtained by the APS method

Table 2

Correlation table of obtained results

Sample	Microhardness, HV0.1/10	Abrasive tests		Corrosion tests		
		Weight loss, g	Wear resistance coefficient	m, g	l, cm	R_{corr} cm/year
TiN 1	1250	0.035	2.08	0.317	0.078	0.078
TiN 2	1183	0.040	1.87	3.556	0.905	0.905
TiN 3	1205	0.042	1.73	1.910	0.486	0.486

Conclusion

This article presents the results of research work on obtaining coatings from titanium nitride by air plasma spraying, as well as an analysis of the evaluation of microhardness values, corrosion and abrasion characteristics. The received results allow to draw the following conclusions. It is established that the use of inert gas at the APS of thin-film coatings from titanium nitride allows to change the chemical composition of the coating and its structure. Under optimal gas pressure conditions of deposition, thin film coatings of stoichiometric composition with improved antifriction properties are formed. At nitrogen pressure equal to 2.3 bar (mode 1), the wear resistance coefficient of the formed coatings decreases practically 1.5 times compared to its value for modes 2 and 3. Increasing nitrogen pressure up to 3 bar causes the formation of a porous coating structure with a developed surface relief and, as a consequence, leads to a deterioration of the coatings' tribological properties.

It was determined that the value of microhardness increased and amounted to 1250 $HV_{0.1}$, which apparently contributed to a decrease in wear of TiN coatings in the realized friction conditions.

It was revealed that the application of TiN coatings improves the corrosion resistance of stainless steel 12X18H10T; in particular the corrosion rate is reduced, indicating that the coating has good stability and excellent protection.

Thus, the conducted studies have shown the prospects and feasibility of using the APS technology to improve the wear resistance of stainless steel 12Kh18N10T.

Acknowledgments

This research is funded by the Science Committee of the Ministry of Science and Higher Education of the Republic of Kazakhstan (Grant No. AP14972882)

References

1 Сотников Д.А. Разработка технологии нанесения пленок нитрида титана / Д.А. Сотников, Л.Л. Колесник // Вакуумная техника и технология: материалы Девятой Рос. студ. науч.-техн. конф. — 2019. — С. 188–189.

2 Лавро В.Н. и др. Исследование триботехнических свойств ионно-плазменных покрытий TiN,(TiAl) N,(TiAlSi)N / В.Н. Лавро и др. // Современные материалы, техника и технологии. — 2016. — №2 (5). — С. 136–141.

3 Махмуд А.М. Влияние технологических параметров получения покрытий из нитрида титана на их износостойкость / А.М. Махмуд. — 2011.

4 Xian G. Investigations on microstructure, mechanical and tribological properties of TiN coatings deposited on three different tool materials / G. Xian, J. Xiong, H. Fan, F. Jiang, Z. Guo, H. Zhao, & Y. Liu // International Journal of Refractory Metals and Hard Materials. — 2022. — Vol. 102, 105700.

5 Rakhadilov B.K. Structure and phase composition of high-speed steels / B.K. Rakhadilov, W. Wieleba, M.K. Kylyshkanov, A.B. Kenesbekov, M. Maulet // Bulletin of the University of Karaganda-Physics. — 2020. — No. 2 (98). — P. 83-92.

6 Murthy J.K.N. Effect of grinding on the erosion behavior of a WC–Co–Cr coating deposited by HVOF and detonation gun spray processes. / J.K.N. Murthy, D.S. Rao, & B. Venkataraman. — Wear. — 2001. — No. 249(7). — P. 592-600.

7 Zhang X. Comparison on multi-angle erosion behavior and mechanism of Cr3C2-NiCr coatings sprayed by SPS and HVOF / X. Zhang, F. Li, Y., Li, Q., Lu, Z., Li, H. Lu, X. Qi // Surface and Coatings Technology. — 2020. — Vol. 403, 126366.

8 Sagdoldina Z. Effect of irradiation with Si+ ions on phase transformations in Ti–Al system during thermal annealing. / Z. Sagdoldina, B. Rakhadilov, S. Kurbanbekov, R. Kozhanova, A. Kengesbekov. — Coatings. — 2021. — No. 11(2). — P. 205.

9 Luo L. Progress update on extending the durability of air plasma sprayed thermal barrier coatings / L. Luo, Y. Chen, M. Zhou, X. Shan, J. Lu, X. Zhao. —Ceramics International. — 2022.

10 Rakhadilov B.K. Development of air-plasma technology for hardening cutting tools by applying wear-resistant coatings./ B.K. Rakhadilov, A.B. Kenesbekov, P. Kowalevski, Y.A. Ocheredko, Z.B. Sagdoldina // News of the National Academy of Sciences of the Republic of Kazakhstan, Series of Geology and Technical Sciences. — 2020. — No. 3(441). — P. 54-62.

11 Basha G.M.T. A critical review on nano structured coatings for alumina-titania (Al_2O_3-TiO_2) deposited by air plasma spraying process (APS) / G.M.T. Basha, A. Srikanth, B.Venkateshwarlu. Materials today: proceedings. — 2020. — No. 22. — P. 1554-1562.

12 Патент на изобретение № 34334. Плазматрон для напыления. Дата регистрации в Государственном реестре полезных моделей 14.08.2020 / И.А. Очередько, Б.К. Рахадилов, Б.Т. Туякбаев, А.Б. Кенесбеков.

13 Измерение микротвердости вдавливанием алмазных наконечников. ГОСТ 9450-76. — Введ. 01.01.1977. — М.: Изд-во стандартов, 1993 — 36 с.

14 Rakhadilov B. Hydrogen and deuterium storage in tungsten when irradiation with plasma beam. / B. Rakhadilov, M. Skakov, A. Miniyzov, A. Kenesbekov. Paper presented at the *METAL 2018 — 27th International Conference on Metallurgy and Materials, Conference Proceedings,* (pp. 1216-1221). — 2018.

15 Mayrhofer P.H. Microstructural design of hard coatings / P.H. Mayrhofer, C. Mitterer, L. Hultman, H. Clemens // Prog. Mater. Sci. — 2006. — Vol. 51. — P. 1032–1114.

16 Zou D. Reactive Plasma Sprayed TiN Coating and Its Thermal Stability / D. Zou, D. Yan, J. He, X. Li, Y. Dong, J. Zhang // Journal of Iron and Steel Research, International. — 2007. — Vol. 14(5). — P.71–75.

17 Shinde S.V. Factors governing segmentation crack characteristics in air plasma sprayed ceramics / S.V. Shinde, S. Sampath // Journal of the European Ceramic Society. — 2022. — No. 42(3). — P. 1077-1087.

18 Li G. Characterization and corrosion behaviors of TiN/TiAlN multilayer coatings by ion source enhanced hybrid arc ion plating. / G. Li, L. Zhang, F. Cai, Y. Yang, Q. Wang, S. Zhang // Surface and Coatings Technology. — 2019. — No. 366. — P. 355-365.

А.Б. Кеңесбеков, Б.К. Рахадилов, Л.Ғ. Журерова, Г.К. Уазырханова, Е.Е. Қамбаров

Ауа-плазмалық бүрку арқылы TiN жабындарын қалыптастыру

Титан нитриді (TiN) жабындары 12Х18Н10Т болатының бетіне TiN ұнтақтарын ауа-плазмалық бүрку (АПБ) әдісімен, өзіміз әзірлеген доғалық плазмотронда алынды. Аталған плазмотронда сақиналы енгізу және ұнтақты газодинамикалық фокустау торабы бар, сондай-ақ саптама-анодтың шығу тесіктері тікбұрышты конустық-кеңейетін арналар түрінде орындалған (№ 34334 ҚР: МПК H05H 1/42). Ұнтақты жабындарды бүрку үшін плазмотронның жұмыс режимдеріне зерттеу жүргізілді. TiN жабындарының құрылымдық-фазалық күйі, микроқаттылығы және тозуға төзімділігі жүйелі түрде зерттелді. TiN жабынын алу үшін ауа-плазмалық бүркудің оңтайлы режимі анықталды: ток 250 А, кернеу 68 В, аргон газының шығыны 34 л/мин, бүрку қашықтығы 150 мм. Ауа-плазмалық бүрку процесінде TiN ұнтағының тотығуын азайту үшін саптаманың — анодтың шығысында азотты ортаны құру әдісі қолданылды, азот шығыны 2,3 бар болды. Құрылымдық талдау нәтижелері TiN жабынның негізгі фазасы TiN екенін көрсетті. TiN құрылымдарының түзілу механизмі TiN жабынының беткі морфологиясын және үлгі бетіне шашыраған TiN тамшыларын СЭМ талдауымен сипатталды. Нәтижелер TiN(1) жабынының TiN(2) және TiN(3) жабындарына қарағанда тозуға төзімділігі жақсы екенін көрсетті. TiN жабынының көлденең және бойлық қималарының микроқаттылығы зерттелді. TiN жабынының көлденең қимасының ең жоғары қаттылығы 1250 $HV_{0,1}$ көрсетті. TiN жабынын қолдану 12Х18Н10Т тот баспайтын болаттың коррозияға төзімділігін жақсартатыны анықталды, атап айтқанда коррозия жылдамдығы төмендейді, бұл жабынның жақсы тұрақтылығы мен тамаша қорғанысы бар екенін көрсетеді.

Кілт сөздер: плазмотрон, ауа-плазмалық бүрку, TiN, тозуға төзімділік.

А.Б. Кенесбеков, Б.К. Рахадилов, Л.Г. Журерова, Г.К. Уазырханова, Е.Е. Камбаров

Формирование TiN покрытий методом воздушно-плазменного напыления

Покрытия из нитрида титана (TiN) были получены на поверхности стали 12Х18Н10Т методом воздушно-плазменного напыления порошков TiN с помощью дугового плазмотрона собственной разработки. Плазмотрон имеет узел кольцевого ввода и газодинамической фокусировки порошка, а также выходные отверстия сопла-анода выполнены в виде прямоугольных ссужающихся-расширяющихся каналов (№ 34334 РК: МПК H05H 1/42). Проведено исследование режимов работы плазмотрона для напыления порошковых покрытий. Систематически исследованы структурно-фазовое состояние, микротвердость и износостойкость покрытий TiN. Определен оптимальный режим ВПН для нанесения порошка TiN: ток 250 А, напряжение 68 В, расход газа аргон 34 л/мин, дистанция напыления 150 мм. Для снижения окисления порошка TiN в процессе APS был использован способ создания азотной среды на выходе из сопла-анода, расход азота — 2,3 бар. Результаты структурного анализа показали, что TiN является основной фазой покрытия. Механизм формирования TiN структур был охарактеризован путем анализа СЭМ результатов морфологии поверхности покрытия TiN и капель TiN, распыленных на поверхность образца. Результаты показали, что покрытие TiN (1) обладает лучшей износостойкостью, чем полученные по режимам TiN (2) и TiN (3). Исследована была микротвердость поперечного и продольного сечений покрытия TiN. Наибольшая твердость поперечного сечения покрытия TiN составила 1250 HV 0.1, что соответствует режиму 1.

Ключевые слова: плазмотрон, воздушно-плазменное напыление, TiN, износостойкость, анализ СЭМ, сопло-анод.

References

1 Sotnikov, D.A., & Kolesnik, L.L. (2019). Razrabotka tekhnologii naneseniia plenok nitrida titana [Development of technology for applying titanium nitride films]. *Vakuumnaia tekhnika i tekhnologiia*: *materialy Deviatoi Rossiiskoi studencheskoi nauchno-tekhnicheskoi konferentsii — Vacuum engineering and technology: Materials of the Ninth Russian Student Scientific and Technical Conference.* 2019, 188, 189 [in Russian].

2 Lavro, V.N. & et al. (2016). Issledovanie tribotekhnicheskikh svoistv ionno-plazmennykh pokrytii TiN, (TiAl), N, (TiAlSi)N [Investigation of tribotechnical properties of ion-plasma coatings TiN,(TiAl) N,(TiAlSi) N]. *Sovremennye materialy, tekhnika i tekhnologii – Modern materials, equipment and technologies*, 2(5), 136–141 [in Russian].

3 Mahmud, A.M. (2011). Vliianie tekhnologicheskikh parametrov polucheniia pokrytii iz nitrida titana na ikh iznosostoikost [The influence of technological parameters of titanium nitride coatings on their wear resistance] [in Russian].

4 Xian, G., Xiong, J., Fan, H., Jiang, F., Guo, Z., Zhao, H., & Liu, Y. (2022). Investigations on microstructure, mechanical and tribological properties of TiN coatings deposited on three different tool materials. *International Journal of Refractory Metals and Hard Materials*, 102, 105700.

5 Rakhadilov, B.K., Wieleba, W., Kylyshkanov, M.K., Kenesbekov, A.B., Maulet, M. (2020). Structure and phase composition of high-speed steels. *Bulletin of the University of Karaganda-Physics*, 2 (98), 83-92.

6 Murthy, J.K.N., Rao, D.S., & Venkataraman, B. (2001). Effect of grinding on the erosion behavior of a WC–Co–Cr coating deposited by HVOF and detonation gun spray processes. *Wear*, 249(7), 592-600.

7 Zhang, X., Li, F., Li, Y., Lu, Q., Li, Z., Lu, H., & Qi, X. (2020). Comparison on multi-angle erosion behavior and mechanism of Cr3C2-NiCr coatings sprayed by SPS and HVOF. *Surface and Coatings Technology*, 403, 126366.

8 Sagdoldina, Z., Rakhadilov, B., Kurbanbekov, S., Kozhanova, R., & Kengesbekov, A. (2021). Effect of irradiation with Si+ ions on phase transformations in Ti–Al system during thermal annealing. *Coatings*, 11(2), 205.

9 Luo, L., Chen, Y., Zhou, M., Shan, X., Lu, J., & Zhao, X. (2022). Progress update on extending the durability of air plasma sprayed thermal barrier coatings. *Ceramics International*.

10 Rakhadilov, B.K., Kenesbekov, A.B., Kowalevski, P., Ocheredko, Y.A., & Sagdoldina, Z.B. (2020). Development of air-plasma technology for hardening cutting tools by applying wear-resistant coatings. *News of the National Academy of Sciences of the Republic of Kazakhstan, Series of Geology and Technical Sciences*, 3(441), 54-62.

11 Basha, G.M.T., Srikanth, A., & Venkateshwarlu, B. (2020). A critical review on nano structured coatings for alumina-titania (Al2O3-TiO2) deposited by air plasma spraying process (APS). *Materials today: proceedings*, 22, 1554-1562.

12 Ocheredko, I.A., Rahadilov, B.K., Tuyakbaev, B.T., & Kenesbekov, A.B. Plazmatron dlia napyleniia. Data registratsii v Gosudarstvennom reestre poleznykh modelei 14.08.2020 [Plasmatron for sputtering] Date of registration in the State Register of Utility Models 14.08.2020.

13 (1993). Izmerenie mikrotverdosti vdavlivaniem almaznykh nakonechnikov [Measurement of microhardness by indentation of diamond tips]. GOST 9450-76 from 01.01.1977. — Moscow: Izdatelstvo standartov.

14 Rakhadilov, B., Skakov, M., Miniyzov, A., & Kenesbekov, A. (2018). Hydrogen and deuterium storage in tungsten when ir-radiation with plasma beam. Paper presented at the *METAL 2018 — 27th International Conference on Metallurgy and Materials, Conference Proceedings*, 1216-1221.

15 Mayrhofer, P.H., Mitterer, C., Hultman, L., Clemens, H. Microstructural design of hard coatings // Prog. Mater. Sci. — 2006. — Vol.51. — P.1032–1114.

16 Zou D., Yan D., He J., Li X., DongY., Zhang J. Reactive Plasma Sprayed TiN Coating and Its Thermal Stability. *Journal of Iron and Steel Research, International*. — 2007. — Vol. 14(5). — P.71–75.

17 Shinde, S.V., & Sampath, S. (2022). Factors governing segmentation crack characteristics in air plasma sprayed ceram-ics. Journal of the European Ceramic Society, 42(3), 1077-1087.

18 Li, G., Zhang, L., Cai, F., Yang, Y., Wang, Q., & Zhang, S. (2019). Characterization and corrosion behaviors of TiN/TiAlN multilayer coatings by ion source enhanced hybrid arc ion plating. Surface and Coatings Technology, 366, 355-365.

DOI 10.31489/2022PH4/32-47

UDC 532.528.5:537.56:661.96

[1]K.A. Kuterbekov, [1]K.Zh. Bekmyrza, [1]A.M. Kabyshev,
[1]M.M. Kubenova, [1]N.K. Aidarbekov, [2]S.A. Nurkenov

[1]L.N. Gumilyov Eurasian National University, Astana, Kazakhstan;
[2]Astana International University, Astana, Kazakhstan
(E-mail: kbekmyrza@yandex.kz)

Investigation of the Characteristics of Materials with the Ruddlesden-Popper Structure for Solid Oxide Fuel Cells

This article presents the results of a study of the characteristics of materials based on lanthanum nickelate $La_2Ni_{1-x}Co_xO_{4+\delta}$ ($0 \le x \le 0.3$) and $Pr_2NiO_{4+\delta}$. Their crystal structure and interaction with YSZ and GDC electrolyte materials at 900 °C are analyzed. The thermal expansion coefficients are determined and the temperature dependences of the conductivities are studied. The polarization resistance of these materials in contact with the electrolyte material YSZ is also measured. As a result of the study, the following cathode materials were investigated: $La_2Ni_{1-x}Co_xO_4$ ($0 \le x \le 0.3$), Pr_2NiO_4. In this case, the influence of low concentrations of Co on the characteristics of lanthanum nickelate was studied for the first time. Materials based on lanthanum nickelate and praseodymium nickelate were characterized by a structure of the K_2NiF_4 type (Ruddlesden-Popper phases) with rhombic symmetry. A study of the thermal expansion of cathode materials showed that all the studied materials are characterized by higher CTEs than YSZ and GDC electrolytes. Based on the studies performed, cathode materials were chosen for the formation of composites with GDC electrolyte: La_2NiO_4, $La_2Ni_{0.8}Co_{0.2}O_4$, Pr_2NiO_4. A study of the sintering kinetics and CTE of composites showed that their thermal characteristics are much closer to those of electrolytes than those of pure cathode materials.

Key words: SOFC, cathode materials, conductivity, thermal expansion coefficient, nanopowders.

Introduction

Solid oxide fuel cells (SOFCs) are promising electrochemical devices that directly convert the chemical energy of a fuel into electrical and thermal energy. The main advantages of SOFC are the high theoretical efficiency of energy conversion (up to 60 % when using only electric power and up to 90 % when using combined electric and thermal energy) and environmental friendliness. In this regard, scientific and technological issues related to the creation of SOFC are widely studied. At the same time, an important task remains to increase the specific power of the cells, which directly depends on their internal resistance, which consists of the ohmic resistance of the electrolyte layers and electrodes, as well as polarization losses due to electrochemical processes on the electrodes. Thus, to reduce the internal resistance of SOFC, it is desirable to reduce both of these components.

One of the possible solutions to this problem is the creation of a non-porous cathode-electrolyte structure instead of the generally accepted one — porous cathode — dense electrolyte. In this case, the layer of cathode material, as well as the electrolyte, will prevent the mixing of fuel and oxidizing gases, which will reduce the thickness of the electrolyte layer and, consequently, its contribution to the internal resistance of SOFC.

Research methodology

Source materials

The initial nanosized powders of $Zr_{0.84}Y_{0.16}O_{2-\delta}$ (YSZ) and $Ce_{0.73}Gd_{0.27}O_{3-\delta}$ (GDC) electrolyte materials were obtained by laser evaporation [1].

Cathode materials, both with a perovskite structure based on praseodymium ferro-cobaltite, and with a Ruddlesden-Popper structure based on lanthanum nickelate and Pr_2NiO_4, were fabricated by the method of self-propagating high-temperature synthesis (SHS). The synthesis process was based on a variant of the Pechini method described in [2]. The reagents used were $Pr(NO_3)_3$ (analytical grade), $Fe(NO_3)_3$ (analytical grade), $Co(NO_3)_2$ (chemically pure), La_2O_3 (chemically pure), NiO (analytical grade), and $SrCO_3$ (analytical grade). Stoichiometric mixtures of reagents were dissolved in a 0.1 N HNO_3 solution until a homogeneous solution was obtained, which was evaporated to wet salts. As a combustible organic substance, a twofold volume of ethylene glycol $HOCH_2CH_2OH$ (chemically pure) was used, which was both a solvent and a rea-

gent. The reaction mixture was heated until the development of the SHS process. The reaction products were remixed and annealed step by step to remove residual organic phases at temperatures of 400, 700, and 900 °C with holding for 6 hours for each temperature. The final stage of processing was annealing at 1100 °C for 30 min.

Characteristics of source materials

The specific surface of the synthesized powders was determined by low-temperature nitrogen vapor sorption by the BET method on an automatic analyzer TriStar 3000. The measurement results are presented in Table 1.

The morphology of the obtained powders was studied by electron microscopy using a JEOL JEM 2100 transmission electron microscope and LEO 982 and JEOL JSM-6390LA scanning electron microscopes.

Figure 1 shows micrographs of the initial YSZ and GDC solid electrolyte powders. The particles of YSZ powder obtained by laser evaporation have a shape close to spherical. GDC powder particles are closer in shape to cubes rounded along the edges. At the same time, microscopy confirms the estimate of the average particle size of powders made on the basis of S_{BET}: about 15 nm for YSZ and 25 nm for GDC.

Micrographs of powders of cathode materials are shown in Figure 2. Powder particles obtained by SHS are irregularly shaped agglomerates. The average particle sizes determined by the BET method (Table 1) correlate with microscopy data.

Table 1

Nomenclature and characteristics of initial powders

Designation	Chemical composition	S_{BET}, m^2/g	d_{BET}, nm	Structure
Electrolyte materials				
YSZ	$Zr_{0,84}Y_{0,16}O_{2-\delta}$	48.1	21.0	Fluorite
GDC	$Ce_{0,73}Gd_{0,23}O_{2-\delta}$	34.2	24.3	Fluorite
Cathode materials				
LN	La_2NiO_4	2.71	320	Ruddlesden Popper
LNC-10	$La_2Ni_{0.9}Co_{0.1}O_4$	2.45	350	Ruddlesden Popper
LNC-20	$La_2Ni_{0.8}Co_{0.2}O_4$	3.05	270	Ruddlesden Popper
LNC-30	$La_2Ni_{0.7}Co_{0.3}O_4$	2.44	340	Ruddlesden Popper
PN	Pr_2NiO_4	1.71	490	Ruddlesden Popper

The phase composition of powders of electrolyte materials was determined by X-ray phase analysis performed on a D8 DISCOVER diffractometer using copper radiation (Cu $K_{\alpha 1,2}$ λ = 1.542 Å) with a graphite monochromator using a diffracted beam. Processing was performed using the TOPAS 3 program with the Rietveld algorithm for refinement of structural parameters. When estimating the average crystallite size, we used the correction factor K (in the Scherer formula) = 0.89. The phase composition of the cathode materials during synthesis was monitored using a Shimadzu XRD-7000 S X-ray diffractometer. The X-ray patterns were processed using the FULLPROF program.

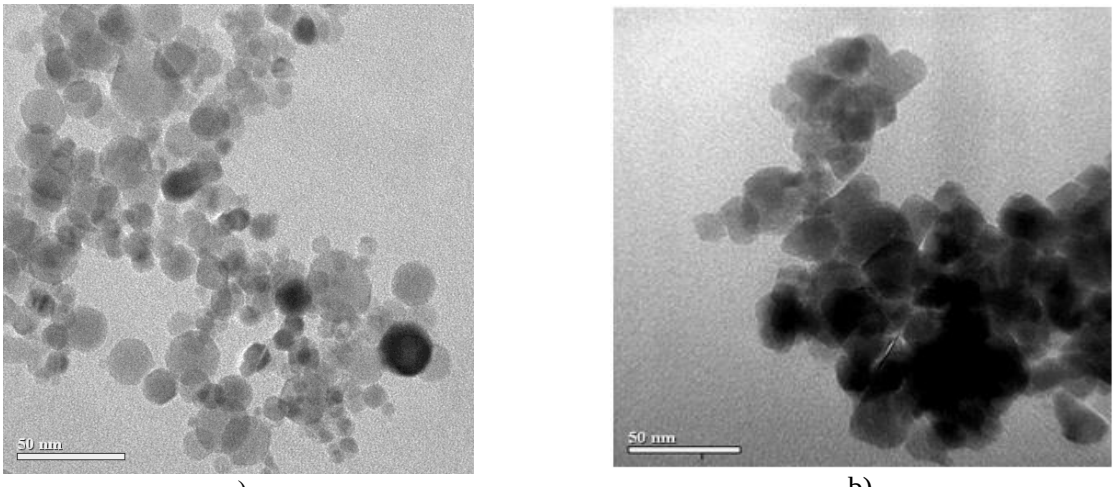

a) b)

Figure 1. Micrographs of the initial powders of solid electrolytes (a) YSZ and b) GDC

Powders of electrolyte materials YSZ and GDC are single-phase and are solid solutions with space group Fm-3m. The cubic lattice parameters a were 5.143 and 5.424 Å for YSZ and GDC, respectively. X-ray phase analysis of powders of cathode materials showed that they are mostly single-phase, but there are traces (less than 2 %) of unidentified secondary phases. Perovskite cathode materials based on praseodymium ferrocobaltite had a rhombic structure after the synthesis procedure, while materials based on lanthanum nickelate and praseodymium nickelate were characterized by a structure of the K_2NiF_4 type.

Study of the structure and interaction with electrolytes.

Disk samples 15 mm in diameter were made from the initial powders to study the structure of dense ceramics. The powders were pressed on a uniaxial hydrostatic press PG30 UHL4. Sintered at 1400 °C for 10 hours.

Samples for studying the chemical interaction between cathode and electrolyte materials were prepared according to the following procedure. The required powders were mixed in a weight ratio of 1:1. They were filled with isopropyl alcohol and sonicated with a UZG8-0.4/22 disperser for 10 min. This procedure makes it possible to “break up” the agglomerates formed in nanosized powders and ensure a uniform distribution of the powders throughout the suspension. Further mixing was carried out using a gravity mixer for 2 days. YSZ balls were added to the slurry as interfering bodies. The resulting mixtures were dried with constant stirring using an RH B S000 (IKA) magnetic stirrer. The resulting mixtures were compacted using a uniaxial press into discs 10 mm in diameter and ~2 mm high. Then the disk samples were sintered at a certain temperature (Tables 3, 4) with an exposure of 5 hours.

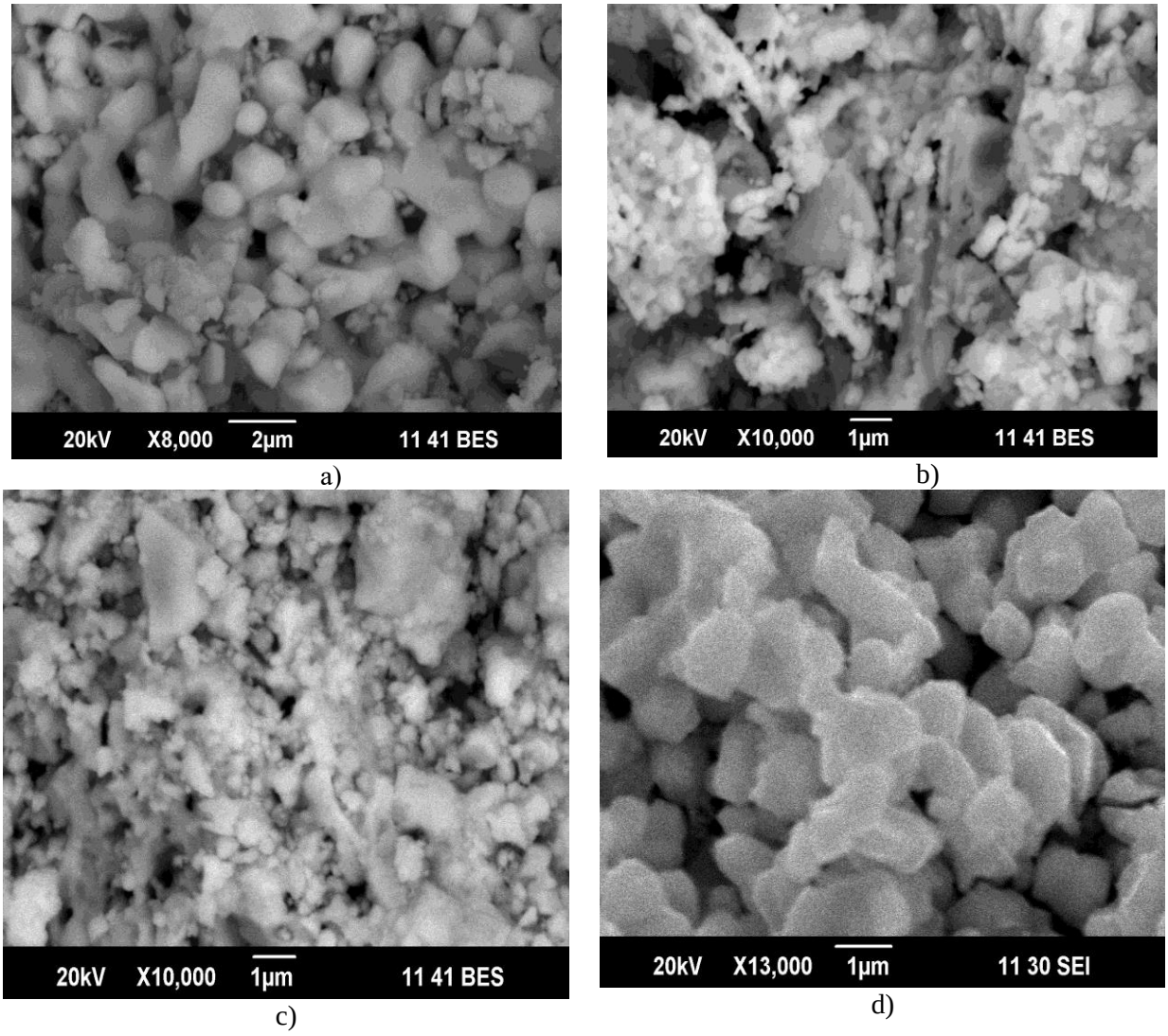

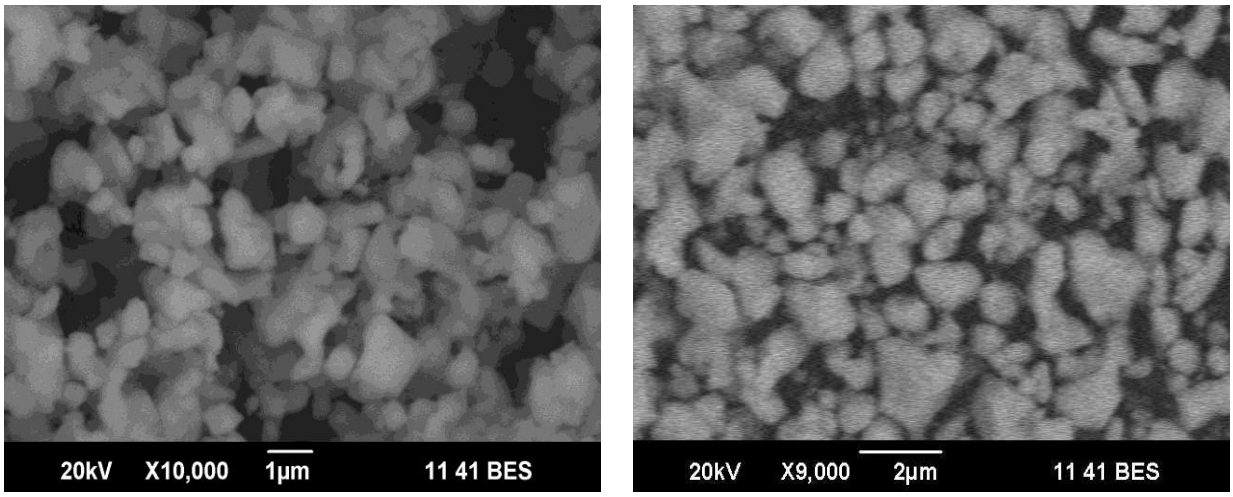

e) f)

Figure 2. Micrographs of initial powders of cathode materials: a) $PrFe_{0.8}Co_{0.2}O_3$, b) $Pr_{0.7}Sr_{0.3}Fe_{0.8}Co_{0.2}O_3$, c) $Pr_{0.7}Sr_{0.3}Fe_{0.5}Co_{0.5}O_3$, d) La_2NiO_4, e) $La_2Ni_{0.8}Co_{0.2}O_4$, f) Pr_2NiO_4

The phase composition of samples of cathode materials and mixtures was determined by X-ray phase analysis performed on a diffractometer. Processing was performed using the TOPAS 3 program with the Rietveld algorithm for refinement of structural parameters.

Study of the coefficient of thermal expansion

The measurement of the linear expansion of cathode materials was carried out on samples in the form of bars with characteristic dimensions of 4 × 4 × 9.5 mm, which were preliminarily sintered to densities close to theoretical (1400 °C, holding for 10 h).

Determination of the thermal expansion coefficient (TEC) of the samples was carried out in an air atmosphere in the temperature range of 20-1200 °C. The measurements were performed on a Dil 402C dilatometer. The heating rate was 5 °C per minute.

Conductivity study

To measure the conductivity, powders of cathode materials were pressed into rectangular bars with characteristic dimensions of 3×2×30 mm. The samples were compacted using a PG30 UHL4 press. The resulting compacts were sintered in an air atmosphere. The sintering temperature of the samples is 1400 °C. The holding time was 10 h.

The density of sintered samples was determined by hydrostatic weighing.

Probes made of platinum wire with a diameter of 0.2 mm were deposited on the sintered samples. To ensure good electrical contact between the probes and the sample, the probes were smeared with platinum paste, which was baked at 1000 °C for 1 h.

Conductivity was measured in air by a 4-probe method at direct current in the temperature range of 20–950 °C using a Solartron Sl-1260/1287 impedance meter. The measurements were carried out in the potentiodynamic mode (U_{max} = 0.1 V).

Study of polarization resistance

The determination of the polarization resistance of cathode materials in contact with the YSZ electrolyte was performed on symmetrical samples.

Disk samples of YSZ carrier electrolyte were obtained by uniaxial pressing using a PG30 UHL4 press and subsequent sintering at a temperature of 1200 °C with a holding time of 6 hours. The characteristic dimensions of the resulting disk samples are: diameter, 12 mm; thickness, 1 mm. The density of the disk samples was at least 98 % of the theoretical density ($\gamma_{XRD\ YSZ}$=5.92 g/cm^3).

The electrodes under study were applied symmetrically on both sides of the YSZ disk samples by staining. The electrode diameter was 8 mm. To apply the electrodes, cathode pastes were prepared by mixing the initial cathode powders (90 wt.%) and rosin (10 wt.%) as a binder. The solvent was isopropyl alcohol. The

sintering temperatures of the electrodes varied from 900 to 1100 °C with an exposure of 1 hour. The thickness of the electrode layers was about 0.1 mm.

Symmetrical samples prepared as described above (Figure 3) for measuring the polarization resistance were placed in a measuring cell, in which they were clamped between platinum grids (Figure 4). Each grid has two probes (potential and current) made of platinum wire 0.5 mm in diameter. The measuring cell was placed in a tubular furnace, which allows you to set the temperature of the samples in the range of 20–900 °C.

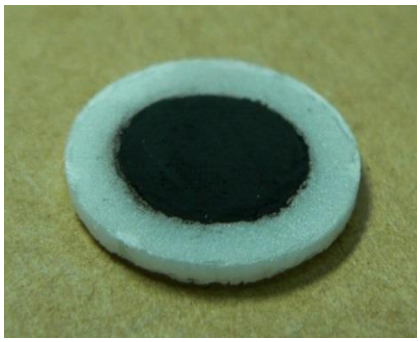

Figure 3. Appearance of the sample for research.

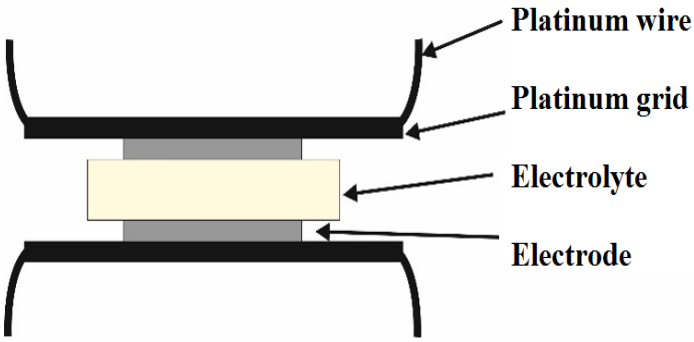

Figure 4. Diagram of a measuring cell for studying the polarization resistance of cathodes.

The impedance spectra were recorded at a voltage of 15 mV in the frequency range of 1 MHz–0.1 Hz using a Solartron Sl-1260/1287. The measurements were carried out in stagnant air in the temperature range of 850–650 °C.

The resulting impedance spectra were calculated using the equivalent circuit shown in Figure 5 using the ZView program. Where R_1 corresponds to the so-called series resistance, which includes the ohmic resistance of the electrolyte, probes. The resistance R_2 corresponds to the polarization resistance of the electrodes under study. Taking into account the fact that there are two identical electrodes in the measured system, the polarization resistance R_η was determined as half of R_2.

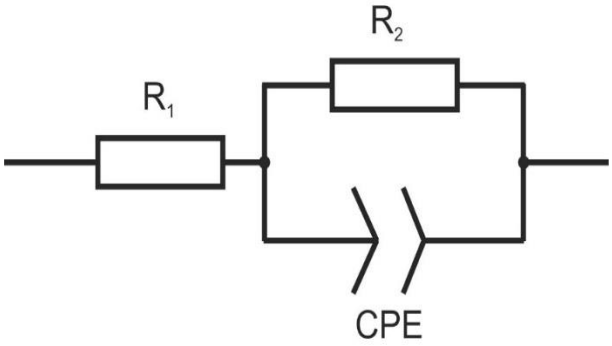

Figure 5. Equivalent circuit for calculating impedance spectra.

Experimental results

Crystal structure

On Figure 6 X-ray diffraction patterns of samples of cathode materials based on lanthanum nickelate and praseodymium nickelate sintered at 1400 °C are presented. Table 2 shows their crystallographic data.

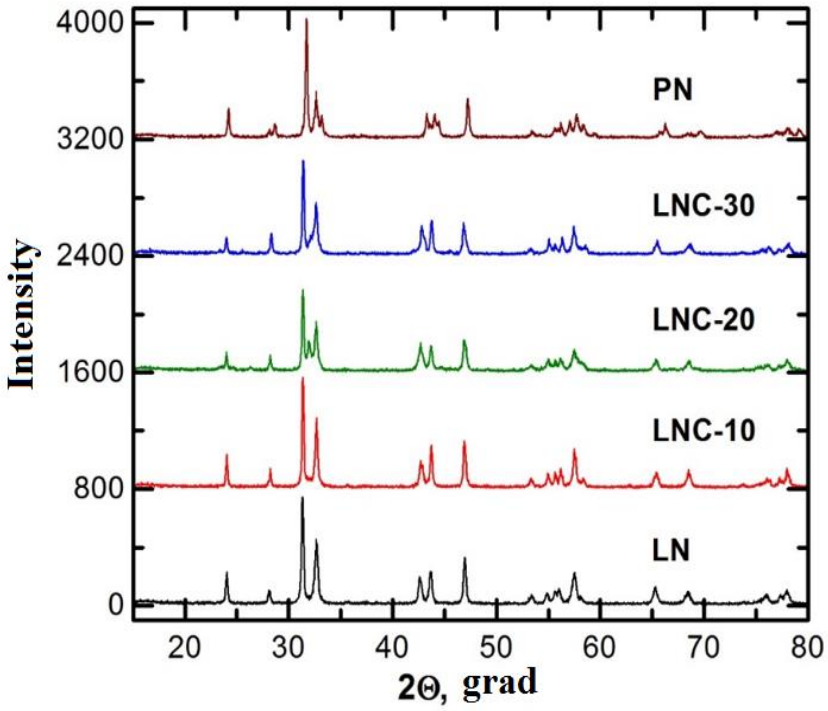

Figure 6. X-ray diffraction patterns of materials $La_2Ni_{1-x}Co_xO_4$, and Pr_2NiO_4.

All samples have a structure of the K_2NiF_4 type. In this case, the main type of symmetry of solid solutions is rhombic Fmmm. However, the LNC samples with 20 and 30 % Co also contain about 10 % of the tetragonal structure of the P4/m type, as well as trace structures symmetry of which can be identified as F4/mmm and R-3cH for LNC-20 and LNC-30, respectively. The PN material contains a sufficiently large amount of the structure with the P42/ncmZ symmetry corresponding to the formula $Pr_2NiO_{4.2}$, i.e. containing an excess amount of oxygen.

Table 2

Crystallographic data of $La_2Ni_{1-x}Co_xO_4$ and $Pr_2NiO_{4+\delta}$ compositions.

Material	Space group	a, Å	b, Å	c, Å	Reference
This work					
LN	100 % Fmmm	5.465(3)	5.489(3)	12.679(7)	
LNC-10	100 % Fmmm	5.469(3)	5.487(3)	12.639(5)	
LNC-20	88 % Fmmm 12 % P4/m	5.491(5) 11.149(9)	5.466(5)	12.637(9) 3.986(4)	
LNC-30	91 % Fmmm 9 % P4/m	5.492(3) 11.147(7)	5.473(3)	12.595(6) 3.883(4)	
PN	69 % Fmmm 31 % P42/ncmZ	5.482(3) 5.452(3)	5.391(3)	12.433(5) 12.438(8)	
Literature data					
$La_2NiO_{4+\delta}$	Fmmm	5.4499	5.4574	12.6724	[3]
$La_2CoO_{4,1}$		5.543	5.493	12.684	[4]

The X-ray density determined for the LN composition is 6.995 g/cm^3.

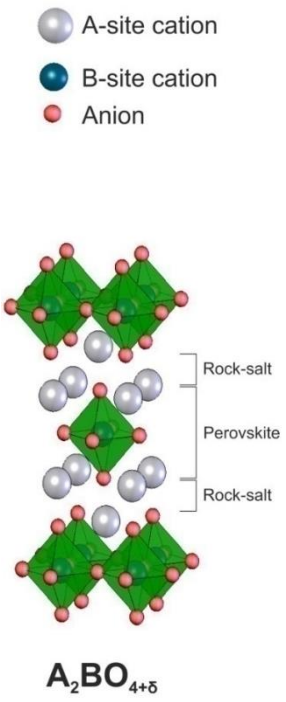

Figure 7. Ideal structure of Ruddlesden-Popper phases.

It is known from the literature [4-6] that in the high-temperature region $La_2MO_{4+\delta}$ materials are characterized by the tetragonal structure I4/mmm. In this state, the MO_6 octahedra are perfectly aligned along the c axis (Figure 7). As the temperature decreases, the structure is deformed, which is expressed in the cooperative deviation of the octahedra from the c axis, leading to the rhombic structure Fmmm. The transition temperature from Fmmm to I4/mmm for the $La_2NiO_{4+\delta}$ material is estimated at about 425 °C in [5] and about 200 °C in [6]. Whereas for the $La_2CoO_{4+\delta}$ material, the transition temperature to the I4/mmm structure is about 580 °C [4]. The literature data on the parameters of elementary cells given in Table 2 are close to the values obtained in our study.

As can be seen from Table 2 with an increase in the content of cobalt in the composition of lanthanum nickelate, there is a slight increase in the parameter ***a***, and a decrease in the parameters ***b*** and ***c***. These data correlate with the data of [7], where the compositions $La_2Ni_{1-x}Co_xO_{4+\delta}$ were also obtained by the Peccini method, but the symmetry of the solid solutions was determined as F4/mmm. Thus, the introduction of cobalt leads to structural distortions. Moreover, the data obtained, together with the dependence of $\boldsymbol{\delta}$ on the cobalt content [8], allow us to state that the c-parameter is strongly related to the electronic state of cobalt ions. Thus, it was suggested in [9] that the decrease in c is due to the replacement of the high-spin Ni^{2+} ion (r_i=0.69 Å at CN=6) by a much smaller low-spin Co^{3+} ion (r_i=0.545 Å at CN=6).

In addition, a decrease in the c parameter with the introduction of Co can also be interpreted as an increase in the "thickness" of the rock salt layer along this direction [10]. Thus, this increase can be expected to lead to an improvement in the mobility of oxide ions in the ab plane.

Chemical interaction with electrolytes.

On Figure 8 shows X-ray diffraction patterns for mixtures of Ruddlesden-Popper electrolyte and cathode materials that were sintered at 900 °C for 5 hours. For comparison, in Figure 8 also shows separate X-ray diffraction patterns of electrolyte (YSZ and GDC) and cathode (LN, LNC-30 and PN) cathode materials. The results of the analysis of X-ray phase data are summarized in Table 3.

The data in Table 3 confirm the well-established opinion that the CeO_2-based electrolyte is more chemically Table to interaction with cathode materials than the ZrO_2-based electrolyte [11, 12]. Literature data also confirm rather high chemical activity of La_2NiO_4 towards YSZ, and Pr_2NiO_4 towards both YSZ and GDC [13-15]. For example, in [14], secondary phases $La_2Zr_2O_7$, $La_3Ni_2O_7$ were found in a mixture of lanthanum nickelate and YSZ after 2 h exposure at 900°C. Whereas no interaction was found with the GDC electrolyte under the same conditions [14]. Exposure for 24 hours at 900 °C of a mixture of Pr_2NiO_4 and

GDC led to the formation of $Pr_4Ni_3O_{10}$ and Pr_6O_{11}, while in a mixture with YSZ, $Pr_2Zr_2O_7$ was additionally formed at a similar exposure [15].

It is also believed that an increase in the content of cobalt in the composition of the cathode material increases its chemical activity with respect to the electrolyte material [12, 16]. Data on the interaction of LN and LNC-20 with GDC electrolyte confirm this pattern. However, it is unexpected that the introduction of Co into the composition of lanthanum nickelate seems to reduce the chemical activity with respect to the YSZ electrolyte (lower content of the secondary phase according to XRD data). The reasons for this behavior are currently unclear and require further research.

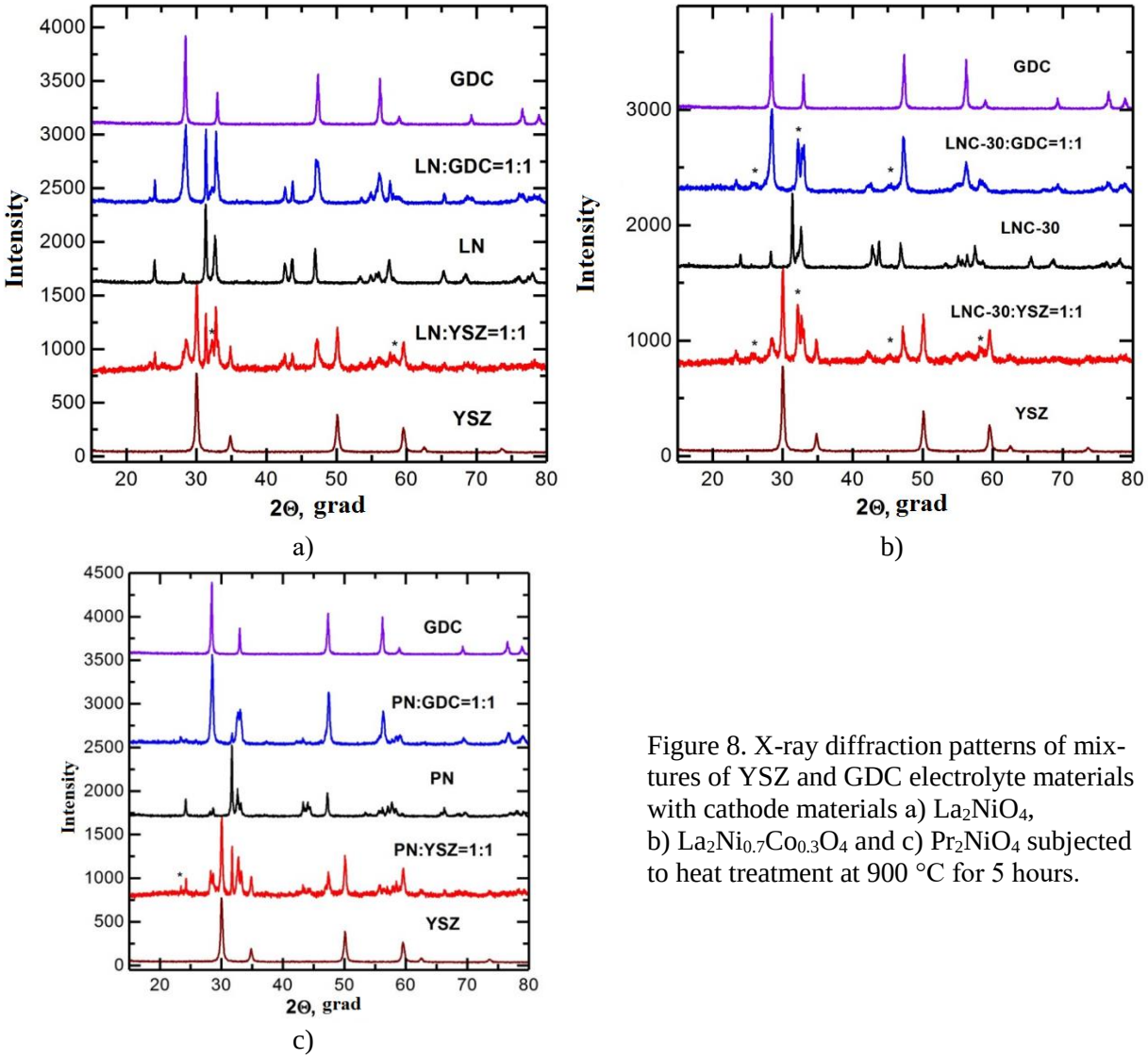

Figure 8. X-ray diffraction patterns of mixtures of YSZ and GDC electrolyte materials with cathode materials a) La_2NiO_4, b) $La_2Ni_{0.7}Co_{0.3}O_4$ and c) Pr_2NiO_4 subjected to heat treatment at 900 °C for 5 hours.

Table 3

Interaction of materials based on La_2NiO_4 and Pr_2NiO_4 with electrolytes

Designation	Cathode material	Electrolyte	$T_{sintering}$, °C	Interaction
LN: YSZ	La_2NiO_4	YSZ	900	41 % secondary phase
LN: GDC	La_2NiO_4	GDC	900	No
LNC-30: YSZ	$La_2Ni_{0.7}Co_{0.3}O_4$	YSZ	900	12 % secondary phase
LNC-30: GDC	$La_2Ni_{0.7}Co_{0.3}O_4$	GDC	900	8 % secondary phase
PN: YSZ	Pr_2NiO_4	YSZ	900	38 % secondary phase
PN: GDC	Pr_2NiO_4	GDC	900	37 % secondary phase

Thermal expansion

On Figure 9 shows the results of measuring the linear expansion of the studied cathode materials in the temperature range of 20-1200 °C.

In the literature, the values of the coefficient of thermal expansion (CTE) averaged over the entire temperature range are usually given. For example, the CTE of $La_2NiO_{4+\delta}$ is 13.0×10^{-6} K^{-1} (20-1000 °C) [3]. However, on the curves of linear expansion obtained by us, a not very obvious inflection is observed in the region of 850 °C. Therefore, the CTE of the studied samples was calculated both for the entire temperature range (20–1200 °C) and separately for the low temperature (200–850 °C) and high temperature (850–1200 °C) regions. The calculation results, together with the coefficients of determination R^2, are summarized in Table 4. It can be seen that the approximation consisting of two linear regions describes the experimental data better.

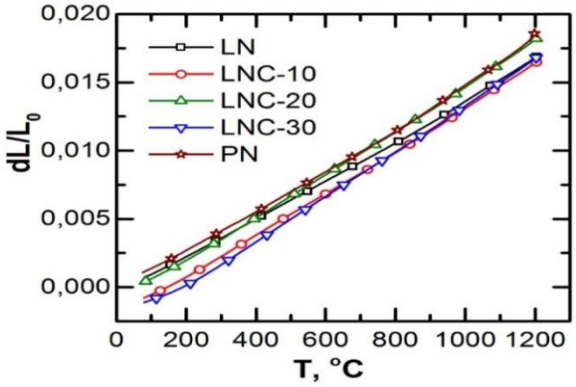

Figure 9. Temperature dependence of the change in the dimensions of samples of cathode materials.

Table 4

Calculation of CTE for various temperature ranges

Compound	200-850 °C		850-1200 °C		20-1200 °C	
	TEC ($\times10^{-6}$), K^{-1}	R^2	TEC ($\times10^{-6}$), K^{-1}	R^2	TEC ($\times10^{-6}$), K^{-1}	R^2
LN	13.89	0.99999	16.29	0.99822	14.39	0.99863
LNC-10	15.19	0.99992	16.81	0.99953	15.45	0.99932
LNC-20	15.72	0.99997	17.45	0.99901	15.93	0.99927
LNC-30	16.49	0.99993	17.51	0.99941	16.35	0.99978
PN	13.82	0.99991	16.50	0.99956	14.48	0.99788

Figure 10 shows the dependence of the change in CTE $La_2Ni_{1-x}Co_xO_{4+\delta}$ (x=0, 0.1, 0.2, 0.3) on the cobalt content for low- and high-temperature sections. It can be seen that with an increase in the content of cobalt in the composition of lanthanum nickelate, the CTE increases both in the low-temperature (20–800 °C) and high-temperature (800–1200 °C) regions. At the same time, in the low-temperature region, the introduction of cobalt has a stronger effect on the CTE of lanthanum nickelate than in the high-temperature region. Thus, from the point of view of CTE, LN and PN are the most suitable cathode materials with the Ruddlesden-Popper structure for YSZ and GDC electrolytes.

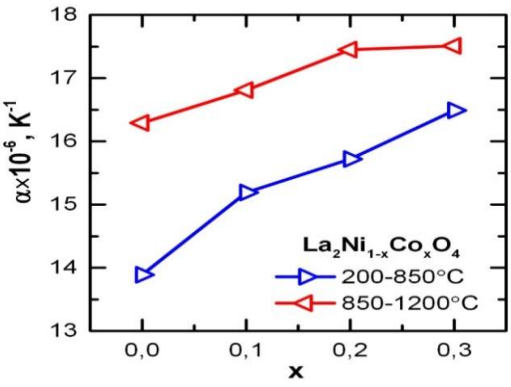

Figure 10. CTE of $La_2Ni_{1-x}Co_xO_{4+\delta}$ samples calculated for two temperature ranges 200-850 and 850-1200 °C

Conductivity

Figure 11 presents data on the total conductivity of the studied materials. It can be seen that a maximum is observed in the temperature dependences of the conductivity. According to [6], this behavior does not apply to the insulator-metal transition, but is due to the fact that at temperatures below 250 °C the chemical composition of $La_2NiO_{4+\delta}$ is stable and the change in conductivity reflects the behavior of the semiconductor type, that is, thermally activated Arrhenius-type conductivity. At higher temperatures, the materials lose some oxygen, which leads to a decrease in the M3+ content and, accordingly, a decrease in charge carrier densities and, consequently, a decrease in conductivity. Thus, competing phenomena (thermal activation and a decrease in the number of charge carriers) determine the presence of a maximum in the temperature dependence of the conductivity.

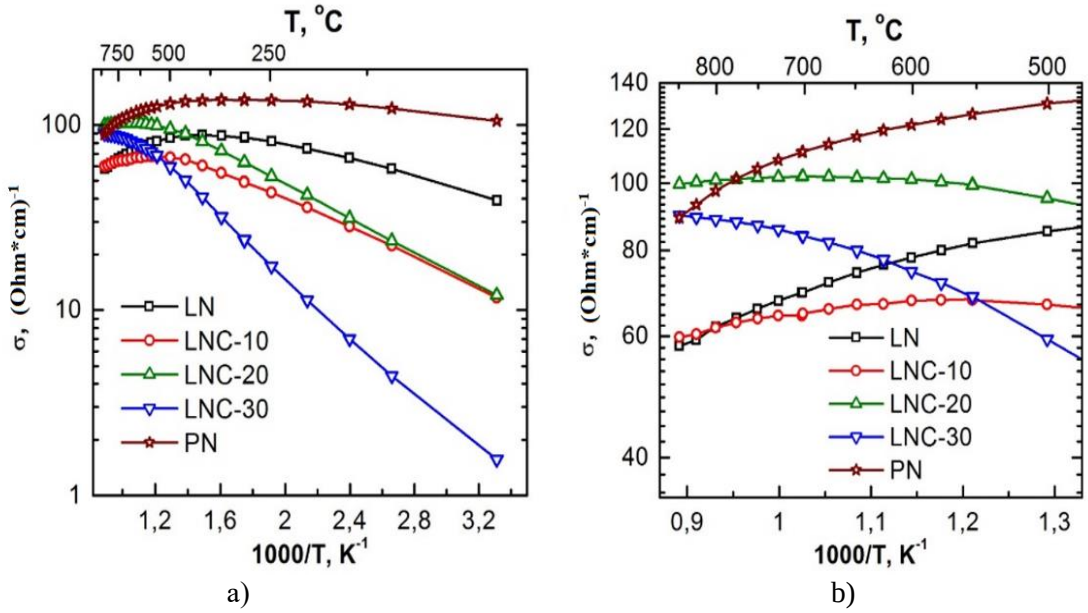

Figure 11. Temperature dependences of the conductivity of the studied materials:
a) — the entire temperature range, b) — high temperature range (500-850 °C).

If we compare the obtained data on the conductivity for the La_2NiO_4 material with the literature data [6, 9], it turns out that the value of the maximum conductivity is close — 80–90 S/cm. However, the temperature at which the maximum conductivity is reached differs significantly: in our study it is about 400 °C, while in [6, 9] it is about 650 °C.

It was shown in [9] that the conductivity of $La_2Ni_{1-x}Co_xO_{4+\delta}$, (x=0.1, 0.5, 1) decreases with increasing cobalt content. This was explained by the fact that in layered systems of the K_2NiF_4 type, the B-O-B bond is mainly responsible for the electrical properties [17]. Exchange interactions along the c axis are much weaker and occur through two oxygen ions. Consequently, with the introduction of cobalt, the Ni(Co)-O bond length increases, which leads to a weakening of the B-O covalent interaction and, consequently, to a decrease in electronic conductivity.

However, our study shows a different picture. If at x=0.1 the conductivity of $La_2Ni_{1-x}Co_xO_{4+\delta}$ decreases compared to $La_2NiO_{4+\delta}$, its value is 65 S/cm at 700 °C, which is close to the data of [9] — about 45 S/cm at 700 °C. Then at x=0.2 and 0.3, although there is a decrease in conductivity in the low-temperature region (which can be explained by the reason described above), in the high-temperature region, the conductivity increases. Most likely, this phenomenon is associated with the presence of a secondary phase observed in the LNC-20 and LNC-30 samples (section 2.1).

Figure 11 shows that PN has a higher conductivity compared to materials based on lanthanum nickelate in the temperature range of 20-800 °C. The obtained values of the conductivity PN and its temperature dependence correlate with the literature data [3, 18-19].

Thus, from the point of view of conductivity, the most suitable materials for a non-porous cathode are PN and LNC-20.

Polarization resistance.

On Figure 12 shows the impedance spectrum of a sample with LNC-10 electrodes. The shape of the spectrum is typical for all studied compositions and measurement temperatures, except for the sample with LNC-30 electrodes sintered to YSZ at 900 °C. For this sample, it was impossible to distinguish the components Rel-ta and Rη in the spectrum, so its polarization resistance is not discussed further. The method for calculating the polarization resistance of cathodes is described in Section 1.6.

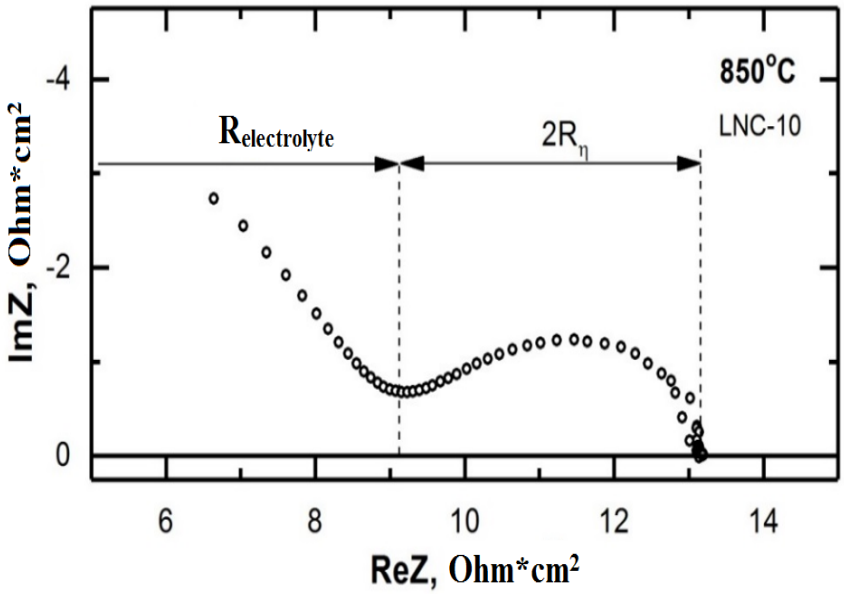

Figure 12. Impedance spectrum of a symmetrical sample with LNC-10 electrodes taken at 850 °C.

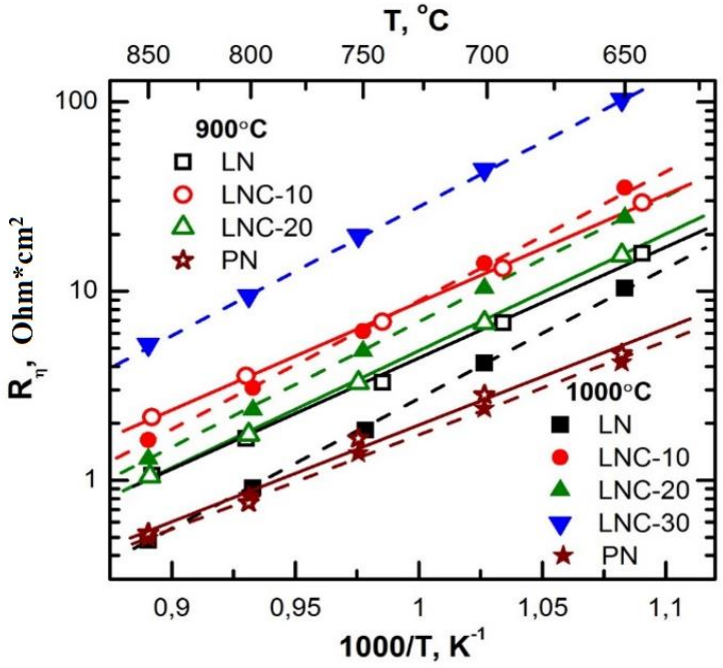

Figure 13. Temperature dependences of the polarization resistance of cathode materials sintered at 900 and 1000 °C.

Figure 13 shows the temperature dependences of the polarization resistance of the investigated cathodes. It can be seen that the electrodes sintered at 1000 °C are characterized by a lower polarization resistance than the electrodes sintered at 900 °C. Most likely, this is due to the formation of a better electrode-electrolyte contact. At the same time, LN and PN materials are characterized by the lowest polarization resistance. The introduction of Co into the composition of lanthanum nickelate leads to an increase in the polarization resistance of the cathode, however, this dependence is not linear.

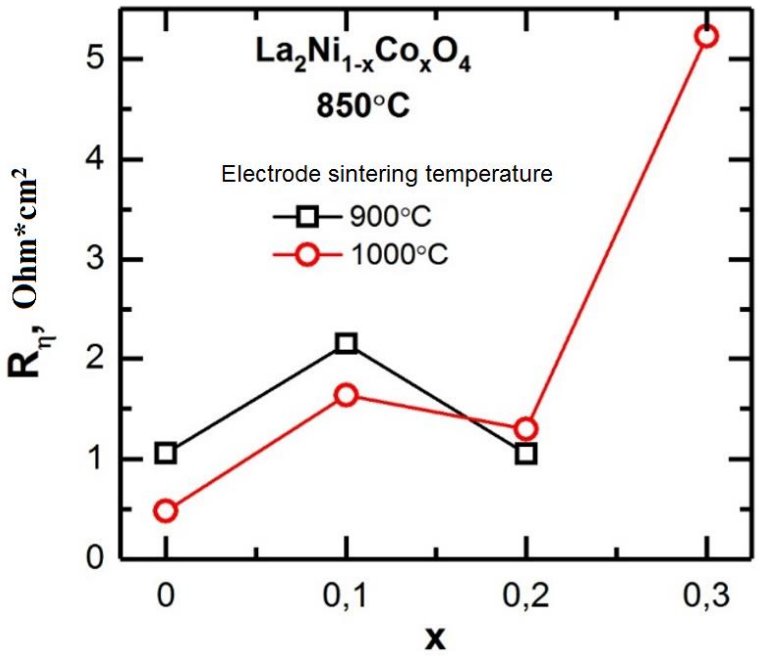

Figure 14. Dependence of polarization resistance of $La_2Ni_{1-x}Co_xO_{4+\delta}$ cathodes sintered to YSZ electrolyte at 900 and 1000 °C on cobalt content (x).

Figure 14 shows the dependence of the polarization resistance of $La_2Ni_{1-x}Co_xO_{4+\delta}$ cathodes on the cobalt content (x). It can be seen that the dependence is complex and non-linear. This is explained by the fact that the introduction of cobalt affects two characteristics of the material at once: conductivity and sintering kinetics. In the course of work on this project in 2018, it was shown that an increase in the content of Co in the composition of lanthanum nickelate leads to a shift in the shrinkage curve to a high-temperature region. Thus, the contact of the cathode material with the YSZ electrolyte formed at the same temperature should deteriorate with increasing Co in the LNC composition. On the other hand, according to the literature data [10, 20], the introduction of cobalt into the composition of La_2NiO_4 should lead to an increase in the oxygen diffusion coefficient and, thus, to a decrease in the polarization resistance. As shown above (see paragraph 2.4), the addition of 10 mol. % Co leads to a decrease in conductivity, which also affects the polarization resistance. While the conductivity of LNC-20 at high temperatures is higher than LN. However, the adhesion of the cathode to the YSZ electrolyte adversely affects the polarization resistance. Consequently, the "confrontation" of two factors (conductivity and sintering kinetics) causes a local minimum of polarization resistance at a content of 20 mol.% Co in the composition of $La_2NiO_{4+\delta}$.

Table 5 summarizes the data on the polarization resistance of the studied cathode materials with the Ruddlesden-Popper structure at 800 °C, and also presents the literature data. The Table shows data on electrodes baked at 1000 °C. As mentioned earlier, solid electrolytes based on CeO2 are more chemically inert to interaction with cathode materials than YSZ. Therefore, in the literature, the polarization resistance of cathodes with the K_2NiF_4 structure is studied mainly in contact with electrolytes based on CeO_2. As can be seen from Table 5, the polarization resistances of our cathodes in contact with the YSZ electrolyte are comparable with the literature data, in which the polarization of the cathodes was studied in contact with the CeO_2-based electrolyte.

Table 5

Polarization resistances of electrodes with the Ruddlesden-Popper structure at 800 °C.

Electrode	Electrolyte	R_η, Ohm*cm^2	Reference
$La_2NiO_{4+\delta}$	YSZ	0.9	this work
$La_2Ni_{0,9}Co_{0,1}O_{4+\delta}$	YSZ	3.0	this work
$La_2Ni_{0,8}Co_{0,2}O_{4+\delta}$	YSZ	2.4	this work
$La_2Ni_{0,7}Co_{0,3}O_{4+\delta}$	YSZ	5.2	this work
$Pr_2NiO_{4+\delta}$	YSZ	0.8	this work
$La_2NiO_{4+\delta}$	SmDC	0.2	[21]
$La_2Ni_{0,9}Co_{0,1}O_{4+\delta}$	GDC	3.0	[7]

Thus, the LN and PN materials have the highest catalytic activity among the studied ones.

Conclusions

As a result of the study, the following cathode materials were investigated: $La_2Ni_{1-x}Co_xO_4$ ($0 \leq x \leq 0.3$), Pr_2NiO_4. In this case, the influence of low concentrations of Co on the characteristics of lanthanum nickelate was studied for the first time. Materials based on lanthanum nickelate and praseodymium nickelate were characterized by a structure of the K_2NiF_4 type (Ruddlesden-Popper phases) with rhombic symmetry. Ruddlesden-Popper materials have been shown to be chemically compatible with $Zr_{0.84}Y_{0.16}O_{2-\delta}$ (YSZ) and $Ce_{0.73}Gd_{0.27}O_{2-\delta}$ (GDC) (GDC) electrolyte materials.

A study of the thermal expansion of cathode materials showed that all the studied materials are characterized by higher CTEs than YSZ and GDC electrolytes. Based on the studies performed, cathode materials were chosen for the formation of composites with GDC electrolyte: La_2NiO_4, $La_2Ni_{0.8}Co_{0.2}O_4$, Pr_2NiO_4. A study of the sintering kinetics and CTE of composites showed that their thermal characteristics are much closer to those of electrolytes than those of pure cathode materials.

Financing

The work was carried out within the framework of project No. AP09261208 with the support of the Ministry of Science and Higher Education of the Republic of Kazakhstan.

References

1 Ivanov M. Laser synthesis of oxide nanopowders / M. Ivanov, V. Osipov, Yu. Kotov et al. // Advances in Science and Technology. — 2006. — No. 45. — P. 291–296.

2 Чупахина Т.И. Синтез, структурные и морфологические характеристики ультрадисперсных порошков и керамики на основе твердых растворов La2-xSr0.125PrxNiO4 ($0 \leq x \leq 1.775$). / Т.И. Чупахина, О.И. Гырдасова, Г.В. Базуев // Известия РАН. Серия Физическая. — 2013. — Т. 77. № 9. — С. 1276–1280.

3 Boehm E. Oxygen diffusion and transport properties in non-stoichiometric $Ln_{2-x}NiO_{4+\delta}$ oxides. Solid State Ionics / E. Boehm, J.-M. Bassat, P. Dordor et al. — 2005. — No. 176. — P. 2717–2725.

4 Mohan Ram R.A. Preparation and characterization of $La_2CoO_{4+\delta}$. / R.A. Mohan Ram, P. Ganguly, C.N.R. Rao // Materials Research Bulletin. — 1988. — No. 23. — P. 501-505.

5 Hayashi A. Successive structural phase transitions in stoichiometric La_2NiO_4 observed by X-ray diffraction / A. Hayashi, H. Tamura, Y. Ueda. — Physica C. — 1993. — No. 216. — P. 77-82.

6 Boehm E. Oxygen transport properties of $La_2Ni_{1-x}Cu_xO_{4+\delta}$ mixed conducting oxides / E. Boehm, J.-M. Bassat, M.C. Steil, et al. // Solid State Sciences. — 2003. — No. 5. — P. 973–981.

7 Amow G. Structural and sintering characteristics of the $La_2Ni_{1-x}Co_xO_{4+\delta}$ series / G. Amow, P.S. Whitfield, I.J. Davidson, R.P. Hammond // Ceramics International. — 2004. — No. 30. — P. 1635–1639.

8 Kilner J.A. Mass transport in $La_2Ni_{1-x}Co_xO_{4+\delta}$ oxides with the K_2NiF_4 structure / J.A. Kilner, C.K.M. Shaw // Solid State Ionics. — 2002. — P. 154–155, 523– 527.

9 Amow, G. Structural and physical property trends of the hyperstoichiometric series $La_2Ni_{(1-x)}Co_xO_{4+\delta}$. / G. Amow, P.S. Whitfield, I.J. Davidson, et al. // Materials Research Society Symposia Proceedings. Solid State Inorganic Materials IV. — 2002. — P. 755, DD8.10.1-6.

10 Munnings C.N. Oxygen transport in the $La_2Ni_{1-x}Co_xO_{4+d}$ system / C.N. Munnings, S.J. Skinner, G. Amow, et al. // Solid State Ionics. — 2005. — No. 176. — P. 1895 — 1901.

11 Tsipis E.V. Electrode materials and reaction mechanisms in solid oxide fuel cells: a brief review. II. Electrochemical behavior vs. materials science aspects / E.V. Tsipis, V.V. Kharton // Journal of Solid State Electrochemistry. — 2008. — No. 12. — P. 1367–1391.

12 Mahato N. Progress in material selection for solid oxide fuel cell technology: A review / N. Mahato, A. Banerjee, A. Gupta, et al. // Progress in Materials Science. — 2015. — No. 72. — P. 141–337.

13 Zhao H. New cathode materials for ITSOFC: Phase stability, oxygen exchange and cathode properties of $La_{2-x}NiO_{4+\delta}$. / H. Zhao, F. Mauvy, et al. // Solid State Ionics. — 2008. — No. 179. — P. 2000–2005.

14 Hernandez A.M. $La_2NiO_{4+\delta}$ as cathode for SOFC: Reactivity study with YSZ and CGO electrolytes / A.M. Hernandez, L. Mogni, et al. // International Journal of Hydrogen Energy. — 2010. — No. 35. — P. 6031–6036.

15 Montenegro-Hernandez A. Thermal stability of $Ln_2NiO_{4+\delta}$ (Ln=La, Pr, Nd) and their chemical compatibility with YSZ and CGO solid electrolytes / A. Montenegro-Hernandez, J. Vega-Castillo, et al. // International Journal of Hydrogen Energy. — 2011. — No. 36. — P. 15704–15714.

16 Nikonov A.V. A brief review of conductivity and thermal expansion of perovskite-related oxides for SOFC cathode / A.V. Nikonov, K.A. Kuterbekov, Bekmyrza et al. // Eurasian Journal of Physics and Functional Materials. — 2018. — No. 2. — P. 274-292.

17 Richter J. Materials design for perovskite SOFC cathodes. / J. Richter, P. Holtappels et al. // Monatshefte für Chemie. — 2009. — No. 140. — P. 985–999.

18 Sadykov V.A. Tailoring the structural, thermal and transport properties of $Pr_2NiO_{4+\delta}$ through Ca-doping strategy / V.A. Sadykov, E.Yu. Pikalova, Z.S. Vinokurov et al. // Solid State Ionics. — 2019. — No. 333. — P. 30–37.

19 Rakhadilov B.K. Research of regimes of applying coats by the method of plasma electrolytic oxidation on Ti-6Al-4V / B.K. Rakhadilov, D.R. Baizhan, Zh.B. Sagdoldina, K. Torebek // Bulletin of the University of Karaganda-Physics. — 2022. — No. 1(105). — P. 99-106.

20 Zhao H. Ln_2MO_4 cathode materials for solid oxide fuel cells / H. Zhao, Q. Li, L. Sun // Science China Chemistry. — 2011. — No. 54. — P. 898–910.

21 Kolchugin A.A. Structural, electrical and electrochemical properties of calcium-doped lanthanum nickelate / A.A. Kolchugin, E.Yu. Pikalova, N.M. Bogdanovich et al. — Solid State Ionics. — 2016 — No. 288. — P. 48–53.

К.А. Кутербеков, К.Ж. Бекмырза, А.М. Кабышев,
М.М. Кубенова, Н.К. Айдарбеков, С.А. Нуркенов

Қатты оксидті отын элементтеріне арналған Радлесден-Поппер құрылымы бар материалдардың сипаттамаларын зерттеу

Мақалада $La_2Ni_{1-x}Co_xO_{4+\delta}$ ($0 \le x \le 0.3$) және $Pr_2NiO_{4+\delta}$ лантан никелаты негізіндегі материалдардың сипаттамаларын зерттеу нәтижелері келтірілген. Олардың кристалдық құрылымы және ysz және GDC электролиттік материалдарымен өзара әрекеттесуі 900 °C температурада талданды. Сондай-ақ, ysz электролиттік материалымен байланыста осы материалдардың поляризациялық кедергісі өлшенді. $La_2Ni_{1-x}Co_xO_4$ ($0 \le x \le 0.3$), Pr_2NiO_4 катод материалдары зерттелген. Бұл жағдайда Co-ның төмен концентрациясының лантан никелатының сипаттамаларына әсері алғаш рет қарастырылған. Лантан никелаты мен празеодим никелатына негізделген материалдар ромбтық симметриямен K_2NiF_4 типті (Радлсден-Поппер фазасы) құрылымымен сипатталды. Радлсден-Поппер құрылымы бар материалдар $Zr_{0.84}Y_{0.16}O_{2-\delta}$ (YSZ) және $Ce_{0.73}Gd_{0.27}O_{2-\delta}$ (GDC) электролиттік материалдармен химиялық үйлесімді екендігі көрсетілген. Катодты материалдардың термиялық кеңеюін зерттеу барлық зерттелетін материалдар YSZ және GDC электролиттеріне қарағанда жоғары ТКК-мен сипатталатыны дәлелденген. Жүргізілген зерттеулер негізінде GDC электролиті бар композиттерді қалыптастыру үшін келесі катодты материалдар таңдалды: La_2NiO_4, $La_2Ni_{0.8}Co_{0.2}O_4$, Pr_2NiO_4. Композиттердің агломерация кинетикасы мен ТКК зерттеуі — олардың термиялық сипаттамалары таза катодты материалдарға қарағанда электролиттердің сипаттамаларына едәуір жақын екенін көрсетті.

Кілт сөздер: ҚООЭ, катодты материалдар, өткізгіштік, температуралық кеңею коэффициенті, нано ұнтақтар.

К.А. Кутербеков, К.Ж. Бекмырза, А.М. Кабышев,
М.М. Кубенова, Н.К. Айдарбеков, С.А. Нуркенов

Исследование характеристик материалов со структурой Раддлсдена-Поппера для твердооксидных топливных элементов

В статье представлены результаты исследования характеристик материалов на основе никелата лантана La2Ni1-xCoxO4+δ (0≤x≤0,3) и Pr2NiO4+δ. Проанализированы их кристаллическая структура и взаимодействие с электролитными материалами YSZ и GDC при 900 °C. Определены коэффициенты термического расширения и исследованы температурные зависимости проводимостей. А также измерено поляризационное сопротивление данных материалов в контакте с электролитным материалом YSZ. Были исследованы следующие катодные материалы: $La_2Ni_{1-x}Co_xO_4$ ($0\leq x\leq 0{,}3$), Pr_2NiO_4. При этом впервые было изучено влияние малых концентраций Co на характеристики никелата лантана. Материалы на основе никелата лантана и никелата празеодима характеризовались структурой типа K_2NiF_4 (фазы Раддлсдена-Поппера) с ромбической симметрией. Было показано, что материалы со структурой Раддлсдена-Поппера химически совместимы с электролитными материалами $Zr_{0.84}Y_{0.16}O_{2-\delta}$ (YSZ) и $Ce_{0.73}Gd_{0.27}O_{2-\delta}$ (GDC). Исследование термического расширения катодных материалов показало, что все исследуемые материалы характеризуются более высокими КТР, чем электролиты YSZ и GDC. На основании проведенных исследований были выбраны катодные материалы для формирования композитов с электролитом GDC: La_2NiO_4, $La_2Ni_{0.8}Co_{0.2}O_4$, Pr_2NiO_4. Исследование кинетики спекания и КТР композитов показало, что их термические характеристики значительно ближе к характеристикам электролитов, чем у чистых катодных материалов.

Ключевые слова: ТОТЭ, катодные материалы, проводимость, коэффициент температурного расширения, нанопорошки.

References

1 Ivanov, M., Osipov, V., Kotov, Yu. et al. (2006). Laser synthesis of oxide nanopowders. *Advances in Science and Technology, 45, 291–296.*

2 Chupahina, T.I., Gyrdasova, O.I., & Bazuev, G.V. (2013). Sintez, strukturnye i morfologicheskie kharakteristiki ultradispersnykh poroshkov i keramiki na osnove tverdykh rastvorov La2-xSr0.125PrxNiO4 (0 ≤ x ≤ 1.775) [Synthesis, structural and morphological characteristics of ultrafine powders and ceramics based on solid solutions La2-xSr0.125PrxNiO4 (0 ≤ x ≤ 1.775)]. *Izvestiia Rossiiskoi akademii nauk. Seriia Pizicheskaia — The journal Izvestia of the Russian Academy of Sciences. The series physical, 77, 9, 1276–1280* [in Russian].

3 Boehm, E., Bassat, J.-M., Dordor, P. et al. (2005). Oxygen diffusion and transport properties in non-stoichiometric $Ln_{2-x}NiO_{4+\delta}$ oxides. *Solid State Ionics, 176, 2717–2725.*

4 Mohan Ram, R.A., Ganguly, P., Rao, C.N.R. (1988). Preparation and characterization of $La_2CoO_{4+\delta}$. *Materials Research Bulletin, 23, 501-505.*

5 Hayashi, A., Tamura, H., Ueda, Y. (1993). Successive structural phase transitions in stoichiometric La_2NiO_4 observed by X-ray diffraction. *Physica C, 216, 77-82.*

6 Boehm, E., Bassat, J.-M., Steil, M.C. et al. (2003). Oxygen transport properties of $La_2Ni_{1-x}Cu_xO_{4+\delta}$ mixed conducting oxides. *Solid State Sciences, 5, 973–981.*

7 Amow, G., Whitfield, P.S., Davidson, I.J., Hammond, R.P. (2004). Structural and sintering characteristics of the $La_2Ni_{1-x}Co_xO_{4+\delta}$ series. *Ceramics International, 30, 1635–1639.*

8 Kilner, J.A., Shaw, C.K.M. (2002) Mass transport in $La_2Ni_{1-x}Co_xO_{4+\delta}$ oxides with the K_2NiF_4 structure. *Solid State Ionics, 154–155, 523– 527.*

9 Amow, G., Whitfield, P.S., Davidson, I.J., et al. (2002). Structural and physical property trends of the hyperstoichiometric series $La_2Ni_{(1-x)}Co_xO_{4+\delta}$. Materials Research Society Symposia Proceedings. *Solid State Inorganic Materials IV, 755, DD8.10.1-6.*

10 Munnings, C.N., Skinner, S.J., Amow, G., et al. (2005). Oxygen transport in the $La_2Ni_{1-x}Co_xO_{4+d}$ system. *Solid State Ionics, 176, 1895—1901.*

11 Tsipis, E.V., Kharton, V.V. (2008). Electrode materials and reaction mechanisms in solid oxide fuel cells: a brief review. II. Electrochemical behavior vs. materials science aspects. *Journal of Solid State Electrochemistry, 12, 1367–1391.*

12 Mahato, N., Banerjee, A., Gupta, A. et al. (2015). Progress in material selection for solid oxide fuel cell technology: A review. *Progress in Materials Science, 72, 141–337.*

13 Zhao, H., Mauvy, F. et al. (2008). New cathode materials for ITSOFC: Phase stability, oxygen exchange and cathode properties of $La_{2-x}NiO_{4+\delta}$. *Solid State Ionics, 179, 2000–2005.*

14 Hernandez, A.M., Mogni, L. et al. (2010). $La_2NiO_{4+\delta}$ as cathode for SOFC: Reactivity study with YSZ and CGO electrolytes. *International Journal of Hydrogen Energy, 35, 6031–6036.*

15 Montenegro-Hernandez, A., Vega-Castillo, J. et al. (2011). Thermal stability of $Ln_2NiO_{4+\delta}$ (Ln=La, Pr, Nd) and their chemical compatibility with YSZ and CGO solid electrolytes. *International Journal of Hydrogen Energy, 36, 15704–15714.*

16 Nikonov, A.V., Kuterbekov, K.A., Bekmyrza, K.Zh., Pavzderin, N.B. (2018). A brief review of conductivity and thermal expansion of perovskite-related oxides for SOFC cathode. *Eurasian Journal of Physics and Functional Materials, 2, 274-292.*

17 Richter, J., Holtappels, P. et al. (2009). Materials design for perovskite SOFC cathodes. *Monatshefte für Chemie, 140, 985–999.*

18 Sadykov, V.A., Pikalova, E.Yu., Vinokurov, Z.S. et al. (2019). Tailoring the structural, thermal and transport properties of $Pr_2NiO_{4+\delta}$ through Ca-doping strategy. *Solid State Ionics, 333, 30–37.*

19 Rakhadilov, B.K., Baizhan, D.R., Sagdoldina, Zh.B., Torebek, K. (2022). Research of regimes of applying coats by the method of plasma electrolytic oxidation on Ti-6Al-4V. *Bulletin of the University of Karaganda-Physics, 1(105), 99-106.*

20 Zhao, H., Li, Q., Sun, L. (2011). Ln_2MO_4 cathode materials for solid oxide fuel cells. *Science China Chemistry, 54, 898–910.*

21 Kolchugin, A.A., Pikalova, E.Yu., Bogdanovich, N.M. et al. (2016). Structural, electrical and electrochemical properties of calcium-doped lanthanum nickelate. *Solid State Ionics, 288, 48–53.*

ТЕХНИКАЛЫҚ ФИЗИКА
ТЕХНИЧЕСКАЯ ФИЗИКА
TECHNICAL PHYSICS

DOI 10.31489/2022PH4/48-55

UDC 621.37

K.M. Makhanov*, N.B. Kurmanaliyev, S.B. Musepov, A.K. Naptalov, K.Z. Kenzhalieva

Karaganda University of the name of academician E.A. Buketov, Kazakhstan
**E-mail: makanov@inbox.ru*

Development of the wiring diagram of the device based on the LoRa module RAK3172

The paper presents the results of the development of circuitry of electronic device for the acquisition and transmission of telemetry data. The purpose of this work is to design and develop circuitry of the device for data acquisition using LoRa technology. The integrated end-to-end design environment Altium Designer was used to develop the electronic part of the device. The STM32F407VGT6 series microcontroller was used as the central control unit. A LoRa RAK3172 radio module is provided in the circuit for receiving and transmitting data. Unlike previous series, this module is equipped with a UART interface, which greatly simplifies the process of designing and writing a program for control. In this article the relevance of developing device with the use of LoRa-technology is considered. The theoretical basis of LoRa-modulation is briefly considered. The main section presents the results of the circuit design of the device, in particular, the inclusion diagram of the module and the control microcontroller. The information presented in the paper reflects only that part of the developed device, which is related to LoRa technology. In general, this work is part of a much larger project, which involves the use of GSM, Wi-Fi, RFID technology. Circuit of power supply is designed for 220 volt AC voltage with further transformation to +12V.

Keywords: LoRa module, STM32 microcontroller, LFM modulation, electric circuit, modulation, gateway, design, circuitry, development, Altium Designer, radio channel.

Introduction

In the context of global digitalization, Internet of Things (IoT) technologies are gaining momentum [1-3]. New types of LPWAN (Low Power Wide Area Networks) have emerged to effectively solve the problems associated with energy consumption. Technologies that enable the connection of autonomous devices to the WAN appeared in 2015-2016 and are now rapidly gaining popularity [4]. The most polar among such technologies are LoRa, SIGFOX, NB-IoT, Weightless P, etc. In most of the published papers [5] it is noted that the use of LoRaWAN protocol in various industries and housing and communal services (HCS) has good prospects.

A module operating in the frequency range 868/433 MHz is embedded in each meter. These are the unlicensed frequencies used by the LoRa standard. LoRa (Long Range) modulation technology is a modulation method that provides a significantly greater communication range (coverage area) than other competing methods. The method is based on spread spectrum modulation and a variation of linear frequency modulation (Chirp Spread Spectrum, CSS) with integrated Forward Error Correction (FEC).

An important element of the system is the base station (gateway), the purpose of which is to collect readings from meters and transmit them over the Internet to the data collection server for further processing and analysis. Theoretically, in a city environment, the base station can cover a zone with a radius of up to 15 km. In practice, the coverage radius is about 2-3 km.

All of the meters from nearby houses that are within its range transmit data to it via radio channel. The base station transmits the received information to the data collection server, where it is further processed under the control of the software.

Application of LoRa technology makes it possible to assemble a variety of devices into a single system: security devices, lighting lamps, metering devices for resource consumption (heat, electricity, water, gas), vehicle sensors (which are used to control movement and fuel consumption), etc.

Thus, fundamentally new solutions in the field of communication services, monitoring, telematics, telemechanics, dispatching, Smart House, Smart City systems, etc. are created.

In the basis of the considered technology LoRa signals are oscillations with linear frequency modulation (LFM-modulation), the frequency of these oscillations can both linearly increase and linearly decrease. LFM signals are complex signals with a basis much larger than unity, respectively, their correlation function will be sufficiently narrow compared to the simple signals [5]. Mathematical description can be expressed by formula (1):

$$s = A * \cos * \left(2\pi \left(f * t_1 + \frac{mt^2}{2} \right) \right) \tag{1}$$

here f_1 is the lower frequency (frequency at which the LFM oscillation begins); m is the signal frequency change rate, determined by the formula:

$$m = \frac{BW}{T_S} \tag{2}$$

where BW is the signal spectrum width (125, 250 and 500 kHz);

Ts — duration of one LFM oscillation:

$$T_S = \frac{2^{SF}}{BW} \tag{3}$$

here SF (Spreading Factor) — spectrum expansion factor, it takes the following values SF = 7...12. It determines the bit depth of the data symbol (in bits) transmitted during Ts, and also affects the signal base. Increase SF greatly increases noise immunity of the transmitted message up to transfer at a negative signal/noise ratio, but at the same time increases the transfer time. The signal base is calculated by the formula

$$B = BW * T_S = 2^{SF} \tag{4}$$

According to [6] the coded information symbol defines the frequency by the value of which the LFM oscillation is shifted. That is, the frequency with which LFM oscillation generation begins is determined by the value of the information symbol in decimal notation system (5):

$$df = \frac{k}{T_S} \tag{5}$$

here k is the current value of the information symbol.

At time T_S — T_0 (6) the LFM oscillation reaches the maximum frequency, after which the generation of a new LFM oscillation begins from the lower frequency $f_1$and stops when it reaches the frequency df. The duration of the new LFM oscillation is T_0:

$$T_0 = \frac{k}{BW} \tag{6}$$

In general, according to [7], the modulated oscillation is described by the expression (7):

$$s(t) = \begin{cases} A\cos\left(2\pi\left(f_0 t + dft + \frac{mt^2}{2}\right)\right), 0 \le t < T_0 \\ A\cos\left(2\pi\left(f_0 t + dft + \frac{mt^2}{2}\right)\right), T_0 \le t < T_S \end{cases} \quad (7)$$

Despite the presence of a large number of publications, currently there are no publications devoted directly to the development of devices based on LoRa-module. The review has shown [1-4] that practically all available developments are based on the application of ready-made modular solutions. Mainly based on the Arduino platform.

The purpose of this work is to develop and design the circuitry of a combined data acquisition device using LoRa technology.

This paper presents the results of design and development of a combined telemetry data acquisition and transmission device. In particular, one of the data acquisition-transfer interfaces is a LoRa module RAK3172. As the control unit used microcontroller series STM32F407XX. The development of the device circuit was performed in the integrated end-to-end design environment Altium Designer.

Experimental

The developed scheme of the device is designed for use in data collection systems from heat meters. Currently meters (water, gas, heat and electricity) have either pulse output or interface output. Pulse output is considered obsolete and has a number of shortcomings. Meters with an interface output are the most promising, but they are also more complex to implement. Unfortunately, there is no "universal" approach that provides zero-modem connection. The fact that counter manufacturers often do not care about minimizing traffic when developing their devices, which is very important for LoRa-technology. This will inevitably lead to loss of stability of LoRa-network even at its low density. Therefore, in the framework of the implemented work, we plan to solve these contradictions at the level of the "driver" of the developed device. In this paper, the primary results related to the circuit design of the device are presented. As the next stages are completed, we plan to publish additional materials.

Figure 1 shows the wiring diagram of the RAK3172 module. Two interfaces are provided for communication in this module. A high speed, synchronous SPI interface and a lower speed, two wire UART interface. There are two UART interfaces on board this module. As you can see from the figure, we have used UART 2 in the schematic.

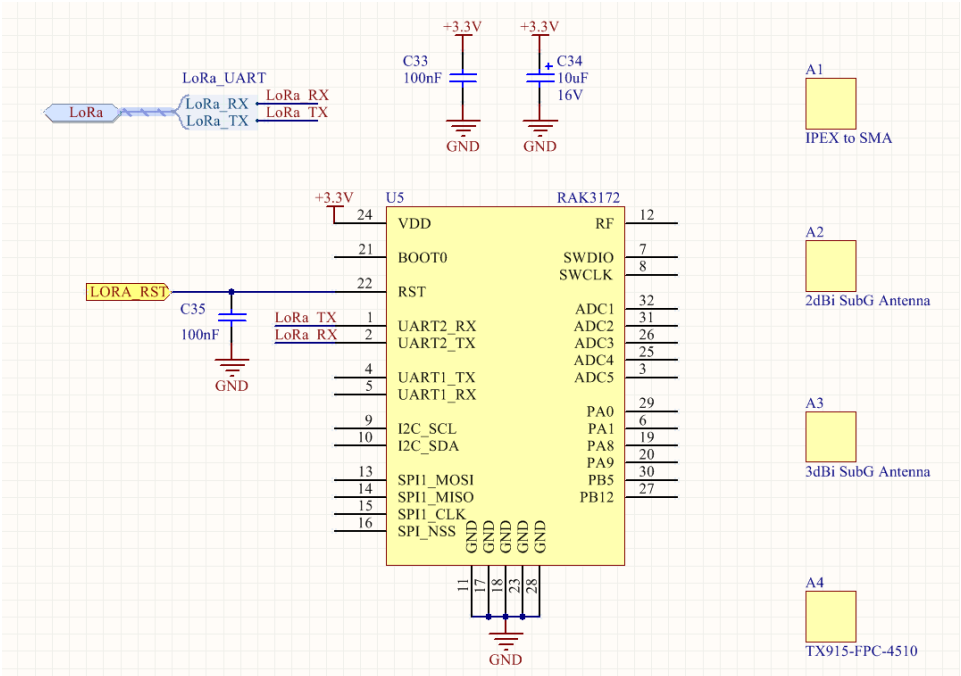

The use of the module RAK3172 in this work is due to the fact that it provides the possibility of using the UART interface. In earlier versions of the module, the use of this interface is not provided, which in turn affected the volume and complexity of the control program.

Both hardware and software options are available to "reset" the module. In this case the output "LORA_RST" provides the possibility to reset the microcontroller programmatically. This function will be used when it is necessary to remotely re-flash or update the control program of the microcontroller.

As noted above, the circuits presented in the paper are part of a more complex combined device circuit. Accordingly, the component numbers in the circuits are also in through order. For example, the power supply circuit of the module, as a rule, includes the device protection for power supply and pulse filtering. And as we can see from this circuit (Figure 1), capacitors *C33* and *C34* are provided for this purpose. It should also be noted that the connection to the main components of the circuit is organized using the “Harness”, which increases the simplicity and at the same time clarity of the connections used in the circuit.

Figure 2 shows the appearance of the circuit, which can be conditionally called "basic". It combines the inclusion of both LoRa module and other functional units not reflected in this article (GSM, USB, temperature sensor).

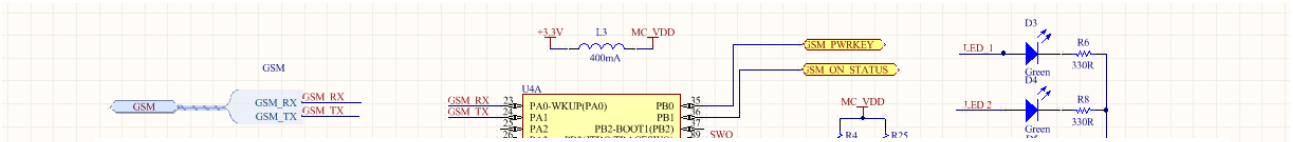

Figure 1. LoRa module RAK3172 wiring diagram

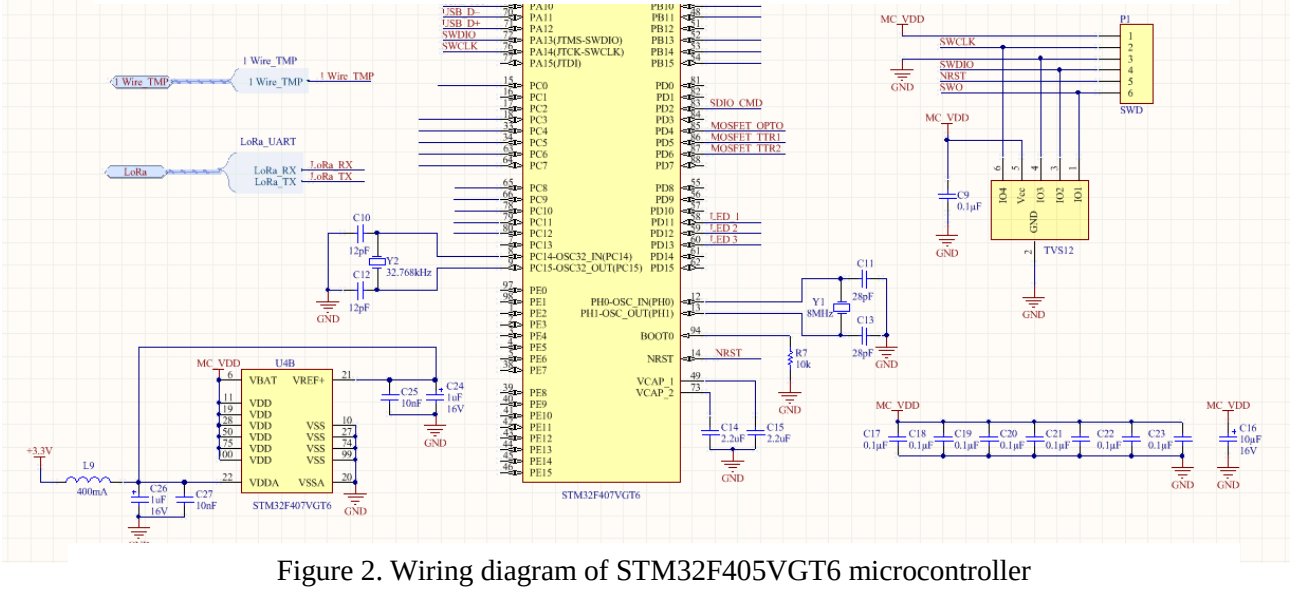

Figure 2. Wiring diagram of STM32F405VGT6 microcontroller

This schematic shows the inclusion of the LoRa interface discussed in the article, the programming node and components to stabilize the microcontroller power.

As can be seen from this figure, two quartz resonators are used in the circuit. One for 32.768 MHz (ECX-31B), the other for 8 MHz (ABM3-8.000MHZ-D2Y-T). According to the "technical documentation" it is recommended to install 12 pF capacitors on the 32.768 MHz resonator. However, at frequencies above 20 MHz quartz resonators are known to operate without interruption and require no additional tuning. In the case of low frequency resonators, the calculation of the capacitance of the used capacitors is required. In the "technical documentation" for the ABM3-8.000MHZ-D2Y-T resonator, it is noted that the load capacitance is determined by the parameters of the external capacitors C_{L1} and C_{L2} and the parasitic capacitance of the circuit board and connections (*Cs*). In this case the capacitance value for C_{L1} and C_{L2} recommended by the manufacturer is 18pF.

In order to accurately determine the parasitic capacitance of the microcontroller ports and the PCB capacitance, measurements must be made. To make preliminary calculations, manufacturers recommend assuming a *Cs* value in the range of 3 — 5pF. Manufacturers recommend these values based on requirements for keeping the quartz resonator as close as possible to the microcontroller's chassis. These *Cs* values accordingly take into account two specific cases. For shortest possible proximity *Cs* = 3pF. For the longest possible distant resonator position *Cs* = 5pF. The value *Cs* = 4 corresponds to the average position distance of the quartz resonator.

Thus, we have the following input data:

C_L = 18 pF, *Cs* = 3 pF, *Cs* = 4 pF, *Cs* = 5 pF

To calculate the capacity of external capacitors ($C_{L1,2}$) including parasitic capacitance, expression (8) recommended by the manufacturer was used:

$$C_L = \frac{C_{L1} * C_{L2}}{C_{L1} + C_{L2}} + C_S \qquad (8)$$

It follows that the capacitance of the capacitors must be:

For *Cs* = 3 pF $\quad C_{L1,2} = 2(C_L - C_S) = 2(18-3) = 30\,pF$

For *Cs* = 4 pF $\quad C_{L1,2} = 2(C_L - C_S) = 2(18-4) = 28\,pF$

For *Cs* = 5 pF $\quad C_{L1,2} = 2(C_L - C_S) = 2(18-5) = 26\,pF$

At this point, we have pre-included 28 pF capacitors into the circuit.

However, when testing the finished device, additional measurements will be taken to determine the loading capacity (C_L), since the manufacturer's recommended value is given as the maximum possible value.

Figure 3 shows a schematic of the electrical power supply. AC voltage from 220 volt mains is used as the main power supply. The circuit is provided with protection against electromagnetic interference and mains voltage ripple. As a converter of alternating voltage CBM70S120 (production Cincon) is used. Small dimensions (61x57.9x17 mm) allow installing the converter directly on the surface of a printed circuit board. The circuit node consisting of Schottky diode (*D10*), *p*-channel field effect transistor (*VT1*) and two resistors (*R23* and *R24*) performs the function of power switch to battery *J3*. The logic behind this node is as follows: when there is electrical power at the *+Vout* output of the *U12* converter, the «drain-source» channel of transistor *VT1* is closed. The device receives 12 volt electrical power from the *12_VDD* point. In the case where there is no 12 volts at the *+Vout* output of the *U12* converter, the «drain-source» channel of transistor *VT1* opens. In this case, the device receives electric power from the emergency battery pack. However, as noted in the technical documentation of *VT1* (Si3493DDV) transistor, the total turn-on and turn-off delay of the «drain-source» junction is less than 200 ns. This allows this transistor to be used as a high-speed switch.

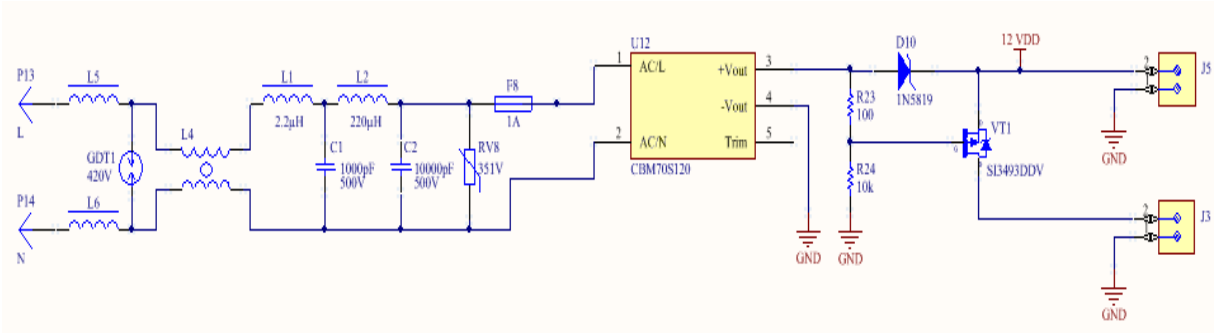

Results and discussion

To create a network using LoRAWAN technologies it is necessary to use a base station for data collection, called — gateway. The device developed in this work is a kind of "end-device" that directly collects data from the connected sensors.

The central link in the chain "end-device — gateway — server" is the gateway. The gateway's task is to receive data from the "end device" and then transmit it to the server for further processing or storage.

As a base station, we use the gateway brand RAK7258. To use this unit as a base station, you need to register it on the network and attach it to a server. The server can be either private or public. In our case, we

Figure 3. Schematic diagram of the electrical power supply to the device

used "The Things Network" server. This server is provided for free by the LoRa technology manufacturers for their customers. After registration on the server, we received a "Key Gateway" key. With the help of this key we need to connect the "end device" to the base station.

Figure 4 shows the appearance of the registration page on the server.

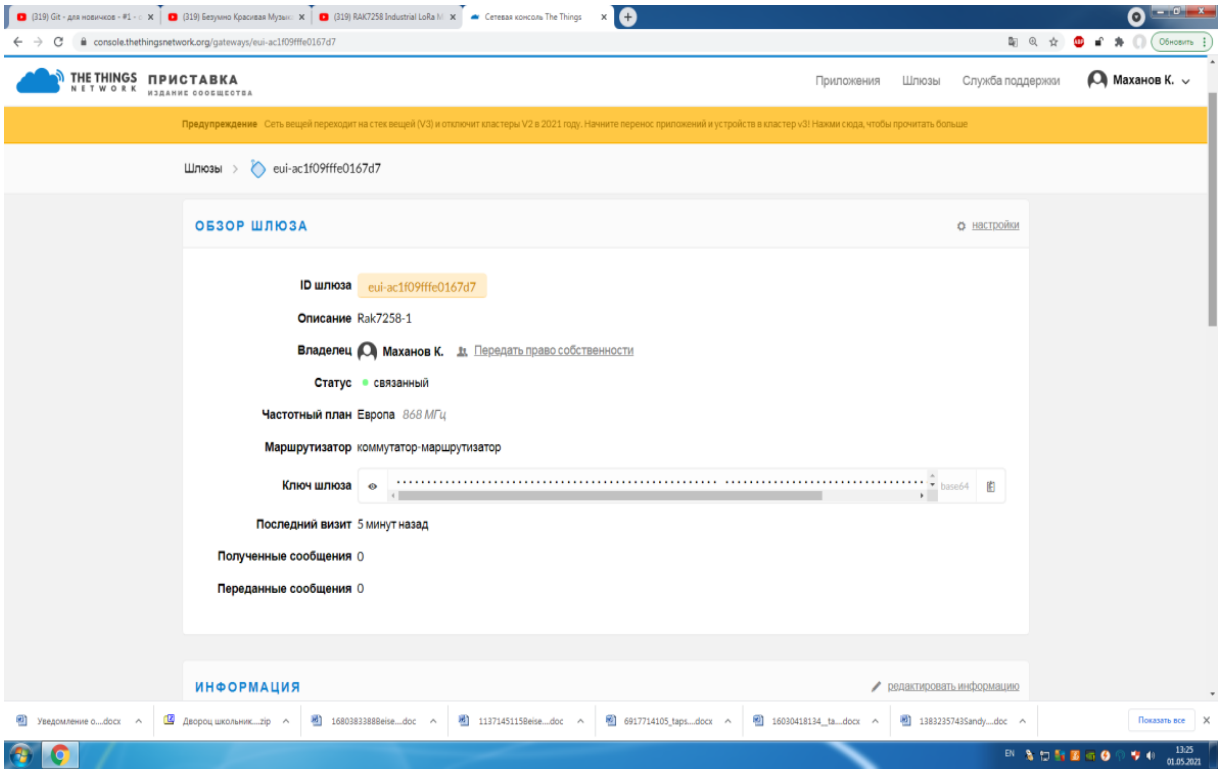

Figure 4. Registration on The Things Network server

Conclusion

In the course of the work the wiring diagram for the design of the circuit board and the whole device based on the wireless LoRa transmitter RAK3172 was developed. The choice of this series was due to the possibility of using UART interface and easier to implement AT commands.

The device power supply circuitry provides protection against electromagnetic interference and electrostatic discharges. Parameters of used components are calculated with regard to the requirements of GOST 30804.4.4-2013 (2 — degree of rigidity).

Because of limiting values of circuit board stray capacitance Cs = 3pF — 5pF and manufacturer's recommended load capacitance C_L = 18pF the capacitance of external capacitors ($C_{L1,2}$) is calculated for 8 MHz quartz resonator. However, it should be noted that the manufacturer has recommended limiting values *of Cs*. Hence it follows that in the process of making the PCB of the device it is necessary to

make an additional value of *Cs*. And if necessary, make an additional calculation of the capacitance of external capacitors.

To control operation of the developed device and subsequent data collection, we carried out work on registration of the gateway RAK7258. At the moment, registration has been successfully completed and an access key from "The Things Network" server has been obtained to connect "end devices" to the base station.

References

1 Кучерявый А.Е. Интернет вещей / А.Е. Кучерявый // Электросвязь. — 2013. — № 1. — С. 21–24.

2 Кучерявый А.Е. Самоорганизующиеся сети / А.Е. Кучерявый, Е.А. Кучерявый, А.В. Прокопьев. — СПб.: Любавич, 2011. — С. 312.

3 Киричек Р.В. Эволюция исследований в области беспроводных сенсорных сетей / Р.В. Киричек, А.И. Парамонов, А.В. Прокопьев, А.Е. Кучерявый // Информационные технологии и телекоммуникации. — 2014. — Т. 4. — № 8. — С. 29–41.

4 Кучерявый А.Е. Перспективы научных исследований в области сетей связи на 2017–2020 годы / А.Е. Кучерявый, А.Г. Владыко, Р.В. Киричек, М.А. Маколкина, А.И. Парамонов, А.И. Выборнова, Р.Я. Пирмагомедов // Информационные технологии и телекоммуникации. — 2016. — Т.4. — № 3. — С. 1–14.

5 Сарьян В.К. Прошлое, настоящее и будущее стандартизации Интернета вещей / В.К. Сарьян, Н.А. Сущенко, И.А. Дубнов // Тр. Научно-исследовательского института: радиожурнал. — 2014. — № 1. — С. 2–7.

6 Талаев А.Д. Стандарты LPWAN для группового взаимодействия мобильных узлов / А.Д. Талаев, В.В. Бородин // Тр. Моск. авиацион. ин-та. — 2018. — № 99. — С. 22–28.

7 Белов С.П. Исследование функции неопределенности псевдослучайных сигналов с линейной частотной модуляцией / С.П. Белов, Е.Г. Жиляков, И.А. Сидоренко // Вопросы радиоэлектроники. Сер. «РЛТ». — 2008. — № 4. — С. 100–109.

Қ.М. Маханов, Н.Б. Құрманалиев, С.Б. Мүсепов, А.Қ. Напталов, Қ.З. Кенжалиева

RAK3172 LoRa модулінің негізінде құрылғыны қосу схемасын әзірлеу

Жұмыста телеметриялық мәліметтерді жинауға және таратуға арналған электрондық құрылғының схемасын әзірлеу нәтижелері келтірілген. Бұл жұмыстың мақсаты LoRa технологиясын қолдана отырып, деректерді жинауға арналған құрылғы схемасын жобалау және әзірлеу. Құрылғының электронды бөлігін әзірлеу үшін басынан соңына дейін жобалауға мүмкіндік беретін Altium Designer ортасы пайдаланылды. Орталық басқару блогы ретінде STM32F407VGT6 сериясының микроконтроллері қолданылды. Деректерді қабылдау және тарату үшін схемада LoRa RAK3172 модулін қолдану ескерілген. Алғашқы сериялармен салыстырғанда, бұл модуль UART интерфейсімен жабдықталғандықтан басқару бағдарламасын жобалау және жазу процестері айтарлықтай жеңілдетілген. Мақалада LoRa технологиясын қолданатын құрылғыларды әзірлеудің өзектілігі талқыланған. LoRa модуляциясының теориялық негіздері қысқаша қарастырылған. Негізгі бөлімде құрылғының схемасын құрастыру нәтижелері берілген. Атап айтқанда, модульді және басқару микроконтроллерін қосу схемасы. Сонымен қатар мақалада келтірілген ақпарат LoRa технологиясымен байланыстырылатын құрылғының бір бөлігін ғана көрсетеді. Жалпы, бұл жұмыс GSM, Wi-Fi, RFID технологияларын қолдануды көздейтін әлдеқайда ауқымды жобаның бөлігі болып табылады. Қоректендіру тізбегі айнымалы 220 В кернеуден қоректендіріліп, кейін +12 В-қа түрлендіріледі.

Кілт сөздер: LoRa модулі, STM32 микроконтроллері, СЖМ модуляциясы, электр тізбегі, модуляция, шлюз, дизайн, схема, әзірлеу, Altium Designer, радиоарна.

К.М. Маханов, Н.Б. Курманалиев, С.Б. Мусепов, А.К. Напталов, К.З. Кенжалиева

Разработка схемы подключения устройства на базе LoRa модуля RAK3172

В статье представлены результаты разработки схемотехники электронного устройства сбора и передачи данных телеметрии. Целью данной работы является проектирование и разработка схемы устройства для сбора данных с использованием технологии LoRa. Для разработки электронной части устройства использовалась интегрированная среда сквозного проектирования Altium Designer. В качестве центрального блока управления применен микроконтроллер серии STM32F407VGT6. В схеме

предусмотрен модуль LoRa RAK3172 для приема и передачи данных. В отличие от предыдущих серий, этот модуль оснащен интерфейсом UART, что значительно упрощает процесс проектирования и написания программы для управления. В данной работе рассмотрена актуальность разработки устройств с использованием LoRa-технологии. Кратко изучены теоретические основы LoRa-модуляции. В основном разделе представлены результаты схемотехнического проектирования устройства, в частности, схема включения модуля и управляющего микроконтроллера. Информация, представленная авторами статьи, отражает только ту часть разрабатываемого устройства, которая связана с технологией LoRa. В целом, эта работа является частью гораздо более крупного проекта, в котором предполагается использование технологий GSM, Wi-Fi, RFID. Схема питания рассчитана на переменное напряжение 220 В с последующим преобразованием в +12 В.

Ключевые слова: модуль LoRa, микроконтроллер STM32, модуляция ЛЧМ, электрическая схема, модуляция, шлюз, проектирование, схемотехника, разработка, Altium Designer, радиоканал.

References

1 Kucheriavyi, A.E. (2013) *Internet veshchei [Internet of Things]*. Elektrosviaz — Telecommunications, 1, 21–24 [in Russian].

2 Kucheriavyi, A.E. (2011). *Samoorganizuiushchiesia seti [Self-organizing networks]*. Saint Petersburg: Liubavich [in Russian].

3 Kirichek, R.V., Paramonov, A.I., Prokopev, A.V., & Kucheriavyi, A.E. (2014). Evoliutsiia issledovanii v oblasti besprovodnykh sensornykh setei [The evolution of wireless sensor network research]. *Informatsionnye tekhnologii i telekommunikatsii — Information technology and telecommunications*, 4, 8, 29–41 [in Russian].

4 Kucheriavyi, A.E., Vladyko, A.G., Kirichek, R.V., Makolkina, M.A., Paramonov, A.I., Vybornova, A.I., & Pirmagomedov, R.Ya. (2016). Perspektivy nauchnykh issledovanii v oblasti setei sviazi na 2017–2020 gody [Prospects for scientific research in the field of communication networks for 2017–2020]. *Informatsionnye tekhnologii i telekommunikatsii — Information technology and telecommunications*, 4, 3, 1–14 [in Russian].

5 Sarian, V.K., Sushchenko, N.A., & Dubnov, I.A. (2014). Proshloe, nastoiashchee i budushchee standartizatsii Interneta veshchei [The Past, Present and Future of IoT Standardization]. *Trudy Nauchno-issledovatelskogo instituta: radiozhurnal — Proceedings of the Scientific Research Institute radio magazine*, 1, 2–7 [in Russian].

6 Talaev, A.D., & Borodin, V.V. (2018). Standarty LPWAN dlia gruppovogo vzaimodeistviia mobilnykh uzlov [LPWAN standards for group communication of mobile nodes]. *Trudy Moskovskogo aviatsionnogo instituta — Proceedings of the Moscow Aviation Institute*, 99, 22–28 [in Russian].

7 Belov, S.P., Zhiliakov, E.G., & Sidorenko, I.A. (2008). Issledovanie funktsii neopredelennosti psevdosluchainykh signalov s lineinoi chastotnoi moduliatsiei [Investigation of the uncertainty function of pseudo-random signals with linear frequency modulation]. *Voprosy radioelektroniki. Seriia «RLT» — Questions of radio electronics. Series "RLT"*, 4, 100–109 [in Russian].

DOI 10.31489/2022PH4/56-64

UDC 621.3.01

S. Katsyv[1], V. Kukharchuk[1], V. Madyarov[1], V. Holodiuk[1],
V. Kucheruk[2,3], P. Kulakov[2], M. Hribov[4]

[1]Vinnytsia National Technical University, Vinnytsia, Ukraine;
[2]Uman National University of Horticulture, Uman, Ukraine;
[3]Vinnytsia National Agrarian University, Vinnytsia, Ukraine;
[4]National Academy of Internal Affairs, Kyiv, Ukraine.
(E-mail: vladimir.kucheruk@gmail.com)

Non-standard analysis in electrical engineering. Transient analysis in second-order electrical circuits with violation of switching laws

For the first time, the authors proposed the use of the mathematical apparatus of non-standard analysis to solve certain non-trivial problems of theoretical electrical engineering. It was established that the axiomatics of non-standard analysis allows to simplify the analysis of transient processes in high-order electric circuits when the switching laws are violated. It is shown that the application of non-standard analysis methods in theoretical electrical engineering provides an opportunity to use the traditional classical method of transient processes analysis of circuits with violation of switching laws. Only by using methods of non-standard analysis, it is possible to strictly prove the fulfillment of the law of energy conservation in such schemes. Also, examples of solving such tasks are given. It is recommended to expand the scope of application of non-standard methods of analysis in problems of various branches of science and technology, which use differential calculus and boundary transitions, and the solution of which is limited or impossible by standard approaches.

Keywords: infinitesimal number, infinitely large number, hyperreal number, non-standard number, standard number, second-order transition process.

Introduction

In solving various scientific and technical problems, such as calculating derivatives and determining the coefficients of infinite series in mathematical analysis, DC circuit analysis with ideal reactive elements and determining the coefficients of ideal reactive four-pole circuits in theoretical electrical engineering, the researcher occasionally meets uncertainty like $\frac{0}{0}$. At the same time, there is a number of problems when using classical methods that quite often lead to certain complications. In the case of classical mathematical analysis, derivative calculations sometimes is time-consuming, but generally accepted and does not cause any problems, then in problems of theoretical electrical engineering, the situation is more complicated. So, for example, to analyze the steady modes of DC circuits with ideal inductances and capacitances by classical method, it is necessary to calculate the transient process and obtain the established value based on these results. If the electrical circuit is relatively simple, then this task does not cause complications. But if a circle has a significant number of reactive elements, the characteristic equation of the transition process has a large order, then the solution can be obtained only by numerical methods. Therefore, for such tasks it is proposed to use ideas and methods of non-standard analysis. It is interesting that the ideas of non-standard analysis (viz. the direct use of infinitesimal numbers) were the foundation on which Leibniz and Newton intuitively built the principles of differential and integral calculations. But later, in the works of Cauchy and other mathematicians, infinitesimal numbers were "withdrawn from circulation" and the mathematical apparatus of differential and integral calculus was based on numerical and functional sequences and limit ratios [1-5]. This increased the axiomatic rigor of the mathematical apparatus, but unfortunately made it difficult to solve a certain range of problems.

The revival of the ideas of non-standard analysis took place in the 60s of the last century, when A. Robinson proposed a new axiomatics of mathematical analysis, which is based on a set of hyperreal numbers, containing in addition to the so-called standard (ordinary real), non-standard numbers (infinitely large and their combinations with ordinary real) numbers [6-8].

In previous works, the problems of DC circuits analysis with ideal reactive elements in steady state [9-10], as well as the transient analysis with violation of the switching laws in first-order circuits [11]. Methods of nonstandard analysis are being developed at the present time and are used in different fields of science

[12-15]. Of interest is the use of nonstandard analysis methods in the problems of identifying the internal parameters of electrical motors, which in many cases cannot be solved by traditional methods [16-20].

Typically, the energy characteristics of inductors and capacitors are used in conjunction with the laws of electrical engineering to solve such problems, which greatly complicates the analysis of such circuits, especially for complex circuits. Therefore, it is important to use the mathematical apparatus of non-standard analysis, which will use known unified methods to calculate such circuits.

The purpose of this work is to analyze the transients with the violation of the switching laws in the second order circuits. The following section summarizes the basic principles of non-standard analysis that are needed to solve the above electrical problems.

Basic principles of non-standard analysis

Let R be an ordered set of real numbers. The number α will be called infinitesimal number if and only if

$$\forall r \in R(\alpha < r), \tag{1}$$

where r is an arbitrary real number.

We will call the number $\beta = \frac{1}{\alpha}$ an infinitely large number. In this case, it is possible to write

$$\forall r \in R(\beta > r). \tag{2}$$

All algebraic operations (addition, subtraction, multiplication, division, squaring, etc.) and theorems (commutativity, associativity, etc.) can be applied to infinitesimal and large numbers.

We will distinguish between infinitesimal and large numbers of different orders, such as:

- $\alpha > \alpha^2 > \alpha^3 > \alpha^k$- infinitesimal numbers of the first, second, third, k-th order;
- $\beta < \beta^2 < \beta^3 < \beta^k$- infinitely large numbers of the first, second, third, k-th order.

Together with real numbers $r \in R$, infinitesimal and large numbers form an ordered set of hyperreal numbers $*R$. It is customary to call real numbers $r \in R$ standard or Archimedean in contrast to non-standard (non-Archimedean) numbers $*r \in *R$.

Each non-standard number contains a standard part

$$*r = r \pm \alpha, \tag{3}$$

i.e.

$$r = st(*r), \tag{4}$$

in other words, an ordinary real number is a standard part of some non-standard number (obviously, such numbers quantity can be infinite).

Two standard numbers a and b are called equal if and only if

$$a - b = 0. \tag{5}$$

Two non-standard numbers $*a$ and $*b$ are called equivalent (or infinitely close to each other) if and only if

$$*a - *b \approx \alpha. \tag{6}$$

The notation $\approx$ will mean the equivalence of two non-standard numbers.

For standard numbers m and n write some relations that follow from (1 — 6):

$$\frac{1}{\alpha^k} = \beta^k, \frac{m}{\alpha} = m\beta, \frac{m}{\alpha^k} = m\beta^k \tag{7}$$

$$\frac{m\alpha}{n\alpha} = \frac{m}{n}, \frac{m\alpha}{n} = \frac{m}{n}\alpha, \frac{m}{n\alpha} = \frac{m}{n}\beta \tag{8}$$

$$m\alpha + n \approx n, m\beta + n \approx m\beta, m\alpha^k + n \approx n, m\beta^k + n \approx m\beta^k \tag{9}$$

$$\sin\alpha \approx \alpha, \cos\alpha \approx 1, tg\alpha \approx \alpha, ctg\alpha \approx \beta \tag{10}$$

Here are some examples of usage. These methods in mathematical analysis.

Find, for example, the first derivative of the function $y = x^5$, for which we introduce a substitution $dx = \alpha$.

$$\frac{dy}{dx} = \frac{(x+\alpha)^5 - x^5}{\alpha} = \frac{x^5 + 5x^4\alpha + 10x^3\alpha^2 + 10x^2\alpha^3 + 5x\alpha^4 + \alpha^5 - x^5}{\alpha} =$$
$$= 5x^4 + 10x^3\alpha + 10x^2\alpha^2 + 5x\alpha^3 + \alpha^4 \approx 5x^4.$$

The derivative of the function $y = \frac{1}{x^2}$ can be found as

$$\frac{dy}{dx} = \frac{\frac{1}{(x+\alpha)^2} - \frac{1}{x^2}}{\alpha} = \frac{\frac{1}{x^2+2x\alpha+\alpha^2} - \frac{1}{x^2}}{\alpha} = \frac{\frac{x^2-x^2-2x\alpha-\alpha^2}{x^4+2x^3\alpha+x^2\alpha^2}}{\alpha}$$
$$= \frac{-2x\alpha-\alpha^2}{x^4\alpha+2x^3\alpha^2+x^2\alpha^3} = \frac{-2x-\alpha}{x^4+2x^3\alpha+x^2\alpha^2} \approx \frac{-2x}{x^4} = \frac{-2}{x^3}.$$

For $y = sin\, x$ get

$$\frac{dy}{dx} = \frac{sin(x+\alpha)-sin\, x}{\alpha} = \frac{sin\, x \cdot cos\, \alpha + sin\, \alpha \cdot cos\, x - sin\, x}{\alpha} \approx \frac{sin\, x \cdot 1 + \alpha \cdot cos\, x - sin\, x}{\alpha} \approx cos\, x.$$

Let $y = cos\, x$. Then

$$\frac{dy}{dx} = \frac{cos(x+\alpha)-cos\, x}{\alpha} = \frac{cos\, x \cdot cos\, \alpha - sin\, x \cdot sin\, \alpha - cos\, x}{\alpha} \approx \frac{cos\, x \cdot 1 - sin\, x \cdot \alpha - cos\, x}{\alpha} \approx -sin\, x.$$

If $y = tgx$

$$\frac{dy}{dx} = \frac{\frac{sin(x+\alpha)}{cos(x+\alpha)} - \frac{sin\, x}{cos\, x}}{\alpha} = \frac{\frac{sin\, x \cdot cos\, \alpha + sin\, \alpha \cdot cos\, x}{cos\, x \cdot cos\, \alpha - sin\, x \cdot sin\, \alpha} - \frac{sin\, x}{cos\, x}}{\alpha} =$$
$$\frac{cos\, x \cdot sin\, x \cdot cos\, \alpha + sin\, \alpha \cdot cos^2 x - sin\, x\, cos\, x \cdot cos\, \alpha + sin^2 x \cdot sin\, \alpha}{\alpha\, cos^2 x \cdot cos\, \alpha - \alpha\, cos\, x \cdot sin\, x \cdot sin\, \alpha} \approx$$
$$\approx \frac{\alpha(cos^2 x + sin^2 x)}{\alpha\, cos^2 x - \alpha^2\, cos\, x \cdot sin\, x} \approx \frac{cos^2 x + sin^2 x}{cos^2 x - \alpha\, cos\, x \cdot sin\, x} \approx \frac{1}{cos^2 x}.$$

In the case of $y = ctgx$

$$\frac{dy}{dx} = \frac{\frac{cos(x+\alpha)\, sin(x+\alpha)}{sin(x+\alpha)} - \frac{cos\, x}{sin\, x}}{\alpha} = \frac{\frac{cos\, x \cdot cos\, \alpha - sin\, x \cdot sin\, \alpha}{sin\, x \cdot cos\, \alpha + sin\, \alpha \cdot cos\, x} - \frac{cos\, x}{sin\, x}}{\alpha} =$$
$$\frac{sin\, x\, cos\, x \cdot cos\, \alpha - sin^2 x \cdot sin\, \alpha - cos\, x\, sin\, x \cdot cos\, \alpha - sin\, \alpha \cdot cos^2 x}{\alpha\, sin^2 x \cdot cos\, \alpha + \alpha\, sin\, \alpha \cdot cos\, x\, sin\, x} \approx$$
$$\approx \frac{-\alpha(sin^2 x + cos^2 x)}{\alpha\, sin^2 x + \alpha^2\, cos\, x \cdot sin\, x} \approx \frac{-(sin^2 x + cos^2 x)}{sin^2 x + \alpha\, cos\, x \cdot sin\, x} \approx \frac{-1}{sin^2 x}.$$

In addition, the problems of classical transient analysis in electrical circuits require the direct use of standard numbers 0 and infinite quantities ∞, so we formulate their non-standard interpretation.

The standard number 0 in non-standard analysis can be considered as an infinitesimal number of infinitely large order, that is $0 \approx \alpha^{\beta}$, therefore

$$\frac{0}{\alpha} \approx 0,\ 0 \cdot \beta \approx 0,\ e^{-\beta \cdot 0} \approx 1,\ e^{-\alpha} \approx 1 \quad (11)$$

An infinite quantity ∞ in a non-standard analysis can be represented as an infinitely large number of infinitely large order, that is $\infty \approx \beta^{\beta}$, therefore

$$\frac{\infty}{\beta} \approx \infty,\ \infty \cdot \alpha \approx \infty,\ e^{-\infty \cdot \alpha} \approx \alpha,\ e^{-\beta} \approx \alpha \quad (12)$$

Before proceeding to the use of the above expressions to solve various applied problems, we will note that there are no general rules for choosing a parameter that should be equated to an infinitesimal (or infinitely large) number. This choice is made by the researcher depending on the context of a particular task. It should be borne in mind that in the case of the need to replace infinitesimal numbers of several dissimilar parameters of one problem, determining the relationship between these numbers is a difficult problem and sometimes requires additional research.

Transient analysis in the 2nd order circuits with violation of switching laws

Example. Determine the transient voltages at the capacitors and the current in the inductor in the circuit shown in Fig. 1, *a*.

Circuit parameters: $U = 100$ V, $r_1 = 50$ Ohm, $L_1 = 100$ mH, $C_2 = 100$ uF, $C_3 = 150$ uF.

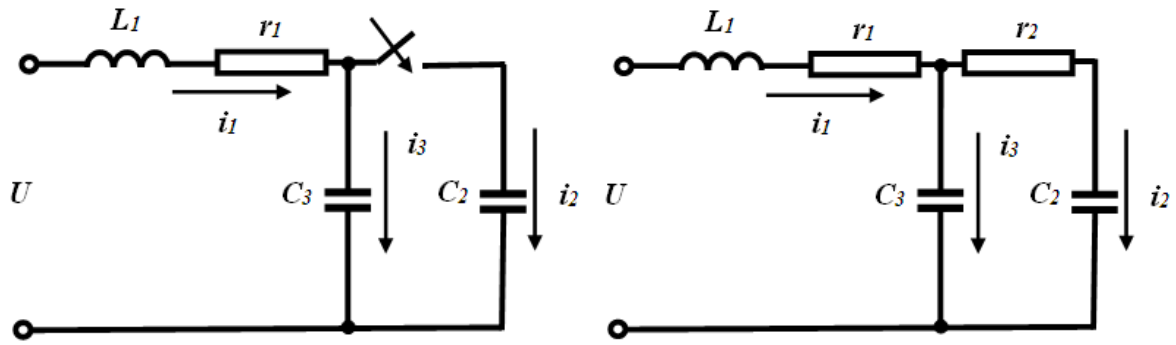

a) b)

Figure 1

To ensure the possibility of using the second law of switching, we assume that the branch with capacitance C_2 contains a resistor $r_2 = \alpha \approx 0$ (Fig. 1, *b*).

The initial conditions can be found as

$$u_{C_3}(0+) = U = 100 \text{ V}, u_{C_2}(0+) = 0 \text{ V}, i_1(0+) = 0 \text{ A}. \quad (13)$$

Forced components are defined as

$$u_{C_2 np} = U = 100 \text{ V}, u_{C_3 np} = U = 100 \text{ V}, i_{1np} = 0 \text{ A}. \quad (14)$$

By the method of input resistance

$$Z_{вх}(p) = r_1 + pL_1 + \frac{\left(r_2 + \frac{1}{pC_2}\right)\frac{1}{pC_3}}{r_2 + \frac{1}{pC_2} + \frac{1}{pC_3}} = r_1 + pL_1 + \frac{\left(\alpha + \frac{1}{pC_2}\right)\frac{1}{pC_3}}{\alpha + \frac{1}{pC_2} + \frac{1}{pC_3}} = \quad (15)$$

$$= \frac{r_1\left(\alpha C_2 C_3 p^2 + (C_2 + C_3)p\right) + pL_1\left(\alpha C_2 C_3 p^2 + (C_2 + C_3)p\right) + \alpha C_2 p + 1}{\alpha C_2 C_3 p^2 + (C_2 + C_3)p},$$

form a characteristic equation:

$$\alpha L_1 C_2 C_3 p^3 + [\alpha r_1 C_2 C_3 + L_1(C_2 + C_3)]p^2 + [r_1(C_2 + C_3) + \alpha C_2]p + 1 = 0, \quad (16)$$

or in numerical form

$$15 \cdot 10^{-10}\alpha p^3 + [75 \cdot 10^{-8}\alpha + 25 \cdot 10^{-6}]p^2 + [0.0125 + 15 \cdot 10^{-5}\alpha]p + 1 = 0, \quad (17)$$

This cubic equation has three roots, the first two of which we determine by performing the transformation

$$15 \cdot 10^{-10}\alpha p^3 + [75 \cdot 10^{-8}\alpha + 25 \cdot 10^{-6}]p^2 + [0.0125 + 15 \cdot 10^{-5}\alpha]p + 1 \approx$$

$$\approx 25 \cdot 10^{-6}p^2 + 0.0125p + 1 = 0, \quad (18)$$

where $p_1 = -400$ s^{-1}, $p_2 = -100$ s^{-1}.

The third root is found using the theorem of factorization, according to which expression (17) can be represented as $15 \cdot 10^{-10}\alpha(p - p_1)(p - p_2)(p - p_3) = 0$.

It follows from this theorem that $(-15 \cdot 10^{-10}\alpha p_1 p_2 p_3) = 1$,

where $p_3 = -\frac{1}{15 \cdot 10^{-10}\alpha p_1 p_2} = -\frac{16667}{\alpha}$ s^{-1}.

Then

$$u_{C_2}(t) = U + A_1 e^{p_1 t} + A_2 e^{p_2 t} + A_3 e^{p_3 t} = 100 + A_1 e^{-400t} + A_2 e^{-100t} + A_3 e^{-\frac{16667}{\alpha}t}, \quad (19)$$

and

$$u_{C_3}(t) = u_{C_2}(t) + \alpha C_2 \frac{du_{C_2}(t)}{dt} = 100 + A_1 e^{-400t} + A_2 e^{-100t} + A_3 e^{-\frac{16667}{\alpha}t} +$$

$$+10^{-4}\left(-400A_1e^{-400t}-100A_2e^{-100t}-\frac{16667}{\alpha}A_3e^{-\frac{16667}{\alpha}t}\right)\alpha\approx \quad (20)$$

$$\approx 100+A_1e^{-400t}+A_2e^{-100t}-0.6667A_3e^{-\frac{16667}{\alpha}t}.$$

The current in the inductor is defined as

$$i_1(t)=C_2\frac{du_{C_2}(t)}{dt}+C_3\frac{du_{C_3}(t)}{dt}=10^{-4}\left(-400A_1e^{-400t}-100A_2e^{-100t}-\frac{16667}{\alpha}A_3e^{-\frac{16667}{\alpha}t}\right)+$$

$$+1.5\cdot10^{-4}\left(-400A_1e^{-400t}-100A_2e^{-100t}+\frac{11111}{\alpha}A_3e^{-\frac{16667}{\alpha}t}\right)= \quad (21)$$

$$=-0.1A_1e^{-400t}-0.025A_2e^{-100t}.$$

To determine the integration constants it is necessary to substitute the value of the initial moment of time $t=0_+\approx\alpha_1$ in expressions (19) and (20) instead of the variable *t* (the initial moment of time is denoted by a symbol α_1, because it differs from resistance in its physical nature $r_3=\alpha$). Uncertainty arises $e^{-16667\frac{\alpha_1}{\alpha}}$.

The ratio of infinitesimal numbers α and α_1 is impossible to establish purely mathematically, because they belong to heterogeneous parameters. Let's analyze them from a physical point of view. Recall that α_1 this is the starting point of time, and α this is the active conductivity of the circuit breaker, which we specifically introduce to fulfill the standard switching laws. Since these values are independent of each other, it is always possible to choose their value to ensure the condition $\alpha_1\approx\alpha^2$. This way it is possible to write

$$e^{-16667\frac{\alpha_1}{\alpha}}=e^{-16667\frac{\alpha^2}{\alpha}}=e^{-16667\alpha}\approx1. \quad (22)$$

From expressions (19), (20) and (21), taking into account (22) we find the integration constants, for which we compose a system of equations:

$$\begin{aligned}u_{C_2}(0+)&=100+A_1+A_2+A_3=0,\\ u_{C_3}(0+)&=100+A_1+A_2-0.6667A_3=100,\\ i_1(0+)&=-0.1A_1-0.025A_2=0.\end{aligned} \quad (23)$$

Hence $A_1=13.333$, $A_2=-53.333$, $A_3=-60$
Thus, the transient voltages on the capacitors

$$u_{C_2}(t)=100+13.333e^{-400t}-53.333e^{-100t}-60e^{-\frac{16667}{\alpha}t}\approx$$

$$\approx100+13.333e^{-400t}-53.333e^{-100t}\text{ V}, \quad (24)$$

$$u_{C_3}(t)=100+13.333e^{-400t}-53.333e^{-100t}+40e^{-\frac{16667}{\alpha}t}\approx$$

$$\approx100+13.333e^{-400t}-53.333e^{-100t}\text{ V}, \quad (25)$$

and the transient current in inductance

$$i_1(t)=-1.333e^{-400t}+1.333e^{-100t}\text{ A}. \quad (26)$$

Let now consider what values the voltages on the capacitors and the current in the inductance at the moments $t=0$ and $t=0_+$ in the real circuit for which $r_2=0\approx\alpha^\beta$.
As already determined, before switching at $t<0$ (in particular at $t=0_-$) $u_{C_3}=100$ V, $u_{C_2}=0$ V, $i_1=0$ A.
At the time, $t=0_+\approx\alpha_1$ expressions (24) and (25), taking into account (12), will take the form

$$u_{C_2}(0_+)=100+13.333e^{-400\alpha_1}-53.333e^{-100\alpha_1}-60e^{-\frac{16667}{0}\alpha_1}\approx$$

$$\approx100+13.333e^{-400\alpha_1}-53.333e^{-100\alpha_1}-60\alpha\approx60\text{ V},$$

$$u_{C_3}(0_+) = 100 + 13.333e^{-400\alpha_1} - 53.333e^{-100\alpha_1} + 40e^{-\frac{16667}{0}\alpha_1} \approx$$

$$\approx 100 + 13.333e^{-400\alpha_1} - 53.333e^{-100\alpha_1} + 40\alpha \approx 60 \text{ V},$$

and current in inductance

$$i_1(t) = -1.333e^{-400\alpha_1} + 1.333e^{-100\alpha_1} \approx 0 \text{ A}.$$

At the moment of time the $t = 0 \approx {\alpha_1}^{\beta}$ expression $e^{-16667\frac{0}{0}}$ becomes uncertain, because time and resistance are heterogeneous parameters, so the exact value of voltages at this time cannot be determined. We can only know the intervals of their possible values, like that

$$0 \le u_{C_2}(0) \le 60,$$

$$60 \le u_{C_3}(0) \le 100.$$

Let now consider the energy ratios in a circle. Since before switching ($t < 0$) the current in the inductor and the voltage on the capacitor C_2 was zero, the energy was stored only in the capacitor C_3 and was equal to

$$W(0_-) = \frac{C_3 u_{C_3}^2(0_-)}{2} = \frac{150\cdot10^{-6}\cdot100^2}{2} = 0.75 \text{ J}.$$

At the first moment of time after switching ($t = 0_+$) the energy is already stored in both capacitors and is equal to

$$W(0_+) = \frac{(C_3+C_2)u_{C_3}^2(0_+)}{2} = \frac{250\cdot10^{-6}\cdot60^2}{2} = 0.45 \text{ J}.$$

Thus, the energy deficit is $\Delta W = 0.75 - 0.45 = 0.3$ J.
In traditional electrical engineering textbooks, the presence of this deficiency is explained by the loss of energy when charging the capacitor, which is turned on, but does not provide any mathematical evidence. Let's try to prove this within the framework of non-standard analysis.
To do this, first determine the current in the capacitor C_2

$$i_2(t) = C_2\frac{du_{C_2}(t)}{dt} = 10^{-4}\frac{d\left(100 + 13.333e^{-400t} - 53.333e^{-100t} - 60e^{-\frac{16667}{\alpha}t}\right)}{dt} =$$

$$= -0.533e^{-400t} + 0.533e^{-100t} + \frac{100}{\alpha}e^{-\frac{16667}{\alpha}t} \text{ A}$$

Then

$$\Delta W = \int_0^\infty i_2^2(t)r_2dt = \int_0^\infty \left(-0.533e^{-400t} + 0.533e^{-100t} + \frac{100}{\alpha}e^{-\frac{16667}{\alpha}t}\right)^2 \alpha dt =$$

$$= \int_0^\infty \begin{pmatrix} 0.284\alpha e^{-800t} + 0.284\alpha e^{-200t} + \frac{10000}{\alpha}e^{-\frac{33333}{\alpha}t} - 0.568\alpha e^{-500t} - \\ -106.6e^{-\left(400+\frac{16667}{\alpha}\right)t} + 106.6e^{-\left(100+\frac{16667}{\alpha}\right)t} \end{pmatrix} dt =$$

$$= \left(\begin{matrix} -3.55\cdot10^{-4}\alpha e^{-800t} - 1.42\cdot10^{-3}\alpha e^{-200t} - 0.3e^{-\frac{33333}{\alpha}t} + 1.136\cdot10^{-3}\alpha e^{-500t} + \\ + \frac{106.6}{400+\frac{16667}{\alpha}}e^{-\left(400+\frac{16667}{\alpha}\right)t} - \frac{106.6}{100+\frac{16667}{\alpha}}e^{-\left(100+\frac{16667}{\alpha}\right)t} \end{matrix}\right)\Bigg|_0^\infty \approx$$

$$\approx -0.3e^{-\frac{33333}{\alpha}\infty} + 0.3e^{-\frac{33333}{\alpha}0} \approx 0.3e^{-33333\cdot0} \approx 0.3 \text{ J}.$$

The law of energy conservation is fulfilled.

Conclusions

1. The application of ideas and methods of non-standard analysis in the field of theoretical electrical engineering makes it possible to use the traditional classical method of transient analysis of circuits with violation of the switching laws.

2. Only using the methods of non-standard analysis, it is possible to strictly prove the implementation of the energy conservation law in such circuits.

3. In order to expand the scope of non-standard analysis methods, it is necessary to distinguish similar problems from various fields of science and technology, which use differential calculus and boundary transitions and which solution is limited or impossible by standard approaches.

References

1 Donaldson J.A. The abstract Cauchy problem / J.A. Donaldson // Journal of Differential Equations. — 1977. — Vol. 25. — Iss. 3. — P. 400-409.

2 De Laubenfels R. Entire solutions of the abstract Cauchy problem / R. De Laubenfels // Semigroup Forum. — 1991. — Vol. 42. — P. 83–105.

3 Vedmitskyi Y.G. Newton binomial in the generalized Cauchy problem as exemplified by electrical systems / Y.G. Vedmitskyi, V.V. Kukharchuk, V.F. Hraniak, I.V. Vishtak, P. Kacejko, A. Abenov // Proc. SPIE 10808, Photonics Applications in Astronomy, Communications, Industry, and High Energy Physics Experiments. — 2018. — Vol. 108082M.

4 Zhen Wang, Xiaqi Ding. Uniqueness of generalized solution for the Cauchy problem of transportation equations / Wang Zhen, Ding Xiaqi // Acta Mathematica Scientia. — 1997. — Vol. 17. — Iss. 3. — P. 341-352.

5 Sanchez-Ortiz. Cauchy Problem for a Stochastic Fractional Differential Equation with Caputo-Itô Derivative / Sanchez-Ortiz, Jorge, U. Omar, Lopez-Cresencio, J. Francisco, Ariza-Hernandez, P. Martin // Mathematics. — 2021. — V. 9. — P. 1-10.

6 Robinson A. Introduction to the Theory of Models and to the Metamathematics of Algebra / A. Robinson. — Amsterdam: North-Holland Publishing Co. — 1963. — 284 pp.

7 Robinson A. Non-Standard Analysis / A. Robinson. Princeton: Princeton Univ. Press. — 1996. — 308 pp.

8 Jensen A.A Computer oriented approach to “nonstandard analysis” / A. Jensen // Studies in Logic and the Foundations of Mathematics. — 1972. — Vol. 69. — P. 281-289.

9 Karpov Y.O. Expanding the domain of applying a symbolic method of estimation of electric circuits through the methods of non-standard analysis (Part 1) / Y.O. Karpov, S.Sh. Katsyv, A.V. Kozlovskiy // Bulletin of the Engineering Academy of Ukraine. — 2013. — Vol. 1. — P. 236-239.

10 Karpov Y.O. Expanding the domain of applying a symbolic method of estimation of electric circuits through the methods of non-standard analysis (Part 2) / Y.O. Karpov, S.Sh. Katsyv, A.V. Kozlovskiy // Bulletin of the Engineering Academy of Ukraine. — 2013. — Vol. 2. — P. 262-265.

11 Kukharchuk V.V. Transient analysis in 1st order electrical circuits in violation of commutation laws / V.V. Kukharchuk, S.V. Pavlov, S.Sh. Katsyv, A.M. Koval, V.S. Holodiuk, M.V. Lysyi, A. Kotyra, O. Mamyrbaev, A. Kalabayeva // Przegląd Elektrotechniczny. — 2021. — Vol. 9. — P. 26-30.

12 Девис М. Прикладной нестандартный анализ / М. Девис, пер. с англ. — М.: Мир, 1980. — 240 с.

13 Gordon E.I. Infinitesimal analysis / E.I. Gordon, A.G. Kusraiev, S.S. Kuteladze. Novosibirsk: Publishing of the Institute for Mathematics. — 2006. — 526 p.

14 Bell J. A Primer of Infinitesimal Analysis / J. Bell. — Cambridge University Press. — 1998. — 140 p.

15 Lutz R. Nonstandard Analysis. A Practical Guide with Applications / R. Lutz, M. Goze. — Berlin: Springer-Verlag. — 1981. — 261 p.

16 IEEE Standard Test Procedure for Polyphase Induction Motors and Generators. IEEE Std 112–2004 from 12th May 2004 (Revision of IEEE Std 112–1996). New York: American National Standard Institute. — 2004.

17 Kucheruk V.Yu. Computer-measuring system of the induction motor’s dynamical torque-speed characteristics / V.Yu. Kucheruk, I.P. Kurytnik, Ye.Z. Oshanov, P.I. Kulakov, A.A. Semenov, D.Zh. Karabekova, A.K. Khassenov // Bulletin of the University of Karaganda-Physics. — 2019. — No. 2(94). — P. 92–100.

18 Hraniak V.F. Phase noncontact method and procedure for measurement of axial displacement of electric machine`s rotor / V.F. Hraniak, V.V. Kukharchuk, V.V. Bogachuk, Yu.G. Vedmitskyi // Proc. SPIE 10808, Photonics Applications in Astronomy, Communications, Industry, and High-Energy Physics Experiments. — 2018, Vol. 1080866.

19 Aree P. Analytical approach to determine speed-torque curve of induction motor from manufacturer data / P. Aree // Procedia Computer Science. — 2016. — Vol. 86. — P. 293–296.

20 Kojooyan-Jafari H., Monjo L., Corcoles F., Pedra J. Parameter Estimation of Wound-Rotor Induction Motors from Transient Measurements / H. Kojooyan-Jafari, L. Monjo, F. Corcoles, J. Pedra // IEEE Transactions on Energy Conversion. — 2014. — Vol. 29. — P. 300–308.

С. Кацыв, В. Кухарчук, В. Мадьяров, В. Голодюк,
В. Кучерук, П. Кулаков, М. Грибов

Электротехникадағы стандартты емес талдау. Ауысу заңдылықтарын бұза отырып екінші ретті электр тізбектеріндегі өтпелі процестерді талдау

Авторлар теориялық электротехниканың кейбір тривиальды емес мәселелерін шешу үшін талдаудың стандартты емес математикалық аппаратын пайдалануды алғаш ұсынып отыр. Стандартты емес талдау аксиоматикасы ауысу заңдылықтары бұзылған кезде жоғары ретті электр тізбектеріндегі өтпелі процестерді талдауды жеңілдетуге мүмкіндік беретіні анықталды. Теориялық электротехникада стандартты емес талдау әдістерін қолдану ауысу заңдылықтарын бұзатын тізбектердің өтпелі процестерін талдаудың дәстүрлі классикалық әдісін қолдануға мүмкіндік беретіні көрсетілген. Стандартты емес талдау әдістерін қолдану арқылы ғана мұндай схемаларда энергияның сақталу заңының орындалуын дәлелдеуге болады. Сонымен қатар, мұндай есептерді шешу мысалдары келтірілген. Дифференциалдық есептеулер мен шекаралық өтулерді қолданатын және стандартты тәсілдермен шешімі шектелетін немесе мүмкін болмайтын ғылым мен техниканың әртүрлі салаларындағы есептерде стандартты емес талдау әдістерін қолдану аясын кеңейту ұсынылады.

Кілт сөздер: шексіз аз сан, шексіз үлкен сан, гипернақты сан, стандартты емес сан, стандартты сан, екінші ретті өтпелі процесі.

С. Кацыв, В. Кухарчук, В. Мадьяров, В. Голодюк,
В. Кучерук, П. Кулаков, М. Грибов

Нестандартный анализ в электротехнике. Анализ переходных процессов в электрических цепях второго порядка с нарушением законов переключения

Авторы впервые предложили использовать математический аппарат нестандартного анализа для решения некоторых нетривиальных задач теоретической электротехники. Установлено, что аксиоматика нестандартного анализа позволяет упростить анализ переходных процессов в электрических цепях высокого порядка при нарушении законов переключения. Показано, что применение нестандартных методов анализа в теоретической электротехнике дает возможность использовать традиционный классический метод анализа переходных процессов цепей с нарушением законов переключения. Только с помощью методов нестандартного анализа можно строго доказать выполнение закона сохранения энергии в таких схемах. Также приведены примеры решения таких задач. Рекомендовано расширить область применения нестандартных методов анализа в задачах различных отраслей науки и техники, использующих дифференциальное исчисление и граничные переходы, решение которых ограничено или невозможно стандартными подходами.

Ключевые слова: бесконечно малое число, бесконечно большое число, гипердействительное число, нестандартное число, стандартное число, переходный процесс второго порядка.

References

1 Donaldson, J.A. (1977). The abstract Cauchy problem. *Journal of Differential Equations, Vol. 25, Issue 3, 400-409.*

2 De Laubenfels, R. (1991). Entire solutions of the abstract Cauchy problem. *Semigroup Forum, Vol. 42, 83–105.*

3 Vedmitskyi, Y.G., Kukharchuk, V.V., Hraniak, V.F., Vishtak, I.V., Kacejko, P., & Abenov, A. (2018). Newton binomial in the generalized Cauchy problem as exemplified by electrical systems. *Proc. SPIE 10808, Photonics Applications in Astronomy, Communications, Industry, and High Energy Physics Experiments. Vol. 108082M.*

4 Zhen Wang, Xiaqi Ding. (1997). Uniqueness of generalized solution for the Cauchy problem of transportation equations. *Acta Mathematica Scientia, Vol. 17, Issue 3, 341-352.*

5 Sanchez-Ortiz, Jorge, Omar, U. Lopez-Cresencio, Francisco, J. Ariza-Hernandez, & Martin, P. Cauchy (2021). Problem for a Stochastic Fractional Differential Equation with Caputo-Itô Derivative. *Mathematics, Vol. 9, 1-10.*

6 Robinson, A. (1963). Introduction to the Theory of Models and to the Metamathematics of Algebra. *Amsterdam: North-Holland Publishing Co.*

7 Robinson, A. (1996). Non-Standard Analysis. *Princeton: Princeton Univ. Press.*

8 Jensen, A.A. (1972). Computer oriented approach to “nonstandard analysis”. *Studies in Logic and the Foundations of Mathematics, Vol. 69, 281-289.*

9 Karpov, Y.O., Katsyv, S.Sh., & Kozlovskiy, A.V. (2013). Expanding the domain of applying a symbolic method of estimation of electric circuits through the methods of non-standard analysis (Part 1). *Bulletin of the Engineering Academy of Ukraine, Vol. 1, 236-239.*

10 Karpov, Y.O., Katsyv, S.Sh., & Kozlovskiy, A.V. Expanding the domain of applying a symbolic method of estimation of electric circuits through the methods of non-standard analysis (Part 2) (2013). *Bulletin of the Engineering Academy of Ukraine. Vol. 2, 262-265.*

11 Kukharchuk, V.V., Pavlov, S.V., Katsyv, S.Sh., Koval, A.M., Holodiuk, V.S., Lysyi, M.V., Kotyra, A., Mamyrbaev, O., & Kalabayeva, A. Transient analysis in 1st order electrical circuits in violation of commutation laws // Przegląd Elektrotechniczny. — 2021. — Vol. 9 — P. 26-30.

12 Devis, M. (1980). Prikladnoi nestandartnyi analiz [Applied non-standard analysis]. (Transl.). Moscow: Mir [in Russian].

13 Gordon, E.I., Kusraiev, A.G., & Kuteladze, S.S. (2006). Infinitesimal analysis. Novosibirsk: Publishing of the Institute for Mathematics.

14 Bell, J. (1998). A Primer of Infinitesimal Analysis. Cambridge University Press.

15 Lutz, R., & Goze, M. (1981). Nonstandard Analysis. A Practical Guide with Applications. Berlin: Springer-Verlag.

16 IEEE Standard Test Procedure for Polyphase Induction Motors and Generators (2004). IEEE Std 112–2004 from 12th May 2004 (Revision of IEEE Std 112–1996). New York: American National Standard Institute.

17 Kucheruk, V.Yu., Kurytnik, I.P., Oshanov, Ye.Z., Kulakov, P.I., Semenov, A.A., Karabekova D.Zh., & Khassenov A.K. (2019). Computer-measuring system of the induction motor's dynamical torque-speed characteristics. *Bulletin of the University of Karaganda-Physics, 2(94), 92–100.*

18 Hraniak, V.F., Kukharchuk, V.V., Bogachuk, V.V., Vedmitskyi, Yu.G. (2018). Phase noncontact method and procedure for measurement of axial displacement of electric machine`s rotor. *Proc. SPIE 10808, Photonics Applications in Astronomy, Communications, Industry, and High-Energy Physics Experiments, Vol. 1080866.*

19 Aree, P. (2016). Analytical approach to determine speed-torque curve of induction motor from manufacturer data. Procedia Computer Science, Vol. 86, 293–296.

20 Kojooyan-Jafari, H., Monjo, L., Corcoles, F., & Pedra, J. (2014). Parameter Estimation of Wound-Rotor Induction. *Motors from Transient Measurements. IEEE Transactions on Energy Conversion, Vol. 29, 300–308.*

DOI 10.31489/2022PH4/65-71

UDC: 621.315.592, 530, 574

G.M. Mammadova

Institute of Physics, Baku, *Azerbaijan Republic*
(E_mail: gizbesmamedova@gmail.com*)*

The frequency of current fluctuations in two-valley semiconductors in an external electric and strong magnetic ($\mu H > c$) fields

Boltzmann's kinetic equations have not been used to date to study nonequilibrium phenomena in semiconductors, and therefore, to obtain analytical expressions for the oscillation frequency inside the semiconductor and the critical external electric field, it is of theoretical interest. In this theoretical work, the frequency of oscillations occurring inside a two-valley semiconductor of the GaAs type in an external constant electric field and in an external strong magnetic field ($\mu H \gg c$, μ-mobility of charge carriers, H-magnetic field strength, c-speed of light) is calculated. It has been proved that the critical values of the external electric field fully correspond to the values of the electric field, which were obtained by the Gunn experiment. It is proved that unstable waves are excited in GaAs if the crystal dimensions are $L_y > 4L_z$ and $L_x \ll L_y$. Analytical expressions are obtained by theoretical calculation for an external constant magnetic field, when unstable oscillations are excited inside the sample. It is proved that the growth rate of the excited waves is much less than the wave propagation frequency$\gamma \ll \omega_0$. Numerical comparisons of theoretical expressions for the frequency of oscillations are carried out using the data of the Gunn experiment $\omega_0 \sim 10^7 \div 10^9$ Hz.

Keywords: oscillations, frequency, distribution function, electric field, magnetic field, current-voltage characteristic, multi-line semiconductors, Boltzmann's kinetic equations.

Introduction

In theoretical works [1-4], current oscillations in two-valley semiconductors of the GaAs type in an external electric field, and in external electric and strong magnetic fields are investigated by solving the Boltzmann kinetic equation. In these works, the critical values of the electric and magnetic fields were calculated from the condition

$$\frac{dj}{dE} = \sigma_d = 0 \quad (1)$$

(j is the current flux density, E is the electric field, σ_d is the differential conductivity). However, from condition (1) it is impossible to determine the frequency of the current oscillation. Therefore, it is of great interest to determine the current fluctuation in the presence of condition (1). In this theoretical work, we will calculate the frequency of current oscillation and the critical value of the electric and magnetic fields by applying the Boltzmann kinetic equation.

In [5] a theoretical study was made of the radiation of energy in strong electric and magnetic fields from two valley semiconductors of the GaAs type, in which the Gunn effect was discovered. It is known that during radiation a GaAs sample is in a nonequilibrium (unstable) state. In this theoretical work, the condition for the emission of energy from two valley semiconductors is theoretically investigated by applying the Boltzmann kinetic equation. Such a theoretical approach is not considered in periodic and theoretical works and is of scientific interest. The application of the Boltzmann equation proves that the condition of energy emission from the GaAs sample, (i.e. the frequency of the current oscillation corresponding to the value of the electric field in this case), fully corresponds to the Gunn experiment.

Theory

Typical examples of the dependence of the current density in a spatially uniform system on the field strength under conditions when there is a falling section on the current-voltage characteristic are shown in

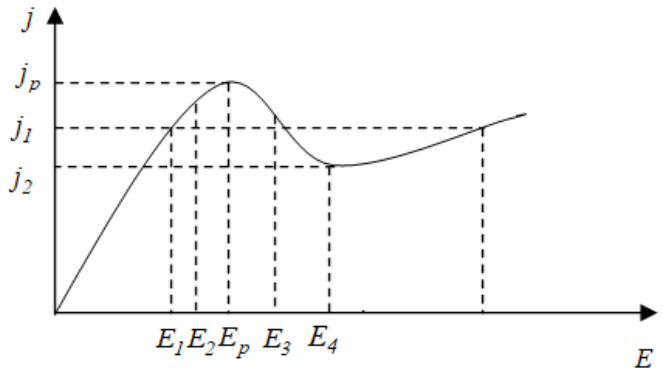

Figure 1. The dependence of the current density on the electric field in two-valley semiconductors of the GaAs type is an N-shaped characteristic.

An essential feature of the characteristic in Figure 1 is that in a certain range of currents $j_2 < j < j_p$, the field strength is a multivalued function of the current density. In this current range, the system can be in one of three spatially homogeneous states. The Gunn effect is associated with an N-shaped characteristic. With negative differential conductivity, electric charges in the system are distributed unevenly, i.e. spatial regions with different values of charges appear in the system (i.e., electrical domains appear). One of the mechanisms for the appearance of domains is the Ridley-Watkins-Hillsum mechanism [6, 7]. In electronic gallium arsenide GaAs, the dispersion law is as follows

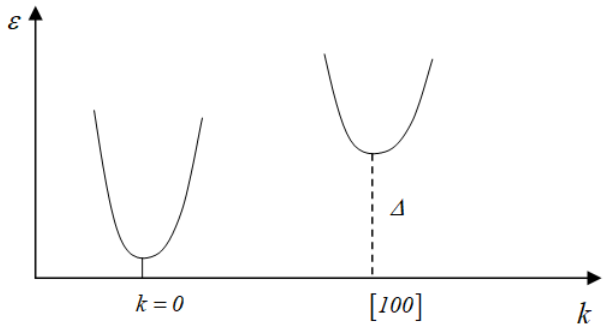

Figure 2. Electron energy versus wave vector in GaAs.

Since the energy distance between the minima is relatively large ($\Delta = 0{,}36eV, \Delta \gg T_p$, T_p is the lattice temperature) under conditions of thermodynamic equilibrium, the presence of upper valleys (minima) practically does not affect the statistics of electrons.

However, with a sufficiently strong heating of electrons by an electric field, some of them pass into the upper minimum. The effective mass of electrons in the lower valley m_a is much less than the mass of electrons in the upper valley m_b. Therefore, the electron mobilities in the corresponding valleys are related by the relation

$$\mu_b \gg \mu_a \quad (2)$$

If we designate the concentrations in the valleys n_a and $n_{\acute{o}}$, we can write an expression for the current in the form

$$\vec{j} = en_a\mu_a\vec{E} + en_b\mu_b\vec{E} \quad (3)$$

$$n = n_a + n_b = const \quad (4)$$

(we neglect the diffusion current due to $eEl \gg k_0T$, e is the elementary charge, is the electron mean free path). In works [5-6], without taking into account the intervalley scattering (it is considered small in comparison with the intravalley one), by solving the Boltzmann equation, more specific conditions for the

appearance of current oscillations were obtained. In the scientific literature, there are no works devoted to theoretical studies of the Gunn effect taking into account the intervalley scattering based on the solution of the Boltzmann kinetic equation. We will theoretically analyze the influence of a strong magnetic field on the Gunn effect, taking into account the intervalley scattering, and calculate the frequency of the current oscillation under the above conditions by solving the Boltzmann kinetic equation.

Basic Equations Of The Problem

Under the action of external forces, the state of charge carriers is described by the distribution function $f(\vec{k},\vec{r})$, the value that is necessary when considering transport phenomena, $f(\vec{k},\vec{r})$ is the probability that an electron with a wave vector $\vec{k}$ (quasimomentum $\hbar\vec{k}$) is located near the point $\vec{r}$. We consider stationary processes, then $f(\vec{k},\vec{r})$ is clearly independent of time. The distribution function is found from the kinetic Boltzmann equation. It is known that the distribution function changes under the influence of external factors and under the influence of collisions with lattice vibrations (phonons) and crystal defects. In the considered stationary state, the influence of these factors mutually compensate each other.

$$\left(\frac{\partial f}{\partial t}\right)_{external} + \left(\frac{\partial f}{\partial t}\right)_{coll} = 0 \quad (5)$$

In the presence of external electric and magnetic fields, equation (5) has the form [8]

$$\vec{v}\nabla_{\vec{r}} f + \frac{e}{\hbar}\left\{\vec{E} + \frac{1}{c}\left[\vec{v}\vec{H}\right]\right\}\nabla_{\vec{k}} f = \left(\frac{\partial f}{\partial t}\right)_{coll} \quad (6)$$

Here $\vec{v} = \frac{1}{\hbar}\nabla_k \varepsilon(\vec{k})$ is the electron velocity, $\nabla_{\vec{r}}\, u\, \nabla_{\vec{k}}$ is the gradient in the space of coordinates and wave vectors.

When solving the problem, we neglect the anisotropy. The fact that no orientation dependence was found in studies of the Gunn effect on GaAs samples speaks in favor of this assumption. We will assume that for the lower valley the intervalley scattering prevails over the intravalley one, and for the upper valley, the intravalley scattering prevails over the intervalley one. Then the Boltzmann equation for the lower valley can be written in the form

$$\left(\frac{\partial f^a}{\partial t}\right)_{internal} + \left(\frac{\partial f^a}{\partial t}\right)_{intervalley} = 0 \quad (7)$$

And for the upper valley — in the form

$$\left(\frac{\partial f^b}{\partial t}\right)_{internal} + \left(\frac{\partial f^b}{\partial t}\right) = 0 \quad (8)$$

Davydov [8] showed that in a strong electric field the distribution function has the form:

$$f = f_0 + \frac{\vec{p}}{p}\overrightarrow{f_1} \quad (9)$$

f_0 is the equilibrium distribution function, is the momentum of charge carriers. It is clear that you can write

$$f^a = f_0^a + \frac{\vec{p}}{p}\vec{f}_1^a, f^b = f_0^b + \frac{\vec{p}}{p}\vec{f}_1^b \quad (10)$$

Distribution function f^b found from equation (8) in [9]

$$f_0^a = Be^{-\alpha_a(\varepsilon-\Delta)^2} \quad (11)\ f_1^b = -\frac{em_b l_b}{p}\vec{p}\frac{\partial f_0^b}{\partial p} \quad (12)$$

Here

$$l_b = \frac{\pi\hbar^4\rho u_0^2}{D^2 m_b^2 k_0 T} \quad (13)\ \alpha_b = \frac{3D^4 m_b^5 k_0 T}{e^2\pi^2\hbar^8\rho^2 u_0^2} \quad (14)$$

It is clear that for the valley "a" you can write similar formulas (13-14) replacing "a" with "b". l_b is the mean free path, D is the deformation potential, T is the temperature of the lattice, ρ is the density of the crystal, u_0 is the speed of sound in the crystal.

Let's calculate the total current

$$\vec{j} = \vec{j}_a + \vec{j}_b \quad (15)$$

$$\vec{j} = \frac{2e}{(2\pi)^3}\int_0^\infty \frac{\vec{p}}{p}\vec{f}\,\vec{v}d\vec{k} \quad (16)$$

Davydov [9] showed that in the case of intravalley scattering f_1^b in an external electric and magnetic field f_1^b has the following form

$$f_1^b = -\frac{el_b m_b}{p}\frac{\partial f_0^b}{\partial p}\cdot\frac{\vec{E}+\left(\frac{el_b}{cp}\right)[\vec{E}\vec{H}]+\left(\frac{el_b}{cp}\right)^2\vec{H}(\vec{E}\vec{H})}{1+\left(\frac{el_b}{cp}\right)^2H^2} \quad (17)$$

$$\alpha_b = \frac{3D^4m_b^5k_0T\left[1+\left(\frac{el_b}{cp}\right)^2H^2\right]}{e^2\pi^2\hbar^8\rho^2u_0^2\left[E^2+\left(\frac{el_b}{cp}\right)^2(\vec{E}\vec{H})^2\right]} \quad (18)$$

f_1^a and α_a are obtained if we replace "b" with "a" in (17-18). After an easy calculation of the current density j_a and j_b from (16) we get:

$$\vec{j}_a = \frac{e^2l_a\alpha_aA}{12\pi^2\hbar^2m_a^2}\left\{\vec{E}\frac{c^2}{e^2l_a^2H^2}\left(\frac{4m_a^2}{\alpha_a}\right)^2+[\vec{E}\vec{H}]\frac{c\Gamma(7/4)}{el_aH^2}\left(\frac{4m_a^2}{\alpha_a}\right)^{7/4}+\vec{H}(\vec{E}\vec{H})\frac{\Gamma(3/2)}{H^2}\left(\frac{4m_a^2}{\alpha_a}\right)^{3/2}\right\} \quad (19)$$

After calculating the total current by the formula

$$\vec{j} = \vec{j}_a + \vec{j}_b \quad (20)$$

$$j_z' = \frac{8nc^2m_a^{1/2}}{3\sqrt{2}\Gamma(3/2)l_a}\frac{E_z'}{H^2}\cdot\frac{\alpha_a^{-1/4}}{1+\gamma^{-3/2}z^{3/4}\beta}\left\{1+t\gamma_z^{-2}\beta+\frac{e^2l_a^2\alpha_a^{1/2}}{2c^2m_a}H^2\Gamma(3/2)\left[1+t\gamma^{-1}z^{1/2}\beta\right]\right\} \quad (21)$$

Here

$$A = tz^{-1/2}\gamma^{-1} = \frac{m_b}{m_a}, \gamma = \frac{m_a}{m_b},\ z = \frac{\alpha_a}{\alpha_b}, t = \frac{l_b}{l_a}, \beta = z^{-1}e^{-\alpha_a\Delta^2}$$

$$e^{-\alpha_a\Delta^2} = e^{-\left(\frac{E_x}{E}\right)^2} = \left(1-\frac{E_x}{E}\right)^2, E_x^2 = \frac{3D^4m_0m_a^3k_0T}{\pi^2e^2\hbar^8\rho^2u_0^2} \quad (22)$$

We write (21) in the following form

$$\vec{j} = \sigma\vec{E} + \sigma_1[\vec{E}\vec{h}] + \sigma_2\vec{h}[\vec{E}\vec{h}] \quad (23)$$

$\vec{h}$ is unit vector in the magnetic field. Comparing (23) with (21), one can easily write the expressions $\sigma+\sigma,\ \sigma_1,\sigma_2$. When obtaining an expression for the current density j_z' (21) we direct the electric field and the magnetic field H_0 as follows

$$\vec{E}_0 = \vec{h}E_0, \vec{H}_0 = \vec{h}H_0 \quad (24)$$

The E_x value is obtained from the following condition

$$\frac{dj_z'}{dE_z'} = 0 \quad (25)$$

When estimating E_x^2 for GaAs, the value

$$E_x^2 = 43{,}84\left(V/_{SM}\right)^2 \quad (26)$$

For all strong electric fields

$$E \gg E_x \quad (27)$$

quite satisfied. Now let's calculate the frequency of the current oscillation. When an alternating electric field E' is excited inside the medium, an alternating magnetic field H' arises, which satisfies Maxwell's equation

$$\frac{\partial\vec{H}'}{\partial t} = -crot\vec{E}' \quad (28)$$

The current density in the presence of electric and magnetic fields has the form

$$\vec{j} = \sigma\vec{E} + \sigma_1[\vec{E}\vec{H}] + \sigma_2\vec{H}[\vec{E}\vec{H}] \quad (29)$$

Let us direct the external electric and magnetic field as follows

$$\vec{E}_0 = \vec{h}E_0, \vec{H}_0 = \vec{h}H_0 \quad (30)$$

($\vec{h}$ is the unit vector in z). We find the variable value j_x', j_y', j_z' from (29) taking into account (28-30), then we get

$$j_x' = \sigma\left(1-\frac{\mu k_zE_0}{\omega}\right)E_x' + \sigma_1\left[\left(1+\frac{ck_xE_0}{\omega H_0}\right)-\frac{2\sigma_2ck_zE_0}{\omega H_0}\right]E_y' + \frac{2\sigma_2ck_yE_0}{\omega H_0}E_z' \quad (31)$$

$$j_y' = -\sigma_1E_x' + \left(\sigma-\frac{\sigma_1ck_zE_0}{\omega H_0}\right)E_y' + \sigma_1\left(1+\frac{ck_yE_0}{\omega H_0}\right)E_z' \quad (32)$$

$$j_z' = (\sigma+\sigma_2)E_z' - \frac{2\sigma_2ck_yE_0}{\omega H_0}\left(E_x'+E_y'\right) \quad (33)$$

Equating $j_x^{'} = 0$ and $j_y^{'} = 0$ to zero, we find $E_z^{'}$ and $E_y^{'}$ from (31-32) and supplying $E_z^{'}, E_y^{'}$ in (33), we obtain for $j_z^{'}$ the following expressions

$$j_z^{'} = \left[\sigma_2 + \frac{2\sigma_2 ck_x E_0}{\omega H_0}\left(1 + \frac{c}{\mu H}\frac{ck_z \mu E_0}{\omega} + \frac{c}{\mu H_0}\frac{ck_y k_z \mu E_0}{\omega^2}\cdot\frac{E_0}{H_0} - \frac{ck_y}{\omega}\frac{c}{\mu H_0}\frac{E_0}{H_0}\right) + \frac{2\sigma_2 ck_y}{\omega}\frac{E_0}{H_0}\left(\frac{ck_y}{\omega} + \frac{c\mu k_z ck_y E_0}{\omega^2}\right)\frac{E_0}{H_0}\right] E_z^{'} \quad (34)$$

When deriving expression (34), we used the conditions of a strong magnetic field $\mu H_0 \gg c$. Equating expressions (34) and (21), we obtain the following dispersion equation for determining the frequency of current oscillation

$$(\sigma_2 - \tilde{\sigma}\Phi)\omega^3 + \frac{2\sigma_2 ck_x E_0}{H_0}\left(1 + \frac{E_0}{H_0}\right)\omega^2 + \frac{2\sigma_2 ck_x E_0}{H_0}\omega + \frac{\sigma_2 ck_x E_0}{H_0} ck_y \mu k_z E_0 \left(\frac{c}{\mu H_0}\cdot\frac{E_0}{H_0} + 2\frac{E_0}{H_0}\right) = 0 \quad (35)$$

Here

$$\tilde{\sigma} = \frac{8nc^2 m_a^{1/2}\alpha_a^{-1/4}}{3\sqrt{2}\Gamma(3/2) l_a H^2},\ \Phi = \frac{1}{1+\gamma^{-3/2}Z^{9/4}\beta}\left[1 + t\gamma^{-2}Z\beta + \frac{e^2 l_a^2 H^2 \alpha_a^{1/2}}{2c^2 m_a}\Gamma(3/2) + \left(1 + t\gamma^{-1}Z^{1/2}\beta\right)\right] \quad (36)$$

Equating $\sigma_2 = \tilde{\sigma}\Phi$ we easily obtain

$$\left(\frac{H_x}{H_0}\right)^2 = 1, \text{ т.е. } H_x = H_0 = \left[\frac{8c^2 m_a^{1/2}\alpha_a^{-1/4}}{3\sqrt{2}\Gamma(3/2) e\mu l_a}\right]^{1/2} \quad (37)$$

Putting the values of $\alpha_a^{-1/4}$ in (37), we easily obtain

$$H_0 = \left[\frac{8}{3\sqrt{2}\Gamma(3/2)}\right]^{1/2}\cdot\left(\frac{k_0 T}{3m_0 u_0^2}\right)^{1/8}\cdot\left(\frac{c^2 m_a^{1/2}}{\mu}\right)^{1/2}\cdot\left(\frac{1}{el_a}\right)^{1/4} E_0^{1/4} \quad (38)$$

From (38) we get

$$E_0 = \left(\frac{\mu}{c^2 m_a^{1/2}}\right)^2 el_a\left(\frac{H_0}{\varphi}\right)^4 \quad (39)$$

$$\varphi = \left[\frac{8}{3\sqrt{2}\Gamma(3/2)}\right]^{1/2}\cdot\left(\frac{k_0 T}{m_0 u_0^2}\right)^{1/8}$$

Thus, the value of the electric field is obtained during current fluctuations in the above two-valley semiconductors of the GaAs type. In [8], it was obtained that taking into account (26)

$$E_0 = E_{кр} = 1500\, V/_{SM} \quad (40)$$

Supplying (40) to (39), it is easy to see that

$$\mu H_0 \gg c$$

From the solution of the dispersion equation (35), we easily obtain

$$\omega_{1,2} = -\frac{ck_z E_0}{2H_0} \pm i\frac{ck_z E_0}{H_0}\left(\frac{L_z}{L_y}\right)^{1/2} \quad (41)$$

For growing fluctuations

$$\omega = -\frac{ck_z E_0}{2H_0} + i\frac{ck_z E_0}{H_0}\left(\frac{L_z}{L_y}\right)^{1/2} = \omega_0 + i\gamma \quad (42)$$

From (42) it is seen that in the crystal $L_y > 4L_z$ (43)

$$\gamma \ll \omega_0$$

Thus, with the size (43) (L_x-can be any), current oscillations (i.e., instability) are excited under an electric field (39) In the calculation, we direct E_0 along H_0. Of course, any orientation of the electric and magnetic fields could be chosen. For other orientations, it is necessary to obtain expressions (21) and (34) in the same orientations, and then find the vibration frequencies in the same orientations.

Discussion Of The Results

In valley semiconductors of the GaAs type, current oscillations occur under the influence of an external electric and strong ($\mu H_0 \gg c$) magnetic field. The frequency of this oscillation ω_0 (42) is close to the frequency of the Gunn effect, i.e. $\omega_0 \sim 10^7 \div 10^9\, Herz$. This proves that the application of the Boltzmann equation is quite valid, although the Boltzmann equation in strong fields is not always applied. By directing

$E_0 = \vec{i}E_0$, $E_0 = \vec{j}E_0$, $H_0 = \vec{i}H_0$, $H_0 = \vec{j}H_0$, one can carry out a theoretical calculation and determine the critical value of the electric field (including the magnetic field) and the frequency of current oscillation. Of course, with such calculations, conditions (43) will most likely change. Theoretical analysis of current fluctuations in multi-valley semiconductors of the GaAs type shows that the sample size at current fluctuations is significant. This fact was confirmed in the experiment of Gunn. It should be noted that it is necessary to solve the problem in a non-linear approximation, which requires the solution of partial differential equations. This problem can be solved only by the asymptotic solution of a differential equation with the Bogolyubov-Metropolsky method. The conclusion is to obtain an expression for the critical value of the electric field (39) and for the oscillation frequency (42). They are indicated in the derivation and evaluated numerically using experimental data.

Reference

1 Hasanov E.R. Current oscillations in semiconductors with deep traps in strong electric and magnetic fields / E.R. Hasanov, A.R. Hasanova, Sh.G. Khalilova, R.K. Mustafayeva // IOSR Journal of Applied Physics. — 2019. — Vol. 11. — P. 13–18.

2 Hasanov E.R. Current oscillations in semiconductors with deep traps in strong electric and magnetic fields / E.R. Hasanov, Sh.G. Khalilova, Z.A. Tagiyeva, S.S. Asadova // 15th International Conference on “Technical and Physical Problems of electrical Engenering”. — 2019. — No. 22. — P. 103–107.

3 Hasanov E.R. Non-linear fluctuations of concentration of charge carriers and electrical field in semiconductors / E.R. Hasanov, J.J. Mustafayev // International Journal on “Technical and Physical Problems of Engenering”. — 2017. — Vol. 9(3). — P. 39–43.

4 Hasanov E.R. Instability in two gaas valley semiconductors in electric and magnetic fields / E.R. Hasanov, Sh.G. Khalilova, R.K. Mustafayeva // 17th International Conference on “Technical and Physical Problems of electrical Engenering”. — 2021. — No. 12. — P. 60–63.

5 Hasanov E.R. Excitation of Growing Waves in Impurity Semiconductors with Two Current Fluctuations in Two-Valley Semiconductors in Strong Electric and Magnetic Fields / E.R. Hasanov, R.K. Mustafayeva, G.M. Mammadova, Sh.G. Khalilova, E.O. Mansurova // IOSR Journal of Applied Physics (IOSR-JAP). — 2021. — No. 13(1). — P. 55-62.

6 Ridley B.K. *The Possibility of Negative Resistance Effects in Semiconductor* / B.K. Ridley, T.B. Watkins // Proc.Phys.Soc. – 1961. — Vol.78. — P. 293.

7 Hilsum C.H. Transferred Electron Amplifiers and Oscillators / C.H. Hilsum // Proc. IRE. — 1962. — Vol.50. — P. 185.

8 Ансельм А.И. Введение в теорию полупроводников / А.И. Ансельм. — М.– Л.: Гос. изд-во физ.-мат. литературы, 1962. — 418 с.

9 Davydov A.B. On the theory of the motion of electrons in gases and in semiconductors / A.B. Davydov // ZhETF. — 1937. — Vol. 7. — P. 1069.

Г.М. Мамедова

Сыртқы электрлік және күшті магниттік өрістердегі (μh>c) екі валентті жартылайөткізгіштердегі токтың флуктуация жиілігі

Жартылайөткізгіштердегі тепе-теңсіз құбылыстарды зерттеу үшін қазіргі уақытқа дейін Больцманның кинетикалық теңдеуі қолданылмады және жартылай өткізгіштегі тербеліс жиілігінің және критикалық сыртқы электр өрісінің аналитикалық өрнегін алу теориялық қызығушылық тудырады. Бұл теориялық жұмыста сыртқы тұрақты электр өрісі мен сыртқы күшті магнит өрістерінде екі жолақты GaAs типтегі жартылайөткізгіш ішінде туындайтын тербеліс жиілігі есептелген (μH>>*c* — зарядты тасымалдаушылардың қозғалғыштығы, *H* — магнит өрісінің кернеуі, *c* — жарық жылдамдығы). Ішкі және сыртқы тізбектің жиілігін қоздыру үшін үлгінің өлшемі анықталған болуы қажет екені дәлелденді. Үлгі ішінде және сыртқы тізбекте тұрақсыз тербелістердің пайда болуы үшін үлгінің белгілі бір ұзындығы болуы керек. Сыртқы электр өрісінің критикалық мәндері Ганн тәжірибесімен алынған электр өрісінің мәндеріне толық сәйкес келетіні айқындалды. Егер кристалдың өлшемі L_y>4L_z, L_x<< L_y болса, тұрақсыз толқындар GaAs-де қоздырылатыны дәлелденген. Теориялық есептеу арқылы үлгінің ішінде тұрақсыз тербелістер қозған кезде сыртқы тұрақты магнит өрісінің аналитикалық өрнегі алынды. Теориялық есептеулер сыртқы тұрақты электр өрісі мен сыртқы магнит өрісі бір бағытта бағытталған кезде орындалады, яғни, $\vec{H}_0 = \vec{h}H_{0z}$, $\vec{E}_0 = \vec{h}E_{0z}$. Қоздыратын толқынның өсуі толқынның таралуымен γ<< ω_0 салыстырғанда әлдеқайда аз екені нақтыланды. Ганн тәжірибесінің деректерін пайдалана отырып $\omega_0 \sim 10^7 \pm 10^9$ Hz тербеліс жиілігінің теориялық өрнектерін сандық салыстыру жүзеге асырылды. Үлгі ішіндегі тербелістерді қоздыру үшін сыртқы электр өрісі мен сыртқы магнит өрісінің бағыты маңызды рөл атқаратыны анықталған.

Кілт сөздер: тербеліс, жиілік, таралу функциясы, электр өрісі, магнит өрісі, вольт-амперлік сипаттамасы, көп сызықты жартылай өткізгіштер, Больцманның кинетикалық теңдеуі.

Г.М. Мамедова

Частота флуктуаций тока в двухвалентных полупроводниках во внешних электрических и сильных магнитных (μh>c) полях

Кинетические уравнения Больцмана до настоящего времени для исследования неравновесных явлений в полупроводниках не использованы и поэтому для получения аналитических выражений для частоты колебания внутри полупроводника и критического внешнего электрического поля представляют теоретический интерес. В настоящей работе вычисляется частота возникающих колебаний внутри двухдолинного полупроводника типа GaAs во внешнем постоянном электрическом поле и во внешнем сильном магнитном поле ($\mu H \gg c$ — подвижность носителей заряда; H — напряженность магнитного поля; c — скорость света). Доказано, что размер образца для возбуждения колебаний внутри и во внешней цепи должны быть определенным. Показано, что для появления неустойчивых колебаний внутри образца и во внешней цепи образец должен иметь определенную длину. Определено, что критические значения внешнего электрического поля вполне соответствуют значению электрического поля, которые получены экспериментом Ганна. Доказано, что неустойчивые волны возбуждаются в GaAs, если размеры кристалла $L_y > 4L_z; L_x \ll L_y$Lx≪Ly. Теоретическим расчетом получены аналитические выражения для внешнего постоянного магнитного поля, при возбуждении неустойчивых колебаний внутри образца. Теоретические расчеты выполнены, когда внешнее постоянное электрическое поле и внешнее магнитное поле направлены одинаково, то есть $\vec{H}_0 = \vec{h}H_{0z}$; $\vec{E}_0 = \vec{h}E_{0z}$. Доказано, что инкремент нарастания возбуждаемых волн намного меньше, чем частота распространения волны $\gamma \ll \omega_0$. Проведены численные сравнения теоретических выражений для частоты колебаний с помощью данных эксперимента Ганна $\omega_0 \sim 10^7 \div 10^9$ Hz. Доказано, что направление внешнего электрического поля и внешнего магнитного поля для возбуждения колебаний внутри образца играют существенную роль.

Ключевые слова: колебания, частота, функция распределения, электрическое поле, магнитное поле, вольт-амперная характеристика, многолинейные полупроводники, кинетические уравнения Больцмана.

Reference

1 Hasanov, E.R., Khalilova, Sh.G., & Mustafayeva R.K. (2019). Current oscillations in semiconductors with deep traps in strong electric and magnetic fields. *IOSR Journal of Applied Physics, Vol. 11, 13–18.*

2 Hasanov, E.R., Khalilova, Sh.G., Tagiyeva, Z.A., & Asadova, S.S. (2019). Current oscillations in semiconductors with deep traps in strong electric and magnetic fields. *15th International Conference on "Technical and Physical Problems of electrical Engenering", 22, 103–107.*

3 Hasanov, E.R., & Mustafayev, J.J. (2017). Non-linear fluctuations of concentration of charge carriers and electrical field in semiconductors. *International Journal on "Tehnical and Physical Problems of Engenering", Vol. 9(3), 39–43.*

4 Hasanov, E.R., Khalilova, Sh.G., & Mustafayeva, R.K. (2021). Instability in two gaas valley semiconductors in electric and magnetic fields. *17th International Conference on "Technical and Physical Problems of electrical Engenering", 12, 60-63.*

5 Hasanov, E.R., Mustafayeva, R.K., Mammadova, G.M., Khalilova, Sh.G., & Mansurova E.O. (2021). Excitation of Growing Waves in Impurity Semiconductors with Two Current Fluctuations in Two-Valley Semiconductors in Strong Electric and Magnetic Fields. *IOSR Journal of Applied Physics (IOSR-JAP), 13(1), 55-62.*

6 Ridley, B.K., & Watkins, T.B. (1961). *The Possibility of Negative Resistance Effects in Semiconductor*. *Proc. Phys. Soc., Vol. 78, 293.*

7 Hilsum, C.H. (1962). Transferred Electron Amplifiers and Oscillators. *Proc. IRE, Vol. 50, 185.*

8 Anselm, A.I. (1962). Vvedenie v teoriiu poluprovodnikov [Introduction to the theory of semiconductors]. Moscow; Leningrad: Gosudarstvennoe izdatelstvo fiziko-matematicheskoi literatury [in Russian].

9 Davydov, A.B. (1937). On the theory of the motion of electrons in gases and in semiconductor. *ZhETF, Vol. 7, 1069.*

DOI 10.31489/2022PH4/72-84

UDC 621.315.6

A. Leonov[1], T. Soldatenko[1]

[1]*National Research Tomsk Polytechnic University, Tomsk, Russia*
(E-mail: ruhtinatm@tpu.ru)

Resistance evaluation of electrical insulating polymer materials used in flexible cables to operational impact

The article presents the test results of polymer material properties taking into account the possibility of their application for flexible cables insulation. The main types of cable constructions and their operation features are considered. Existing test determination methods of insulation resistance to thermal, mechanical, electrical and environmental conditions are analyzed. Requirements for laboratory equipment and test conditions are given. Evaluation criteria of test results are noted. Experimental evaluation was carried out for change degree in the properties of the main types of electrical insulation materials used currently during the flexible cable production: polyvinyl chloride compound (PVC), rubber, ethylene propylene rubber (EPR), thermoplastic elastomer (TPE), fluoropolymer. Tests were carried out under the influence of high and low temperatures, aggressive environments, ozone, mechanical loads. The main processes that determine the changes in electrophysical, physical and mechanical properties of the studied materials are described. Resistance of EPR, TPE and fluoropolymer insulation to a wide range of temperatures, mechanical loads, diesel fuel and transformer oil are shown. An increased resistance of EPR to ozone was also noted. Rubber and PVC compound did not pass the tests under the influence of low and high temperatures, showed "poor" resistance to aggressive environments, but passed the mechanical stress tests. Recommendations on tests and application of polymer insulation taking into account the specifics of flexible cables working are presented.

*Keywords***:** flexible cables, insulation, sheath, polyvinyl chloride compound, thermoplastic elastomer, fluoropolymer, ethylene propylene rubber, ozone resistance, oil resistance, mechanical strength, tests.

Introduction

Development of power industry, improvement of electrical devices for generation, transmission, distribution and consumption of electrical energy, determines the growing need for cables and wires. Electrical cables improvement is connected with increase of carrying capacity, application of new polymer materials for electric insulation, having considerable technological and operational advantages. At the same time, improving the cable products quality is one of the main tasks due to their mass production, versatility of application and very high material consumption [1].

The flexible cables are one of the main cable types. These cables are used for installation of various electronic units and devices; automation, control and management systems; connection to power grids of mobile mechanisms intended for work in open and underground mines; control of conveyor and lifting equipment, laying of security and fire alarm systems, etc.

Flexible cables are made with conductors of copper or tinned copper wires. Pure tin or tin-lead alloy is used as tinning material. Depending on the conditions of the cable application, the conductors can be stranded in a core around a central element of rubber or reinforcing aramid fibers. Some cables types are produced with parallel laying conductors. The main typical designs are flexible cables with twisted insulated conductors in the core, with outer jacket (Figure 1 (a)), individual shields over core (Figure 1 (b)), overall shield (Figure 1 (c)), individual shields over core and common shield (Figure 1 (d)) [2].

As can be seen from Figure l, the insulation and sheath are the common element that protects the design of flexible cables from external influences. Reliability and service life are determined by the ability of the polymer material to maintain its integrity and mechanical properties during operation [3].

Rubbers, ethylene propylene rubber, polyvinyl chloride compound (PVC), thermoplastic elastomers (TPE), cross-linked polyethylene (XLPE), and fluoropolymers are used for insulation and sheath of flexible cables [4].

Rubbers have high electrical resistance and moisture resistance. One of the main advantages is elasticity, but most rubbers have low ozone resistance [5].

Ethylene propylene rubber is suitable for use in cables with operating voltages up to 35 kV. The chemical stability of the material, including in relation to ozone and UV radiation, allows to guarantee operation in harsh conditions of industrial plant, subway tunnels, construction site and mining facilities. An important

advantage of cables insulated with ethylene propylene rubber is the extended operating temperature range with a lower permissible temperature of — 60 ^{0}C + 90^{0}C [6, 7].

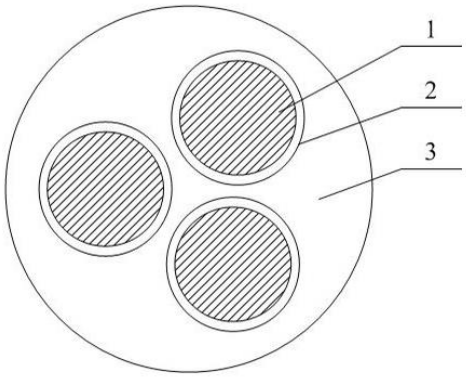

a) 1 — core; 2 — insulation; 3 — cable sheath.

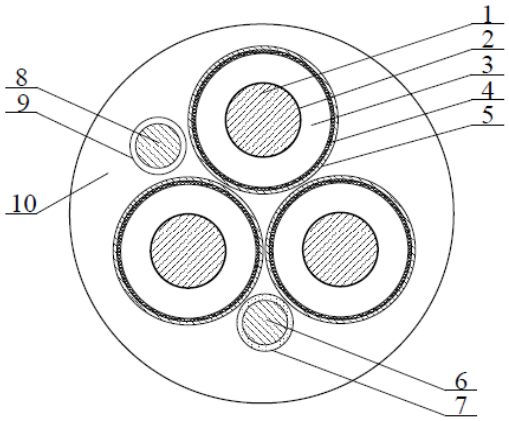

b) 1 — core; 2 — inner conductive shield; 3 — insulation; 4 — outer conductive shield; 5 — metal shield; 6,8 — grounding wire; 7,9 — grounding wire insulation; 10 — cable sheath.

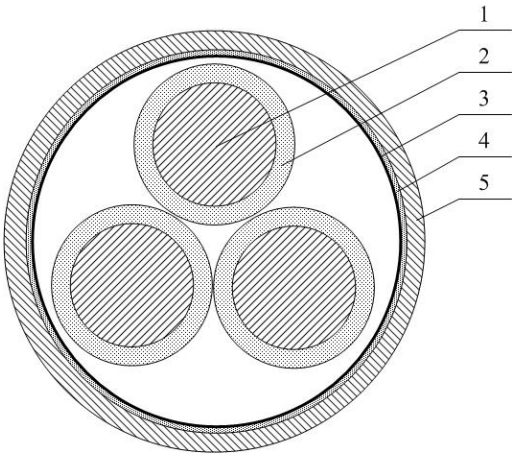

c) 1 — core; 2 — insulation; 3 — inner sheath; 4 — shield; 5 — outer cable sheath.

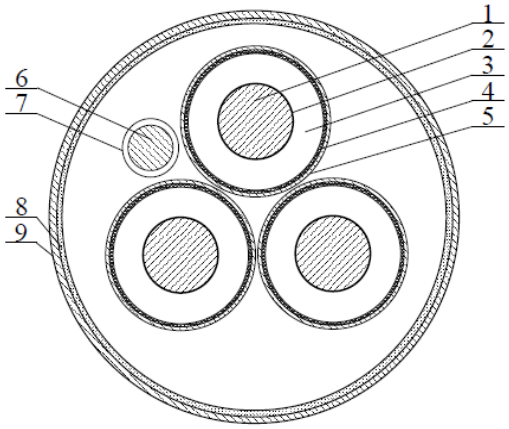

d) 1 — core; 2 — inner conductive shield; 3 — insulation; 4 — outer conductive shield; 5 — metal shield; 6 — grounding wire; 7 — grounding wire insulation; 8 — overall shield, 9 — cable sheath.

Figure 1. The main designs of flexible cables

PVC is a colorless, transparent plastic, thermoplastic polymer of vinyl chloride. It is characterized by chemical resistance to alkalis, acids and solvents, moisture resistance, sufficient flexibility, relative resistance to solar radiation. However, it should be noted that the aging of cable made of PVC is much faster. Permissible operating temperature of 70 ^{0} C. With further increase in temperature heating begins to release harmful hydrogen halogen chloride, which is dangerous to humans [8].

Thermoplastic elastomers combine the high elastic properties of rubbers and the ability to melt above the yield point and be processed by extrusion. The advantages of TPE in comparison with rubbers are as follows: reduction of material intensity due to lower density, increase in productivity and reduction of labor and energy costs during processing. The disadvantage as compared to rubbers in terms of application in cables and wires is an inherent ability of any thermoplastic material to melt at high temperatures. They have a higher cost: their formulation cannot be "diluted" with more fillers. In addition, TPEs have insufficient chemical resistance and heat resistance [9].

Polyethylene has a high chemical resistance to acids, alkalis and various chemical liquids. However, at high temperatures PE swells or even dissolves in toluene, benzene, carbon tetrachloride. PE at room temperature is resistant to nitric acid, but at +50 ^{0}C is completely destroyed after two days of exposure to this acid. The mechanical characteristics of PE are related to its molecular weight, degree of branching and crystallinity [10, 11].

Fluorine-containing polymers are characterized by high heat resistance, high electrical insulation properties, chemical and corrosion resistance. In addition, they have good weather ability and high frost resistance, low friction coefficient, low water absorption and gas permeability, high electrical strength. They have temperature operation in the range from — 269 ^{0}C to + 260 ^{0}C. Fluoropolymers are insoluble or poorly soluble in many organic solvents, resistant to acids, alkalis, oil products. The disadvantages are high cost, difficulties in processing in the cable industry [12].

Depending on the purpose and operating conditions, flexible cables must be resistant to a wide range of operating temperatures, mineral oils and diesel fuels, electrical voltages, mechanical loads and other factors (Figure 2) [13-15].

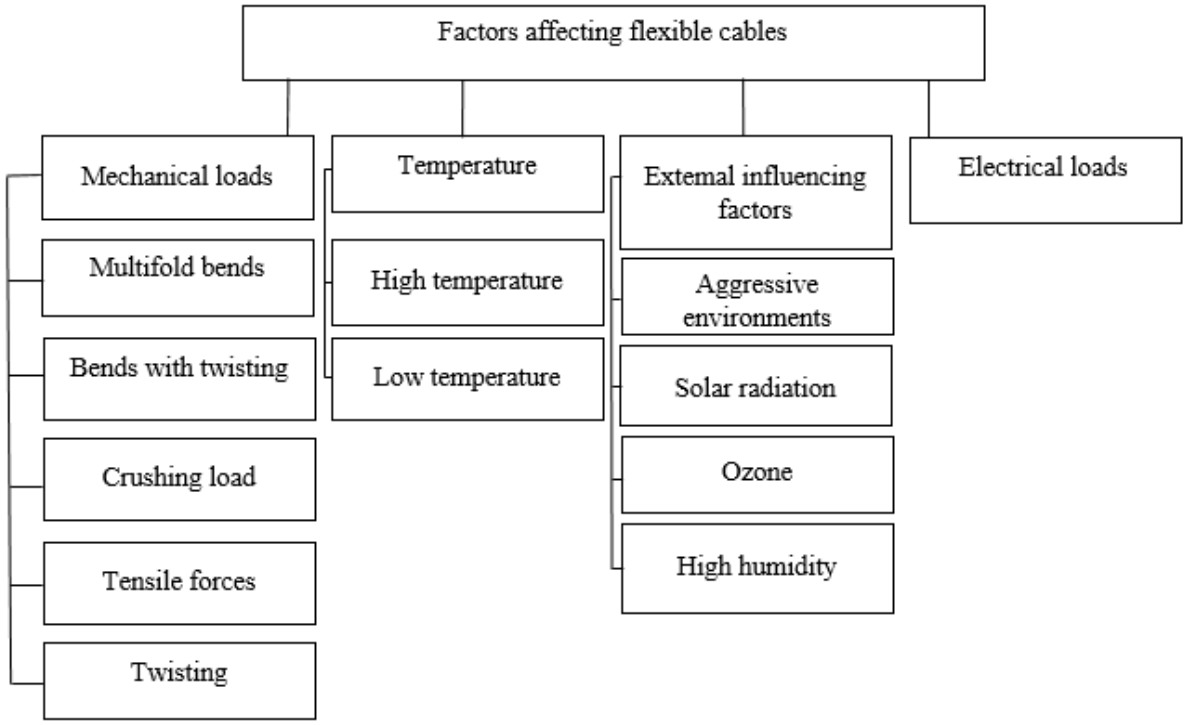

Figure 2. Factors affecting flexible cables

Thus, the reliability of electrical equipment is generally determined by the quality and reliability of cable design. At another point, polymer insulation is an element determining the flexible cables reliability during operation.

There are several methods to assess the performance flexible cables properties according to criteria:

– mechanical loads (multifold bends, bends with axial torsion, crushing loads, tensile force);

– electrical loads;

– external factors (high, low temperatures).

Determining the methods in formativeness, taking into account the significance for each flexible cables types, will simplify the task of selecting electrical insulation materials and reduce the time spent on the stage of preliminary tests.

Overview of flexible cables test methods

A generalized analysis of the test methods for the resistance of flexible cables to the operational effects is given in Table 1.

Table 1

Test methods for flexible cables

Type of test	Test method	Evaluation criterion (result)
Multifold bending resistance [16]	Cable samples are fixed in the clamping device and bent around the cylinder at an angle of $\pm\pi/2$ with a load creating a pressing force. Sample length, load weight, number of bending cycles and rollers diameter should be specified in the technical documentation for cables.	High voltage test, no cracks on the insulation and sheath surface, the number of wire breaks and metal shields should not exceed 30 %.
Multifold bendig resistance trough a roll system [17]	Tests are carried out on samples with a length of at least 3.5 m, with the application of current load to the cable at rated alternating voltage with frequency of 50 Hz specified in the normative document. Cable samples are fixed on a device consisting of a carriage with exchangeable rollers, a mechanism providing end-to-end motion, a tensioning device or a set of weights and clamps limiting the sample movement. Number of bending cycles, rollers diameter shall be specified in the specifications for cables.	No current interruption, no short circuit between conductors, no short circuit between sample and stand rollers.
Bending resistance with twisting [18]	Tests are carried out on samples with a length of at least 3.5 m. Samples of cables are fixed on a device consisting of a clamp with end-to-end motion, a mechanism ensuring rotation of the clamp. The test specimen is clamped at one end of the clamp and a load is hung at the other end. The test cycle consists of the clamp rotating in full turn, the specimen must be bent along a given radius at all points alternately contacting with the clamp as it rotates.	Overvoltage test, visual inspection.
Crushing resistance [19]	The test consists in compressing the sample between the dies. The dies form, the pressure value on the sample, the mutual arrangement of dies and the sample between them must be specified in the regulatory documentation for the cables.	No short circuit between conductors or between conductors and shield.
Resistance to high temperature impact [20]	Tests are carried out on three cable samples coiled in coils with an inner diameter not exceeding three minimum allowable bending radius during operation. Time and temperature of tests should be specified in the normative document on cables.	No cracks on the insulation and sheath surface, insulation resistance must meet the requirements of regulatory and technical documentation.
Resistance to low temperature impact [21]	Depending on the nominal cross section of conductors, the test procedure is different. For cables with an outer diameter of up to 12.5 mm, the samples are kept for at least 4 h and wound on a metal rod. The diameter of the rod, the windings number are chosen depending on the outside cable diameter. For cable products with a diameter of more than 12.5 mm, the samples are kept in a cold chamber for at least 4 h. After exposure, the sample must be subjected to three bending cycles around the rollers in opposite directions at an angle of at least 90^0. The bending cycle shall include right (left) bending, straightening, left (right) bending and straightening. Rollers diameter, test temperature shall be specified in the regulatory documentation for cables.	Over-voltage test, no cracks on the insulation and sheath surface.
Resistance to temperature changes [22]	The tests are carried out by three consecutive cycles on three samples coiled in coils. Coil diameter, cycles number and test temperature shall be specified in the specifications of the cables.	Overvoltage test, no cracks on the insulation and sheath surface.
Resistance to solar radiation [23]	Tests are carried out on three cable samples with a length of at least 1 m. Samples are placed in the chamber, turn on the radiation source, and then set the temperature in the chamber (in the shade) 55 ± 2 ^{0}C. Exposure time is 5 days.	No cracks on the insulation and sheath surface.
Ozone resistance [24]	The samples are placed in a test chamber with an ozone concentration of at least 0.0015 % and withstood for at least 180 min. The samples are bent at ambient temperature around	No cracks on the insulation and sheathing surface.

Type of test	Test method	Evaluation criterion (result)
	a brass, aluminum or wooden rod. The bent samples together with the rod are kept in the air at ambient temperature without any additional treatment for 30-45 min before starting the tests. The samples are then kept in a desiccator for at least 16 h at (23±5) °C. Both ends are fixed in the clamping device, stretch it by (33±2) % and leave in this device.	
Oil resistance [25]	Tests are carried out in the environment of industrial oil I-40A or I-50A according to GOST 20799 or diesel fuel. Exposure time and heating temperature of oil (diesel fuel) must be specified in technical conditions for specific cable brands.	The deviation of tensile strength and elongation at break before and after exposure does not exceed 40 %.
Resistance to high air humidity [26]	Tests are carried out on three cable samples with a length of at least 2 m. Cable samples are placed in the moisture chamber. Temperature, humidity and holding time shall be specified in the regulatory document for the cables.	No cracks on the insulation and sheath surface, insulation resistance must meet the requirements of regulatory and technical documentation.
Determination of physical and mechanical characteristics after exposure to high and low temperatures [27], [28]	Measurement of physical and mechanical characteristics is carried out on samples in the form of double-sided blades. The number of samples should be at least 5 for each test point.	The change in relative elongation and tensile strength should be no more / no less (%), must comply with the requirements of regulatory and technical documentation.

Depending on the purpose of the flexible cables, some or other methods are used in various combinations.

Methodical part

The representatives of the main groups of electrical insulating polymer materials currently used for manufacture of flexible cables were selected as the test object: rubber, EPR, PVC, polyolefin and urethane TPE, photopolymer.

The choice of test method is determined by standards recommendations, depending on the type of operational impact (Table l).

Test conditions and equipment requirements are stipulated in the regulatory and technical documentation: rollers, cylinders for cable coiling test and cable bending test through a roll system (error of measurements ± 0.5 %), equipment for testing cables through a roll system (measurement error of ± 10 %), breaking machines (measurement error of ± 0.5 %), climatic chamber of heat/cold (measurement error of ± 3 ^{0}C) micrometer (measurement error of ± 0,01 mm), microscope (measurement error of ± 0,003 mm), high-voltage tester (measurement error of ± 3 %), ozone resistance tester for rubber and cables (measurement error of ±10 %).

Experimental part

Heat resistance tests

Heat resistance is the ability of materials to maintain performance properties at high temperatures.

Temperature is a common factor affecting all cables. Thermal heating of insulation occurs due to dielectric losses when electric current flows through conductors and exposure to external ambient temperature. Long-term exposure to temperature leads to insulation aging and its gradual degradation with deterioration of physical, mechanical and electrical properties of the material, which ultimately reduces the service life.

Samples of cables without mechanical damage, cracks, pollutions and defects according to [27, 28] were selected for testing. Ageing time was 168 h. Test temperature was selected in accordance with the normative documents for flexible cables.

Evaluation criterion is the change in physical and mechanical characteristics not more than ±20 %. Aging temperature and evaluation results are shown in Table 2 and Figure 3.

Table 2

Aging temperature of polymeric materials

Insulation materials	Rubber	EPR	PVC	TPE (polyolefin, urethane)	Flouropolymers
Aging temperature, °C	80	135	100	100	280

Cold resistance tests

Implementation of programs for the Arctic region development determines the increased demand for cable products that are resistant to low temperatures.

The cables cold resistance is determined by the choice of electrical insulating polymer materials. It is the cable insulation fault that determines its breakdown at critically low temperatures. Compound frost resistance is the ability to maintain its performance properties at specified negative temperatures. Frost resistance criteria may be different depending on the requirements related to the conditions of its application. There are limited reductions of deformability or limited increase of frost resistance, absence of brittleness for insulation and sheath of cable products. The choice of polymer materials mainly has a significant impact on the operation efficiency and cable line reliability.

Three samples with a cable length of 1.5 m without mechanical damage, cracks, pollutions and defects were selected for testing according to [21]. Each sample was wound on a metal rod after 4 hours of staying in a cold chamber. The test temperature was from -10 to -60 ^{0}C. The coils number was selected based on the cable product diameter.

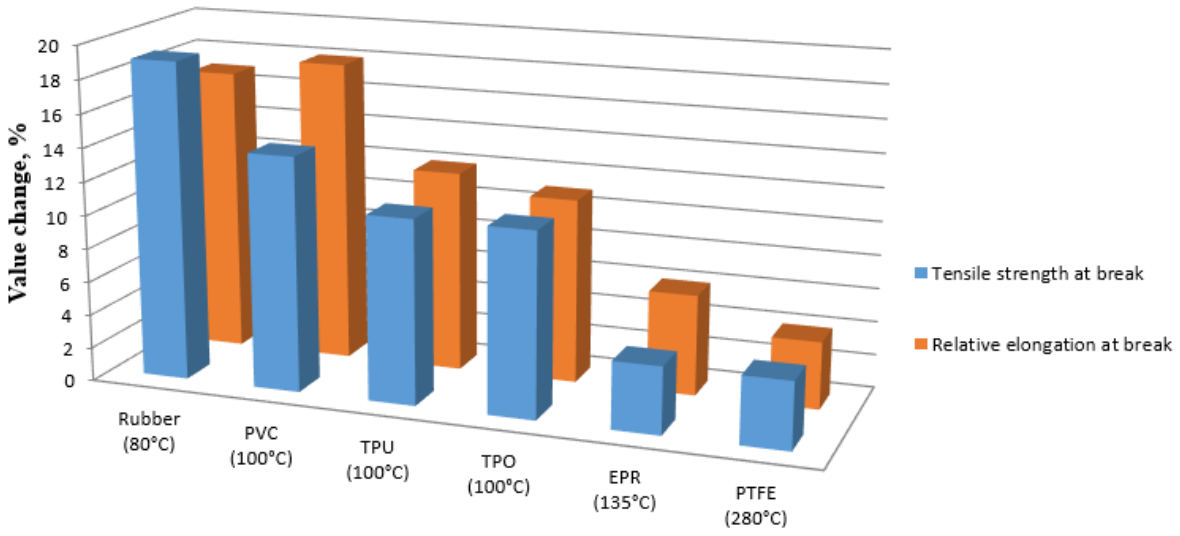

Figure 3. Physical and mechanical properties after thermal aging (test temperature indicated)

The evaluation criterion is the absence of cracks on the samples surface (Table 3).

Table 3

Installation bend resistance test results

Temperature, ºC	Material					
	EPR	PVC	Polyolefin TPE	Urethane TPE	Rubber	Fluoropolymer
-10	+	+	+	+	+	+
-15	+	+	+	+	+	+
-30	+	+	+	+	+	+
-40	+	-	+	+	+	+
-50	+	-	+	+	-	+
-60	+	-	+	+	-	+

Determination of cable resistance to the low temperature impact was also determined indirectly [27, 28] by determining the change in physical and mechanical characteristics (Table 4). The exposure time of the samples in the cold chamber was 4 h. Test temperature was chosen in accordance with the technical guide for flexible cables. Samples in the form of a double-sided blades were fixed in the tensile machine within the cold chamber. After the set exposure time, the relative elongation at break *Δl/l* was determined.

Evaluation criterion — the relative elongation must be at least 20 %.

Table 4

Elongation value after low temperature impact

Temperature, ºC	Material					
	EPR	PVC	Polyolefin TPE	Urethane TPE	Rubber	Fluoropolymer
-10	345 %	150 %	230 %	304 %	240 %	295 %
-15	334 %	102 %	210 %	295 %	180 %	289 %
-30	320 %	60 %	198 %	288 %	90 %	270 %
-40	307 %	-	156 %	270 %	40 %	268 %
-50	306 %	-	121 %	260 %	-	268 %
-60	302 %	-	120 %	251 %	-	267 %

Oil resistance test

Low-voltage cables are operated in conditions where the sheath and insulation are exposed to many factors simultaneously, including the aggressive environment impact. In production and transportation, liquid hydrocarbons exposure (diesel fuel (DF) and transformer oil (TO)) is one of the most important aging factors for low-voltage cables. To a greater extent, the cable service life depends on the sheath ability to withstand these fluids action.

The polymer materials oil resistance evaluation was carried out according to the results of change in tensile strength (σ_p) and change in relative elongation (*Δl/l)* after soaking samples in diesel fuel and transformer oil. The methodology recommended by [25, 27] was taken as the basis. Ageing time was 1000 hours, every 50 hours a batch of samples was taken out, and σ_p и *Δl/l* were determined. Aging time and evaluation results are shown in Figure 4 and Figure 5.

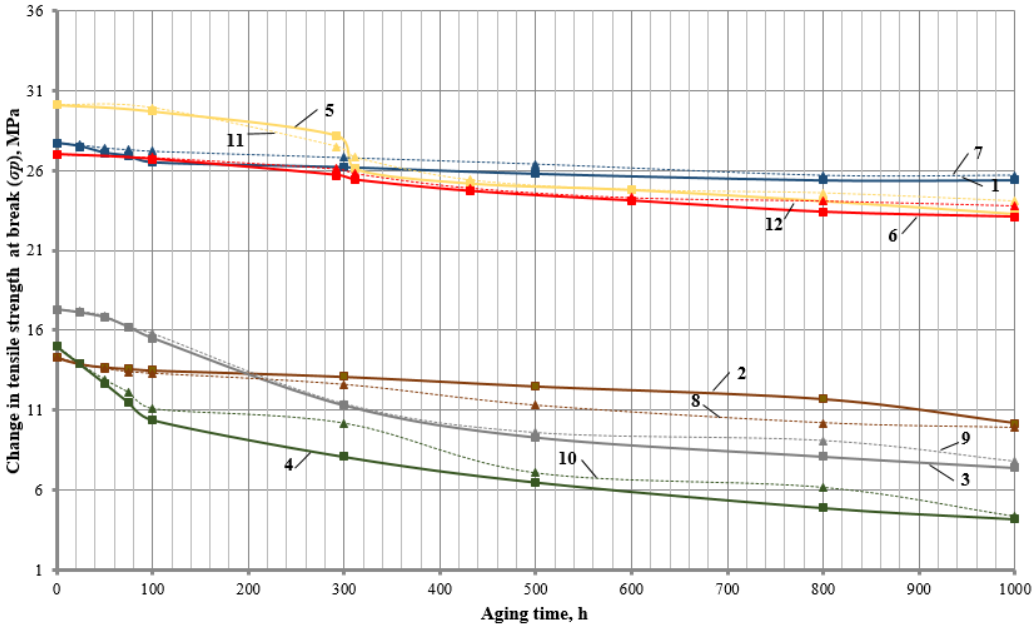

Figure 4. The tensile strength at break (σ_p) as a function of ageing time in diesel fuel and transformer oi, where 1 is PTFE in DF; 2 is PVC in DF; 3 is EPR in DF; 4 is rubber in DF; 5 is TPU in DF; 6 is TPO in DF; 7 is PTFE in TO; 8 is PVC in TO; 9 is EPR in TO; 10 is rubber in TO; 11 is TPU in TO; 12 is TPO in TO.

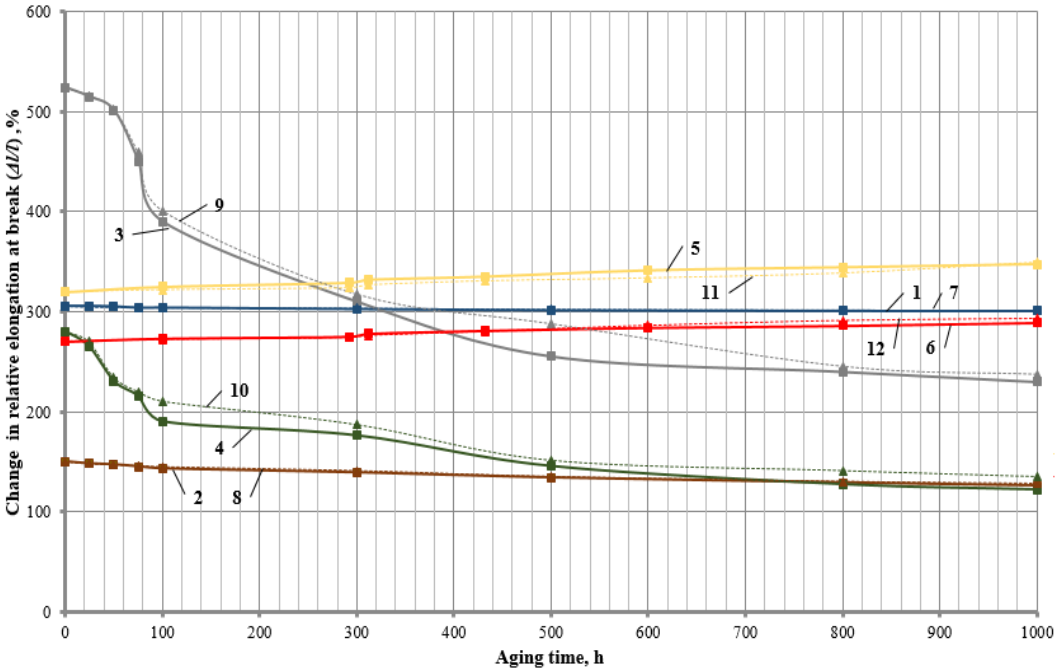

Figure 5. The relative elongation at break (*Δl/l)* as a function of aging time in diesel fuel and transformer oil, where 1 is PTFE in DF; 2 is PVC in DF; 3 is EPR in DF; 4 is rubber in DF; 5 is TPU in DF; 6 is TPO in DF; 7 is PTFE in TO; 8 is PVC in TO; 9 is EPR in TO; 10 is rubber in TO; 11 is TPU in TO; 12 is TPO in TO.

Ozone resistance tests

Ozone resistance is the ability of insulating material or insulation to remain in an atmosphere with high ozone content without damage or significant deterioration of properties [29]. Ozone exposure leads to accelerated aging and degradation of rubbers, and to a much lesser extent plastics. Ozone is especially dangerous for rubber-insulated/sheathed cables used outdoors, as even small ozone concentrations (e.g. after a thunderstorm) will cause the crack insulation. Because rubber-insulated/sheathed cables are flexible and designed to be connected to moving electrical equipment (walking excavators, industrial robots, etc.), they are often subjected to bending. Ozone exposure causes the crack insulation at the point of bending, causing the insulation to break and exposing the conductors.

Rubber and EPR aging were carried out for 8 hours with sample removal at 3, 5, and 8 hours, with an ozone concentration of 0.015 % according to [24]. At the end of the aging time, physical and mechanical characteristics were measured and visual inspection was performed. Results of ozone resistance tests of EPR and rubber are shown in Table 5.

Table 5

Results of ozone resistance tests of EPR and rubber

Aging time (hours)	EPR		Rubber	
Physical and mechanical characteristics	*σp*, MPa	*Δl*, %	*σp*, MPa	*Δl*, %
Aging temperature (150 ºC)				
0	5,5	348	Sample break (after 45 minutes the samples are completely destroyed)	
3	5,9	280		
5	5,9	280		
8	5,9	280		

Mechanical load tests

As a rule, flexible cables break down not as a result of electrical loads, but because of dynamic effects. Therefore, it is important to ensure equal strength of all design elements: core, insulation, shields and protective sheath under mechanical influences.

Tests are regulated by [17]. Tests are carried out on samples with a length of 5 m under current loading applied to the cable. Number of bending cycles is 30000. Evaluation criterion: there should be no short circuit between the conductors, short circuit between the sample and the stand rollers. Tests results for mechanical loads are shown in Table 6.

Table 6

Tests results for mechanical loads

Number of cycles	Material					
	EPR	PVC	Polyolefin TPE	Urethane TPE	Rubber	Fluoropolymer
30000	+	+	+	+	+	+

Results and Discussion

1. The existing approach makes it possible to effectively assess the polymer insulation heat resistance both at the stage of cable products manufacturing and during the incoming inspection of materials. After thermal aging all materials showed satisfactory resistance. Change of physical and mechanical characteristics was not more than 18 %. It is quite admissible, as according to normative and technical guide of cables with similar electric insulating materials the change of properties by more than ± 20 % is critical.

2. After low temperature exposing to materials (as PVC -30ºC, rubber -40ºC, thermoplastic elastomers, EPR and fluoropolymer -60ºC) relative elongation change $\Delta l/l$ of samples from EPR, TPE and fluoropolymer is insignificant. At the same time insulation materials from rubber and PVC also have not passed tests at temperatures from -40 to -60ºC in connection with "embrittlement" of materials.

3. Physical and mechanical properties changing after exposing to aggressive environments fully enough indicates the ability of the material and the design as a whole, to resist the action of hydrocarbon liquids. Among the polymers considered, fluoropolymer is the most resistant. Fluoropolymer samples showed "good" resistance to the action of both diesel fuel and transformer oil. The tensile strength changing at break σ_p and relative elongation $\Delta l/l$ does not exceed 10 %. Resistance of fluoroplastic to hydrocarbon liquids is explained by high value of bonding energy "carbon-fluorine", by specific structure of polymer macromolecules expressed in the fact that fluorine atoms completely "screen" the carbon skeleton of macromolecules [30-31]. Samples made by rubber and ethylene propylene rubber, thermoplastic elastomers showed "poor" resistance to aggressive media. The change of physical and mechanical characteristics was about 37 %. However, such values are admissible due to the fact that in normative and technical documentation the evaluation criterion is the change of physical and mechanical characteristics by not more than 40 %. Samples from PVC were not passed, as the change in relative elongation was more than 50 %. These materials are weakly polar. The polymers chemical nature affects the diffusion rate of physically aggressive environment into them. Weak resistance of samples to penetration of hydrocarbon liquids means that there is a high affinity between the polymer molecules and the aggressive environment (diesel fuel, transformer oil), the measure of which is the change in free energy. The greater the decrease in free energy during mixing, the more hydrocarbon liquid penetrates into the polymer. The dissolution intensity of polar liquids in polar materials significantly exceeds the dissolution intensity in non-polar materials [32].

4. The ozone effect on rubber in its destructive power is one of the most aggressive. Ozone aging of rubber is expressed in the appearance of characteristic cracks on the surface and loss of the original physical and mechanical characteristics and other properties. The resistance of ethylene propylene rubber is due to the insignificant content of double bonds.

5. All polymer materials have successfully passed the test for mechanical tests. This approach makes it possible to evaluate not only the properties of the materials, but also the reliability of the design as a whole.

Conclusions

According to the test results, promising materials for insulation and sheath of flexible cables can be identified:

- EPR, TPE and fluoropolymer for use in flexible cables operating at low and high temperatures, as well as when exposed to hydrocarbon liquids;
- EPR as insulation and sheath of flexible cables operating under ozone exposure.

The success of the passed tests with all samples confirms the correctness of the preliminary selection.

References

1 Nematia H.M. Reliability evaluation of power cables considering the restoration characteristic / H.M. Nematia, A. Sant'Anna, S. Nowaczyka, J.H. Jürgensenb, P. Hilberb // Enternational Journal of Electrical Power & Energy Systems. — 2019. — Vol. 105. — P. 277.

2 Wang J. Adaptive event-triggered PDE control for load-moving cable systems / J. Wang, M. Krstic // Automatica. — 2021. — Vol. 129. — P109637-109657.

3 Blivet C. Non-Arrhenius behavior: Influence of the crystallinity on lifetime predictions of polymer materials used in the cable and wire industries. / C. Blivet, L. Jean-François, Y. Israëli, P.-O. Bussière // Journal of Polymer Degradation and Stability. — 2022. Vol. 199. — P. 109890.

4 Bonneric M. Finite element simulation of a steel cable — rubber composite under bending loading: Influence of rubber penetration on the stress distribution in wires / M. Bonneric, V. Aubin, D. Durville // International Journal of Solids and Structures. — 2019. — Vol. 160. — P. 158-167.

5 Saman N.M. Barrier effect on electrical tree growth characteristics in silicon rubber / N.M. Saman, C.L.G.P. Kumar, M.H. Ahmad, Z. Nawawi, M.A.B. Sidik, M.I. Jambak // Journal of Electrostatics. — 2022. — Vol. 115. — P. 103682.

6 Lei Z. Mechanism of bulk charging behavior of ethylene propylene rubber subjected to surface charge accumulation / Z. Lei, C. Li, R. Men // Journal of Applied Physics. — 2018. — Vol. 124. — P. 244103.

7 Jing Y. Improved ethylene-propylene rubber /silica interface via in-situ polymerization / Y. Jing, Nui Hiu, Y. Li // Journal of Polymer. — 2019. — Vol. 172. — P. 117-125.

8 Wang Z. Thermal degradation kinetics study of polyvinyl chloride (*PVC*) sheath for new and aged *cables* / Z. Wang, T. Xie, X. Ning, Y. Liu, J. Wang // Journal of Waste Management. — 2019. — Vol. 99. — P. 146 — 153.

9 Zanchin G. Polyolefin thermoplastic elastomers from polymerization catalysis: Advantages, pitfalls and future challenges. / G. Zanchin, G. Leone // Journal of Progress in Polymer Science. — 2021. — Vol. 113. — P. 103342.

10 Lu Y. Operational state assessment of cross-linked polyethylene power cable on the basic of an optimized cloud matter-element theory / Y. Lu, G. Zhang, J. Qi, Y. Huang // Journal of Sustainable Energy Technologies and Assessment. — 2021. — Vol. 48. — P. 101584.

11 Gulski E. Discussion of electrical thermal aspect of offshore wind warms' power cable reliability / E. Gulski, G.J. Andres, R.A. Jongen, J. Parciak, J. Siemiński, E. Piesowicz, S. Paszkiewicz, I. Irska // Journal of Renewable and Sustainable Energy Reviews. — Vol. 151. — P. 11580.

12 Ebnesajjad S. Applications of Fluoropolymers / S. Ebnesajjad // Introduction to Fluoropolymers. — 2021. — P. 253-269.

13 Lv N. A review of techniques for modeling flexible cables / N. Lv, I. Liu, H. Xia, J. Ma, X. Yang // Journal of Computer-Aided Design. — 2020. — Vol. 122. — P. 102826.

14 Lin L. Aging life evaluation of coal mining flexible EPR cables under multi-stresses / L. Lin, C. Lin, P. Geng, Zh. Lei, J. Song, M. Tian // Journal of Physics: Conference Series. — 2020. — No. 8. — P. 53539-53546.

15 Bowler N. Dielectric and Mechanical Behavior of Thermally Aged EPR/CPE Cable Materials. / N. Bowler, S.W. Glass, S. Leonard, A.S. Fifield, S.W. Glass, L.S. Fifield // Conference on Electrical Insulation and Dielectric Phenomena (CEIDP). — 2018. — P. 11-17.

16 ГОСТ 12182.8–80. Кабели, провода и шнуры. Метод проверки стойкости к изгибу. — М.: Стандартинформ Российской Федерации, 1982. — 3 с.

17 ГОСТ 12182.1–80. Кабели, провода и шнуры. Методы проверки стойкости к многократному перегибу через систему роликов. — М.: Стандартинформ Российской Федерации, 1982. — 16 с.

18 ГОСТ 12182.3-80. Кабели, провода и шнуры. Методы проверки стойкости к изгибу с осевым кручением. — М.: Стандартинформ Российской Федерации, 1982. — 3 с.

19 ГОСТ 12182.5–80. Кабели, провода и шнуры. Метод проверки стойкости к растяжению. — М.: Стандартинформ Российской Федерации, 1982. — 2 с.

20 ГОСТ 20.57.406–81 (метод 201–1.1). Комплексная система контроля качества. Изделия электронной техники, квантовой электроники и электротехнические. Методы испытаний. — М.: Стандартинформ Российской Федерации, 1982. — 133 с.

21 ГОСТ 17491–80. Кабели, провода и шнуры с резиновой и пластмассовой изоляцией и оболочкой. Методы испытания на холодостойкость. — М.: Стандартинформ Российской Федерации, 1981. — 5 с.

22 ГОСТ 20.57.406–81 (метод 205–1). Комплексная система контроля качества. Изделия электронной техники, квантовой электроники и электротехнические. Методы испытаний. — М.: Стандартинформ Российской Федерации, 1982. — 133 с.

23 ГОСТ 20.57.406–81 (метод 211–1). Комплексная система контроля качества. Изделия электронной техники, квантовой электроники и электротехнические. Методы испытаний. — М.: Стандартинформ Российской Федерации, 1982. — 133 с.

24 ГОСТ IEC 60811–403–015. Кабели электрические и волоконно-оптические. Методы испытаний неметаллических материалов. Ч. 403. Разные испытания. Испытания сшитых композиций на озоностойкость. — М.: Стандартинформ Российской Федерации, 2016. — 12 с.

25 ГОСТ IEC 60811–404–2015. Кабели электрические и волоконно-оптические. Методы испытаний неметаллических материалов. Ч. 404. Разные испытания. Испытания оболочек кабеля на стойкость к минеральному маслу. — М.: Стандартинформ Российской Федерации, 2016. — 12 с.

26 ГОСТ 16962.1–89. Изделия электротехнические. Методы испытаний на устойчивость к климатическим внешним воздействующим факторам. — М.: Государственный комитет СССР по управлению качеством продукции и стандартам, 1990. — 84 с.

27 ГОСТ IEC 60811–501–2015. Кабели электрические и волоконно-оптические. Методы испытаний неметаллических материалов. Ч. 501. Механические испытания. Испытания для определения механических свойств композиций изоляции и оболочек. — М.: Стандартинформ Российской Федерации, 2016. — 16 с.

28 ГОСТ IEC 60811–401–2015. Кабели электрические и волоконно-оптические. Методы испытаний неметаллических материалов. Ч. 401. Разные испытания. Методы теплового старения. Старение в термостате. — М.: Стандартинформ Российской Федерации, 2016. — 20 с.

29 Zheng T. Study on the ozone aging mechanism of Natural Rubber / T. Zheng, X. Zheng, Sh. Zhan, J. Zhou, S. Liao // Journal of Polymer Degradation and Stability. — 2021. — Vol. 186. — P. 109514.

30 Peng B. Activation of different C-F bonds in fluoropolymers for Cu(o) –mediated single electron transfer radical polymerization / B. Peng, J.Wang, M. Li, M. Wang, Sh. Tan, Zh. Zhang // Journal Polymer Chemistry. — 2021. — No. 12. — P. 3132-3141.

31 Yarkimbaev Sh.S. Study of physical control methods for metric parameters of extended products in cable industry. / Sh.S. Yarkimbaev, E.M. Fedorov, V.V. Redko, O.V. Galtseva, X. Jiang // Bulletin of the University of Karaganda-Physics. —2022. — No. 2(106). — P. 7-17.

32 Leon A. High performance polymers for oil and gas applications / A. Leon, Í.G.M. Silva, K.D. Pangilinan, Q. Chen, E.B. Caldona, R.C. Advincula // Journal of Reactive and Functional Polymers. — 2021. — Vol. 162. — P. 104878.

А. Леонов, Т. Солдатенко

Икемді кабельдерге қолданылатын полимерлі электр оқшаулағыш материалдардың эксплуатациялық әсерлерге төзімділігін бағалау

Мақалада оқшаулау ретінде икемді кабельдерді пайдалану мүмкіндігін ескере отырып, полимерлі материалдардың қасиеттерін зерттеу нәтижелері берілген. Кабельдік бұйымдардың құрылымдарының негізгі түрлері және олардың жұмыс істеу ерекшеліктері қарастырылған. Оқшаулаудың жылу, механикалық, электрлік және сыртқы әсер етуші факторларға төзімділігін тәжірибелік анықтаудың қолданыстағы әдістеріне талдау жүргізілген. Зертханалық жабдыққа қойылатын талаптар және сынақ жағдайлары сипатталған. Сынақ нәтижелерін бағалау критерийлері атап өтілген. Қазіргі уақытта икемді кабельдер өндірісінде қолданылатын электр оқшаулағыш материалдардың негізгі түрлерінің қасиеттерінің өзгеру дәрежесін эксперименталды түрде анықтау жүргізілді: поливинилхлоридті пластикат (ПВХ-пластикат), резеңке, этиленпропиленді резеңке (ЭПР), термопластик (ТЭП), фторполимер. Сынақтар жоғары және төмен температуралардың, агрессивті орталардың, озонның және механикалық жүктемелердің әсерінен жүргізілді. Зерттелетін материалдардың электрофизикалық және физика-механикалық қасиеттерінің өзгеруін анықтайтын негізгі процестер сипатталған. ЭПР, ТЭП және фторполимерлі оқшаулау температураның кең диапазонына, механикалық жүктемелерге, дизельдік отынға және трансформатор майына төзімді екені көрсетілген. Сондай-ақ ЭПР озонға төзімділігінің жоғарылауы байқалды. Резеңке және ПВХ-пластикат төмен және жоғары температура әсерінен сынақтардан өтпеді, сонымен қатар агрессивті орталарға «нашар» қарсылық көрсетті, бірақ, өз кезегінде, механикалық әсер кезінде сынақтардан өтті. Икемді кабельдердің ерекшеліктерін ескере отырып, полимерлі оқшаулауды сынау және қолдану бойынша ұсыныстар жасалған.

Кілт сөздер: икемді кабель, оқшаулау, қабық, ПВХ пластикат, термоэластопласт, фторполимер, этиленпропиленді резеңке, озонға төзімділік, майға төзімділік, механикалық беріктік, сынақтар.

А. Леонов, Т. Солдатенко

Оценка стойкости полимерных электроизоляционных материалов, применяемых в гибких кабелях, к эксплуатационным воздействиям

В статье приведены результаты исследования свойств полимерных материалов с учетом возможности применения в качестве изоляции гибких кабелей. Рассмотрены основные типы конструкций кабельных изделий и особенности их эксплуатации. Проведен анализ существующих методов экспериментального определения стойкости изоляции к тепловым, механическим, электрическим и внешним воздействующим факторам. Описаны требования к лабораторному оборудованию и условиям проведения испытаний. Отмечены критерии оценки результатов испытаний. Проведено экспериментальное определение степени изменения свойств основных типов электроизоляционных материалов, применяемых в настоящее время при производстве гибких кабелей: поливинилхлоридный пластикат (ПВХ–пластикат), резина, этиленпропиленовая резина (ЭПР), термоэластопласт (ТЭП), фторполимер. Испытания были проведены при воздействии повышенных и пониженных температур, агрессивных сред, озона, механических нагрузок. Описаны основные процессы, определяющие изменение электрофизических и физико-механических свойств исследованных материалов. Показано, что ЭПР, ТЭП и фторполимерная изоляция обладают стойкостью к воздействию широкого диапазона температур, механических нагрузок, устойчивы к воздействию дизельного топлива и трансформаторного масла. Также отмечена повышенная устойчивость ЭПР к воздействию озона. Резина и ПВХ–пластикат не прошли испытания при воздействии пониженных и повышенных температур, а также показали «плохую» устойчивость к воздействию агрессивных сред, но, в свою очередь, прошли испытания при механических воздействиях. Сделаны рекомендации по испытаниям и применению полимерной изоляции с учетом специфики работы гибких кабелей.

Ключевые слова: гибкие кабели, изоляция, оболочка, поливинилхлоридный пластикат, термоэластопласт, фторполимер, этиленпропиленовая резина, озоностойкость, маслостойкость, механическая прочность, испытания.

References

1 Nematia, H.M., Sant'Anna, A., Nowaczyka, S., Jürgensenb, J.H., & Hilberb, P. (2019). Reliability evaluation of power cables considering the restoration characteristic. *Enternational Journal of Electrical Power* & *Energy Systems, 105*, 277.

2 Wang, J., & Krstic, M. (2021). Adaptive event-triggered PDE control for load-moving cable systems. *Automatica, 129*, 109637-109657.

3 Blivet, C., Jean-François, L., Israëli, Y., & Bussière, P.-O. (2022). Non-Arrhenius behavior: Influence of the crystallinity on lifetime predictions of polymer materials used in the cable and wire industries. *Journal of Polymer Degradation and Stability, 199*, 109890.

4 Bonneric, M., Aubin V., & Durville, D. (2019). Finite element simulation of a steel cable — rubber composite under bending loading: Influence of rubber penetration on the stress distribution in wires. *International Journal of Solids and Structures, 160*, 158-167.

5 Saman, N.M., Kumar, C.L.G.P., Ahmad, M.H., Nawawi, Z., Sidik, M.A.B., & Jambak, M.I. (2022). Barrier effect on electrical tree growth characteristics in silicon rubber. *Journal of Electrostatics, 115*, 103682.

6 Lei, Z., Li, C., & Men, R. (2018). Mechanism of bulk charging behavior of ethylene propylene rubber subjected to surface charge accumulation. *Journal of Applied Physics, 124*, 244103.

7 Jing Y., Hiu Nui, & Li, Y. (2019). Improved ethylene-propylene rubber /silica interface via in-situ polymerization. *Journal of Polymer, 172*,117—125.

8 Wang, Z., Xie, T., Ning, X., Liu, Y., & Wang, J. (2019). Thermal degradation kinetics study of polyvinyl chloride *(PVC)* sheath for new and *aged cables*. *Journal of Waste Management, 99*, 146—153.

9 Zanchin, G., & Leone, G. (2021). Polyolefin thermoplastic elastomers from polymerization catalysis: Advantages, pitfalls and future challenges. *Journal of Progress in Polymer Science, 113*, 103342.

10 Lu, Y., Zhang, G., Qi, J., & Huang, Y. (2021). Operational state assessment of cross-linked polyethylene power cable on the basic of an optimized cloud matter-element theory. *Journal of Sustainable Energy Technologies and Assessment, 48*, 101584.

11 Gulski, E., Andres, G.J., Jongen, R.A., Parciak, J., Siemiński, J., Piesowicz, E., Paszkiewicz, S., & Irska, I. (2021). Discussion of electrical thermal aspect of offshore wind warms' power cable reliability. *Journal of Renewable and Sustainable Energy Reviews, 151*, 11580.

12 Ebnesajjad, S. (2021). Applications of Fluoropolymers. *Introduction to Fluoropolymers*, 253—269.

13 Lv, N., Liu, I., Xia, H., Ma, J., & Yang, X. (2020). A review of techniques for modeling flexible cables. *Journal of Computer-Aided Design, 122*, 102826.

14 Lin, L., Lin, C., Geng, P., Lei, Zh., Song, J., & Tian, M. (2020). Aging life evaluation of coal mining flexible EPR cables under multi-stresses, *Journal of Physics: Conference Series, 8*, 53539-53546.

15 Bowler, N., Glass, S.W., Leonard, S., Fifield, A.S., Glass, S.W., & Fifield, L.S. (2018). Dielectric and Mechanical Behavior of Thermally Aged EPR/CPE Cable Materials. *Conference on Electrical Insulation and Dielectric Phenomena (CEIDP)*, 11—17.

16 GOST 12181.8–80. (1982). *Kabeli, provoda i shnury. Metod proverki stoikosti k izgibu [Cables, wires and cords. Methods of control of bending strength]*. Moscow: Standartinform Rossiiskoi Federatsii [in Russian].

17 GOST 12181.1–80. (1982). *Kabeli, provoda i shnury. Metody proverki stoikosti k mnogokratnomu peregibu cherez sistemu rolikov [Cables, wires and cords. Methods of multifold bendig resistance trough a roll system]*. Moscow: Standartinform Rossiiskoi Federatsii [in Russian].

18 GOST 12182.3–80. (1982). *Kabeli, provoda i shnury. Metody proverki stoikosti k izgibu s osevym krucheniem [Cables, wires and cords. Methods of control of bending resistance with twisting]*. Moscow: Standartinform Rossiiskoi Federatsii [in Russian].

19 GOST 12182.5–80. (1982). *Kabeli, provoda i shnury. Metod proverki stoikosti k rastiazheniiu [Cables, wires and cords. Method of checking for elongation resistance]*. Moscow: Standartinform Rossiiskoi Federatsii [in Russian].

20 GOST 20.57.406–81 (metod 201–1.1). (1982). *Kompleksnaia sistema kontrolia kachestva. Izdeliia elektronnoi tekhniki, kvantovoi elektroniki i elektrotekhnicheskie. Metody ispytanii [Complex quality control system. Electronic, quantum electronic and electrotechnical components. Test methods*]. Moscow: Standartinform Rossiiskoi Federatsii [in Russian].

21 GOST 17491–80. (1981). *Kabeli, provoda i shnury s rezinovoi i plastmassovoi izoliatsiei i obolochkoi. Metody ispytaniia na kholodostoikost [Cable wires and cords with rubber and plastic insulation and sheath. Methods of frostproofness test]*. Moscow: Standartinform Rossiiskoi Federatsii [in Russian].

22 GOST 20.57.406–81 (metod 205-1). (1982). *Kompleksnaia sistema kontrolia kachestva. Izdeliia elektronnoi tekhniki, kvantovoi elektroniki i elektrotekhnicheskie. Metody ispytanii [Complex quality control system. Electronic, quantum electronic and electrotechnical components. Test methods*]. Moscow: Standartinform Rossiiskoi Federatsii [in Russian].

23 GOST 20.57.406-81 (metod 211–1). (1982). *Kompleksnaia sistema kontrolia kachestva. Izdeliia elektronnoi tekhniki, kvantovoi elektroniki i elektrotekhnicheskie. Metody ispytanii [Complex quality control system. Electronic, quantum electronic and electrotechnical components. Test methods*]. Moscow: Standartinform Rossiiskoi Federatsii [in Russian].

24 GOST IEC 60811–403–2015. (2016). *Kabeli elektricheskie i volokonno-opticheskie. Metody ispytanii nemetallicheskikh materialov. Chast 403. Raznye ispytaniia. Ispytaniia sshitykh kompozitsii na ozonostoikost [Electric and optical fiber cables. Test methods for non-metallic materials. Part 404. Miscellaneous tests. Ozone resistance test on cross-linked componds]*. Moscow: Standartinform Rossiiskoi Federatsii [in Russian].

25 GOST IEC 60811–404–2015. (2016). *Kabeli elektricheskie i volokonno-opticheskie. Metody ispytanii nemetallicheskikh materialov. Chast 404. Raznye ispytaniia. Ispytaniia obolochek kabelia na stoikost k mineralnomu maslu [Electric and optical fiber cables. Test methods for non-metallic materials. Part 404.Miscellaneous tests. Mineral oil immersion tests for sheaths]*. Moscow: Standartinform Rossiiskoi Federatsii [in Russian].

26 GOST 16962.1–89. (1990). *Izdeliia elektrotekhnicheskie. Metody ispytanii na ustoichivost k klimaticheskim vneshnim vozdeistvuiushchim faktoram [Electrical articles. Test methods as to environments climatic factors resistance]*. Moscow: Gosudarstvennyi komitet SSSR po upravleniiu kachestvom produktsii i standartam [in Russian].

27 GOST IEC 60811–501–2015. (2016). *Kabeli elektricheskie i volokonno-opticheskie. Metody ispytanii nemetallicheskikh materialov. Chast 501. Mekhanicheskie ispytaniia. Ispytaniia dlia opredeleniia mekhanicheskikh svoistv kompozitsii izoliatsii i obolochek [Electric and optical fibre cables. Test methods for non-metallic materials. Part 501. Mechanical tests. Tests for determining the mechanical properties of insulating and sheathing compounds]*. Moscow: Standartinform Rossiiskoi Federatsii [in Russian].

28 GOST IEC 60811–401–2015. (2016). *Kabeli elektricheskie i volokonno-opticheskie. Metody ispytanii nemetallicheskikh materialov. Chast 401. Raznye ispytaniia. Metody teplovogo stareniia. Starenie v termostate [Electric and optical fibre cables. Test methods for non-metallic materials. Part 401. Miscellaneous tests. Thermal ageing methods. Ageing in an air oven]*. Moscow: Standartinform Rossiiskoi Federatsii [in Russian].

29 Zheng, T., Zheng, X., Zhan, Sh., Zhou, J., & Liao, S. (2021). Study on the ozone aging mechanism of Natural Rubber. *Journal of Polymer Degradation and Stability, 186*, 109514.

30 Peng, B., Wang, J., Li, M., Wang, M., Tan, Sh., & Zhang, Zh. (2021). Activation of different C-F bonds in fluoropolymers for Cu(o) — mediated single electron transfer radical polymerization. *Journal Polymer Chemistr*y, *12*, 3132-3141.

31 Yarkimbaev, Sh.S., Fedorov, E.M., Redko, V.V., Galtseva, O.V., & Jiang, X. (2022). Study of physical control methods for metric parameters of extended products in cable industry. *Bulletin of the University of Karaganda-Physics, 2(106)*, 7—17.

32 Leon, A., Silva, Í.G.M., Pangilinan, K.D., Chen, Q., Caldona, E.B., & Advincula, R.C. (2021). High performance polymers for oil and gas applications. *Journal of Reactive and Functional Polymers, 162*, 104878.

DOI 10.31489/2022PH4/85-93

UDC 621.74.011:669.017

E.N. Eremin

Omsk State Technical University, Omsk, Russia
(E-mail: weld_techn@mail.ru)

Influence of modification of the cast metal structure by solid phase particles on the nucleation of crystallization centers and their stability

The inoculation method has wide possibilities for improving the mechanical and operational properties of cast metal, which makes it possible to create artificial centers of crystallization due to the direct introduction of dispersed refractory particles into the melt. The efficiency of such particles serving as crystallization centers is due to the presence of an activated transition layer on their surface. In this regard, it is promising to use complex modification, in which activating additives are introduced into the melt together with dispersed refractory particles, which form a transition layer with the desired properties on the particles. At the same time, the features of the interaction of particles with activating additives have not been sufficiently studied. A theoretical assessment of the influence of dispersed particles on the nucleation of crystallization centers and their stability was carried out on the basis of a study of the phenomena of wetting, adsorption, and dissolution using the relationship between the critical size of additional nuclei, their wetting angle, and supercooling of the melt. It is shown that if between the particle and the cladding layer the difference in chemical potentials of the contacting phases will exist throughout the entire process, and on the surface of the complex it will have a low value of surface tension, then such a particle will be stable, which takes place during adsorption of a surface-active component from a melt. Therefore, the efficiency of melt heterogenization and modification of the cast metal structure is determined by the thermodynamic activity of the substance of the transition layer to the material of the solid phase particle. The obtained conclusions make it possible to select the composition of complex modifiers that allow controlling the structure of castings in the process of their crystallization.

Key words: cast metal, suspension, modification, particles, crystallization, adsorption, wetting, interfacial energy, structure

Introduction

Of considerable interest for improving the quality of cast metal is the use of the modification method by creating artificial crystallization centers due to the direct introduction of refractory inoculant particles into the melt [1–9]. The efficiency of such particles as crystallization centers is characterized by the presence of an activated transition layer on their surface. Therefore, it is advisable to use complex modification, in which certain elements are introduced into the melt together with inoculator particles as activating additives (protectors), with the help of which it is possible to form a transition layer with the desired properties on the particles [10, 11]. However, the features of the interaction between the inoculant particle and the protector metal have not been sufficiently studied. This work is devoted to this problem.

Analysis of the processes of nucleation of crystallization centers and their stability during the complex modification of foundry metal with particles of dispersed powders

To assess the effect of complex modification of dispersed powder particles on the nucleation of crystallization centers and their stability, the concepts presented by B. Chalmers [12] were used, based on the relationship between the critical size r^* of prenuclei, their wetting angle θ and supercooling of the melt ΔT, shown in the diagram (Figure 1), from which it follows that with a decrease in θ, ΔT decreases. This provision can be taken as a working hypothesis when solving the issue of increasing the efficiency of modifying the structure of steels and alloys using natural and artificial solid-phase substrates (inoculator) activated by surface-active elements (protector) or intermetallic compounds and heterogenizing the melt as a result of selective adsorption of chemical elements from the alloy.

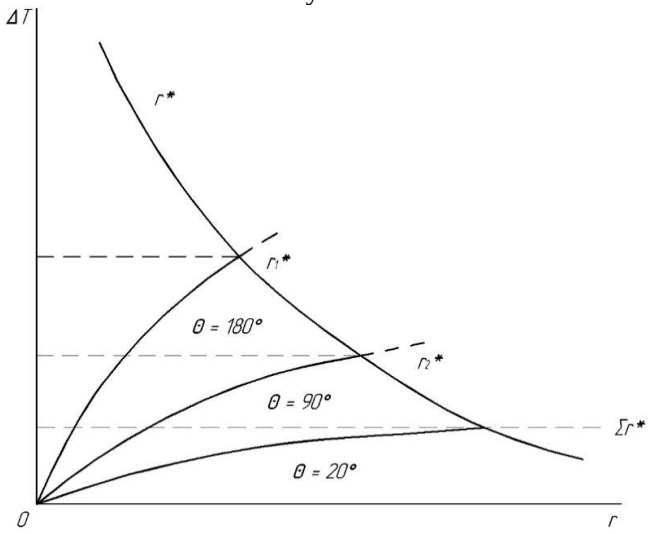

Figure 1. Conditions for heterogeneous nucleation of crystallization centers with radius r at different contact angles θ

The study of the phenomena of wetting, adsorption, dissolution, and nucleating activity of solid phase particles was carried out on the model of the structure of a suspension with particles in a metal melt, shown in Figure 2.

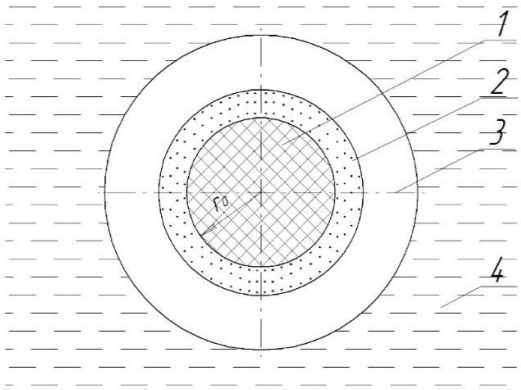

Figure 2. Model of the structure of a particle of a complex modifier in a metal melt: 1 — particle core; 2 — transition layer; 3 — adsorbed layer; 4 — metal melt

The core of such a complex is a refractory particle of the solid phase 1 with radius $r_0<r^*$, the surface of which is clad with a layer of substance 2 formed by the product of the interaction of the protector metal with the material of the particle and chemical elements adsorbed from some volume 3 of the melt 4. The boundary between 3 and 4 However, in volume 3, which is depleted in the content of chemical elements that have reacted with the material of the cladding layer, adhesion forces can act on the surface of the particle, forming a concentration fluctuation [13].

Wettability in the system solid (s) — liquid (l) — gas (g) is usually considered by the example of the contact of a flat substrate with a melt drop [14]. If a flat substrate is rolled into a sphere of radius r, then the wetting conditions — the values of the wetting angle (θ) and the values of surface tension (σ_{sl}) will change, σ_{sl} will decrease, and the work of adhesion between the solid and liquid phases WA will increase, since from the Dupre equation follows:

$$\sigma_{sl} = \sigma_{lg} + \sigma_{sg} - W_A, \quad (1)$$

$$W_A = W_A^e + W_A^{none.}, \quad (2)$$

where W_A^e and $W_A^{none.}$ are the equilibrium and nonequilibrium parts of W_A: $W_A^e = W_A^x + W_A^{VDW}$. Here W_A^x is the energy of cohesion of the liquid and solid phases at a steady state equilibrium of chemical bonds; W_A^{VDW} is the energy of the Van der Waals interaction. As r decreases, the contribution of W_A^{VDW} to W_A^e increases. Therefore, in equilibrium systems, the interfacial energy σ_{sl} is the smaller, the smaller the difference in the structure of the contacting phases.

If there is a chemical interaction between the S and L phases, then σ_{sl} will change with time and can be extremely low [15].

It follows from Dupre's equation (1) that the more intensively the phases interact, the less σ_{sl}. When the system approaches equilibrium, when the chemical potentials of the phases are equalized ($\mu_i^s \approx \mu_i^l$), σ_{sl} can increase due to the action of the transition layer (the effect of A.A. Zhukhovitsky) [16].

This property of the interacting phases ensures the stability of the solid phase in the melt in the case of the formation of a refractory transition layer with a low diffusion mobility of atoms, which is characteristic of metallides or intermetallides.

Change σ_{sl} depends on the difference in chemical potentials of the contacting phases $\Delta\mu$ and is found by the formula

$$\Delta\sigma_{sl} = M \cdot \Delta\mu, \quad (3)$$

where M is a constant.

The stability of suspension particles with a transition layer between a solid core and a melt can be estimated by a criterion obtained from formal thermodynamic relations [17]:

$$K = \sigma_{sg} - \sigma_{sl} - 0{,}5\sigma_{lg}. \quad (4)$$

The system is considered stable if K>0, i.e. $\sigma_{sg} > \sigma_{sl} - 0{,}5\sigma_{lg}$. This condition is satisfied when σ_{sl} is sufficiently small. If a chemical potential difference $\Delta\mu$ exists between the particle and the cladding layer throughout the entire process, then, according to formula (3), $\Delta\sigma_{sl}$ is sufficiently large, and a low value $\mu_i^1 \approx \mu_i^s$ will occur on the surface of the complex at σ_{sl}, and such a particle will be stable. This is noted during the adsorption of some surface-active component from the melt, the transition of one of the components through the phase boundary, or during partial dissolution of the solid phase. According to the Neumann equation $K = \sigma_{lg}(\cos\theta - 0{,}5)$, and considering adhesion to a solid $K = W_A - (3/2)\sigma_{sl}$. The boundary between K>0 and K<0 is at $\theta \approx 60°$, and the evaluation criterion acquires a positive sign, which is a sign of suspension stability.

Based on the studies of the mechanism of homogeneous nucleation during steel deoxidation, carried out by S.I. Popel and M.P. Dokhov [18, 19], and the possibility of using the Gibbs equation instead of the Helmholtz function for small volume changes during the formation of a spherical nucleus with a critical size *r**, can be written:

$$r^* = 2\sigma \cdot V_0 / \Delta G, \tag{5}$$

where σ is the interfacial energy; V_0 — molar volume of the embryo; ΔG is the total change in the free energy of the system. With a small change in volume, the change in stresses in the old phase can be neglected, then ΔG can be represented by the sum:

$$\Delta G = \Delta G_V + \Delta G_S. \tag{6}$$

$\Delta G_v = -4L\Delta T\pi r^3/(3T_e)$ is the change in volumetric and surface free energy, where T_e is the equilibrium melting temperature; ΔT is the difference in melting and crystallization temperatures (supercooling); L is the volumetric heat of transformation. Then the critical radius of the equilibrium embryo is determined:

$$r_e^* = 2\sigma V_0 T_e /(L\Delta T). \tag{7}$$

The calculation of r_P^* according to expression (7), performed by Yu.Z. Babaskin [20], showed that at ΔT =320 °C for pure iron r_e^* = 1.3 nm. If a surfactant is introduced into the melt, then the value of σ can decrease, for example, to 10^{-5} J/cm^2. Then the nucleus will reach the critical size at supercooling ΔT ≈ 160 °C.

A change in the chemical composition of the liquid metal will certainly affect the value of the interfacial energy σ_{sl}, but for transition metal alloys, the general pattern of formation of metal-like compounds should be preserved due to the similarity in the electronic structure and high values of the adhesion work WA. Calculations show that the probability of heterogeneous nucleation crystallization centers by carbide phases in iron-carbon alloys, in accordance with the change in the free energy of formation of compounds, 33 decreases in the following series of chemical elements: Zr → Ti → Ta → Nb → Cr → V → Si → Fe [18, 19].

If ready-made nucleation centers are introduced into the melt, for example, particles of ultrafine powders (UDP) TiC, TiN, TiCN, strong carbide-, nitride- and oxide-forming elements Ti, Cr, Mo, V, Y, Zr, Ta, and the melt will contain C, N, and O, then the scheme of suspension formation may look like that shown in Figure 3.

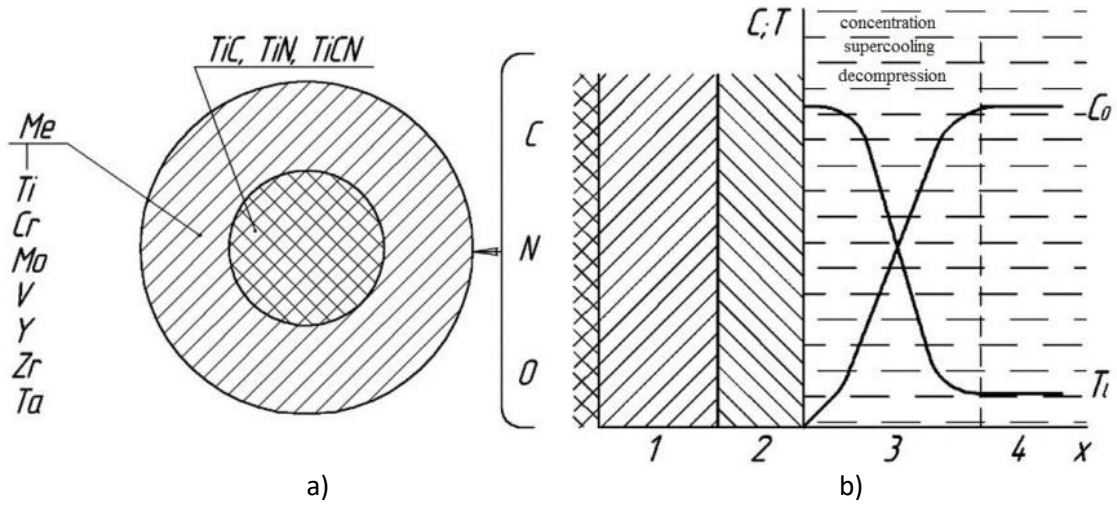

Figure 3. Schemes of the formation of a suspension with an ultrafine particle (a) and transition layers (1-2) on UDP (b) and a change in the concentration of the adsorbed element C_0 and the melting temperature T_l in the adsorbed layer (3) and the volume of the melt (4)

In this case, the equilibrium constant K_e of the reaction of a metal cladding a particle with a non-metal — carbon C (Me + C = MeC) will be inversely proportional to the product of the activity of the components:

$$K_e = 1/(a_{Me} \cdot a_C). \quad (8)$$

Then, near the interfacial surface, the carbon activity will be close to zero; therefore, the melting temperature of the alloy T_l (Fig. 3b) in melt layer 3 will approach the melting temperature of pure metal T_{Me}. In this case, concentration supercooling can form in layer 3, which slows down the destruction of the complex.

Studies of the crystallization of alloys in the concentration and temperature fields are given in [21]. Using the results of these studies, the heterogenization of a metal-carbon-alloying element alloy belonging to a pseudobinary system can be represented considering local concentration fluctuations in heterophase complexes. The composition of alloy 4 in subsequent sources (Fig. 3b) will be depleted in the outcome (component).

Crystallization of an ordinary alloy under non-equilibrium conditions will begin according to a metastable diagram in the temperature range T_L-T_S with supercooling ΔT relative to the equilibrium diagram. Crystallization of the heterogenized melt will begin according to the metastable diagram with a larger metastability range than that of the original alloy. At a content of 107 particles in 1 cm^3 of the melt, the spheres of action of adsorption forces can overlap, and to start crystallization, an atom needs to overcome the sum of the adsorption forces G_r and the activation energy of the transition to the solid phase G_b.

But G_r and G_b have opposite signs, so G_b compensates G_r if $|G_r|>|G_m|$, G_m is the change in free energy during the formation of a solid phase. Then $G_r–G_m=G_z$, and the atom needs to overcome the energy barrier G_z (potential well) in order to occupy a position in the crystal lattice of the solid phase with a higher level of free energy. Therefore, the crystallization of such an alloy will begin with a metastability interval exceeding this value for the original alloy, and may be accompanied by a decrease in density (decompression). If the impurity concentration C_0 in the transition layer is close to zero (Fig. 3b), then the cooling curve should show a plateau due to the precipitation of pure metal, and crystallization will be completed earlier than in the initial alloy, since clustering and adsorption forces change integral free energy of the system, and the duration of crystallization of the treated melt will be less than that of the original.

The kinetic law of continuous growth [22] is expressed by the formula

$$V_P = -D_L \cdot \Delta H_m \cdot \Delta T_K / (a \cdot k_{id} \cdot T^2), \quad (9)$$

where V_P is the growth rate; D_L — diffusion coefficient in the liquid phase; ΔH_m — molecular (atomic) heat of fusion; ΔT_K — kinetic supercooling; a — interplanar distance, which determines the position of the interfacial boundary. As can be seen, the rate of advancement of the interfacial boundary linearly depends on supercooling. An increase in kinetic supercooling during melt heterogenization increases the growth rate. The integral characteristic of the crystallization of a heterogenized eutectic alloy, in accordance with the hypothesis put forward, can be expressed by the course of the process in the temperature range with an inflection of the curve within the crystallization range. The low stability of the crystallization front during directional solidification of a conventional alloy is due to the value of the equilibrium impurity distribution coefficient $k_{id} < 1$, which causes the growth of columnar crystals at high crystallization overcooling (Figure 4a). In a heterogenized alloy, because of modification, concentration supercooling at the crystallization front may be absent, and kinetic supercooling may increase significantly. The growth of a dendrite in a metal suspension is hampered by a barrier of particles at the crystallization front, which causes splitting of the stem and separation of the axes. Excess phases are formed on the substrates in the early stages of solidification and can grow into the dendrite shaft, being in the metal in the volume of grains, and then the alloy will have a fine-grained structure (Figure 4b).

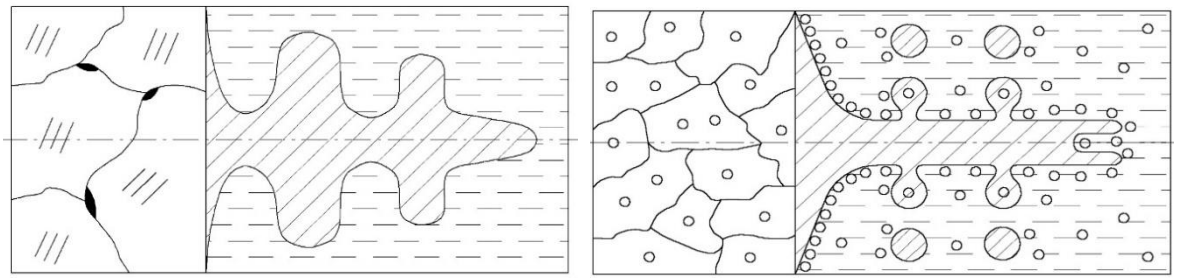

a) b)

Figure 4. Scheme of crystallization of suspensions: *a* — ordinary alloy; *b* — modified alloy

The criterion of concentration supercooling, originally obtained by B. Chalmers [12], in the absence of convective mixing, characterizes the stability of a flat crystallization front:

$$\frac{T_L}{V_P} \geq -\frac{m_i \cdot C_0(1-\omega)}{\omega \cdot D_L}, \tag{10}$$

where T_L is the temperature gradient; mi is the slope of the liquidus line; C_0 is the impurity concentration in the melt.

Impurity adsorption on heterophase complexes reduces the concentration of C_O in the bulk of the melt, and the growth rate of V_P with a flat crystallization front, other things being equal, can be increased. In addition, an increase in the stability of a dispersed thermodynamic system will make it possible to increase the temperature gradient ahead of the crystallization front without the danger of the nucleation and growth of crystallization centers in the melt volume remote from the growing solid phase.

Thus, the efficiency of melt heterogenization and modification of the cast metal structure is determined by the thermodynamic activity of the substance of the transition layer to the material of a solid phase particle, to an impurity, or to one of the chemical elements that make up the alloy. Since all real metal melts are suspensions to one degree or another, the interaction of solid phase particles with thermodynamically active additives of modifiers will inevitably have a positive effect on the kinetics of the nucleation of crystallization centers.

The performed analysis makes it possible to select the composition of complex modifiers for their successful practical use [23].

Conclusion

On the basis of the foregoing, it is possible to formulate the basic principles of the crystallization activity of solid phase particles and the stability of metal suspensions during modification: the particle size of the solid phase must be commensurate with the critical size of the nucleus of the crystallizing phase; the surface of the particles of the suspension must be activated by the adsorbed substance, in which the thermodynamic potential of the interaction of the particle with the non-metal (O, N, C, B, etc.) must be higher than that of the metal of the solid phase; between the substance of the solid phase and the adsorbed layer, there must be a chemical interaction with the release of excess energy; the adsorbed layer should heterogenize the melt due to the increased chemical affinity for one of the chemical elements from the composition of the alloy that forms the eutectic.

References

1 Кузнецов М.А. Управление структурой и свойствами металлов методом модифицирования (обзор) / М.А. Кузнецов, Д.Е. Колмогоров, Е.А. Зернин // Технология машиностроения. — 2012. — № 2. — С. 5–8.

2 Комшуков В.П. и др. Модифицирование металла нанопорошковыми инокуляторами в кристаллизаторе сортовой машины непрерывного литья заготовок / В.П. Комшуков и др. // Механичекие и металлографические исследования. Изв. вузов. Черная металлургия. — 2008. — № 8. — С. 10, 11.

3 Xiong Y. Grain refinement of Superalloy IN 718C by the addition of Inoculants. / Y. Xiong, J. Du, X. Wie, A. Yang, L. Liu Metallurgical and Materials Transactions A. — 2004. — Vol. 35(A). — P. 2111-2114.

4 Binczyk F. Ceramic filters for bulk inoculation of nickel alloy castings / F. Binczyk, J. Śleziona, P. Gradoń // Archives of Foundry Engineering. — 2011. — No. 11 (spec. 3). — P. 29-33.

5 Фаткулин О.Х. Модифицирование жаропрочных никелевых сплавов дисперсными частицами тугоплавких соединений / О.Х. Фаткулин, А.А. Офицеров // Литейное производство. — 1993. — № 4. — С. 13, 14.

6 Liu L. Grain refinement of superalloy K4169 by addition of refineries: cast structure and refinement mechanisms / L. Liu, T. Huang, Y. Xiong // Materials Science and Engineering A. — 2005. — Vol. 394. — P. 1—8.

7 Zielińska M. Effect of modification on microstructure and mechanical properties of cobalt casting superalloy / M. Zielińska, J. Sieniawski, M. Wierzbińska // Archives of Metallurgy and Materials. — 2008. — No. 53(3). — P. 887—893.

8 Binczyk F. Effect of modification on the mechanical properties of IN-713C alloy / F. Binczyk, J. Śleziona // Archives of Foundry Engineering. — 2010. — No. 10(1). — P. 195—198.

9 Binczyk F. Mechanical properties and creep resistance behaviour of IN-713C alloy castings / F. Binczyk, J. Śleziona // Archives of Foundry Engineering. — 2010. — No. 10(4). — P. 9—13.

10 Комаров О.С. Комплексное модифицирование стали / О.С. Комаров, В.И. Волосатиков, И.Б. Проворова // Материаловедение и термическая обработка металлов. — 2013. — № 3 (693). — С. 48–51.

11 Андреев И.Д. Влияние технологических параметров модифицирования комплексными модификаторами на свойства отливок / И.Д. Андреев, А.В. Афонаскин, Г.Ю. Бажова, В.Д. Дорожный // Литейное производство. — 2002. — № 6. — С. 13–15.

12 Chalmers B. Principles Solidification. John Willey and sons [Text] / B. Chalmers. — New York, 1964. — 259 p.

13 Поташинский А.З. Флуктуационная теория фазовых переходов / А.З. Поташинский, В.Л. Покровский. — М.: Наука, 1982. — 382 с.

14 Есин О.А. Физическая химия пирометаллургических процессов / О.А. Есин, П.В. Гельд. — М.: Металлургиздат, 1962. — Ч. 1. — 671 с.

15 Еременко В.Н. Замочування редкими металлами твердых поверхонь тугоплавких сполук / В.Н. Еременко, Ю.В. Найдич. — Киев: АН УССР, 1958. — 20 с.

16 Жуховицкий А.А. Поверхностный эффект химического процесса / А.А. Жуховицкий, В.А. Григорян, Е. Михалик // Докл. АН СССР. — 1964. — Т. 155, № 2. — С. 392–394.

17 Минаев Ю.А. Термодинамическая устойчивость поверхностных слоев при смачивании твердых тел расплавами металла // Изв. вузов. Черная металлургия. — 1973. — № 3. — С. 19–22.

18 Попель С.И. Зарождение неметаллических включений в стали / С.И. Попель // Процессы разливки стали и формирование слитка. Тр. VIII науч.-техн. конф. — М.: Металлургия, 1981. — С. 23–26.

19 Дохов М.П. О поверхностной энергии на границе раздела «твердая фаза–расплав» / М.П. Дохов, С.Н. Задумкин // Смачиваемость и поверхностные свойства расплавов и твердых тел. — Киев: Наук. думка, 1972. — С. 13–20.

20 Бабаскин Ю.З. Механизм влияния тугоплавких дисперсных частиц на высокотемпературные свойства жаропрочных сплавов / Ю.З. Бабаскин, В.Б. Брик, Л.В. Иванисенко // Литейное производство. — 1979. — № 3. — С. 5, 6.

21 Федоров О.П. О механизме преобразования ветвей дендритов двухкомпонентного сплава / О.П. Федоров, Д.Е. Овсиенко, Н.Б. Кривошей // Металлофизика. — 1987. — Т. 9, № 2. — С. 68–75.

22 Флемингс М. Процессы затвердевания / М. Флемингс; пер. с англ., под ред. А.А. Жукова и Б.В. Рабиновича. — М.: Мир, 1977. — 424 с.

23 Eremin E.N. Selection inoculated additives for modifying nickel alloys / E.N. Eremin // Bulletin of the University of Karaganda-Physics. — 2022. — No. 1(105). — P. 81—88.

Е.Н. Еремин

Қатты фазалы бөлшектермен толтырылған металл құрылымының модификациясының кристалдану орталықтарының қалыптасуына және олардың тұрақтылығына әсері

Құйылған металдың механикалық және пайдалану қасиеттерін арттырудың кең мүмкіндіктері дисперсті отқа төзімді бөлшектерді балқымаға тікелей енгізу арқылы жасанды кристалдану орталықтарын құруға мүмкіндік беретін модификация әдісіне ие. Кристалдану орталықтары ретінде қызмет ететін мұндай бөлшектердің тиімділігі олардың бетінде белсендірілген өтпелі қабаттың болуына байланысты. Дисперсті отқа төзімді бөлшектер қосылған ерітіндіге бөлшектерде қажетті қасиеттерге ие өтпелі қабат түзетін белсендірілген қоспалар қосылады, бұл жағдайда кешенді түрлендіруді қолдану перспективті болып табылады. Сонымен қатар, бөлшектердің белсендіруші қоспалармен әрекеттесу ерекшеліктері толық зерттелмеген. Кристалдану орталықтарының пайда болуына және олардың орнықтылығына дисперсті бөлшектердің әсерін теориялық бағалау сулау, өскіннің критикалық өлшеміне дейінгі сіңіру мен еруі арасындағы тәуелділікті қолдану, оларды сулау бұрышы және балқудың суытылуы құбылысын зерттеу негізінде жүргізілді. Егер бөлшек пен қаптама қабаты арасындағы бай-

ланысатын фазалардың химиялық потенциалдарының айырмашылығы толық процесс барысында бар болса, ал кешеннің бетінде—беттік керілу аз мәнге ие болса онда бұндай бөлшек орнықты болады, ол беттік—белсенді компонентінің балқымадан адсорбция барысында орынға ие болады. Сондықтан балқудың гетерогенизациясы және құйылған металдың құрылымын түрлендіру қатты фаза бөлшегі материалына заттың өтпелі қабатының термодинамикалық белсенділігі арқылы анықталады. Алынған қорытындылар құйманың құрылымы мен кристалдану процестерін басқаруға жүзеге асыратын кешенді модификаторлардың құрамын таңдауға мүмкіндік береді.

Кілт сөздер: құйылған металл, суспензия, түрлену, бөлшектер, кристалдану, сіңіру, сулау, фаза аралық қуат көзі, құрылым.

Е.Н. Еремин

Влияние модифицирования структуры литого металла частицами твердой фазы на зарождение центров кристаллизации и их устойчивость

Широкими возможностями повышения механических и эксплуатационных свойств литого металла обладает метод модифицирования, позволяющий создавать искусственные центры кристаллизации за счет прямого введения в расплав дисперсных тугоплавких частиц. Эффективность таких частиц, служащих центрами кристаллизации, обусловлена наличием на их поверхности активированного переходного слоя. В этом отношении перспективно использовать комплексное модифицирование, при котором в расплав совместно с дисперсными тугоплавкими частицами вводятся активирующие добавки, формирующие на частицах переходный слой с нужными свойствами. В то же время особенности взаимодействия частиц с активирующими добавками изучены недостаточно. Теоретическая оценка влияния дисперсных частиц на зарождение центров кристаллизации и их устойчивость проведена на основании изучения явлений смачивания, адсорбции и растворения с использованием зависимости между критическим размером дозародышей, углом их смачивания и переохлаждением расплава. Показано, что если между частицей и плакирующим слоем разность химических потенциалов контактирующих фаз будет существовать на протяжении всего процесса, а на поверхности комплекса будет иметь низкое значение поверхностного натяжения, то такая частица будет устойчивой, что имеет место при адсорбции из расплава поверхностно-активного компонента. Поэтому эффективность гетерогенизации расплава и модифицирования структуры литого металла определяется термодинамической активностью вещества переходного слоя к материалу частицы твердой фазы. Полученные выводы позволяют осуществлять выбор состава комплексных модификаторов, позволяющих управлять структурой отливок в процессе их кристаллизации.

Ключевые слова: литой металл, суспензия, модифицирование, частицы, кристаллизация, адсорбция, смачивание, межфазная энергия, структура.

References

1 Kuznetsov, M.A., Kolmogorov, D.E., & Zernin, E.A. (2012). Upravlenie strukturoi i svoistvami metallov metodom modifitsirovaniia (obzor) [Management of structure and properties of metals by a modification method (review)]. *Tekhnologiia mashinostroeniia — Mechanical engineering technology*, 2, 5–8 [in Russian].

2 Komshukov, V.P. (2008). Modifitsirovanie metalla nanoporoshkovymi inokuliatorami v kristallizatore sortovoi mashiny nepreryvnogo litia zagotovok [Modification of metal by nanopowder inoculators in the mold of a long-range continuous casting machine]. *Mekhanichekie i metallograficheskie issledovaniia. Izvestiia vysshikh uchebnykh zavedenii. Chernaia metallurgiia — Mechanical and metallographic studies. News of higher educational institutions. Ferrous metallurgy*, 8, 10, 11 [in Russian].

3 Xiong, Y., Du, J., Wie, X., Yang, A. & Liu, L. (2004). Grain refinement of Superalloy IN 718C by the addition of Inoculants. *Metallurgical and Materials Transactions A, Vol.* 35(A), 2111-2114.

4 Binczyk, F., Śleziona J., Gradoń P. (2011). Ceramic filters for bulk inoculation of nickel alloy castings. Archives of Foundry Engineering, No. 11 (spec. 3), 29—33.

5 Fatkulin, O.Kh., & Ofitserov, A.A. (1993). Modifitsirovanie zharoprochnykh nikelevykh splavov dispersnymi chastitsami tugoplavkikh soedinenii [Modification of heat-resistant nickel alloys by dispersed particles of refractory compounds]. *Liteinoe proizvodstvo — Foundry production*, 4, 13, 14 [in Russian].

6 Liu, L., Huang, T., & Xiong, Y. (2005). Grain refinement of superalloy K4169 by addition of refineries: cast structure and refinement mechanisms. Materials Science and Engineering A, Vol. 394, 1—8.

7 Zielińska, M., Sieniawski, J. & Wierzbińska, M. (2008). Effect of modification on microstructure and mechanical properties of cobalt casting superalloy. Archives of Metallurgy and Materials, Vol. 53(3), 887—893.

8 Binczyk, F., & Śleziona J. (2010). Effect of modification on the mechanical properties of IN-713C alloy. Archives of Foundry Engineering, 10 (1), 195-198.

9 Binczyk, F. & Śleziona, J. (2010). Mechanical properties and creep resistance behaviour of IN-713C alloy castings. Archives of Foundry Engineering. 10(4), 9—13.

10 Komarov, O.S., Volosatikov, V.I., & Provorova, I.B. (2013). Kompleksnoe modifitsirovanie stali [Complex modification of steel]. *Materialovedenie i termicheskaia obrabotka metallov — Materials science and heat treatment of metals*, 3 (693), 48–51 [in Russian].

11 Andreev, I.D., Afonaskin, A.V., Bazhova, G.Yu., & Dorozhnyi, V.D. (2002). Vliianie tekhnologicheskikh parametrov modifitsirovaniia kompleksnymi modifikatorami na svoistva otlivok [Influence of technological parameters of modification by complex modifiers on the properties of castings]. *Liteinoe proizvodstvo — Foundry production*, 6, 13–15 [in Russian].

12 Chalmers, B. Principles Solidification. John Willey and sons / B. Chalmers. — New York, 1964. — 259 p.

13 Potashinskii, A.Z, & Pokrovskii, V.L. (1982). Fluktuatsionnaia teoriia fazovykh perekhodov [Fluctuation theory of phase transitions]. Moscow: Nauka [in Russian].

14 Esin, O.A., & Geld, P.V. (1962). Fizicheskaia khimiia pirometallurgicheskikh protsessov [Physical chemistry of pyrometallurgical processes]. Part 1. Moscow: Metallurgizdat [in Russian].

15 Eremenko, V.N., & Naidich, Yu.V. (1958). Zamochuvannia redkimi metallami tverdykh poverkhon tugoplavkikh spoluk [Wetting of solid surfaces of refractory compounds with rare metals] Kyiv: *Akademiia nauk USSR — AN USSR* [in Ukraian].

16 Zhukhovitsky, A.A., Grigorian, V.A., & Mikhalik, E. (1964). Poverkhnostnyi effekt khimicheskogo protsessa [Surface effect of the chemical process]. *Doklady Akademii nauk SSSR — Reports of the USSR Academy of Sciences*, 2, 392–394 [in Russian].

17 Minaev, Yu.A. (1973). Termodinamicheskaia ustoichivost poverkhnostnykh sloev pri smachivanii tverdykh tel rasplavami metalla [Thermodynamic stability of surface layers when wetting solids with metal melts]. *Izvestiia vysshikh uchebnykh zavedenii. Chernaia metallurgiia — News of higher educational institutions. Ferrous metallurgy* 3, 19–22 [in Russian].

18 Popel, S.I. (1981) Zarozhdenie nemetallicheskikh vkliuchenii v stali [The origin of non-metallic inclusions in steel]. Protsessy razlivki stali i formirovanie slitka. Trudy VIII nauchno-tekhnicheskoi konferentsii [Steel casting processes and ingot formation. Proceedings of the VIII Scientific and Technical Conference]. Moscow: Metallurgiia [in Russian].

19 Dokhov, M.P., & Zadumkin, S.N. (1972). O poverkhnostnoi energii na granitse razdela «tverdaia faza–rasplav» [On the surface energy at the solid–melt interface]. *Smachivaemost i poverkhnostnye svoistva rasplavov i tverdykh tel — Wettability and surface properties of melts and solids*, 13–20 [in Russian].

20 Babaskin, Yu.Z., Brik, V.B., & Ivanisenko, L.V. (1979). Mekhanizm vliianiia tugoplavkikh dispersnykh chastits na vysokotemperaturnye svoistva zharoprochnykh splavov [Mechanism of influence of refractory dispersed particles on high-temperature properties of heat-resistant alloys]. *Liteinoe proizvodstvo — Foundry production*, 3, 5–6 [in Russian].

21 Fedorov, O.P., Ovsienko, D.E., & Krivoshei, N.B. (1987). O mekhanizme preobrazovaniia vetvei dendritov dvukhkomponentnogo splava [On the mechanism of transformation of branches of dendrites of a two-component alloy]. *Metallofizika*, 2, 68–75 [in Russian].

22 Flemings, M. (1977). Protsessy zatverdevaniia [Solidification processes]. (Transl.) A.A. Zhukov, B.V. Rabinovich (Eds.). Moscow: Mir [in Russian].

23 Eremin, E.N. (2022). Selection inoculated additives for modifying nickel alloys. *Bulletin of the University of Karaganda-Physics*, 1(105), 81—88.

DOI 10.31489/2022PH4/94-105

UDC 538.93+519.6

B.Z. Kenzhegulov[1], S.B. Kenzhegulova[2], D.B. Alibiyev[3], A.Sh. Kazhikenova[3]

[1]*Dosmukhamedov Atyrau University, Kazakhstan;*
[2]K. Sagadiev University of International Business, Kazakhstan;
[3]Karaganda Buketov University, Kazakhstan;
(E-mail: aigul-kazhikenova@mail.ru)

Finite element modeling of heat propagation of a complete rod of constant cross-section

In this paper, the definition of the temperature distribution field for a rod made of heat-resistant alloy EI48 is introduced. The authors consider for the study a complete rod of circular cross-section of radius R, of limited length L. Studied body is under the influence of a heat flow q from the surface over the entire cross-sectional area of the left end, and heat exchange with the environment occurs on the cross-sectional area of the right end. The rod is thermally insulated along the side surface. The authors consider two cases: the first is the heat flow with intensity q can be set on the area of a small circle with radius r <R, the second is the heat flow can be set on its part, that is, on the area $\pi\left(\frac{R}{2}\right)^2$. During the study, the authors showed that during the thermomechanical process, the strength of each section of the load-bearing structural elements is significantly influenced by the temperature distribution field. The influence of high temperature on the morphology of heat-resistant alloys is also shown. This leads to the fact that in some parts of the structural elements the temperature will be acceptable, and in some — critical. As a result, rapid wear of structural elements and loss of their physical qualities occur. Therefore, mathematical modeling of temperature distribution field for a body of various configurations is an urgent problem. The article presents a method for constructing a mathematical model and a corresponding computational algorithm that allows solving a class of problems to determine the regularities of the temperature distribution field in the elements of rod-shaped structures. To do this, the authors used the energy-variation principle in combination with the finite element method.

Keywords: mathematical model, complete rod, heat flow, cross-section, functional, heat exchange, thermal insulation, temperature distribution field.

Introduction

The methodology for building a mathematical model and the problem of developing a heat propagation process in one-dimensional and multi-dimensional structural elements of complex configuration, made of heat-resistant alloys is important and relevant.

There are many works devoted to the problem of the effect of thermomechanical process on changing the structure and composition of the material of any technical unit or structure. From this we can distinguish the following authors: Segerlind L., Nozdrev V.F., Kudaykulov A.K., Pisarenko G.S., Birger I.A., Panovko Y.G., Khimushin F.F., Zenkevich O., Critch F., Federov Y.A., Bakulin V.N., Afanasyeva V.V., Oleynikov A.I., Jordar A., Yakobi A.I. and others. Analyzing the above-mentioned works we encounter some shortcomings. These works take into account influence on body temperature distribution of separate external factors: either heat insulation, or heat exchange with environment, or heat flow or temperature, etc. Here we developed a mathematical model of an insulated rod of constant cross-section under the influence of heat flow and heat exchange with the environment.

A mathematical model of the temperature distribution field of a rod of different configuration in the simultaneous presence of heat flow, thermal insulation and heat exchange using minimization of the total heat energy functional can be successfully applied to solve many scientific and applied problems. Basically, such problems are encountered in the intensive development of modern technological processes in the field of metal science. The obtained scientific results are confirmed by solving real test problems, which confirms the high degree of theoretical and practical importance of the topic.

The objects of the research are load-bearing structural elements in the form of a complete rod made of heat-resistant alloys.

Subject. A full rod of limited length, constant cross-section, completely insulated along the side surface, a heat flow is set on the small circle cross-sectional area of the left end, and heat exchange to the environment takes place through the cross-sectional area of the right end.

The aim and objectives of this paper are to investigate the temperature field distribution based on the application of the energy principle using finite elements.

The paper presents a method of heat transfer in one-dimensional bodies, with the problem of temperature distribution over the volume of bodies of various configurations made of heat-resistant alloys formalized and solved based on minimization of the total heat energy. Numerical solutions of test problems of steady-state thermal conductivity for one-dimensional structural elements are new approaches for establishing a pattern of temperature field distribution.

By changing some parameters of the structure of structural elements, such as the radius of the rod cross section, it will be possible to identify all vulnerable places in the structural elements and protect them from deformation or fracture. Such predictions and hypotheses greatly reduce the detection of critical temperatures throughout the body. Therefore, theoretical mathematical modeling of temperature distribution over the volume of bodies of different configuration can be implemented to solve problems of optimization of operation modes of main technological units, turbine units and internal combustion engines.

Research methodology

It is known from the general course of thermophysics that the established process of heat distribution in one-dimensional structural elements is described by the differential equation of the quasi-harmonic form of the parabolic type [1]:

$$\frac{\partial}{\partial x}\left(K_{XX}\frac{\partial T}{\partial x}\right)+Q=0, \tag{1}$$

where the following boundary conditions take place:

$h = 6\ \left[\frac{\text{Вт}}{(cm^2\ \ ^\circ\text{C})}\right]$, on S_1,

$\mathrm{T} = \mathrm{T_s}(2)$

$h = 6\ \left[\frac{\text{Вт}}{(cm^2\ \ ^\circ\text{C})}\right]$, on S_2. (3)

Here is K_{xx} – is the heat transfer coefficient of the rod material, the dimension of which is $\left[\frac{W}{cm\cdot{}^\circ C}\right]$ $\left[\frac{\text{Вт}}{(\text{cm}\cdot\ ^\circ\text{C})}\right]$; Q — internal heat source, the dimension of which is $\left[\frac{W}{cm\cdot{}^\circ C}\right]\left[\frac{\text{Вт}}{(\text{cm}\cdot\ ^\circ\text{C})}\right]$; T_{at} – ambient surface temperature S_2, the dimensionality of which is $[^\circ C]$;T_s — surface temperature S_1, which is considered to be a given and the dimension of which$[^\circ C]$; ℓ_x – the guide cosines of the considered cross-sectional surface of the rod; q– a given heat flux on a certain surface of the rod, the dimensionality of which is $\left[\frac{W}{cm^2}\right]\left[\frac{\text{Вт}}{\text{cm}^2}\right]$. In addition, if the heat flux is brought to some surface of the rod, it is taken with a minus sign, and if it is removed from the rod, it is taken with a plus sign; h– is the value of the coefficient of heat exchange of the rod with its environment, the dimensionality of which is $\left[\frac{W}{cm^2\cdot{}^\circ C}\right].\left[\frac{\text{Вт}}{\text{cm}^2}\right]$ Certain parts of the rod can be surrounded by water, soil, sand, ice, etc. In each case, the values of the heat transfer coefficient of the rod with its environment will be different.

Here it should be noted that the boundary condition (3) cannot simultaneously set q and h. If q is given on some surface of the rod, then on that surface the value of h will be zero, and vice versa, i.e. where h is given, then there the value of q=0.

It is known from the course of calculus of variations that the solution of equation (1), which satisfies boundary conditions (2) and (3) gives a minimum of the following functional:

$$I=\int_V\frac{1}{2}\left[K_{XX}\left(\frac{\partial T}{\partial x}\right)^2-2QT\right]dV+\int_S\left[qT+\frac{h}{2}\left(T-T_{at}\right)^2\right]dS. \tag{4}$$

Then if we find a function $T=T(x)$, which will give a minimum to the functional (4), then it is a solution of equation (1) and will simultaneously satisfy boundary conditions (2) and (3).

This classical theory is applied to a particular applied problem. Consider a complete rod of bounded length L and divide it into $n-1$ parts. In this case we have n nodes. Next, for each individual finite element, taking into account the real conditions, let us write down the functional expressions for each finite element in detail $I_1, I_2, ..., I_{n-1}$ [2-6]. Let's compose the sum of the functionals

$$I = \sum_{k=1}^{n-1} I_k . \tag{5}$$

Minimizing the I- functional by the temperature nodal values, we obtain the following solving system of algebraic equations:

$$\begin{cases} \dfrac{\partial I}{\partial T_1} = 0 \\ \dfrac{\partial I}{\partial T_2} = 0 \\ \ldots \\ \dfrac{\partial I}{\partial T_n} = 0 \end{cases} \tag{6}$$

Here it should be noted that when integrating over the volume and surface integrals in the expression of the functionals $I_1, I_2, ..., I_{n-1}$ there are a lot of peculiar problems connected with specificity of structural elements such as full and gentle rods, variable cross-section, presence of internal cavities in some elements, presence of heat flows on local surface of elements of internal sources, and also given temperature values in some nodes. Depending on these data, the number of algebraic equations in system (6) may be less than n. Therefore, we will show these features on each specific example with corresponding physical and mathematical comments. In doing so, we will proceed from the real formulation of problems regardless of their complexity in the sense of physical and mathematical formulation.

Results and Discussion

In order to test this theory, consider a complete rod of limited length L, the cross section of which is a circle with radius R. This rod is completely insulated along its lateral surface. On the full cross-sectional area of the left end a heat flux of intensity q is given (though the heat flux can be given on the area of a small circle of radius $r < R$). On the cross-sectional area of the right end there is a heat transfer to the environment (heat transfer can take place on a small area). In this case, the values of the heat transfer coefficient denote by h, and the values of the ambient temperature denote by T_{at} (Fig. 1) [1, 7-11].

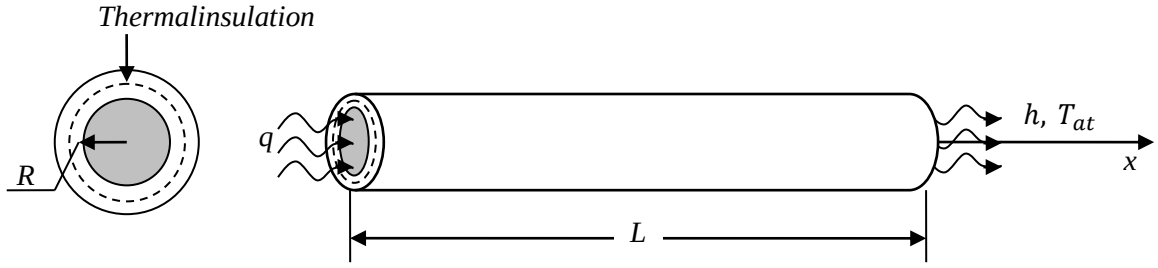

Figure1. Thermally insulated full rod

For convenience, we first discretize the rod in question using three finite elements of equal length $\ell = \dfrac{L}{3}$ (Fig. 2). This will allow us to perform all calculations manually. It should be noted here that it is not necessary to discretize the rod with the same element lengths. The length of each element can be different, i.e. $\ell_1 \neq \ell_2 \neq \ell_3$, etc.

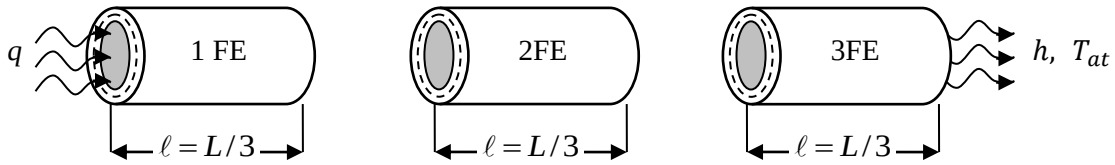

Figure 2 .Three discrete finite elements.

In the considered problem there is no internal heat source, i.e.Q=0. For the 1st finite element the expression of the form function is as follows

$$\left.\begin{aligned}\varphi_1(x) &= \frac{x_2 - x}{\ell_1}\\ \varphi_2(x) &= \frac{x - x_1}{\ell_1}\end{aligned}\right\} \quad \text{when } x_1 \le x \le x_2;\ x_2 - x_1 = l_1$$

The temperature values at any point within the length of the first finite element are determined by the temperature values of the nodes T_1 and T_2 according to the formula

$$T = \varphi_1(x)T_1 + \varphi_2(x)T_2 = \frac{x_2 - x}{\ell_1}T_1 + \frac{x - x_1}{\ell_1}T_2 \tag{7}$$

Then the functional expression for the first finite element is as follows [1, 2, 12-16]:

$$I_1 = \int\limits_{V^{(1)}} \frac{1}{2}\left[K_{xx}^{(1)}\left(\frac{\partial T}{\partial x}\right)^2\right]dV + \int\limits_{S_1} qT_1 dS,$$

where $K_{xx}^{(1)}$ – is the value of the heat transfer coefficient of the material of the first finite element, S_1 – is the cross-sectional area of the left end of the rod, which corresponds to the first node. This functional takes into account the presence of heat flow with intensity $\boldsymbol{q}$ on the cross-sectional area S_1, which corresponds to the first node. From (7) we define the expression for the temperature gradient within the length of the first finite element

$$\frac{dT}{dx} = \frac{d\varphi_1(x)}{dx}T_1 + \frac{d\varphi_2(x)}{dx}T_2 = \frac{T_2 - T_1}{\ell_1}.$$

Then the expression for I_1 it has the following form

$$I_1 = \int\limits_{V^{(1)}} \frac{1}{2}\left[K_{xx}^{(1)}\left(\frac{T_2 - T_1}{\ell_1}\right)^2\right]dV + \int\limits_{S_1} qT_1 dS = \frac{K_{xx}^{(1)}A^{(1)}}{2\ell_1^2}\int\limits_{x_1}^{x_2}(T_2 - T_1)^2 dx + qT_1A_1 =$$

$$= \frac{K_{xx}^{(1)}A^{(1)}}{2\ell_1}(T_2 - T_1)^2 + qT_1A_1,$$

where $A_1 = S_1$ is the cross-sectional area of the left end of the rod, where the heat flux with intensity q, $A^{(1)}$ – is applied, are the values of the cross-sectional area of the first finite element. Thus, for the first finite element we have:

$$I_1 = \frac{K_{xx}^{(1)}A^{(1)}}{2\ell_1}(T_2 - T_1)^2 + qT_1A_1, \tag{8}$$

T_1, T_2 – are the nodal temperature values at nodes 1 and 2, respectively. Similarly, let us write the functional expression for the second (inner) finite element:

$$I_2 = \int\limits_{V^{(2)}} \frac{1}{2}\left[K_{xx}^{(2)} \left(\frac{T_3 - T_2}{\ell_2} \right)^2 \right] dV = \frac{K_{xx}^{(2)} A^{(2)}}{2\ell_2} (T_3 - T_2)^2 \quad . \tag{9}$$

But, for the third finite element, the functional expression I_3 must be written taking into account the heat exchange process of the rod with the environment through the cross-sectional area of the right end of the rod. Where are the values of the heat transfer coefficient *h*, and the ambient temperature T_{at}. Then

$$I_3 = \int\limits_{V^{(3)}} \frac{1}{2}\left[K_{xx}^{(3)} \left(\frac{T_4 - T_3}{l_3} \right)^2 \right] dV + \int\limits_{S_4} \frac{h}{2} \left(T - T_{at} \right)^2 dS,$$

where S_4 – s the cross-sectional area of the right end of the rod, which corresponds to the fourth node, and along which there is heat exchange with the environment. After integrating the expression I_3 we have:

$$I_3 = \frac{K_{xx}^{(3)} A^{(3)}}{2l_3} \left(T_4 - T_3 \right)^2 + \frac{hA_4}{2} \left(T_4 - T_{at} \right)^2 ,$$

(10)

where $A_4 = S_4$. Thus, for the considered rod, taking into account the specificity and formulation of the problem, the full expression of the functional will be:

$$I = I_1 + I_2 + I_3 =$$

$$\frac{K_{xx}^{(1)} A^{(1)}}{2l_1} \left(T_2 - T_1 \right)^2 + qT_1 A_1 + \frac{K_{xx}^{(2)} A^{(2)}}{2l_2} \left(T_3 - T_2 \right)^2 + \frac{K_{xx}^{(3)} A^{(3)}}{2l_3} \left(T_4 - T_3 \right)^2 + \frac{hA_4}{2} \left(T_4 - T_{at} \right)^2 .$$

Then minimizing the functional *I* over the nodal values of temperature T_1, T_2, T_3 и T_4 and obtain the following basic system of solving algebraic equations with respect to the desired nodal values of temperature:

$$\left.\begin{aligned}
&\frac{\partial I}{\partial T_1} = 0 \Rightarrow -\frac{K_{xx}^{(1)} A^{(1)}}{l_1} \left(T_2 - T_1 \right) + qA_1 = 0 \\
&\frac{\partial I}{\partial T_2} = 0 \Rightarrow \frac{K_{xx}^{(1)} A^{(1)}}{l_1} \left(T_2 - T_1 \right) - \frac{K_{xx}^{(2)} A^{(2)}}{l_2} \left(T_3 - T_2 \right) = 0 \\
&\frac{\partial I}{\partial T_3} = 0 \Rightarrow \frac{K_{xx}^{(2)} A^{(2)}}{l_2} \left(T_3 - T_2 \right) - \frac{K_{xx}^{(3)} A^{(3)}}{l_3} \left(T_4 - T_3 \right) = 0 \\
&\frac{\partial I}{\partial T_4} = 0 \Rightarrow \frac{K_{xx}^{(3)} A^{(3)}}{l_3} \left(T_4 - T_3 \right) + hA_4 \left(T_4 - T_{at} \right) = 0
\end{aligned}\right\} \tag{11}$$

In order to obtain numerical results, let us set specific application problems for the parameters in the system (15). Assume that the considered rod is homogeneous and of constant cross-section. Then for the numerical solution we assume the following initial data [1, 2, 17-22]:

$$K_{xx}^{(1)} = K_{xx}^{(2)} = K_{xx}^{(3)} = 100 \left[\frac{W}{cm^\circ C} \right]; \; l_1 = l_2 = l_3 = \frac{L}{3} = \frac{15}{3} = 5[cm]; \; R = 2[cm]$$

$$A_1 = A_4 = A^{(1)} = A^{(2)} = A^{(3)} = \pi R^2 = 4\pi [cm^2].$$

Values of the coefficient of heat exchange with the environment h=6 h = 6 $\left[\frac{\text{Вт}}{(\text{cm}^2\ ^\circ\text{C})}\right]$,of the available heat flow (supply flow) q=-180 q = -180 $\left[\frac{\text{Вт}}{\text{cm}^2}\right]$,ambient temperatures of the cross section of the right end (4th node) T_{at} =16$\left[^\circ C\right]$Tat = 16 [˚C]. Now using the system of equations (11) we find the temperature values at nodes 1, 2, 3 and 4, i.e. T_1, T_2, T_3 и T_4.

Based on the initial data we have:

$\frac{K_{xx}\cdot A}{\ell} = \frac{100\cdot 4\pi}{5} = 80\pi$, $q\cdot A_1 = -180\cdot 4\pi = -720\pi$, $h\cdot A_4\cdot T_{at} = 6\cdot 4\pi\cdot 16 = 384\pi$.

The obtained numerical data are substituted into the system of equations (11) and we obtain the following system of algebraic equations, relative to the temperature nodal values:

$$\begin{cases} -80\pi(T_2 - T_1) - 720\pi = 0, \\ 80\pi(T_2 - T_1) - 80\pi(T_3 - T_2) = 0, \\ 80\pi(T_3 - T_2) - 80\pi(T_4 - T_3) = 0, \\ 80\pi(T_4 - T_3) + 24\pi(T_4 - 16) = 0. \end{cases}$$

By opening the brackets and reducing both parts of the equations, after slight simplifications, we obtain the following final solving system of algebraic equations:

$$\begin{cases} 80T_1 - 80T_2 = 720 \\ -80T_1 + 160T_2 - 80T_3 = 0 \\ -80T_2 + 160T_3 - 80T_4 = 0 \\ -80T_3 + 104T_4 = 384 \end{cases} \quad (12)$$

From the first equation of the original system (12) we have:

$$80T_1 = 80T_2 + 720 \Rightarrow T_1 = T_2 + 9. \quad (13)$$

Substituting $80T_1$, into the second equation of the system (12) we find that

$$T_2 = T_3 + 9 \quad (14)$$

Substituting the found value T_2 into the third equation of the system (12) we obtain that

$$T_3 = T_4 + 9 \quad (15)$$

Finally, substituting the found values into the last equation of the system (12) we find that $80T_4 - 80T_4 - 720 + 24T_4 = 384$. From this we get that

$$24T_4 = 384 + 720 \Rightarrow T_4 = \frac{384 + 720}{24} = 46\ ^\circ C.$$

Substituting the value T_4 into equation (15) we find the temperature in the inner 3rd node $T_3 = T_4 + 9 = 46 + 9 = 55\ ^\circ C$.

Substituting T_3 into equation (14) let's find the temperature in the inner second node

$$T_2 = T_3 + 9 = 55 + 9 = 64\ ^\circ C.$$

Finally, by substituting the value of T_2 into equation (13), we find the temperature value in the 1st node on the cross-sectional area of which the heat flux of intensity is given q=-180 q = -180 $\left[\frac{\text{Вт}}{\text{cm}^2}\right]$,

$$T_1 = T_2 + 9 = 64 + 9 = 73\ ^\circ C.$$

Here we consider the first case, which heat flux intensity q is given on the area of a small circle of a rod with radius $r<R$.

Now consider the second case, when the heat flux with intensity q is applied not to the full area of the left end, but to a part of it, that is, to the area $\pi\left(\frac{R}{2}\right)^2$ (Fig. 3) [1-6, 22-23]:

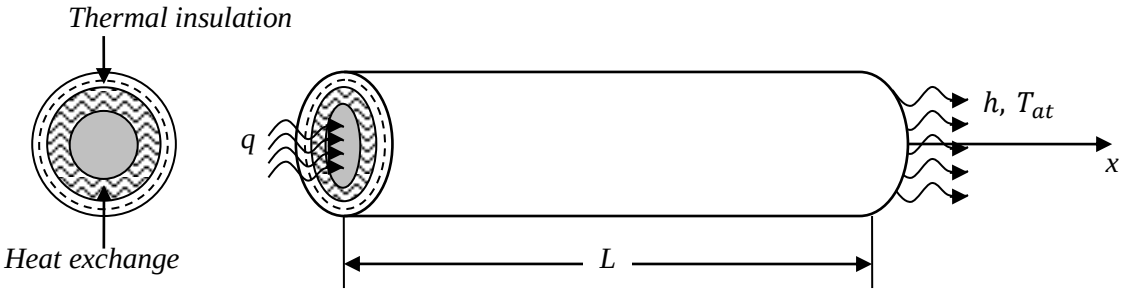

Figure 3. Calculation scheme

At the same time on the remaining cross-sectional area of the left end, i.e. on the $\pi R^2 - \pi\left(\frac{R}{2}\right)^2 = \frac{3\pi R^2}{4} cm^2$ $\pi R^2 - \pi\left(\frac{R}{2}\right)^2 = \frac{3\pi R^2}{4}$ cm^2there is a heat exchange with the environment h_1=6 h = 6 $\left[\frac{Вт}{(cm^2 \cdot °C)}\right]$,$h_1 = 6$ $\left[\frac{Вт}{(cm^2 \cdot °C)}\right]$, there is a heat exchange with the environment $T_{at_1} = 20^\circ C$, $T_{at} = 16^0 C$. The area to which the heat flow is brought

q = -180 $\left[\frac{Вт}{cm^2}\right]$ denote by $S_{11} = \pi\left(\frac{R}{2}\right)^2 = \frac{\pi R^4}{4} cm^2$.

Then we denote the remaining cross-sectional areas of the left end of the rod by $S_{12} = \pi R^2 - \pi\left(\frac{R}{2}\right)^2 = \frac{3\pi R^2}{4} cm^2$.$S_{12} = \pi R^2 - \frac{\pi R^2}{2} = \frac{3\pi R^2}{4}$ cm^2 Over the total area of the right end of the rod there is a heat exchange with the environment h=6 h = 6 $\left[\frac{Вт}{(cm^2 \cdot °C)}\right]$,. As in the previous problem, we discretize the rod in question with length L, using three finite elements lengths of which are respectively $\ell_1 = \ell_2 = \ell_3 = \frac{L}{3}$ (Fig. 2). Then in the considered problem for the first finite element the expression of the functional I_1 instead of (8) will be as follows:

$$I_1 = \int\limits_{V^{(1)}} \frac{1}{2}\left[K_{xx}^{(1)}\left(\frac{T_2 - T_1}{l_1}\right)^2\right]dV + \int\limits_{S_{11}} qT_1 dS_{11} + \int\limits_{S_{12}} \frac{h_1}{2}\left(T - T_{at_1}\right)^2 dS_{12} =$$

$$= \frac{K_{xx}^{(1)} A^{(1)}}{2l_1}\left(T_2 - T_1\right)^2 + qT_1 S_{11} + \frac{h_1 S_{12}}{2}\left(T_1 - T_{at_1}\right)^2.$$

Thus, for the first finite element we have

$$I_1 = \frac{K_{xx}^{(1)} A^{(1)}}{2l_1}\left(T_2 - T_1\right)^2 + qT_1 S_{11} + \frac{h_1 S_{12}}{2}\left(T_1 - T_{at_1}\right)^2.$$

We leave the functionals for the remaining elements (2-3) the same as (9) and (10):

$$I_2 = \int\limits_{V^{(2)}} \frac{1}{2}\left[K_{xx}^{(2)}\left(\frac{T_3 - T_2}{l_2}\right)^2\right]dV = \frac{K_{xx}^{(2)} A^{(2)}}{2l_2}\left(T_3 - T_2\right)^2;$$

$$I_3 = \int\limits_{V^{(3)}} \frac{1}{2}\left[K_{xx}^{(3)}\left(\frac{T_4 - T_3}{l_3} \right)^2 \right] dV + \int\limits_S \frac{h}{2}\left(T - T_{at}\right)^2 dS = \frac{K_{xx}^{(3)} A^{(3)}}{2l_3}\left(T_4 - T_3\right)^2 + \frac{hA_4}{2}\left(T_4 - T_{at}\right)^2.$$

The general expression of the functional for the full rod is as follows

$$I = I_1 + I_2 + I_3 = \frac{K_{xx}^{(1)} A^1}{2l_1}\left(T_2 - T_1\right)^2 + qT_1 S_{11} + \frac{h_1 S_{12}}{2}\left(T_1 - T_{at_1}\right)^2 + \frac{K_{xx}^{(2)} A^{(2)}}{2l_2}\left(T_3 - T_2\right)^2 + \\ + \frac{K_{xx}^{(3)} A^{(3)}}{2l_3}\left(T_4 - T_3\right)^2 + \frac{hA_4}{2}\left(T_4 - T_{at}\right)^2. \quad (16)$$

Now minimize the obtained functional I (16) by the nodal values of temperature T_1, T_2, T_3 и T_4 and obtain the following solving system of algebraic equations:

$$\left.\begin{aligned} &\frac{\partial I}{\partial T_1} = 0 \Rightarrow -\frac{K_{xx}^{(1)} A^{(1)}}{l_1}\left(T_2 - T_1\right) + qS_{11} + h_1 S_{12}\left(T_1 - T_{at_1}\right) = 0 \\ &\frac{\partial I}{\partial T_2} = 0 \Rightarrow \frac{K_{xx}^{(1)} A^{(1)}}{l_1}\left(T_2 - T_1\right) - \frac{K_{xx}^{(2)} A^{(2)}}{l_2}\left(T_3 - T_2\right) = 0 \\ &\frac{\partial I}{\partial T_3} = 0 \Rightarrow \frac{K_{xx}^{(2)} A^{(2)}}{l_2}\left(T_3 - T_2\right) - \frac{K_{xx}^{(3)} A^{(3)}}{l_3}\left(T_4 - T_3\right) = 0 \\ &\frac{\partial I}{\partial T_4} = 0 \Rightarrow \frac{K_{xx}^{(3)} A^{(3)}}{l_3}\left(T_4 - T_3\right) + hA_4\left(T_4 - T_{at}\right) = 0. \end{aligned}\right\} \quad (17)$$

Calculating the values at R=2 cm. We have $S_{11} = \frac{4\pi}{4} = \pi$; $S_{12} = \frac{3\pi \cdot 4}{4} = 3\pi$; $h_1 \cdot S_{12} = 6 \cdot 3\pi = 18\pi$; $h \cdot A_4 = 6 \cdot 4\pi = 24\pi$.

Substituting the coefficients into the system of equations (17) we obtain

$$\begin{cases} -80\pi(T_2 - T_1) - 180\pi + 18\pi(T_1 - 20) = 0, \\ 80\pi(T_2 - T_1) - 80\pi(T_3 - T_2) = 0, \\ 80\pi(T_3 - T_2) - 80\pi(T_4 - T_3) = 0, \\ 80\pi(T_4 - T_3) + 24\pi(T_4 - 16) = 0. \end{cases}$$

Reducing all terms of the equation by and after a slight simplification we have:

$$\begin{cases} 98T_1 - 80T_2 = 540, \\ -80T_1 + 160T_2 - 80T_3 = 0, \\ -80T_2 + 160T_3 - 80T_4 = 0, \\ -80T_3 + 104T_4 = 384. \end{cases} \quad (18)$$

From the first equation of the original system:

$$T_1 = \frac{270}{49} + \frac{40}{49} \cdot T_2, \quad (19)$$

Substituting the found value T_1 into the second equation of the system (18) we obtain that

$$T_2 = \frac{270}{58} + \frac{49}{58} \cdot T_3 \quad (20)$$

Substituting the found T_2 in the third equation of the system (18) we find

$$T_3 = \frac{270}{67} + \frac{58}{67} \cdot T_4 \quad (21)$$

Substituting the obtained value T_3 into the last equation of the system (18), we find the temperature value of the 4th node, which corresponds to the cross-sectional surface of the right end of the full rod, where the heat exchange takes place:

$$-80\left(\frac{270}{67} + \frac{58}{67} \cdot T_4\right) + 104T_4 = 384.$$

From this we have

$$T_4 = \frac{47328}{2328} \approx 20.33\ ^{\circ}C,$$

then substituting T_4 in (21) we obtain the temperature values in the 3-node.

$$T_3 = \frac{270}{67} + \frac{58}{67} \cdot 20.33 \approx 21.63\ ^{\circ}C.$$

From (20) the value T_2 will be:

$$T_2 = \frac{270}{58} + \frac{49}{58} \cdot 21.63 \approx 22.93\ ^{\circ}C.$$

From (19) we find the temperature value of the first node, which corresponds to the cross section of the left end of the rod, where part of the area is subjected to heat flow and the right part is subjected to heat exchange:

$$T_1 = \frac{270}{49} + \frac{40}{49} \cdot 22.93 \approx 24.23\ ^{\circ}C.$$

Conclusions

It should be noted that three types of boundary conditions have been set in this problem:

1) The surface of the cross-sectional area of the left end of the full rod is given a heat flux and two cases are considered:

a) a given heat flux of intensity q can be set on the area of a small circle of radius $r<R$;

b) the heat flux can be set on its part, i.e. on the area $\pi\left(\frac{R}{2}\right)^2$.

2) The lateral surface area along the entire length of the rod is insulated.

The cross-sectional area of the right end is open. It is surrounded by some medium (water, oil, ground, etc.), temperature of which is $T_4 = 16\ ^{\circ}C$. Values of the coefficient of heat exchange of the rod with this environment h=6 $\mathrm{h} = 6\ \left[\frac{\text{Вт}}{(\text{см}^2\ ^{\circ}\text{C})}\right]$,, heat transfer coefficient $\mathrm{h} = 6\ \left[\frac{\text{Вт}}{(\text{см}^2\ ^{\circ}\text{C})}\right]$, and the coefficient of heat exchange of the rod with the environment $T_{at} = 16^{\circ}C$ is determined experimentally and in all problems considered by us are considered to be set. Values of heat flux and internal heat source are also set.

As a result, the initial data for both cases are the same, but for the first case, when the heat flux is set on the area of a small circle of radius $r<R$ the temperature values at the nodal points are as follows: $T_1 = 73^{\circ}C$, $T_2 = 64^{\circ}C$, $T_3 = 55^{\circ}C$, $T_4 = 46^{\circ}C\ \mathrm{T}_1 = 73^{\circ}C$.

Now for the second case, when the heat flux is set on its part, that is, on the area $\pi\left(\frac{R}{2}\right)^2$ the temperature values at the nodal points are as follows: $T_1 = 24.23^\circ C$, $T_2 = 22.93^\circ C$, $T_3 = 21.63^\circ C$, $T_4 = 20.33^\circ C$ $\mathrm{T}_1 = 73\,^\circ C$.

On the basis of the above-stated, practical significance of the conducted research can be determined. The proposed computational algorithm can be used to determine the regularities of the temperature distribution field in rod-type structural elements. Furthermore, the presented method of transferring heat to one-dimensional bodies based on minimizing integral thermal energy allows formalizing and solving the problems of temperature distribution over the volume of bodies of various configurations made of heat-resistant alloys.

References

1 Kenzhegulov, B. (2021). Numerical modeling of multidimensional temperature and one-dimensional nonlinear thermomechanical processes in heat-resistant alloys. Atyrau: ASU Press publishing House.

2 Kenzhegulov, B., Shazhdekeyeva, N., Myrzhasheva, A.N., Kabylhamitov, G.T., & Tuleuova, R.U. (2020). Necessary Optimality Conditions for Determining of the Position of the Boundary of Oil Deposit. *International Journal of Engineering Research and Technology, Vol. 13,* 1204-1209.

3 Kenzhegulov, B., Kultan, J., Alibiyev, D.B., & Kazhikenova, A.Sh. (2020). Numerical Modelling of Thermomechanical Processes in Heat-Resistant Alloys. *Bulletin of the University of Karaganda-Physics*, 2(98), 101—108.

4 Kenzhegulov, B., Shazhdekeyeva, N., Myrzhasheva, A.N., & Tuleuova, R.U. (2020). A Numerical Method for Determining the Dependence of the Thermally Stressed State of a Rod on Ambient Temperature with The Simultaneous Presence of Thermal Processes. *PeriodicoTcheQuimica, Vol. 17, 765-780.*

5 Kenzhegulov, B., Tuleuova, R., Myrzasheva, A., Shazhdekeyeva, N., & Kabylkhamitov, G. (2021). Mathematical modelling and development of a computational algorithm for the study of thermo-stressed state of a heat-resistant alloy. *Site of journal "Periodicals of Engineering and Natural Sciences".* Retrieved from http://pen.ius.edu.ba/index.php/pen/issue/view/31.

6 Kenzhegulov, B., Shazhdekeyeva, N., Myrzasheva, A., Kabylkhamitov, G., & Tuleuova, R. (2021). Numerical methods for solving improper problems of filtration theory. *Journal of Applied Engineering Science*, Vol. 19, Br. 1, 98-108.

7 Li, H.-F., Zhao, J., Cheng, C.-Q., Min, X.-H., Cao, T.-S., & Xu, J. (2018). Prediction of High Temperature Creep Deformation and Rupture Life on HP Heat Resistant Alloy Using Zc Parameter. *Journal of Materials Engineering, Vol. 46,* No. 3, 112-116.

8 Meng, B., Yang, K., Wu, J., & Zhang, X. (2019). Preparation Method of High Conductivity and Heat Resistant Aluminum Alloy. Tezhong Zhuzao Ji Youse Hejin / *Special Casting and Nonferrous Alloys*, Vol. 39, No. 8, 922-924.

9 Wang, J. (2020). Kinetic and Strength Calculation of Age-Hardening Phases in Heat-Resistant Aluminum Alloys with Silver. *Materials Science Forum*, Vol. 993 (pp. 1051-1056).

10 Adaskin, A.M., Kirillov, A.K., & Kutin, A.A. (2020). Improving the Cutting of Heat-Resistant Chromium Alloy. *Russian Engineering Research,* Vol. 40, No. 9, 748-750.

11 Min, P.G., Sidorov, V.V., Vadeev, V.E., & Kramer, V.V. (2020). Development of Corrosion and Heat Resistant Nickel Alloys and their Production Technology with the Aim of Import Substitution. *Power Technology and Engineering, Vol. 54*, No. 2, 225-231.

12 Petrushin, N.V., Evgenov, A.G., Zavodov, A.V., & Treninkov, I.A. (2018). Structure and Strength of the ZhS32-VI Heat-Resistant Nickel Alloy Produced by the Method of Selective Laser Alloying on a Single-Crystal Substrate. *Inorganic Materials: Applied Research, Vol. 9*, No. 4, 620-627.

13 Zhang, N., Cheng, R., Dong, H., Liu, W., Zhan, J., Jiang, B. et al. (2019). Application and Research Progress of Strontium in Heat-resistant Magnesium Alloy. *Cailiao Daobao/Materials Reports*, Vol. 33, No. 8, 2565-2571.

14 Li, G., Liao, H., Suo, X., Tang, Y., Dixit, U.S., & Petrov, P. (2018). Cr-Induced Morphology Change of Primary Mn-Rich Phase in Al-Si-Cu-Mn Heat Resistant Aluminum Alloys and Its Contribution to High Temperature Strength. *Materials Science and Engineering A, Vol. 709*, 90-96.

15 Quan, G.-Z., Zhang, K.-K., An, C., Qiu, H.-M., & Xia, Y.-F. (2018). Analysis of Dynamic Recrystallization Behaviors in Resistance Heating Compressions of Heat-Resistant Alloy by Multi-Field and MultiScale Coupling Method. *Computational Materials Science, Vol. 149,* 73-83.

16 Xu, X., Jin, X., Liu, Z., Zhang, B., Zhang, R., Zhuang, Y., et al. (2019). Microstructure and Properties of a New Al-Cu-Mg-Zn-Zr-Ti Heat Resistant Aluminum Alloy. *Materials Research Express, Vol. 6*, No. 12, article number 1265H8.

17 Facco, A., Couvrat, M., Magné, D., Roussel, M., Guillet, A., & Pareige, C. (2020). Microstructure Influence on Creep Properties of Heat-Resistant Austenitic Alloys with High Aluminum Content. *Materials Science and Engineering A, Vol. 783,* article number 139276.

18 Kvasnytska, Y.H., Ivaskevych, L.M., Balytskyi, O.I., Maksyuta, I.I., & Myalnitsa, H.P. (2020). High Temperature Salt Corrosion of a Heat-Resistant Nickel Alloy. *Materials Science, Vol. 56,* No. 3, 432-440.

19 Sustaita-Torres, I.A., Haro-Rodríguez, S., & Colás, R. (2018). Aging of a Low Carbon Heat Resistant Cast Alloy. *High Temperature Materials and Processes, Vol. 37,* No. 2, 133-139.

20 Patrin, P.V., Karpov, B.V., Aleshchenko, A.S., & Galkin, S.P. (2020). Capability Process Assessment of Radial-Displacement Rolling of Heat-Resistant Alloy HN73MBTYU. *Steel in Translation, Vol. 50,* No. 1, 42-45.

21 Fu, Y., Zhuang, Y., Xu, X., Zhang, J., Liu, Z., Zhang, B., et al (2019). Effect of Ti Content and Hot/Cold Extrusion on Microstructure and Properties of 2219 Heat-Resistant Aluminum Alloy. *Materials Research Express, Vol. 6,* No. 10, article number 1065F2.

22 Fang, J., Huang, Y., Yu, G., & Hu, Z. (2019). Influence of Cold Deformation on Properties and Static Recrystallization of Al-Mg-Si-Zr Heat-Resistant Aluminum Alloy. *Jinshu Rechuli / Heat Treatment of Metals, Vol. 44,* No. 8, 37-40.

23 Bao, H.-S., Yang, G., Chen, Z.-Z., & Liu, Z.-D. (2020). Effects of Long-Term Aging on Microstructure and Properties of a Tungsten Bearing Heat-Resistant Alloy. Journal of Iron and Steel Research International, Vol. 27, No. 4, 477-487.

Б.З. Кенжегулов, С.Б. Кенжегулова, Д.Б. Әлібиев, А.Ш. Қажикенова

Көлденең қимасы тұрақты біртұтас сырықтың ұзына бойына жылу таралу өрісін шекті элементтер әдісімен пішіндеу

Мақалада ЭИ48 жылуға төзімді құймадан жасалған сырықтың ұзына бойы жылу таралу өрісінің заңдылығын анықтау негізделген. Авторлар ұзындығы шектеулі *L*-ге тең, ұзына бойы көлденең қималарының радиустары *R*-ге тең дөңгелек біртұтас сырықты қарастырған. Зерттеуге алынған дененің сол жақ көлденең қимасының толық бетінің ауданына *q* жылу ағыны түсірілген, ал оң жақ көлденең қимасының ауданынан қоршаған ортамен жылу алмасу жүріп жатыр. Сырықтың бүйір бетінің ауданы жылудан оқшауланған. Мақала авторлары екі жағдайды қарастырған: біріншісі — жылу ағыны *q* қарқынымен сол жақ ауданының $r<R$ радиусымен берілген кішкентай дөңгелек ауданын; екіншісі — жылу ағыны сол жақ бетінің ауданының белгілі бір бөлігіне берілген, яғни $\pi\left(\frac{R}{2}\right)^2$ ауданын. Зерттеу көрсеткендей, жылумеханикалық процесте негізгі құрылғы элементтерінің әр бөлігіндегі ыстыққа төзімділікке жылу таралу өрісінің әсері маңызды болады. Сонымен қатар, жоғары температура ыстыққа төзімді құймалардың морфологиясына әсер ететіндігі зерттелген. Бұл құрылғы элементтерінің кейбір бөліктерінде жылу өтімді, ал кейбір бөліктерінде критикалық жағдайға жететіндігін көрсетеді. Осындай құбылыстардың нәтижесінде құрылымдық элементтер жарамсыз күйге (қирауға) тез ұшырайды және физикалық қасиеттерін жоғалтады. Сондықтан әр түрлі формадағы дене үшін температураның таралу өрісін математикалық модельдеу (пішіндеу) өзекті мәселе. Мақалада сырық тәріздес құрылымдық элементтердегі жылу таралу өрісінің заңдылықтарын анықтау бағытында есептер шығару үшін математикалық модельді (пішінді) құру әдістемесі және сәйкесті есептеу алгортмдері келтірілген. Бұл үшін авторлар энергетикалық-вариациялық принцип негізінде шекті элементтер әдісін қолданды.

Кілт сөздер: математикалық модель (пішін) біртұтас сырық, жылу ағыны, көлденен қима, функционал, жылу алмасу, жылудан оқшаулау, жылу таралу өрісі.

Б.З. Кенжегулов, С.Б. Кенжегулова, Д.Б. Алибиев, А.Ш. Кажикенова

Конечно-элементное моделирование распространения тепла полного стержня постоянного поперечного сечения

В статье введено определение поля распределения температуры для стержня, изготовленного из жаропрочного сплава ЭИ48. Авторами для исследования выбран полный стержень кругового поперечного сечения радиуса *R* ограниченной длины *L*. Изучаемое тело находится под воздействием теплового потока *q* со стороны поверхности по всей площади поперечного сечения левого конца, а на площади поперечного сечения правого конца происходит теплообмен с окружающей средой. Стержень теплоизолирован по боковой поверхности. Изучены два случая: первый — тепловой поток интенсивностью *q* может быть задан на площади малого круга радиусом $r<R$; второй — тепловой поток может быть задан на ее части, то есть на площади $\pi\left(\frac{R}{2}\right)^2$. При исследовании авторами показано, что при термомеханическом процессе на прочность каждого участка несущих элементов конструкции существенное влияние оказывает поле распределения температуры. Также отмечено влияние высокой температуры на морфологию жаропрочных сплавов. Это приводит к тому, что на каких-

то участках элементов конструкции температура будет допустимой, а на каких-то — критической. Вследствие этого происходит быстрое изнашивание элементов конструкции и потеря их физических качеств. Поэтому математическое моделирование распределения поля температуры для тела различной конфигурации является актуальной проблемой. В статье приведена методика построения математической модели и соответствующего вычислительного алгоритма, позволяющих решать класс задач по определению закономерностей поля распределения температур в элементах конструкций стержневого вида. Для этого авторы использовали энергетическо-вариационный принцип в сочетании метода конечных элементов.

Ключевые слова: математическая модель, полный стержень, тепловой поток, поперечное сечение, функционал, теплообмен, теплоизоляция, поле распределения температуры.

DOI 10.31489/2022PH4/106-114

UDC 533.682

B.R. Nussupbekov, S.E. Sakipova *, D.A. Ospanova, B.B. Kutum,
K.M. Shaimerdenova, Zh.S. Bekturganov

Karaganda University of the name of academician E.A. Buketov, Kazakhstan
*(*E-mail: sesaule@mail.ru)*

Some technological aspects of cleaning pipes of heat exchangers from solid scale deposits

This article discusses possible solutions to one of the problems associated with the low efficiency of existing thermal power plants. These factors are due to both the depreciation of equipment and the lack of any effective technologies for intensifying heat and mass transfer processes. The relevance of research topics is also confirmed by the fact that at the state level it is proposed to legally oblige the subjects of the heat and power industry to carry out preventive measures aimed at optimizing existing enterprises. The description of the reasons for the occurrence of scale deposits that appear in the in-line cavities is given. Due to the fact that the thermal conductivity of solid deposits is much less than the thermal conductivity of the metals from which the heat exchanger tubes are made, they significantly reduce the intensity of the processes and the intensity of heat transfer. Solid deposits lead to a decrease in the coolant flow rate, an increase in fuel consumption and a violation of the technological mode of operation of the entire heat exchange unit. The authors analyzed various technological aspects of various methods for cleaning heat exchanger tubes from solid scale deposits, on the basis of which the advantages of the electrohydraulic treatment method are substantiated. A schematic diagram of the device is given and a brief description of the method of cleaning the pipes of heat exchangers from solid scale deposits is given using electro-hydro-pulse action. The results of the application of this technology for cleaning heat exchange pipes at specific heat and power enterprises are shown, which confirm its advantages over other cleaning methods, both in terms of processing time and energy costs. The influence of the degree of purification of heat exchange pipes from solid deposits on the thermophysical parameters and efficiency of the heat exchanger is considered.

Keywords: heat exchanger, hard scale deposits, pipe cleaning, electro-hydro-impulse treatment, heat exchange efficiency.

Introduction

The energy-saving use of heat and power resources, the creation of new efficient ones, as well as the improvement of existing technical devices, is an important problem of scientific and technological progress. Heat exchangers are used to implement various thermal processes of heating, cooling, boiling, condensation and more complex physical processes — evaporation, absorption, heat transfer, etc. Heat exchangers are widely used in steam generators of nuclear power plants, gas-pipe installations and technological devices of chemical production, air conditioning systems, refrigeration and transport installations, etc. [1-5].

The development of energy intensity and production volumes requires an increase in the size of heat exchangers, which necessitates the search for ways to save fuel, materials and labor costs. According to JSC KOREM company, our “Kazakhstan's thermal power industry operates with a low efficiency [2, 6, 7]. Moreover, the Ministry of Energy has developed a Law obliging the subjects of the heat and power industry to carry out preventive measures aimed at optimizing existing facilities. The new legislation should ensure the technological renewal of the industry, the possibility of providing reliable, high-quality services to consumers, the reduction of specific and absolute levels of emissions, etc. The adoption of such measures at the state level is due to many technical and economic problems of the thermal power industry, such as a high degree of wear and tear of the main equipment — the national average wear of heating networks is 59 %; low thermal efficiency of existing equipment, high losses of thermal energy in thermal networks, etc. Among them, the problem of “lack of effective organization and planning of repair work to maintain and restore the main and auxiliary equipment of CHPPs, boiler houses and heating networks” is highlighted separately. In the proposed article, the authors consider some aspects of the technology, the application of which can determine possible ways to solve one of the most urgent problems of the domestic thermal power industry.

Problem statement and research method

It is known that the heat transfer largely depends on the cleanliness degree of working surfaces, because the presence of even a thin deposit of in-line deposits sharply worsens the process of heat transfer. Scale deposits have low thermal conductivity; they reduce heat transfer, so the heating of heat exchangers with deposits takes a longer time and requires more energy. Walls of heat exchange tubes in the presence of scale are heated to a higher temperature, which leads to a reduction in their service life. Therefore, in recent years, much attention has been paid to the fight against the occurrence of unwanted deposits in pipes, which not only reduce the efficiency of the boiler, but also increase fuel consumption [8-11]. Classical methods of dealing with scale are associated with the removal of hardness salts from the feed water (their absorption by various ion exchangers) or the addition of chemicals, such as phosphates, to the water [12]. These methods are very expensive, and therefore they are used mainly on large heat exchange devices.

It should be noted that at some technological enterprises, heat exchangers and boilers use pipes made of expensive metals and their alloys, such as brass, copper, LAMsh, etc., which are difficult to clean. Such pipes simply have to be cut and removed along with deposits. This is very costly and time consuming due to the need to stop the operation of the entire heat exchanger. The need to develop and implement an effective method for cleaning heat exchange pipes, which quickly removes solid deposits without deformation and rupture of the metal walls of the pipes directly, is an urgent task not only in Kazakhstan, but also in many CIS countries and far abroad.

Practice shows that the cleaning of heat exchange surfaces from solid deposits using electro-hydropulse (EHP) action is the most effective and environmentally friendly method [13]. In addition to cleaning heat exchange tubes, EHP technology is widely used in a wide variety of production processes and industries, for water disinfection, for crushing and grinding mineral ores, for breaking rocks, for demulsifying liquids, for cleaning oil and phosphorus deposits and others [14-18]. At the same time, the physical phenomena accompanying the processes of interaction between pressure shock waves and macroscopic structures in heterogeneous liquids have not been fully studied. This is due to their complexity and diversity, as well as the impossibility of preliminary calculation of the parameters of the EHP impact, which depend in each particular case on many factors. In this regard, the authors studied some technological aspects of cleaning the heat exchanger tubes from solid deposits using EHP action to determine the most optimal parameters and modes of this method and its effect on the efficiency of the heat exchanger.

The process of formation of scale deposits depends on both the temperature regime of the heat carrier and the water treatment of the source water. As a rule, industrial water, which always contains various impurities in the form of gas bubbles or dispersed solid particles, is used as a high-quality heat carrier at enterprises, technological installations of the chemical, oil and gas industries. Due to the presence of impurities of various salts in the process water in the form of fine-grained particles or dissolved substances, scale and solid deposits form in the heat exchangers during operation [10, 11].

Various impurities contained in water are divided into suspended and dissolved. Suspended substances consist of sand, clay, particles of organic and mineral origin and are removed from the water by clarification in mechanical filters. Of the dissolved salts in the water, magnesium chloride Mg Cl_2, sodium Na Cl, calcium Ca Cl_2, calcium sulfate Ca SO_4 and magnesium Mg SO4, carbonate and bicarbonate salts of calcium or magnesium Ca SO_3, Mg SO_3, Ca $(HCO_3)_2$, Mg $(HCO_3)_2$, as well as compounds of iron, aluminum, silicon [8, 10]. Calcium and magnesium salts have the greatest scale-forming ability. Scale deposits consist of a mixture of various chemical elements, the composition and structure of which also depends on the temperature regime of the coolant.

Numerous boilers, water heaters and other heat exchange devices of small and medium capacity, as a rule, use network water without special treatment. As a result, there is a rapid formation of scale deposits on the walls of heat exchangers. This is confirmed by the results of the analysis of the composition and structure of hard scale deposits formed on the inner surface of the pipes of heat exchangers of a number of operating thermal power facilities. As part of the research, the condition of the pipes of such heat exchangers as boilers and condensers of heat power plant HPP-3 in Karaganda city, the bakery boiler unit E-1/9-1 of Saran city, and others were studied.

The efficiency of cleaning heat exchangers from solid deposits can be ensured by a method based on the well-known electrohydraulic effect (EHE) by Yutkin L. This has been repeatedly confirmed experimentally, both by testing the EHP technology in laboratory conditions and directly by the results of cleaning various heat exchange pipes at operating industrial facilities [13-19].

Let's consider some technological aspects of cleaning the internal surfaces of heat exchanger tubes from solid scale deposits using EHP technology. Under EHP action, the destruction source of solid deposits is powerful impulse pressures at the front of shock waves, which are formed during a high-voltage electric discharge in water. It has been established that, first of all, thicker deposits are destroyed, and for the destruction of thin-layer deposits, it is required to increase the supplied discharge energy. In addition to the fact that this causes additional energy costs and can lead to unwanted ruptures of the pipe wall. Electric discharges are carried out near the cylindrical wall of the pipe. Therefore, it is necessary to take into account multiple reflections of pressure waves, which can enhance the effect of the EHP action, and under certain conditions, and vice versa, reduce it. It is difficult to determine in advance the pressure value at the shock wave front due to cavitation effects, phase changes in the working fluid, reaction of scale deposits, etc. that occur during EHP treatment.

To solve this problem, a team of authors proposed a method for removing solid deposits of various thicknesses that form on the inner surface of pipes, which can be implemented without an additional increase in the electrical parameters of the discharge [11, 17, 18]. According to the idea of the authors, a cable-electrode is inserted into the cavity of the cleaned pipe, which is installed in a cone-shaped nozzle made of durable material. Figure 1 shows a scheme for cleaning the surfaces of heat exchangers from solid scale deposits.

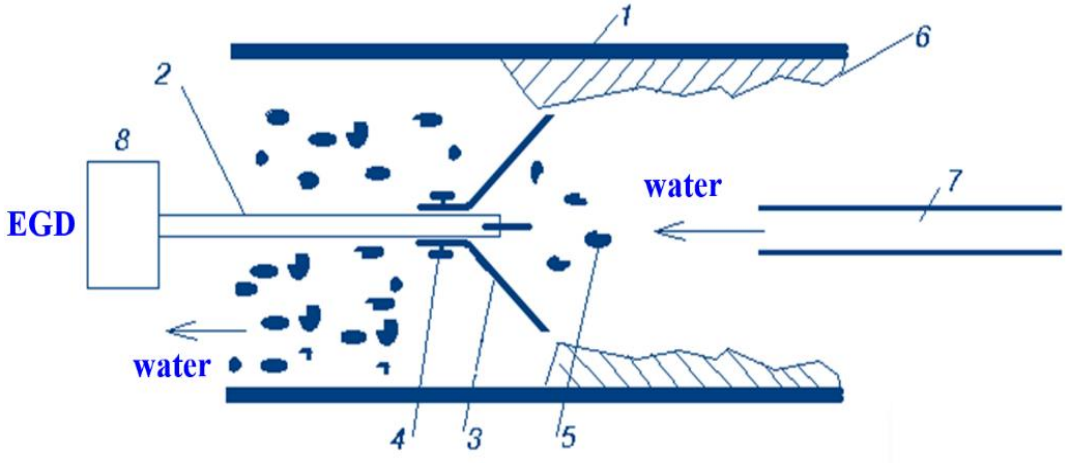

Figure 1. Scheme of the electro-hydro-pulse cleaning method:
1 — wall of the pipe being cleaned, 2 — cable-electrode, 3 — cone-shaped device, 4 — fastening, 5 — destroyed deposits, 6 — scale layer being cleaned, 7 — technical water, 8 — electro-hydraulic device (EGD).

The cone-shaped nozzle is made of steel (1.0÷1.5) mm thick. The outer diameter of the cone is smaller than the inner diameter of the heat exchanger tube being cleaned. During EHE, the shock wave propagates isotropically, in all directions, and the cone-shaped nozzle orients its movement along a certain solid angle, and therefore allows increasing the value of the wave pressure along the pipe axis. This phenomenon is associated with the cumulating effect, which provides an increase in the pressure of the shock wave in a certain direction, and, consequently, the effect of energy concentration.

The greatest increase in the pulse pressure amplitude was obtained when using a nozzle with a taper angle $\alpha=30^0$. The shock wave enhanced by the cumulative effect contributes to faster destruction and flaking of hard and superhard deposits located on the inner surface of the pipe. The periodic action of a powerful shock wave on the treated surface contributes to the destruction of solid deposits, thereby intensifying the process of cleaning the internal cavity of the heat exchanger tube. Destroyed and exfoliated sediment particles are carried away from the working area by the fluid flow. Let us consider examples of the successful application of the developed technology for cleaning pipes and tube bundles of peak boilers of thermal power plants, E1/9 steam boilers, etc.

As a result of the cleaning work using the EHP treatment, the heat exchange tubes are completely cleaned. Along with the cleaning of pipes the pressure testing of pipes and tube bundles was also carried out, and their suitability for further operation is determined.

Results and discussion

Treatment of brass pipes using electro-hydro impulse treatment.

Figures 2 and 3 are photographs of pipes sections of the heat exchangers of various diameters d with hard scale deposits. The solid scale deposits into pipes formed from CHPP-3 (Karaganda city) after operation during the season (about 6 months). It can be seen that inner surfaces of the pipes are completely cleaned after electrohydraulic treatment (Fig. 3b). The metal walls are not deformed, which allows them to be used in the heat exchanger in the future along with new ones.

a *b*

Figure 2. Samples of heat exchange pipes sections from CHPP-3 after operation during the heating season:
a) — boiler pipe, d=19mm; b) — condenser pipe, d=28mm

a b

Figure 3. Samples of condenser pipes sections from CHPP-3, d = 24 mm
a) before processing; b) — completely cleared using the EHI effects.

The significance and practical importance of this technology is that the use of EHP- processing allows manufacturing enterprises to continue working in a short time with improved indicators of energy efficiency and economic profitability of equipment. As a result of the work carried out on the cleaning of heat exchange pipes, a methodology for its application was developed, equipment was created, which was tested and implemented at a number of thermal power facilities.

Treatment of steel pipes of the boiler unit E1/9 using electro-hydro pulse treatment.

The studied steam generator E1/9 worked for 9 months without stopping. Boiler plants of the plant provide production processes with saturated steam with humidity up to 30 % and at the same time cover all technological and heating loads. According to the passport data, the productivity of the E1/9 solid fuel steam generator should be 103 kg of steam per hour. In the E1/9 steam generator, the upper and lower drums are strictly located on the same vertical axis and are interconnected by tube bundles forming convective heating surfaces. Seamless pipes made of grade 10 steel are used. The pipe diameter is 51 mm and the wall thickness is 2.5 mm (Fig. 4).

It can be seen that some pipes after seasonal operation are almost completely filled (“clogged”) with solid deposits. These solid deposits are characterized by a denser, homogeneous, almost stone structure (Fig. 4a). Previously, pipes with such deposits were processed first using chemical reagents, then cleaned using a mechanical cutter. But this method does not allow to remove the formed solid scale deposits, as a result of which the uncleaned pipes used during one season were replaced by new ones. Examination of fragments of spent pipes showed that in almost 70 % of the pipes of the convective bundle, the solid scale thickness reaches about 13-15 m (Fig. 4b). When checking the condition of the equipment, burnt pipes were also found, inside which the scale hardened like a stone.

a b

Figure 4. Samples of boiler pipes before and after cleaning using EHP — treatment: with hard deposits before processing; b) partially cleaned after processing, d = 51 mm

As part of the experiments, the dependence of the scale mass on the treatment time and the change in the thermal parameters of the E1/9 boiler as a result of cleaning using the EHP technology were revealed. Within 5 hours, with the help of EGI technology, 3 rows of 11 convective pipes, 1.1 m to 1.8 m long, were cleaned. A total of 48 m of convective pipes were processed. The total mass of hard scales after EHP treatment was determined [17, 19]. After draining the water from the lower drum, scale deposits were weighed. The total weight of scale deposits from 33 pipes was 83 kg, which is 1.8 kg on average per meter of pipe. The maximum fragment size was 37 98 mm; the appearance and dimensions of some broken and removed scale deposits are shown in Figure 4b.

About influence of EHP pipe treatment on heat exchanger efficiency.

In the course of activities during the EHP treatment of the internal cavities of pipes for cleaning from solid scale deposits, a change in thermophysical characteristics was studied. An analysis of the parameters of the considered steam generator E1/9 after continuous operation for 9 months showed that the heat removal decreased to 47 %, while the consumption of solid fuel increased by 1.75 times. Data on the dependence of the heat transfer of a pipe on the thickness of deposits, which are determined for brass pipes of boilers with a diameter of 18.8 mm, are obtained (without taking into account the contamination of the outer surface of the pipes).

The appearance of deposits with a thickness of δ = 0.5 mm reduces the heat transfer coefficient by 23 %. A further increase in the thickness of the existing scale significantly disrupts the technological mode of operation of the entire heat exchange unit. The flow rate of the coolant is reduced, which reduces the performance of the heat exchanger.

For example, calculations for the E1/9-1 boiler showed that a scale layer of 1 mm thick entails an increase in fuel consumption by 2.5 %, with a thickness of 4 mm — by 7.5 %, which in practice leads to an excess consumption of fuel oil by 770 kg/ day.

The thermal conductivity of scale is tens, often hundreds, times less than the thermal conductivity of the metals from which the heat exchanger tubes are made. The carried out changes showed that even with the appearance of deposits with a thickness of δ = 0.5 mm on the inner surface of the pipe, the heat exchange unit efficiency — η, % decreases (Fig.5). With an increase in scale thickness up to 7 mm on the heat transfer surface of a brass pipe (d=28 mm), the liquid flow through the pipe decreases by 1.5 times, which leads to a 2-times decrease in the efficiency of the installation. After the cleaning work, commissioning work was carried out, which showed that the efficiency of the boiler E1/9-1 η,% of the boiler reached 68 % at a nominal value of 75 %. The steam temperature reached 147ºC, at the norm of 170ºC.

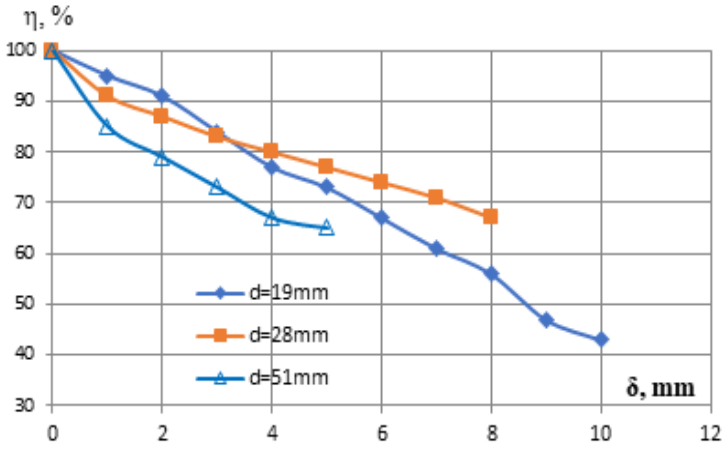

Figure 5. Dependence of the heat exchanger efficiency on the thickness of deposits.

The difference in efficiency values is due to the fact that some of the worn and burnt pipes were cut out and removed. These obtained results confirm that the removal of solid scale deposits in pipes contributes to the intensification of the heat transfer process and, accordingly, to the increase in the heat transfer efficiency of industrial heat exchangers.

Conclusion

Regular cleaning of pipes from solid scale deposits and the mandatory implementation of preventive measures against the occurrence of these deposits remain the most pressing problems of thermal power engineering so far. Obtained results have shown the undeniable advantages of cleaning the pipes of the heat exchanger and boiler units with the help of EHP technology. The speed of cleaning by this method is much higher than the productivity of the mechanical method with much lower power consumption. In general, the use of EHP impact for the destruction and removal of hard scale deposits from the internal cavities of pipes makes it possible to increase the efficiency of heat exchangers, and for heat and power enterprises to revise the cost items for major repairs and new purchases of materials. In the future, for a more effective solution to the problem of cleaning heat exchange pipes, it is necessary to comprehensively study the conditions for the formation of hard scale deposits, the mechanism and kinetics of their growth, structure and thermophysical properties, etc. This will allow not only to develop effective methods for removing scale deposits, but also to develop effective measures to prevent their formation.

Acknowledgments

The study was supported by project No. 0433-F-22 "Creation of an energy-saving installation for the efficiency of heat transfer of industrial heat exchangers"

References

1 Kazakhstan electric power industry: key factors. KEGOC. 16/10/2022. Retrived from https://www.kegoc.kz/en/electric-power/elektroenergetika-kazakhstana/.

2 Смирнов С. Энергетика Казахстана на пороге кризиса [Электронный ресурс] / С. Смирнов // Ритм Евразии. 27.04.2022. — Режим доступа: https://www.ritmeurasia.org/news-2022-04-27-energetika-kazakhstana-naporoge-krizisa-59598.

3 Петровский Ю.В. Современные эффективные теплообменники / Ю.В. Петровский, В.Г. Фастовский. — М.: Госэнергоиздат, 1982. — 256 с.

4 Попов И.А. Теплообменные аппараты с интенсификацией теплоотдачи / И.А. Попов, А.В. Щелчков, М.З. Яркаев и др. // Энергетика Татарстана. — 2014. — № 1 (19). — С. 10–16.

5 Попов И.А. Повышение эффективности котлоагрегатов посредством интенсификации теплообмена / И.А. Попов, А.Б. Яковлев, А.В. Щелчков, Д.В. Рыжков // Энергетика Татарстана. — 2010. — № 3 (19). — С. 31–36.

6 Законопроект «О теплоэнергетике» разработали в Казахстане [Электронный ресурс]. 08.11.2021. — Режим доступа: https://www.zakon. kz/5089880-zakonoproekt-o-teploenergetike.html.

7 Akchulakov B. Amendments in the field of electric power industry, construction of generating plants, the potential for the development of nuclear energy — the state of the thermal power industry in Kazakhstan today. 02.11.2022. Retrieved from

https://primeminister.kz/en/news/elektr-energetikasy-salasyndagy-tuzetuler-zhinaktaushy-kondyrgylar-kurylysy-atom-energetikasyn-damytu-aleueti.

8 Batrakov P.A., et al. The analysis of the deposit formation on the working surfaces of heat exchange industrial equipment. / P.A. Batrakov, A.M. Lasitsa, M.S. Peshko, et al. // Journal of Physics: Conference Series, 012040 IOP Publishing. 2022. doi:10.1088/1742-6596/2182/1/012040/.

9 Бубликов И.А. Структурные особенности и теплофизические свойства внутритрубных отложений на теплообменных поверхностях в системах технической воды / И.А. Бубликов // Теплоэнергетика. — 1998. — № 2. — С. 30–34.

10 Anastasios J. Karabelas. Scale formation in tubular heat exchangers — research priorities / J. Anastasios Karabelas. // International Journal of Thermal Sciences. — 2002. — Vol. 41. — Issue 7. — P. 682—692. https://doi.org/10.1016/S1290-0729(02)01363-7.

11 Сакипова С.Е. Особенности разрушения отложений накипи на теплообменных поверхностях при электрогидравлической очистке / С.Е. Сакипова // Деформация и разрушение материалов. — 2009. — № 9. — С. 42–44.

12 Плинский Г.И. и др. Опыт эксплуатационной химической очистки внутренних поверхностей нагрева парогенераторов ТПП–200 / Г.И. Плинский и др. // Теплоэнергетика. — 1976. — № 11. — С. 72–74.

13 Юткин Л.А. Электрогидравлический эффект и его применение в промышленности / Л.Ф. Юткин. — Л.: Машиностроение, 1986. — 253 с.

14 Nussupbekov B.R., et al. Electrohydraulic method for processing of the phosphorus containing sludges / B.R. Nussupbekov, S.E. Sakipova, A. Edris et al. // Eurasian Physical Technical Journal. — 2022. — Vol. 19, No. 1(39). — P. 99–104. https://doi.org/10.31489/2022No1/99-104.

15 Sakipova S.E. Effect of electric pulse processing on physical and chemical properties of inorganic materials / S.E. Sakipova, B.R. Nussupbekov, D.A. Ospanova, et al. // IOP Conference Series Materials Science and Engineering. — 2015. — No. 81. — P. 12051-12056. DOI:10.1088/1757-899X/81/1/012051.

16 Nussupbekov B.R. Electro-impulse Method of Surface Cleaning / B.R. Nussupbekov, K. Kussaynov, A.K. Khassennov // European Researcher. — 2013. — Vol. 38, No.1—1. — P. 11–14.

17 Kussaiynov K., et al. Electro-hydro-pulse technology for restoring the performance properties of heat exchangers / K. Kussaiynov, S.E. Sakipova, B.R. Nusupbekov et al. // Modern science: research, ideas, results, technologies. — 2013. — No. 2 (13). — P. 86—91.

18 Кусайынов К. и др. Электроимпульсный метод избирательного разрушения материала в жидкой среде / К. Кусайынов, Б.Р. Нусупбеков, С.Е. Сакипова и др. Инновационный патент РК на изобретение № 29005. Опубликован: 15.10.2014.

19 Нүсіпбеков Б.Р. Жылу алмастырғыштарды қалпына келтірудің жаңа технологиясы / Б.Р. Нүсіпбеков, А.К. Хасенов, Д.Ж. Карабекова, М. Стоев, А.Ж. Бейсенбек, Б.И. Қазанқап // Қарағанды университетінің хабаршысы. Физика сериясы. — 2017. — № 1(85). — Б. 67-72.

Б.Р. Нусупбеков, С.Е. Сакипова, Д.А. Оспанова, Б.Б. Кутум,
К.М. Шаймерденова, Ж.С. Бектұрғанов

Жылу алмастырғыш құбырларды қатты қақтардан тазартудың кейбір технологиялық аспектілері

Мақалада жұмыс істеп тұрған жылу энергетикалық кәсіпорындардағы кондырғылардың тиімділігінің төмендеуін болдырмаудың бірден бір мәселелерін шешудің мүмкін жолдары талқыланған. Бұл факторлар жабдықтың тозуына да, жылу масса тасымалдау процестерін арттырудың тиімді технологияларының болмауына да байланысты болуы мүмкін. Зерттеу тақырыптарының өзектілігі негізінен жұмыс істеп тұрған кәсіпорындардағы жылу энергетикасы саласының субъектілерінде алдын алу шараларын жүргізумен қатар, мемлекеттік деңгейде және заң аясында оңтайландыруға бағытталған жұмыстарды міндеттеу көзделіп отыр. Себебі, жылу мен электр энергиясын өндіретін әрбір мекеме, мемлекетіміздегі стратегиялық нысан болып табылады. Сондықтан мақалада құбырішілік қабырғаларда пайда болатын шөгінділердің пайда болу себептерінің сипаттамасы келтірілген. Қатты шөгінділердің жылу өткізгіштігі жылу алмастырғыш құбырлар жасалған металдардың жылу өткізгіштігінен әлдеқайда төмен болғандықтан, жылу беру процестерінің қарқындылығын айтарлықтай азайтып жібереді. Ал сәйкесінше, қатты шөгінділердің пайда болуы салқындатқыштың шығынын азайтып, отын шығынын арттыруға және бүкіл жылу алмасу қондырғысының технологиялық режимін бұзуға әкеледі. Авторлар өз зерттеулерінде, жылу алмастырғыштар құбырларды қатты шөгінділерден тазартудың бірнеше әдістері мен әртүрлі технологиялық аспектілеріне талдаулар жүргізе отырып, электрогидравликалық өңдеу әдісін пайдаланудың артықшылықтарына басымдық берген. Мақалада құрылғының принципиалдық сұлбасы ұсынылып, жылу алмастырғыш құбырларын электро-гидро-импульстік әсерді пайдаланып, қатты қақтардан тазалау әдісіне қысқаша сипаттама берген. Сонымен қатар, жылу алмасу құбырларын тазартудың осы технологиясын нақты жылу энергетикалық кәсіпорындарда қолдану нәтижелері көрсетілген. Ал өңдеу уақыты бойынша да, энергия шығындары бойынша да тазалаудың басқа жолдарымен салыстырғанда, ұсынылған әдістің артықшылықтарын көруге болады. Зерттеулер-

де, жылу алмасу құбырларын қатты шөгінділерден тазарту дәрежесінің жылу-физикалық параметрлері мен жылу алмастырғыштың тиімділігіне әсері де қарастырылған.

Кілт сөздер: жылу алмастырғыш, қатты қақтар, шөгінділер, құбырларды тазарту, электр-гидроимпульсті өңдеу, жылу алмасу тиімділігі.

Б.Р. Нусупбеков, С.Е. Сакипова, Д.А. Оспанова, Б.Б. Кутум,
К.М. Шаймерденова, Ж.С. Бектурганов

Некоторые технологические аспекты очистки труб теплообменников от твердых накипных отложений

В статье обсуждены возможные пути решения одной из проблем, связанных с низкой эффективностью действующих теплоэнергетических предприятий. Эти факторы обусловлены как изношенностью оборудования, так и отсутствием каких-либо эффективных технологий для интенсификации процессов тепломассопереноса. Актуальность тематики исследований подтверждается также и тем, что на государственном уровне предлагается законодательно обязать субъекты теплоэнергетической отрасли проводить профилактические мероприятия, направленные на оптимизацию действующих предприятий. Приведено описание причин возникновения накипных отложений, которые появляются во внутритрубных полостях. Вследствие того, что теплопроводность твердых отложений намного меньше теплопроводности металлов, из которых изготовлены трубы теплообменников, они существенно снижают интенсивность процессов, интенсивность теплоотдачи. Наличие твердых отложений приводит к уменьшению расхода теплоносителя, увеличению расхода топлива и нарушению технологического режима работы всей теплообменной установки. Авторами проведен анализ различных технологических аспектов различных методов очистки труб теплообменников от твердых накипных отложений, на основе которого обоснованы преимущества метода электрогидравлической обработки. Приведена принципиальная схема устройства, и дано краткое описание метода очистки труб теплообменников от твердых накипных отложений с помощью электрогидроимпульсного воздействия. Показаны результаты применения данной технологии очистки теплообменных труб на конкретных теплоэнергетических предприятиях, которые подтверждают ее преимущества по сравнению с другими методами очистки как по времени обработки, так и по энергетическим затратам. Рассмотрено также влияние степени очистки теплообменных труб от твердых отложений на теплофизические параметры и эффективность теплообменника.

Ключевые слова: теплообменник, твердые накипные отложения, очистка труб, электрогидроимпульсная обработка, эффективность теплообмена.

References

1 Kazakhstan electric power industry: key factors. KEGOC. 16/10/2022. Retrived from https://www.kegoc.kz/ru/electric-power/elektroenergetika-kazakhstana/.

2 Smirnov, S. Energetika Kazakhstana na poroge krizisa [Energy industry of Kazakhstan on the verge of crisis]. *Ritm Evrazii — Rhythm of Eurasia*. 27.04.2022. Retrieved from https://www.ritmeurasia.org/news—2022-04-27—energetika-kazahstana-na-poroge-krizisa [in Russian].

3 Petrovsky, Yu.V., & Fastovsky, V.G. (1982). Sovremennye effektivnye teploobmenniki [Modern efficient heat exchangers]. Moscow, Gosenergoizdat [in Russian].

4 Popov, I.A., Shchelchkov, A.V., & Yarkaev, M.Z., et al. (2014). Teploobmennye apparaty s intensifikatsiei teplootdachi [Heat exchangers with heat transfer enhancement]. *Energy of Tatarstan*, 1 (19), 10—16 [in Russian].

5 Popov, I.A., Yakovlev, A.B., & Shchelchkov, A.V., et al. (2010). Povyshenie effektivnosti kotloagregatov posredstvom intensifikatsii teploobmena [Improving the efficiency of boiler units by intensifying heat transfer]. *Energy of Tatarstan*, 3 (19), 31–36 [in Russian].

6 Zakonoproekt "O teploenergetike" razrabotali v Kazakhstane [Draft law "On thermal power engineering" in Kazakhstan]. 08.11. 2021. Retrieved from https://www.zakon. kz/5089880-zakonoproekt-o-teploenergetike.html.

7 Akchulakov B. Amendments in the field of electric power industry, construction of generating plants, the potential for the development of nuclear energy — the state of the thermal power industry in Kazakhstan today. 02/11/2022. Retrieved from https://www.primeminister.kz/ru/news/reviews/popravki-v-oblasti-elektroenergetiki-stroitelstvo-generiruyushchih-ustanovok-potencial.

8 Batrakov, P.A., Lasitsa, A.M., & Peshko, M.S., et al. (2022). The analysis of the deposit formation on the working surfaces of heat exchange industrial equipment. *Journal of Physics: Conference Series*, 012040 IOP Publishing. doi:10.1088/1742-6596/2182/1/012040/.

9 Bublikov, I.A. (1998). Strukturnye osobennosti i teplofizicheskie svoistva vnutritrubnykh otlozhenii na teploobmennykh poverkhnostiiakh v sistemakh tekhnicheskoi vody [Structural features and thermophysical properties of in-line deposits on heat exchange surfaces in industrial water systems]. *Thermal power engineering*, 2, 30-34 [in Russian].

10 Anastasios, J. Karabelas. (2002). Scale formation in tubular heat exchangers — Research priorities. *International Journal of Thermal Sciences*, Vol. 41, Issue 7, 682—692. https://doi.org/10.1016/S1290-0729(02)01363-7.

11 Sakipova, S.E. (2009). Osobennosti razrusheniia otlozhenii nakipi na teploobmennykh poverkhnostiakh pri elertrogidravlicheskoi ochistke [Features of the destruction of scale deposits on heat exchange surfaces during electrohydraulic cleaning]. *Deformatsiia i razrushenie materialov — Deformation and destruction of materials*, 9, 42–44 [in Russian].

12 Plinskiy, G.I., et al. (1976). Opyt ekspluatatsionnoi khimicheskoi ochistki vnutrennikh poverkhnostei nagreva parogeneratorov TPP-200 [Experience of operational chemical cleaning of internal heating surfaces of steam generators TPP-200]. *Thermal Power Engineering*, 11, 72–74 [in Russian].

13 Yutkin, L.A. (1986). Elertrogidravlicheskii effekt i ego primenenie v promyshlennosti [Electrohydraulic effect and its application in industry]. Leningrad, Mashinostroenie [in Russian].

14 Nussupbekov, B.R., Sakipova, S.E., & Edris, A., et al. (2022). Electrohydraulic method for processing of the phosphorus containing sludges. *Eurasian Physical Technical Journal, Vol.*19, 1(39), 99–104. https://doi.org/10.31489/2022No1/99-104.

15 Sakipova, S.E., Nussupbekov, B.R., & Ospanova, D.A., et al. (2015). Effect of electric pulse processing on physical and chemical properties of inorganic materials. *IOP Conference Series Materials Science and Engineering.* 81, 12051-12056. DOI:10.1088/1757-899X/81/1/012051.

16 Nussupbekov, B.R., Kussaiynov, K., Khassennov, A.K. (2013). Electro-impulse Method of Surface Cleaning. *European Researcher, Vol.* 38, 1–1, 11–14.

17 Kussaiynov, K., Sakipova, S.E., & Nusupbekov, B.R., et al. (2013). Electro-hydro-pulse technology for restoring the performance properties of heat exchangers. *Modern science: research, ideas, results, technologies*, 2 (13), 86—91.

18 Kussaiynov, K., Nusupbekov, B.R., & Sakipova, S.E., et al. (2014). Elektroimpulsnyi metod izbiratelnogo razrusheniia materiala v zhidkoi srede [Electropulse method of selective destruction of material in a liquid medium]. Innovative patent of the Republic of Kazakhstan for the invention No. 29005. Published: 10/15/2014 [in Russian].

19 Nussupbekov, B.R., Khassenov, A.K., Karabekova, D.Zh., Stoev, M., Beysenbek, A.Zh., Kazankap, B.I. (2017). Zhylu almastyrgyshtardy qalpyna keltirudin zhana tekhnologiiasy [New technology for the recovery of heat exchangers]. *Bulletin of the Karaganda University. Physics Series*, 1(85), 67–72 [in Kazakh].

АВТОРЛАР ТУРАЛЫ МӘЛІМЕТТЕР
СВЕДЕНИЯ ОБ АВТОРАХ
INFORMATION ABOUT AUTHORS

Aidarbekov, N.K. — Postdoc, L. N. Gumilyov Eurasian National University, Astana, Kazakhstan

Alibiyev, D.B — Candidate of physical and mathematical sciences, Karagandy University of the name of academician E.A. Buketov, Karaganda, University street, 28, 100028, Kazakhstan; e-mail: dalibiev@mail.ru; https://orcid.org/0000-0003-1150-7096

Baltabekov, A.S. — Doctor of PhD, Associate Professor of the Department of Physics and Nanotechnology, Karaganda University named after Academician E.A. Buketov, Karaganda, Kazakhstan; abskargu@mail.ru

Bekmyrza, K.Zh. (contact person) — Ph.D, Associate Professor of the Department of Technical Physics, L.N. Gumilyov Eurasian National University, Astana, Kazakhstan

Bekturganov, Zh.S. — Doctor of Chemical Sciences, Professor of the Department of Radiophysics and Electronics, Karaganda University named after E.A.Buketov, Kazakhstan

Eremin, E.N. (contact person) - Doctor of Technical Sciences; Professor; Dean of the Mechanical Engineering Institute, Head of the Department of Mechanical Engineering and Materials Science; Omsk State Technical University; Omsk; Russia; weld_techn@mail.ru

Golodyuk, V.S. — Postgraduate Student, Department of Computerized Electromechanical Systems and Complexes, Vinnitsa National Technical University, Ukraine, e-mail: vgolodyk@gmail.com

Gribov, M.L. — Doctor of Law, Professor, Professor of the Department of Investigative Activities of the National Academy of Internal Affairs, Ukraine, e-mail: griboff007@gmail.com

Ibrayev, N. — Doctor of Physics and Mathematical Sciences, Professor, Director of the Institute of Molecular Nanophotonics, Karaganda University of the name of academician E.A. Buketov, Kazakhstan

Ishchenko, A. — Doctor of Chemical Sciences, Professor, Institute of Organic Chemistry, NAS of Ukraine, Kyiv, Ukraine

Kabyshev, A.M. — Ph.D, Senior Lecturer of the International Department of Nuclear Physics, new materials and technologies, L.N. Gumilyov Eurasian National University, Astana, Kazakhstan

Kambarov, Ye.Ye. — PhD student, D. Serikbayev East Kazakhstan technical university, Ust-Kamenogorsk, Kazakhstan; e-mail: yedilzhan@gmail.com

Katsyv, S.Sh. — Candidate of Technical Sciences, Associate Professor, Associate Professor of the Department of Computerized Electromechanical Systems and Complexes, Vinnitsa National Technical University, Ukraine, e-mail: katsyvsam@ukr.net

Kazhikenova, A.Sh. — Candidate of technical science, Karagandy University of the name of academician E.A. Buketov, Karaganda, University street, 28, 100028, Kazakhstan; e-mail: aigul-kazhikenova@mail.ru; https://orcid.org/0000-0003-4053-1546

Kazhikenova, A.Sh. (contact person) — Candidate of technical science, Karagandy University of the name of academician E.A. Buketov, Karaganda, University street, 28, 100028, Kazakhstan; e-mail: aigul-kazhikenova@mail.ru; https://orcid.org/0000-0003-4053-1546

Kengesbekov, A.B. (contact person) — Postdoctoral student, PlasmaScience LLP, Ust-Kamenogorsk, Kazakhstan; e-mail: aidar.94.01@mail.ru.

Kenzhalieva, K.Z. — student of 2 years of study. Department of Radiophysics and Electronics, Karaganda University of the name of academician E.A. Buketov, Karaganda, Kazakhstan.

Kenzhegulov, B.Z. — Doctor of Technical Sciences, Professor, Research Institute of Mathematics and Applied Technologies, Dosmukhamedov Atyrau University, Atyrau, Student street, 1, Kazakhstan; e-mail: kenzegulov_bz@mail.ru; https://orcid.org/0000-0001-6230-2926.

Kenzhegulov, S.B. — Master of IS, senior lecturer of "Business informatics" department, K. Sagadiev University of International Business, Almaty, 8A, Kazakhstan; e-mail: kenzegulov_bz@mail.ru; https://orcid.org/0000-0001-8461-8956.

Kuanyshbekova, A.B. — Master student of the Department of Physics and Nanotechnology, Karaganda University named after Academician E.A. Buketov, Karaganda, Kazakhstan, kuanyshbekovaaya@mail.ru

Kubenova, M. — PhD, Senior Lecturer, Department of Standardization and Certification, L.N. Gumilyov Eurasian National University, Astana, Kazakhstan.

Kucheruk, V.Yu. (contact person) — Doctor of Technical Sciences, Professor, Professor of the Department of Information Technologies of the Uman National University of Horticulture, Professor of the Department of Computer Science and Economic Cybernetics of the Vinnitsa National Agrarian University, Ukraine, e-mail: vladimir.kucheruk@gmail.com.

Kudinova, M. — Senior researcher, Candidate of Chemical Sciences, Institute of Organic Chemistry, NAS of Ukraine, Kyiv, Ukraine

Kukharchuk, V.V. — Doctor of Technical Sciences, Professor, Professor of the Department of Computerized Electromechanical Systems and Complexes, Vinnitsa National Technical University, Ukraine, e-mail: BKuch@ukr.net

Kulakov, P.I. — Doctor of Technical Sciences, Professor, Professor of the Department of Information Technologies of the Uman National University of Horticulture, Ukraine, e-mail: kulakovpi@gmail.com

Kurmanaliyev, N.B. — 2 st year undergraduate student. Department of Radiophysics and Electronics, Karaganda University of the name of academician E.A. Buketov, Karaganda, Kazakhstan.

Kuterbekov, K.A. — Doctor of physical and mathematical sciences, professor of the International Department of Nuclear Physics, new materials and technologies, L. N. Gumilyov Eurasian National University, Astana, Kazakhstan.

Kutum, B.B. — Senior lecturer of the Department of Engineering Thermophysics named after prof. Zh.S. Akylbayev Karaganda University named after E.A.Buketov, Kazakhstan; e-mail: kuttykadam@mail.ru

Leonov, A.P. (contact person) — PhD, Associate Professor, School of Energy & Power Engineering, Tomsk Polytechnic University, Tomsk, Russia, e-mail: leonov_ap@tpu.ru

Madyarov, V.G. — Candidate of Technical Sciences, Professor of the Department of Computerized Electromechanical Systems and Complexes, Vinnitsa National Technical University, Ukraine, e-mail: madiarov@vntu.edu.ua

Makhanov, K.M. (contact person) — Candidate of Physical and Mathematical sciences, Associate Professor, Karaganda University of the name of academician E.A. Buketov, Karaganda, Kazakhstan; e-mail: makanov@inbox.ru.

Mammadova, G.M. (contact person) - leading engineer, at Institute of Physics of National Academy of Science of Azerbaijan, Baku Azerbaijan Repablic, e*_mail:* gizbesmamedova@gmail.com

Musepov, S.B. — 1 st year undergraduate student. Department of Radiophysics and Electronics, Karaganda University of the name of academician E.A. Buketov, Karaganda, Kazakhstan.

Naptalov, A. K. — 1 st year undergraduate student. Department of Radiophysics and Electronics, Karaganda University of the name of academician E.A. Buketov, Karaganda, Kazakhstan.

Nurkenov, S.A. — Ph.D, Associate Professor of the Higher School of Education of Astana International University Kazakhstan, Astana, Kazakhstan.

Nussupbekov, B.R. — Candidate of Technical Sciences, Full Professor of the Department of Engineering Thermophysics named after prof. Zh.S.Akylbayev, Karaganda University named after E.A.Buketov, Kazakhstan; e-mail: bek_nr1963@mail.ru

Ospanova, D.A. — PhD student of the Department of Engineering Thermophysics named after prof. Zh.S. Akylbayev, University named after E.A.Buketov, Kazakhstan

Rakhadilov, B.K. — PhD, associate professor; Director «PlasmaScience» LLP, Ust-Kamenogorsk, Kazakhstan; e-mail: rakhadilovb@mail.ru

Sakipova, S.E. (contact person) — Candidate of Physical and Mathematical Sciences, Professor of the Department of Engineering Thermophysics named after prof. Zh.S. Akylbayev, Karaganda University named after E.A.Buketov, Kazakhstan; e-mail: sesaule@mail.ru

Seliverstova, E. — Senior researcher, PhD Physics, Institute of Molecular Nanophotonics, Karaganda University of the name of academician E.A. Buketov, Kazakhstan.

Serikov, T.M. (contact person) — Doctor of PhD, Associate Professor of the Department of Physics and Nanotechnology, Karaganda University named after Academician E.A. Buketov, Karaganda, Kazakhstan; serikov-timur@mail.ru

Shaimerdenova, K.M. — Candidate of Technical Sciences, Professor of the Department of Engineering Thermophysics named after prof. Zh.S. Akylbayev, Karaganda University named after E.A. Buketov, Kazakhstan; e-mail: gulzhan.0106@mail.ru

Soldatenko, T.M. — Senior lecturer, School of Energy & Power Engineering, Tomsk Polytechnic University, Tomsk, Russia, e-mail: ruhtinatm@tpu.ru

Temirbayeva, D. (contact person) — Junior researcher, Institute of Molecular Nanophotonics, Karaganda University of the name of academician E.A. Buketov, Kazakhstan; e-mail: dilara_7-7-7@mail.ru

Uazyrkhanova, G.K. — PhD, associate professor; Associate Professor of the Department of Physics, D. Serikbayev East Kazakhstan technical university, Ust-Kamenogorsk, Kazakhstan; e-mail: GUazyehanova@mail.ru

Zhanbirbayeva, P.A. — Master student of the Department of Physics and Nanotechnology, Karaganda University named after Academician E.A. Buketov, Karaganda, Kazakhstan perizat.zhanbirbaeva@mail.ru

Zhurerova, L.G. — PhD, associate professor; Senior Researcher at the Research Center “Surface Engineering and Tribology”; Sarsen Amanzholov East Kazakhstan University, Ust-Kamenogorsk, Kazakhstan; e-mail: leila_uka@mail.ru.

2022 жылғы
«Қарағанды университетінің хабаршысы. Физика сериясы»
журналында жарияланған мақалалардың көрсеткіші

Указатель статей, опубликованных в журнале
«Вестник Карагандинского университета. Серия Физика»
в 2022 году

Index of articles published in
«Bulletin of the Karaganda University. Physics Series»
in 2022

№ б.
№ с.
№ р.

ТЕХНИКАЛЫҚ ФИЗИКА
ТЕХНИЧЕСКАЯ ФИЗИКА
TECHNICAL PHYSICS

КОНДЕНСАЦИЯЛАНҒАН КҮЙДІҢ ФИЗИКАСЫ
ФИЗИКА КОНДЕНСИРОВАННОГО СОСТОЯНИЯ
PHYSICS OF THE CONDENSED MATTER

ЖЫЛУФИЗИКАСЫ ЖӘНЕ ТЕОРИЯЛЫҚ ЖЫЛУТЕХНИКАСЫ
ТЕПЛОФИЗИКА И ТЕОРЕТИЧЕСКАЯ ТЕПЛОТЕХНИКА
THERMOPHYSICS AND THEORETICAL THERMOENGINEERING